

## INFORMATION TO USERS

This manuscript has been reproduced from the microfilm master. UMI films the text directly from the original or copy submitted. Thus, some thesis and dissertation copies are in typewriter face, while others may be from any type of computer printer.

**The quality of this reproduction is dependent upon the quality of the copy submitted.** Broken or indistinct print, colored or poor quality illustrations and photographs, print bleedthrough, substandard margins, and improper alignment can adversely affect reproduction.

In the unlikely event that the author did not send UMI a complete manuscript and there are missing pages, these will be noted. Also, if unauthorized copyright material had to be removed, a note will indicate the deletion.

Oversize materials (e.g., maps, drawings, charts) are reproduced by sectioning the original, beginning at the upper left-hand corner and continuing from left to right in equal sections with small overlaps.

ProQuest Information and Learning  
300 North Zeeb Road, Ann Arbor, MI 48106-1346 USA  
800-521-0600

UMI<sup>®</sup>



University of Alberta

RECEIVER DESIGN AND COCHANNEL INTERFERENCE MITIGATION FOR  
MICRO-CELLULAR WIRELESS SYSTEMS

by

Kathiravetpillai Sivanesan



A thesis submitted to the Faculty of Graduate Studies and Research in partial  
fulfillment of the requirements for the degree of **Doctor of Philosophy**.

Department of Electrical and Computer Engineering

Edmonton, Alberta

Spring 2005



Library and  
Archives Canada

Bibliothèque et  
Archives Canada

0-494-08299-2

Published Heritage  
Branch

Direction du  
Patrimoine de l'édition

395 Wellington Street  
Ottawa ON K1A 0N4  
Canada

395, rue Wellington  
Ottawa ON K1A 0N4  
Canada

*Your file    Votre référence*

*ISBN:*

*Our file    Notre référence*

*ISBN:*

#### NOTICE:

The author has granted a non-exclusive license allowing Library and Archives Canada to reproduce, publish, archive, preserve, conserve, communicate to the public by telecommunication or on the Internet, loan, distribute and sell theses worldwide, for commercial or non-commercial purposes, in microform, paper, electronic and/or any other formats.

The author retains copyright ownership and moral rights in this thesis. Neither the thesis nor substantial extracts from it may be printed or otherwise reproduced without the author's permission.

#### AVIS:

L'auteur a accordé une licence non exclusive permettant à la Bibliothèque et Archives Canada de reproduire, publier, archiver, sauvegarder, conserver, transmettre au public par télécommunication ou par l'Internet, prêter, distribuer et vendre des thèses partout dans le monde, à des fins commerciales ou autres, sur support microforme, papier, électronique et/ou autres formats.

L'auteur conserve la propriété du droit d'auteur et des droits moraux qui protègent cette thèse. Ni la thèse ni des extraits substantiels de celle-ci ne doivent être imprimés ou autrement reproduits sans son autorisation.

---

In compliance with the Canadian Privacy Act some supporting forms may have been removed from this thesis.

Conformément à la loi canadienne sur la protection de la vie privée, quelques formulaires secondaires ont été enlevés de cette thèse.

While these forms may be included in the document page count, their removal does not represent any loss of content from the thesis.

Bien que ces formulaires aient inclus dans la pagination, il n'y aura aucun contenu manquant.

  
**Canada**

*To the memory of my grandmother*

*Subramaniam Theivannaipillai*

# Abstract

The number of users subscribed to wireless communication services has been growing exponentially during the past decade. New sophisticated wireless services are being added. Demands for high data rates and capacity over the wireless channel at lower cost are enormous. Multipath fading, cochannel interference (CCI), multiple access interference (MAI) and adjacent channel interference (ACI) are the prime factors affecting the capacity and the bit error rate (BER). In the literature, a considerable amount of research thrust has been focused to combat these factors. Many diversity techniques were proposed to combat the multipath fading. Optimal maximum likelihood receivers and many suboptimal receivers were proposed to combat cochannel interference and multiple access interference.

In this thesis, interference whitening receivers and conventional space diversity receivers are investigated to combat the CCI and MAI in micro-cellular fading environments. The interference whitening receivers exploit the correlation in the spectrum of CCI and MAI to mitigate their effects on detection of the desired signal. A whitening matched filter is introduced instead of the conventional matched filter. While maximizing the signal-to-noise plus interference ratio (SNIR), the whitening matched filter introduces intersymbol interference (ISI) in the desired sample. A fractionally spaced linear minimum mean square error (MMSE) equalizer is employed to combat the intersymbol interference. Average BER expressions are derived using characteristic function and Fourier series methods. Notably, the complexity of this system does not grow with the number of users as do the complexities of the optimal or suboptimal multiuser receivers. The whitening matched filter receiver uses the knowledge of the

value of the total interference power and the interferers' pulse shaping, information normally available at the receivers for power control, etc. or inexpensive to obtain.

The accurate BER and outage performances of conventional space diversity receivers in CCI and fading channels are studied. Bandlimited BPSK systems with two Nyquist pulse shapes, namely, spectrum raised-cosine (SRC) and Beaulieu-Tan-Damen (BTD) pulses are considered. Again, characteristic function and Fourier series methods are employed. It is shown that the BTD pulse outperforms the SRC pulse in all the cases considered.

The proposed receivers require only the total interference power and the pulse-shape of the interferers at the receiver. These parameters may be available at the conventional receiver for the power control and some diversity combining schemes. As the receiver structure changes with the parameters thus, these receivers are adaptive single-user receivers.

# Acknowledgements

I take this opportunity to express my sincere gratitude to my supervisor Dr. Norman C. Beaulieu for his valuable guidance, technical advice, encouragement and financial support throughout my stay at the University of Alberta. I would also like to thank all my colleagues in the *i*CORE Wireless Communication Laboratory for their strong support and valuable friendship. I like to thank Sharon and Sandra for helping me out with the administrative matters.

I would like to thank Dr. Valentine Aalo from Florida Atlantic University for agreeing to serve as an external examiner. I would also like to thank Drs. Ioanis Nikolaidis, Chintha Tellambura and Mrinal Mandal for serving on my committee.

I am indebted to all my family members for their continuous love, support, encouragement and for putting up with me being a student for so long.

Finally, I would like to acknowledge the financial support of the Alberta Informatics Circle of Research Excellence (*i*CORE), the Natural Science and Engineering Research Council of Canada (NSERC) and the Mary Louise Imrie Graduate Student Award at University of Alberta. Their support made my graduate studies at the University of Alberta possible.



# Contents

<b>1</b>	<b>Introduction</b>	<b>1</b>
1.1	Background and Motivation . . . . .	1
1.1.1	Cochannel Interference (CCI) . . . . .	2
1.1.2	Fading . . . . .	3
1.1.3	Diversity Combining Schemes . . . . .	9
1.1.4	Spread Spectrum (SS) and Code Division Multiple Access (CDMA) Systems . . . . .	13
1.1.5	Interference Mitigation . . . . .	16
1.2	Thesis Outline and Contributions . . . . .	18
<b>2</b>	<b>Interference Whitening Receivers for Micro-Cellular Systems</b>	<b>21</b>
2.1	Introduction . . . . .	21
2.2	System Model . . . . .	24
2.3	Whitening Matched Filter Receivers . . . . .	29
2.3.1	Bandlimited Pulse-Shaping . . . . .	30
2.3.2	NRZ Pulse-Shaping . . . . .	34
2.4	Conventional Matched Filter and Transversal Filter Receiver . . . . .	35

2.5	Correlating Receiver Structure . . . . .	38
2.6	Fractionally Spaced Correlator and Transversal Filter Receivers . . .	40
2.7	Numerical Results and Discussion . . . . .	44
2.7.1	Bandlimited Pulse-Shaping . . . . .	44
2.7.2	NRZ Pulse-Shaping . . . . .	63
2.8	Summary . . . . .	65
<b>3</b>	<b>Performance Analysis of Bandlimited DS-CDMA Systems in Nak-</b>	
	<b>agami Fading Channels</b>	<b>67</b>
3.1	Introduction . . . . .	67
3.2	System and Channel Model . . . . .	70
3.3	BER Analysis Using Gaussian Approximations . . . . .	72
3.3.1	Characteristic Function Improved Gaussian	
	Approximation (CFIGA) . . . . .	72
3.3.2	Standard Gaussian Approximation (SGA) . . . . .	75
3.3.3	Holtzman's Simplified Improved Gaussian	
	Approximation (HSIGA) . . . . .	76
3.3.4	Improved Holtzman's Gaussian Approximation (IHGA) . . . .	78
3.4	Exact BER Analysis Using Characteristic	
	Function Method . . . . .	79
3.5	Numerical Results and Discussion . . . . .	81
3.6	Summary . . . . .	86
<b>4</b>	<b>Performance Analysis of Bandlimited DS-CDMA Systems with Space</b>	
	<b>Diversity Receivers in Nakagami Fading Channels</b>	<b>88</b>
4.1	Introduction . . . . .	88

4.2	System and Channel Model . . . . .	91
4.3	Performance of Maximal Ratio Combining (MRC) . . . . .	92
4.4	Performance of Equal Gain Combining (EGC) . . . . .	95
4.5	Performance of Selection Combining (SC) . . . . .	97
4.6	Numerical Results and Discussion . . . . .	99
4.7	Summary . . . . .	103
<b>5</b>	<b>Interference Whitening Receivers for Bandlimited DS-CDMA Sys-</b> <b>tems in Nakagami Fading Channels</b>	<b>106</b>
5.1	Introduction . . . . .	106
5.2	System and Channel Model . . . . .	108
5.3	Performance Analysis of Whitening Matched Filter Receiver Structure . . . . .	112
5.4	Numerical Results and Discussion . . . . .	114
5.5	Summary . . . . .	117
<b>6</b>	<b>Performance Analysis of Space Diversity Receivers in Cochannel</b> <b>Interference and Fading Channels</b>	<b>118</b>
6.1	Introduction . . . . .	118
6.2	System and Channel Model . . . . .	122
6.3	BER Analysis of BPSK and QPSK in CCI and Fading with NRZ Pulse- Shaping . . . . .	123
6.3.1	BPSK Analysis . . . . .	124
6.3.2	QPSK Analysis . . . . .	125
6.3.3	BER Analysis Using Gaussian Approximation . . . . .	127

6.4	BER Analysis of Bandlimited BPSK with EGC and SC Diversity in CCI and Nakagami Fading . . . . .	127
6.4.1	Equal Gain Combining (EGC) . . . . .	127
6.4.2	Selection Combining (SC) . . . . .	130
6.5	Outage and BER Analysis of Bandlimited BPSK with MRC Diversity in CCI and Fading . . . . .	131
6.5.1	Outage Probability Analysis . . . . .	131
6.5.2	BER Analysis . . . . .	133
6.6	Numerical Results and Discussion . . . . .	133
6.7	Summary . . . . .	142
<b>7</b>	<b>Precise Outage Analysis of SC Diversity and SWC Diversity in Micro-cellular Systems with CCI</b>	<b>143</b>
7.1	Introduction . . . . .	143
7.2	System Model . . . . .	147
7.3	Selection Diversity . . . . .	148
7.3.1	Maximum Desired Signal Power Selection . . . . .	149
7.3.2	Maximum Signal-to-Interference Power Ratio (SIR) Selection . . . . .	150
7.3.3	Maximum Output Power Selection . . . . .	151
7.4	Switched Diversity . . . . .	153
7.4.1	Desired Signal Power Switching . . . . .	154
7.4.2	Signal-to-Interference Power Ratio (SIR) Switching . . . . .	156
7.4.3	Total Branch Power Switching . . . . .	158
7.5	Numerical Results and Discussion . . . . .	159

7.6 Summary . . . . .	171
<b>8 Conclusions and Suggestions for Future Work</b>	<b>172</b>
8.1 Conclusions . . . . .	172
8.2 Suggestions for Future Work . . . . .	176
<b>References</b>	<b>179</b>
<b>Appendix A</b>	<b>198</b>
<b>Appendix B</b>	<b>200</b>
<b>Appendix C</b>	<b>202</b>
<b>Appendix D</b>	<b>204</b>

# List of Figures

1.1	The seven cell cluster layout illustrating frequency reuse [1]. . . . .	3
1.2	Small-scale fading superimposed on large scale fading. . . . .	4
1.3	Small-scale fading. . . . .	5
1.4	Nakagami fading amplitude probability density function for different fading parameters, $m$ and $\Omega = 1$ . . . . .	8
2.1	The desired user receiver with whitening matched filter and MMSE equalizer. . . . .	29
2.2	The desired user receiver with transversal filter and MMSE equalizer.	35
2.3	The desired user receiver with correlator. . . . .	38
2.4	The desired user fractional correlator receiver with transversal filter and MMSE equalizer. . . . .	41
2.5	Effective pulse shape of the WMF for SNR= 0 dB and SIR = 10 dB.	46
2.6	Effective pulse shape of the WMF for SNR= 10 dB and SIR = 10 dB.	47
2.7	Effective pulse shape of the WMF for SNR= 20 dB and SIR = 10 dB.	48
2.8	Effective pulse shape of the WMF for SNR= 40 dB and SIR = 10 dB.	49
2.9	Performance of continuous time WMF with SRC and BTD pulse-shaping, no fading for the desired user, SIR = 10 dB , $T/4$ spaced MMSE equalizer with 41 taps, $K = 9$ and synchronous CCI. . . . .	50

2.10	Performance of continuous time WMF with SRC and BTD pulse-shaping, $m_s = 8$ for the desired user, SIR = 10 dB, $T/4$ spaced MMSE equalizer with 41 taps, $K = 9$ and synchronous CCI . . . . .	51
2.11	Performance of continuous time WMF with SRC and BTD pulse-shaping, Rayleigh fading for the desired user, SIR = 10 dB and $T/4$ spaced MMSE equalizer with 41 taps, $K = 9$ and synchronous CCI. .	52
2.12	Performance of continuous time WMF with SRC and BTD pulse-shaping, $m_s = 8$ for the desired user, SIR = 10 dB , $T/4$ spaced MMSE equalizer with 41 taps and asynchronous CCI. . . . .	53
2.13	Performance of continuous time WMF with SRC and BTD pulse-shaping, Rayleigh fading for the desired user, SIR = 10 dB , $T/4$ spaced MMSE equalizer with 41 taps, $K = 9$ and asynchronous CCI. .	54
2.14	Performance of transversal filter receiver ( $K_e = 4, N_q = 4$ ) with SRC and BTD pulse-shaping, $m_s = 8$ for the desired user, SIR = 10 dB, $K = 9$ and synchronous CCI. . . . .	55
2.15	Performance with rectangular pulse-shaping, no fading for the desired user, SIR = 10 dB, $K = 6$ and $T/4$ spaced MMSE equalizer with 41 taps	56
2.16	Performance with rectangular pulse-shaping, $m_s = 8$ for the desired user, SIR = 10 dB, $K = 6$ and $T/4$ spaced MMSE equalizer with 41 taps. . . . .	57
2.17	Performance with rectangular pulse-shaping, Rayleigh fading for the desired user, SIR = 10 dB, $K = 6$ and $T/4$ spaced MMSE equalizer with 41 taps. . . . .	58
2.18	The correlating waveform for finite observation interval $[0, T]$ , $K = 6$ and SIR = 10 dB. . . . .	59

2.19	The correlating waveform for finite observation interval $[0, T]$ , $K = 6$ and $SNR = 15$ dB. . . . .	60
2.20	Performance of fractional correlator ( $n_q = 4$ ) and transversal filter ( $K_e = 6$ ) receiver, $m_s = 8$ , $SIR = 10$ dB, $K = 6$ and $T/4$ spaced linear MMSE equalizer with 41 taps. . . . .	61
3.1	The performance of a bandlimited DS/CDMA system in Nakagami fading ( $m = 5$ ) with random spreading ( $N = 64$ ) and $SNR = 10$ dB. . . . .	82
3.2	The performance of a bandlimited DS/CDMA system in Nakagami fading ( $m = 5$ ) with random spreading ( $N = 64$ ) and $K = 10$ . . . . .	83
3.3	The performance of bandlimited DS/CDMA system using a Gold sequence ( $N = 31$ ) for the desired user and random sequences for the interferers in Nakagami fading ( $m = 5$ ) with $SNR = 10$ dB. . . . .	84
3.4	The performance of bandlimited DS/CDMA system using a Gold sequence ( $N = 31$ ) for the desired user and random sequences for the interferers in Nakagami fading ( $m = 5$ ) with $K = 10$ . . . . .	85
4.1	The BER performance of a bandlimited DS-CDMA system estimated using the SGA for MRC, EGC and SC diversity in Nakagami fading ( $m = 2$ ) with random spreading ( $N = 64$ ) and $K = 10$ . . . . .	100
4.2	The BER performance of a bandlimited DS-CDMA system estimated using the SGA for MRC, EGC and SC diversity in Nakagami fading ( $m = 2$ ) with random spreading ( $N = 64$ ) and $SNR = 10$ dB. . . . .	101
4.3	The BER performance of a bandlimited DS-CDMA system estimated using the SGA for MRC, EGC and SC diversity in Nakagami fading ( $m = 2$ ), with random spreading ( $N = 64$ ) and $SNR = 10$ dB. . . . .	102



4.4	The BER performance of a bandlimited DS-CDMA system estimated using the IGA for EGC and SC diversity in Nakagami fading ( $m = 2$ ) with random spreading ( $N = 64$ ) and $K = 15$ . . . . .	104
4.5	The BER performance of a bandlimited DS-CDMA system estimated using the IGA for EGC and SC diversity in Nakagami fading ( $m = 2$ ) with random spreading ( $N = 64$ ) and $SNR = 5$ dB. . . . .	105
5.1	The interference whitening receiver structure for the DS-CDMA system.	109
5.2	The performance of the whitening matched filter with MMSE equalizer receiver for a bandlimited DS/CDMA system in Nakagami fading ( $m = 8$ ) with Gold/random spreading for desired/interfering users ( $N = 31$ ) and $K = 10$ . . . . .	115
5.3	The performance of the whitening matched filter receiver for a bandlimited DS/CDMA system in Nakagami fading ( $m = 8$ ) with Gold/random spreading for desired/interfering users ( $N = 31$ ) and $SNR = 10$ dB. .	116
6.1	The performance of the BPSK system with the Nakagami/Nakagami model, for $m_0 = 8$ , $m_i = 5$ , and $SIR = 10$ dB. . . . .	135
6.2	The performance of the QPSK system with the Nakagami/Rayleigh model, for $m_0 = 8$ , and $SIR = 10$ dB. . . . .	136
6.3	The performance of the bandlimited BPSK system with EGC and SC in Nakagami fading ( $m = 5$ ), with CCI, $K = 6$ , and $SIR = 5$ dB. . . .	137
6.4	The performance of the bandlimited BPSK system with EGC and SC in Rayleigh fading ( $m = 1$ ), with CCI, $K = 6$ , and $SIR = 10$ dB. . . .	138

6.5	The outage performance of the bandlimited BPSK system with MRC in CCI with $m = 5$ , $K = 6$ , and average SIR=5 dB. In the case of unequal interferer powers, the normalized power distribution [0.05, 0.1, 0.15, 0.22, 0.23, 0.25] is assumed for $K = 6$ . . . . .	139
6.6	The outage performance of the bandlimited BPSK system with MRC in CCI with $m = 5$ , $L = 2$ , and average SIR=5 dB. In the case of unequal interferer powers, the normalized power distributions [0.1, 0.9] and [0.05, 0.1, 0.15, 0.22, 0.23, 0.25] are assumed for $K = 2$ and $K = 6$ , respectively. . . . .	140
6.7	The BER performance of the bandlimited BPSK system with MRC in CCI with $m = 5$ , $K = 6$ , and average SIR=2 dB. . . . .	141
7.1	The outage performance of selection diversity with a maximum desired power criterion for average SIR=5 dB. . . . .	160
7.2	The outage performance of selection diversity with a maximum SIR criterion for average SIR=5 dB. . . . .	161
7.3	The outage performance of selection diversity with a maximum output power criterion for average SIR=5 dB. . . . .	162
7.4	Outage performance comparison of selection diversity with maximum desired power, SIR and output power selection criteria for average SIR=5 dB and SRC pulse shape. . . . .	164
7.5	Outage performance comparison of selection diversity with maximum desired power, SIR and output power selection criteria for average SIR=5 dB and BTD pulse shape. . . . .	165
7.6	The outage performance of switched diversity with desired power switching criterion for average SIR=5 dB. . . . .	166

7.7	The optimum switching threshold for switched diversity with desired power switching criterion for average SIR=5 dB. . . . .	167
7.8	The outage performance of switched diversity with SIR switching criterion for average SIR=5 dB. . . . .	168
7.9	The outage performance of switched diversity with total output power switching criterion for average SIR=5 dB. . . . .	169
7.10	The optimum switching threshold for switched diversity with total output power switching criterion for average SIR=5 dB. . . . .	170

# Acronyms

Acronyms	Definition
AWGN	Additive white Gaussian noise
BER	Bit error rate
BPSK	Binary phase shift keying
BTD	Beaulieu-Tan-Damen (pulse)
CCI	Cochannel interference
CDF	Cumulative density function
CDMA	Code division multiple access
CF	Characteristic function
CLT	Central limit theorem
DS-CDMA	Direct-sequence code division multiple access
EGC	Equal gain combining
FDMA	Frequency division multiple access
HSIGA	Holtzman's simplified improved Gaussian approximation
IGA	Improved Gaussian approximation
iid	Independent identically distributed
ISI	Intersymbol interference
LOS	Line-of-sight

MA	Multiple access
MAI	Multiple access interference
MC	Monte Carlo (simulation)
MF	Matched filter
MGF	Moment generating function
ML	Maximum-likelihood
MMSE	Minimum mean square error
MRC	Maximal ratio combining
NRZ	Nonreturn-to-zero
PDF	Probability density function
PN	Pseudo-noise
PSD	Power spectral density
PSK	Phase shift keying
QPSK	Quadrature phase shift keying
RV	Random variable
SC	Selection combining
SGA	Standard Gaussian approximation
SIR	Signal-to-interference ratio
SNIR	Signal-to-noise plus interference ratio
SNR	Signal-to-noise ratio
SRC	Spectrum raised-cosine
SS	Spread spectrum
SWC	Switched combining
TDMA	Time division multiple access
WMF	Whitening matched filter

wrt

With respect to

# List of Symbols

Symbol	Definition
$A(e^{j\omega})$	Transfer function of transversal filter
$a[l]$	Desired user's $l$ -th transmitted symbol $\in [+1, -1]$
$b_i[l]$	$i$ -th interfering user's $l$ -th transmitted symbol $\in [+1, -1]$
$\mathbf{C}$	Tap coefficients of MMSE equalizer
$e$	Base of natural logarithm
$\mathbb{E}[X]$	Expectation of RV $X$
$\text{erf}(x)$	Gaussian error function
${}_1\mathbf{F}_1(\cdot)$	Confluent hypergeometric function
${}_2\mathbf{F}_1(\cdot)$	Gauss hypergeometric function
${}_p\mathbf{F}_q(\cdot)$	Generalized hypergeometric function
$F_X(x)$	Cumulative distribution function (CDF) of RV $X$
$f_c$	Carrier frequency
$f_X(x)$	Probability density function (PDF) of RV $X$
$G$	Decision statistic
$g(t)$	Impulse response of cascade of transmitter and receiver filters
$g_T(\cdot)$	Impulse response of transmitter filter
$H(\omega)$	Transfer function of receiver or transmitter filters

$I(t)$	Interference component
$I_i(t)$	$i$ -th user CCI component
$\mathbf{I}$	Identity matrix
$\mathbf{I}_0(\cdot)$	The 0-th order modified Bessel function of the first kind
$I_c$	Interchip interference
$I_s$	Intersymbol interference
$\mathbf{I}_x(a, b)$	Normalized incomplete beta function
$K$	Number of interferers
$2K_e + 1$	Number of taps of MME equalizer
$K_R$	Rice factor
$K_n(\cdot)$	Autocorrelation function of interference-plus-noise
$2K_t + 1$	Number of taps of transversal filter
$L$	Number of diversity branches
$\mathcal{M}$	Multiple access interference
$\mathcal{M}_i$	$i$ -th user multiple access interference
$m$	Nakagami fading parameter
$m_i$	$i$ -th user Nakagami fading parameter
$N$	Processing gain
$N_e$	Number of tap spacings
$N_0/2$	Power Spectral Density of the AWGN
$n(t)$	Background AWGN
$n_0$	Background noise component in decision statistic
$N_q$	Number of fractional spacings, $N_q = T/T_q$
$P_k$	$k$ -th user transmitted power
$P_e$	Average bit error rate



$P_O$	Outage probability
$P_s$	Desired user transmitted power
$\Pr\{S\}$	Probability of event $S$
$\mathbf{Q}(x)$	Gaussian tail probability function given by $\mathbf{Q}(x) = \frac{1}{\sqrt{2\pi}} \int_x^\infty e^{-\frac{y^2}{2}} dy$
$q(\cdot)$	Time domain effective pulse shape
$R_i$	$i$ -th user fading gain
$R_{i,j}$	$i$ -th user $j$ -th branch fading gain
$R_E$	Sum of the fading gains $(\sum_{j=1}^L R_{0,j})$
$R_M$	Sum of the squared fading gains $\sum_{j=1}^L R_{0,j}^2$
$\mathbf{R}_v$	Correlation matrix
$S_n(f)$	Power Spectral Density of $n$
$S_d(t)$	Desired user transmitted signal
$s_d(t)$	Desired user baseband transmitted signal
$S_i(t)$	$i$ -user transmitted signal
$s_i(t)$	$i$ -user baseband transmitted signal
$T$	Bit time duration
$T_c$	Chip time duration
$T_q$	Fractional symbol time
$T_0$	Parameter that controls the accuracy of Fourier series method
$\mathbf{U}[a, b]$	Uniformly distributed on $[a, b]$
$\mathbf{v}$	Sampled interference-plus-noise vector
$\text{VAR}[X]$	Variance of RV $X$
$\mathbf{x}$	Sampled effective pulse shape vector
$Z$	Decision statistic
$\alpha$	Tap coefficient vector of the transversal filter

$\beta$	Excess bandwidth
$\mathbf{\Gamma}$	Covariance matrix
$\Gamma(\cdot)$	Gamma function
$\Gamma(\cdot, \cdot)$	Upper incomplete gamma function
$\gamma(\cdot, \cdot)$	Lower incomplete gamma function
$\delta(\cdot)$	Dirac delta function
$\theta_s$	Desired user phase
$\theta_i$	$i$ -th user phase
$\xi$	Sampled effective pulse shape
$\sigma_X^2$	Variance of RV $X$
$\tau_k$	$k$ -th user time delay
$\phi(\cdot)$	Autocorrelation function of rectangular pulse
$\phi_k$	$k$ -th user phase offset
$\phi_{k,j}$	$k$ -th user $j$ -th branch phase offset
$\Phi_X(\omega)$	Characteristic function of RV $X$
$\Phi_{\mathbf{J}}$	Covariance matrix of vector $\mathbf{J}$
$\omega_c$	Radian carrier frequency
$\omega_0$	Sampling frequency ( $\frac{2\pi}{T_0}$ )
$\Omega$	Second moment of fading amplitude
$\Omega_i$	Second moment of $i$ -th user fading amplitude

# Chapter 1

## Introduction

### 1.1 Background and Motivation

The wireless communication sector is one of the fastest growing industries in all of electrical engineering. Although, Guglielmo Marconi demonstrated the first radio technology in 1897, its growth was very slow until the last two decades. The growth of two way wireless communication was fueled by efficient digital and radio frequency fabrication, very large system integration techniques and miniaturization technologies. Broadly speaking, wireless communication includes cellular telephony, satellite communication, point-to-point radio links, paging, wireless local area networks (Wi-Fi), etc. Cellular telephony provides the major portion of the revenue in the wireless communication sector. The number of cellular phone customers has grown from 10 million in the early 1990's to approximately 700 million in 2002 and is expected to increase to more than two billion around year 2006-2007 [1], [2].

In commercial cellular communication systems, frequency division multiple access (FDMA), time division multiple access (TDMA), and code division multiple access

(CDMA) are the major access techniques. FDMA assigns individual frequency slots for each user while TDMA assigns individual time slots. Thus, FDMA and TDMA provide orthogonal transmission in frequency or time. The widely accepted GSM system is based on TDMA techniques. The GSM system has the largest number of subscribers, more than any other cellular standard. The CDMA system is based on a spread spectrum technique. Spread spectrum techniques have been very successfully used for military communications for decades. Recently CDMA, has taken a significant role in cellular and personal communication networks, mobile satellite networks and wireless local area networks [3]. The CDMA has been used as the main access method for third generation cellular standards.

### **1.1.1 Cochannel Interference (CCI)**

Unlike wire-line transmission, wireless transmission has many limitations. As all the wireless services share the frequency spectrum, it becomes a very precious resource and its availability is limited. To overcome this, in cellular telephone systems the cell concept and frequency reuse were introduced [1], [4]. Due to frequency reuse, there will be cochannel interference to a particular user from subscribers using the same frequency in surrounding cells. Fig. 1.1 illustrates the frequency reuse concept in a seven cell cluster. The cells labeled with the same letters use the same group of frequency channels and they are called cochannel cells. For a particular user the signals of the users operating on the the same carrier frequency in cochannel cells are interference and this is called cochannel interference (CCI). As the demand for wireless channels increases the cell sizes are reduced to increase the capacity leading to micro-cellular systems. Many research studies have shown that micro-cellular systems are cochannel interference limited and not background noise limited systems [4].

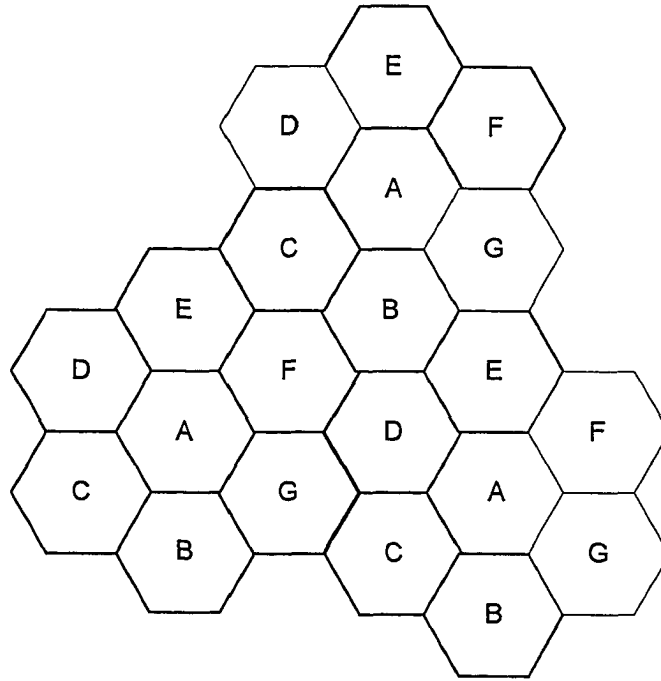


Fig. 1.1. The seven cell cluster layout illustrating frequency reuse [1].

### 1.1.2 Fading

When a signal is transmitted through a wireless channel, it is subject to attenuation, phase rotation, etc. The transmitted signal travels through the medium as a radio wave. Due to the irregularities of the medium, typical wave propagation phenomena such as diffraction, scattering, and reflection, diffuse the transmitted radio wave into a continuum of plane waves with different amplitudes and phases. At the receiver antenna, they are added constructively or destructively causing multipath fading [5], [6]. The fading captures the rapid amplitude and phase fluctuations of a radio signal over a small window of time or distance or wavelength. There are two types of fading effects characterizing wireless communications. They are large-scale and small-scale

fading. The large-scale fading represents the average signal power attenuation or the path loss due to transmission over large areas. This phenomenon is caused by terrain contours, such as: hills, forest, high-rise-buildings etc. between a transmitter and receiver. It is normally described as  $n$ -th law path loss and lognormal shadowing.

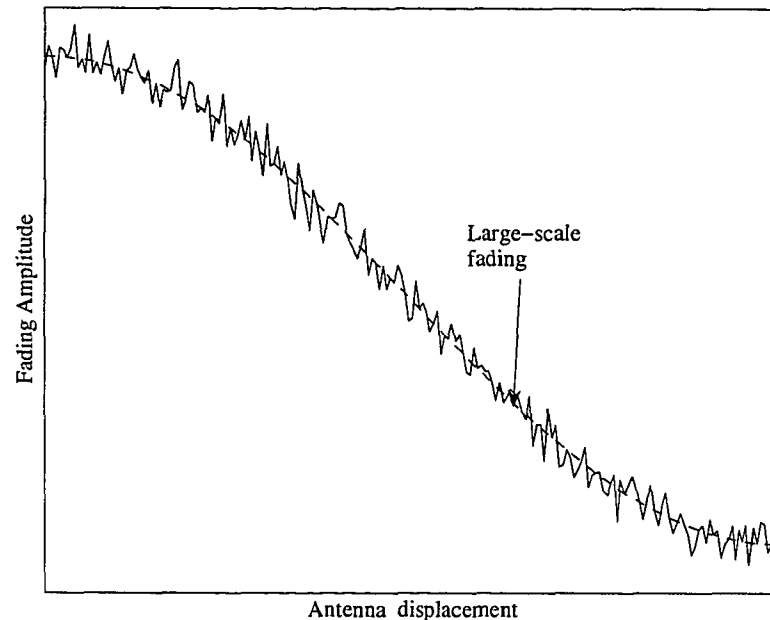


Fig. 1.2. Small-scale fading superimposed on large scale fading.

Small-scale fading refers to the dramatic change in the amplitude and phase of the received signal due to the changes in the positioning of a transmitter and receiver. Two types of phenomena are used in the characterization of small-scale fading. They are time dispersion of the signal and variation of the channel in time.

In time dispersion of the signals, if the delay spread of the channel is greater than the symbol duration then the channel is called a frequency-selective channel, otherwise, it is called a frequency-nonselective channel or flat fading channel. The reciprocal of the delay spread is called the coherence bandwidth of the channel. It represents a frequency range over which signal's frequency components have strong amplitude correlation. In the frequency domain, if the coherence bandwidth of the

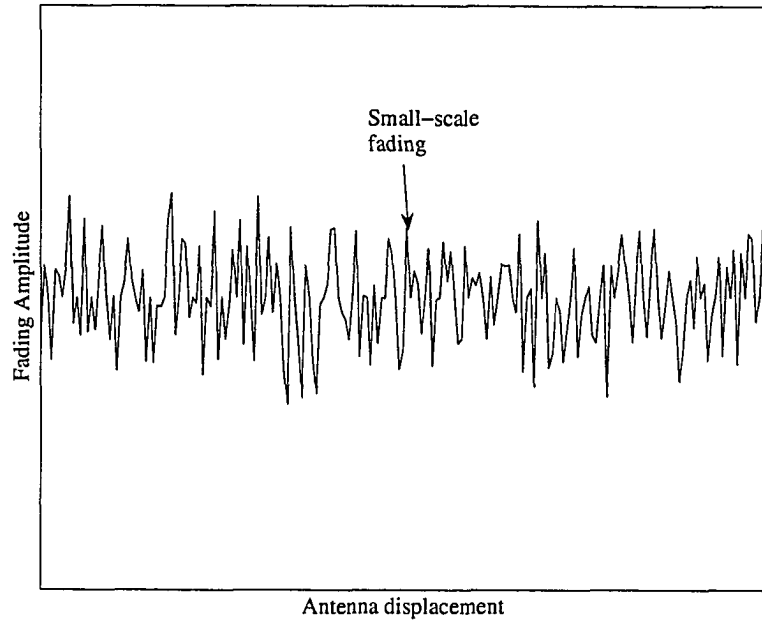


Fig. 1.3. Small-scale fading.

channel is greater than the bandwidth of the signal, then the channel is called a frequency-nonselective channel, otherwise, it is called a frequency-selective channel.

In time variation of the channel phenomenon, if the channel variation is faster than the symbol rate, the channel is called a fast fading channel, otherwise, it is a slow fading channel. In other words, if the coherence time of the channel is less than the symbol time duration, the channel is a fast fading channel, otherwise it is a slow fading channel. The coherence time is described as the expected time duration over which the channel response to a sinusoid is invariant. The reciprocal of the coherence time is called Doppler spread. While the delay spread describes the time dispersion of the channel, Doppler spread manifests the frequency dispersion of the channel. As the delay spread and Doppler spread are two independent phenomenon, we have four types of fading situations. In this thesis we only consider flat (frequency-nonselective) slow fading channels.

Using complex notation, a transmitted signal,  $s(t)$  is written as [7]

$$s(t) = \mathbb{Re}[g(t) e^{j2\pi f_c t}] \quad (1.1)$$

where  $\mathbb{Re}[x]$  is the real part of  $x$ ,  $f_c$  is the carrier frequency and  $g(t)$  is the desired baseband signal. Assuming antenna is moving and there are multiple scatter path each associated with a time variant propagation delay  $\tau_n(t)$  and time variant fading amplitude  $\alpha_n(t)$ . Neglecting the additive noise, the received signal,  $r(t)$  is

$$r(t) = \sum_n \alpha_n(t) s(t - \tau_n(t)). \quad (1.2)$$

Substituting (1.1) in (1.2), it becomes

$$r(t) = \sum_n \alpha_n(t) e^{-j2\pi f_c \tau_n(t)} g(t - \tau_n(t)) e^{j2\pi f_c t}. \quad (1.3)$$

Then, the equivalent baseband signal is given by

$$z(t) = \sum_n \alpha_n(t) e^{-j2\pi f_c \tau_n(t)} g(t - \tau_n(t)). \quad (1.4)$$

For the case of an unmodulated carrier, the received signal becomes

$$z(t) = \sum_n \alpha_n(t) e^{-j\theta_n(t)} \quad (1.5)$$

where the phase,  $\theta_n(t) = 2\pi f_c \tau_n(t)$ . The phase,  $\theta_n(t)$  may change significantly with the change of propagation delay. Thus, the phasors in (1.5) may add up constructively or destructively. Then eq. (1.5) can be compactly written as

$$z(t) = \alpha(t) e^{-j\theta(t)} \quad (1.6)$$

where  $\alpha(t)$  is the resultant fading amplitude and  $\theta(t)$  is the resultant phase. Eq. (1.5) can also be written using two orthogonal components as

$$z(t) = \sum_n x_n(t) + jy_n(t) \quad (1.7)$$



where  $x_n(t) = \alpha_n(t) \cos(\theta_n(t))$  and  $y_n(t) = \alpha_n(t) \sin(\theta_n(t))$ . Assuming the fading process is a widesense stationary (WSS) process, and using a central limit theorem (CLT), when  $n$  is large  $x = \sum_n x_n$  and  $y = \sum_n y_n$  are going to have Gaussian probability density function (PDF). If  $x$  and  $y$  are independent and have zero mean (in other words, there is no line-of-sight (LOS) path component), the PDF of the resultant fading gain  $\alpha$  is [4]

$$f_\alpha(r) = \frac{2r}{\Omega} \exp \left[ -\frac{r^2}{\Omega} \right], \quad r > 0 \quad (1.8)$$

which is called the Rayleigh PDF and  $\mathbb{E}[\alpha^2] = \Omega$ . As  $x$  and  $y$  are independent random variables, the resultant phase is uniformly distributed and resultant fading gain and resultant phase are mutually independent. If there is a LOS path the PDF is called Rice PDF and is given by [4]

$$f_\alpha(r) = \frac{2r(K_R + 1)}{\Omega} \exp \left\{ -K_R - \frac{(K_R + 1)r^2}{\Omega} \right\} I_0 \left( 2r \sqrt{\frac{K_R(K_R + 1)}{\Omega}} \right), \quad r > 0 \quad (1.9)$$

where  $I_0(\cdot)$  is the modified Bessel function of the zeroth order and first kind,  $K_R$  is the Rice factor defined as

$$K_R = \frac{\text{Specular power}}{\text{Scattered Power}} = \frac{s^2}{\Omega_p} \quad (1.10)$$

and  $\mathbb{E}[\alpha^2] = \Omega = s^2 + \Omega_p$ . When  $K_R$  is zero there is no specular component and, thus, the fading PDF becomes the Rayleigh PDF, and when  $K_R$  approaches infinity the channel does not exhibit any fading. The resultant phase distribution is given in [8] and the fading gain and the phase are not independent.

In early 1940's, Nakagami introduced a distribution for fading gain now called the Nakagami distribution [9]. It was shown to have a closer match to empirical data than other fading distributions. The Nakagami fading gain PDF is written as [4]

$$f_\alpha(r) = \frac{2}{\Gamma(m)} \left( \frac{m}{\Omega} \right)^m r^{2m-1} \exp \left\{ -\frac{m}{\Omega} r^2 \right\}, \quad r > 0, \quad m \geq \frac{1}{2} \quad (1.11)$$

where  $\mathbb{E}[\alpha^2] = \Omega$  and  $m$  is the Nakagami fading parameter taking values from 0.5 to infinity. When  $m = 1$ , the Nakagami PDF becomes the Rayleigh PDF, when  $m = \frac{1}{2}$  it becomes a one sided Gaussian PDF and when  $m \rightarrow \infty$ , it becomes an impulse function (no fading). Thus, the severity of the fading reduces with the fading parameter. For different values of Nakagami fading parameter the Nakagami PDF's are sketched in Fig. 1.4. The distribution of the resultant phase is still an open

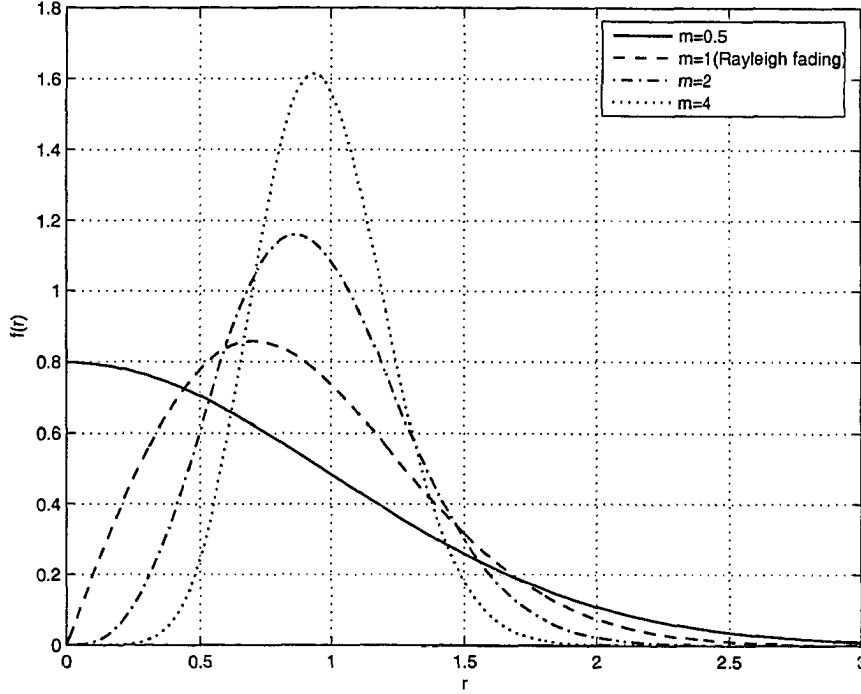


Fig. 1.4. Nakagami fading amplitude probability density function for different fading parameters,  $m$  and  $\Omega = 1$ .

problem when the fading amplitude is Nakagami distributed. The Rice distribution is sometimes closely approximated using Nakagami distribution, and the mapping is given by [6]

$$m = \frac{(1 + K_R)^2}{1 + 2K_R}, \quad K_R > 0 \quad (1.12)$$

$$K_R = \frac{\sqrt{m^2 - m}}{m - \sqrt{m^2 - m}}, \quad m > 1. \quad (1.13)$$

As the Nakagami distribution contains only simple functions, it often leads to convenient closed-form solutions or simple analytical expressions in wireless communication systems analysis.

### 1.1.3 Diversity Combining Schemes

The cochannel interference and fading are major factors affecting the capacity of cellular radio systems. Diversity schemes combat fading and cochannel interference simultaneously. During the past few decades, an enormous amount of research has been done on them [6]. To understand the diversity mechanism, assume  $p$  is the probability of a channel experiencing a deep fade. If there are  $L$  independent diversity branches, the probability of all channels experiencing a deep fade becomes  $p^L$ . Thus, the probability of making error is reduced. Diversity can be achieved in space, angle, multipath, frequency, time, polarization and field [4].

Frequency diversity is obtained by transmitting the same information over multiple ( $\geq 2$ ) carrier frequencies at least separated by the coherence bandwidth of the channel. Time diversity is achieved by transmitting the same information over different time slots separated by at least the coherence time of the channel. Multipath diversity is achieved when the fading is frequency selective. When the signal bandwidth is much greater than the coherence bandwidth of the channel the signal will resolve the multipath components [7]. Thus, the receiver is provided with several independent fading paths. If the delay spread is  $T_m$  and the signal bandwidth  $W$ , there are  $T_m W$  resolvable signal components. The use of wideband signals is a way of obtaining multipath diversity. The optimum receiver for this multipath diversity is called a RAKE receiver and it is widely used in DS-CDMA systems. Angle diversity is implemented using directional antennas and it is also called directional diversity.

The fact that the electromagnetic waves can be transmitted as independent vertically and horizontally polarized waves, is exploited to obtain polarization diversity. Field diversity is based on the fact that the electric and magnetic waves undergo independent fading. In practice, antenna design for field and polarization diversity is much more difficult. Space diversity or antenna diversity employs multiple antennas. Conventionally, a single transmit antenna and multiple receive antennas have been considered. Recently, diversity systems with multiple transmit and receiver antennae drew much attention of researchers due to their high data rate and capacity capabilities [4]. Theoretically, the antennas should be separated by at least a half the wavelength to obtain uncorrelated diversity branches. However, in practice the separation should be at least 10 wave lengths to obtain the independent fading. In this thesis, we only consider space diversity schemes with flat slow fading.

The signals that are received in the diversity branches can be combined in a number of ways. There is a trade-off between complexity and better performance. Widely used combining methods are selection combining (SC), switched combining (SWC), equal gain combining (EGC) and maximal ratio combining (MRC). If the combining is done after the detection process in each branch it is called post-detection combining. Normally post detection combining is performed in baseband. If the combining is performed before the detection process in the branches, it is called predetection combining and it is performed in RF. For the coherent receivers, postdetection and predetection combining schemes provide identical results [4], [6].

Lets assume, there are  $L$  independent diversity branches. Each channel undergoes frequency nonselective slow fading. The  $l$ -th branch lowpass BPSK received signal is written as

$$y_l(t) = \alpha_l e^{j\theta_l} s(t) + n_l(t), \quad l \in [1, \dots, L] \quad (1.14)$$

where  $s(t)$  is the desired signal,  $n_l(t)$  is the additive complex Gaussian noise,  $\alpha_l$  is the fading amplitude and  $\theta_l$  is the phase.

#### 1.1.3.1 Maximal Ratio Combining (MRC)

Regardless of the fading statistics, MRC is the optimum combining scheme for signal detection in the presence of additive white Gaussian noise (AWGN) only. It requires knowledge of the fading amplitudes and phases in all diversity branches. As it requires the phase information it is not feasible with noncoherent or differential detectors. In MRC, the matched filter outputs in diversity branches are multiplied by the corresponding complex conjugate of the fading channel gain,  $(\alpha_l e^{-j\theta_l})$  and then all of them are summed together to obtain the decision statistic. The multiplication is to compensate the phase rotation by the channel and weight the signal by a factor proportional to the fading amplitude. Thus, a strong branch signal is weighted by larger factor than a weaker branch signal. After matched filtering and weighting by the complex conjugate fading gain  $(\alpha_l e^{-j\theta_l})$  and combining, the decision statistic is written as

$$\begin{aligned} U &= \Re \left[ \sum_{l=1}^L \alpha_l^2 + \sum_{l=1}^L \alpha_l n_l \right] \\ &= \sum_{l=1}^L \alpha_l^2 + \sum_{l=1}^L \alpha_l n_{lc} \end{aligned} \quad (1.15)$$

where the desired symbol energy and the symbol duration are assumed unity,  $n_{lc}$  is the real part of the additive Gaussian noise component and  $L$  is the number of diversity branches.

### 1.1.3.2 Equal Gain Combining (EGC)

Predetection EGC is similar to MRC, the branches are cophased but they are not weighted by the fading gains. Thus, EGC has less complexity at the expense of performance. In practice, EGC is employed in systems with equal energy symbols such as MPSK [4]. Postdetection EGC is used in applications where the phase of the received signal cannot be obtained accurately [6]. In such situations, postdetection EGC is employed with noncoherent or differential detectors. In this thesis, only predetection EGC is considered.

If the received signal in (1.14) is cophased, passed through a matched filter and the branches are combined, the decision statistic becomes

$$\begin{aligned} U &= \Re \left[ \sum_{l=1}^L \alpha_l + \sum_{l=1}^L n_l \right] \\ &= \sum_{l=1}^L \alpha_l + \sum_{l=1}^L n_{lc}. \end{aligned} \tag{1.16}$$

### 1.1.3.3 Selection Combining (SC)

Unlike MRC and EGC, in selection combining only one diversity branch is selected to detect the signal depending on the selection criteria. Thus, SC provides inferior performance with less complexity. There are several selection criteria which have been studied in the literature [10], [11]. However, we consider only three selection criteria in this thesis namely, maximum SNR selection, maximum desired signal power selection and maximum output power selection. Among these schemes, the SNR selection scheme provides better performance with higher complexity. The maximum output power selection scheme is more practical to implement. The main drawback of SC in continuous transmission is that the channel parameters in all the branches should be estimated continuously. Moreover, if the channel parameters are estimated it is

better to use EGC or MRC to obtain better performance.

Suppose the  $j$ -th branch is selected in the received signal in (1.14). Then, after coherent detection, the decision statistic is given by

$$\begin{aligned} U &= \operatorname{Re} [\alpha_j + n_j] \\ &= \alpha_j + n_{jc} \end{aligned} \tag{1.17}$$

where the  $j$ -th branch is selected based on the selection criterion.

#### 1.1.3.4 Switched Combining (SWC)

Unlike SC, for SWC the channel parameters in all the branches do not need to be estimated continuously. There are different variants of SWC schemes in the literature [12]. In the SWC considered in this thesis, a switching metric of a particular branch is continuously compared with a predetermined threshold value. If the branch metric is greater than the threshold, the same branch is selected. Otherwise, the output is switched to other branches cyclically until a branch with metric greater than the threshold is found [13], [14]. If all the branch metrics are below the threshold, the output never settles to any branch. The switching metrics considered are desired signal power, signal-to-interference (SIR) power ratio, and total branch power.

#### 1.1.4 Spread Spectrum (SS) and Code Division Multiple Access (CDMA) Systems

Spread spectrum techniques have been employed by the military since World War II. In the last two decades, spread spectrum-based systems have been widely used in cellular and personal communication networks, mobile satellite networks, wireless local area networks, and global positioning systems, etc. Spread spectrum systems may

provide asynchronous data transmission, message privacy, signal hiding and position location within their repertoire. Basically, a spread spectrum system is one in which the transmitted signal is spread over a wide frequency band, in fact, much wider than the minimum bandwidth required to transmit the information being sent. There are some benefits in the signal spreading by means of a code sequence. The signal energy is diluted over the bandwidth while occupying a very large bandwidth. The amount of the power spectral density present at any point within the spread signal is very small. As a result, may be the signal below the noise floor of a conventional receiver and seems invisible in the spectrum, but it can be detected using a spread spectrum receiver. The receiver can reject strong undesired signals even if the undesired signal power is much higher than that of the desired spread spectrum signal. This is because the authorized spread spectrum receiver has a replica of the spreading sequence to despread the signal. The non-spread signals are then suppressed in the detection process. This property in SS systems provides a certain degree of immunity to intentional or unintentional jamming. The most commonly used techniques are direct sequence spread spectrum (DS-SS) and frequency hopping spread spectrum (FH-SS). The DS-SS can be viewed as the modulation of carrier by a digital code sequence whose bit rate is much higher than the information signal bandwidth. The FH-SS occurs when the carrier frequency is shifted in discrete increments according to a pattern dictated by a code sequence. The transmitted frequency jumps from frequency to frequency within a predetermined set determined by a code sequence. The SS systems have the capability of combating a limited amount of multipath fading. Frequency selective fading typically occurs at relatively narrow bandwidths of a wideband system. Thus, the spread signal provides a form of frequency diversity which compensates the faded frequencies by those, that do not experience the same fading. The effective frequency



of deep fades in a multipath channel which results from "echoes" of the same signal arriving at the SS receiver at slightly different times, can be largely reduced. The design of the spreading codes is the key to enhancing the robustness to unwanted signals. Moreover, a single receiver or group of receivers may be addressed by a reference code, compared with other users who have different codes. Thus a code sequence becomes a user's address. When the codes are properly chosen to have low cross correlation properties, minimum interference occurs between users. More than one signal can be unambiguously transmitted in the same bandwidth and at the same time; and selective addressing and code-division multiplexing are implemented by the coded modulation format. The multiple access capability that is achieved by the code-division is termed code division multiple access (CDMA). Direct-sequence code division multiple access (DS-CDMA) and Frequency-hopping code division multiple access (FH-CDMA) are the most commonly used techniques.

Particularly in mobile cellular communication, CDMA has been considered as an attractive alternative to the conventional FDMA and TDMA techniques for the following reasons. First, a large number of users may subscribe to such a system, with the system performance (error rate etc.) primarily dependent on the number of simultaneous users and the nature of the channel. The performance degrades as the number of active users increase and there are no blocked calls in the usual sense, although of course traffic will ultimately be limited by the available resources and the effective BER. Secondly, each user may transmit asynchronously and no scheduling of channel use is required. This enables easy access for new subscribers. However, the signals of the other active users are interference for a particular user. There are a number of disadvantages associated with the CDMA, the two most obvious of which are the problem of "self-jamming" and the related problem of the "near-far" effect.

The self-jamming arises to from the fact that in an asynchronous CDMA network, the spreading sequence of the different users are not orthogonal, and hence in the despreading of a given user's waveform, nonzero contributions to the user's receiver decision statistic arise from the transmissions of the other users in the network. The near-far problem refers to the fact that, signals closer to the receiver of interest are received with smaller attenuation than signals located further away. This means that power control techniques must be used in the cell of interest. Another concern in the CDMA is the smooth handover from one cell to the next requires acquisition by the mobile of the new cell before it relinquishes the old cell. The CDMA systems are self-interference limited. That is, in attempting to have many users communicate simultaneously, the mutual interference sets a limit on the number of simultaneous active users. To the extent that not every user in the network is always transmitting, the capacity of the system is increased. In the CDMA systems, if a given user stops transmitting, and no new user wants to access the channel at that particular instant of time, then all the remaining users on the channel experience less interference, i.e. voice activity levels influence the CDMA system performance.

### **1.1.5 Interference Mitigation**

The CCI and MAI are the prime factors which limit the capacity and performance of wireless communication systems. The conventional matched filter receiver does not take into account the existence of the CCI or MAI. It uses a single-user detection strategy in which each user is detected separately without regard for interferers. Significant capacity increment can theoretically be achieved, if the the negative effect that each user has on other users is cancelled. Instead of the users interfering with each other, they can all be used for their mutual benefit by joint detection.

This detection strategy is called multiuser detection. The important assumption in optimum multiuser detection is that the amount of information available about the desired user (timing offset, phase offset, etc.) at the receiver are also available for the interfering users as well. It is generally difficult to obtain and not practical for many systems. In 1986, Verdu [15] proposed and analyzed the optimum multiuser detector or the maximum-likelihood sequence detector for the CDMA. The optimum detection of a BPSK system was reported in [16], [17], [18] and is complex. The receiver complexity of the optimum maximum-likelihood detection increases exponentially with the number of users and is not suitable for practical systems. Therefore, over the last decade, most of the research has been focused on finding sub-optimal multiuser detectors [19], [20], [21], [22] and improved single-user detectors [23], [24] which are more feasible to implement. It is interesting to note that there is a strong similarity between the problem of MAI and CCI and that of intersymbol interference (ISI) [15]. Comprehensive treatments of optimum and sub-optimum detection of the CDMA can be found in [19] by Verdu, [25] by Duel-Hallen *et al.* and [26] by Moshavi. In this thesis, an improved single user receiver structure with whitening matched filter [27] and linear fractionally spaced minimum mean square error (MMSE) equalizer is considered to mitigate the cochannel interference in fading environments.

#### **1.1.5.1 Whitening Matched Filter (WMF) Receivers**

A whitening matched filter [28], [27], [29] was proposed for signal detection in colored Gaussian noise. It maximizes the signal-to-noise ratio (SNR) and provides the optimum performance in colored Gaussian noise. It consists of a filter which whitens the spectrum of the colored noise followed by a filter matched to the distorted signal output from the whitening filter. As the resultant transfer function does not satisfy

the Nyquist criterion, a WMF introduces ISI to the decision statistic in continuous transmission systems. When bandlimited pulse-shaping is employed the WMF implementation is feasible. However, when the time-limited pulse shapes are used the implementation is feasible only with reasonably long delay [27].

## 1.2 Thesis Outline and Contributions

There are six major chapters in this thesis. Each chapter contains one major contribution. The chapters are organized as follows.

In Chapter 2, several single-user interference whitening receiver structures to combat the CCI in micro-cellular fading environments are proposed. A Nakagami-Rayleigh desired/interfering user fading model is adopted for the micro-cellular environment [4]. The fading is assumed to be flat and slow. While maximizing the SNIR, the WMF introduces ISI in the decision statistic. A fractionally spaced linear MMSE equalizer is employed to suppress the ISI introduced by the WMF. Two Nyquist pulse shapings, namely, spectrum raised-cosine (SRC) and Beaulieu-Tan-Damen (BTD) pulses [30] and nonreturn-to-zero (NRZ) rectangular pulses are employed. The performance analysis is carried out using a characteristic function (CF) method and an approximate Fourier series method [31]. In some cases Monte Carlo computer simulation is used to obtain the BER performance. The performance of the proposed receivers is compared against that of conventional matched filter (MF) receivers. Our results show that the proposed receivers provide substantial performance gains.

In Chapter 3, we study the BER performance of a bandlimited binary DS-CDMA system in Nakagami fading channels. Slow flat fading is assumed and a single-user correlator receiver or a conventional MF receiver structure is considered. Two Nyquist

pulse shapes, SRC and BTD pulse shapes are employed. We consider several Gaussian approximation methods and an exact CF method for the analysis. A new computationally efficient method is introduced by incorporating the CF method into the improved Gaussian approximation (IGA) method [32] proposed by Morrow and Lehnert. In our proposed method, the computational complexity is substantially reduced and it does not depend on the number of users in the system. The accuracy of the Gaussian approximation methods is assessed using Monte Carlo computer simulation. An exact BER analysis using a CF method for systems with deterministic desired user spreading sequences and random interfering users' spreading sequences is also considered. The BER performance of the SRC and BTD pulse shapes are compared under identical system conditions.

In Chapter 4, we extend the work in Chapter 3 for space diversity receivers for bandlimited DS-CDMA systems. The combining schemes considered are MRC, EGC and SC. The IGA and standard Gaussian approximation (SGA) [33] of the MAI are considered using CF and approximate Fourier series methods for the performance analysis. The computational complexity of the BER expressions does not increase with diversity order or number of interferers. The SNR and capacity gains with the diversity order of the different combining schemes are compared.

In Chapter 5, the WMF receiver considered in Chapter 2 is considered for bandlimited DS-CDMA systems in Nakagami fading channels. Again a fractionally spaced linear MMSE chip equalizer is used to combat the ISI introduced by the WMF. We assume deterministic desired user spreading sequences and random spreading sequences for interfering users. The BER expressions are derived using the approximate Fourier series method.

In Chapter 6, performance analysis of narrowband communication systems in

fading and CCI is considered. An exact BER expression for a BPSK system with NRZ rectangular pulse shaping in Nakagami fading and CCI is derived using the CF method. It is computationally more efficient than other reported methods. The accuracy of the Gaussian approximation of the CCI is assessed. A QPSK system with a Nakagami/Rayleigh desired/interfering user fading model is also considered. Then, exact BER expressions for a bandlimited BPSK system with EGC and SC diversity receivers in Nakagami fading and CCI are derived. Two Nyquist pulse shapes, SRC and BTD pulse shapes are used. Again the CF method and the Fourier series methods are employed. The complexity of the BER expressions neither increases with diversity order nor number of interferers. An exact outage probability expression for a bandlimited BPSK system with MRC diversity in CCI and Nakagami/Rayleigh fading is derived. The outage performance of the BTD and SRC pulses are compared.

In Chapter 7, outage probability expressions for a bandlimited BPSK system with SC and SWC in CCI and Nakagami/Rayleigh fading model are derived. Interference limited systems are considered in the analysis. Three selection and switching criteria, namely, desired signal power, SIR and total output power are considered. Unlike previous results, the system model under investigation takes into account the pulse shaping and the random delays and phase offsets of the interfering users. The optimum switching thresholds for different switching criterions are formulated.

Chapter 8 provides our conclusions, summary of the major contributions and suggestions for future work.

# Chapter 2

## Interference Whitening Receivers for Micro-Cellular Systems

### 2.1 Introduction

The transmission environment places a fundamental limitation on the performance of wireless communication systems. There are two main source of degradation of performance. They are fading and CCI. In order to meet the capacity demand, the cell sizes are reduced, as a result in the micro-cellular environment the system performance is limited by cochannel interference rather than background noise [4]. Therefore, cochannel interference mitigation in fading environments is of considerable interest.

Few methods have been proposed to combat CCI in fading environments in the literature. Lo *et al.* [34] studied adaptive equalization to combat the CCI in interference limited systems. A fractionally spaced decision feedback equalizer was employed with least mean square (LMS) and recursive least square (RLS) algorithms. A QPSK

system with raised cosine pulse shaping in quasi-static frequency selective fading channels was considered. Training symbols were transmitted periodically to estimate the channel parameters. Recently, Lo and Letaief [35] also used adaptive equalization to combat the CCI and ISI. The maximum likelihood sequence estimation (MLSE) equalizer with RLS channel estimator was employed. Winters [36] proposed an optimum linear MMSE combining technique with space diversity reception to combat the CCI and fading. For the case of two antenna elements, direct matrix inversion was suggested as a means of updating the antenna weighting coefficients. A receiver structure equipped with space time filter and Viterbi equalizer was proposed by Liang *et al.* [37] to jointly combat the CCI and ISI in slow Rayleigh fading. A performance analysis of successive CCI cancellation using smart antenna systems was reported by Hazna *et al.* [38]. Closed-form expressions for outage probability and bit error rate were derived. Arslan *et al.* [39] proposed a successive CCI cancellation method for TDMA systems. There have been few reported works on optimal maximum-likelihood (ML) receivers for communication systems in the presence of CCI [40], [16], [17], [18]. In these works, fading environments are not considered and the complexity of the solution grows exponentially with the number of users. The ML sequence detection with Viterbi algorithm was employed to combat the CCI by Wales [41] for TDMA systems. In [23] and [24], a WMF or SNR maximizing filter was proposed to reject multiple access interference in DS-CDMA systems. The multiple access interference was assumed to be Gaussian distributed and fading was not considered. As mentioned in [23], the Gaussian assumption is valid only for large numbers of users. While it maximizes the SNR, the WMF introduces ISI into the decision statistic. The effects of the ISI were not considered in [23] and [24]. Yoon and Leib [42] studied the generalized form of matched filter or SNR maximizing filter for the CDMA systems in



improper complex noise environments. The BER performance of digital communication systems in fading and CCI is studied extensively in [43], [44], [45] and the references therein.

In this chapter, we study several WMF or SNIR maximizing filter receiver structures to mitigate the CCI of a BPSK system in micro-cellular fading environments. While maximizing the SNIR, the WMF introduces ISI in the decision statistic. A linear fractionally spaced MMSE equalizer is employed to combat the ISI introduced by the WMF. We assumed the desired user and interfering users undergo Nakagami- $m$  and Rayleigh fading, respectively. This fading scenario normally arises in micro-cellular environments. The fading is assumed to be flat, and slow. Two Nyquist pulse shapes, namely SRC and BTD pulses and the NRZ rectangular pulse are considered. First, an exact continuous time filter WMF structure is considered. Then, another receiver structure with a conventional MF cascaded with a fractionally spaced discrete time transversal filter structure as a SNIR maximizing filter is studied. For the NRZ signaling, the WMF is infinitely long in both directions of the frequency axis. Thus, a long delay has to be introduced to make the WMF a causal filter. The long time delay may not be desirable for many applications. A coherent correlation receiver is proposed to make the data recovery decision based on the information obtained over only one symbol duration. The correlating waveform which maximizes the SNIR is derived. Another receiver structure is considered with fractional correlator and fractionally spaced transversal filter instead of a WMF. This receiver structure requires a relatively short time delay compared to the WMF structure. Again a fractionally spaced MMSE equalizer is employed to combat ISI. An extensive performance comparison study is done using the CF method [46], [45] and an approximate Fourier series method [31], [47] for different cases. Closed-form BER expressions are derived

for a few special cases. Monte Carlo computer simulation is used to obtain the BER in some complex situations. All the performances are compared against the performance of the conventional matched filter receiver structure.

The remainder of this chapter is organized as follows. In Section 2.2, we describe our system and channel model. The receiver structure with continuous time WMF is considered in Section 2.3. In Section 2.4, the analysis in Section 2.3 is extended for a discrete time transversal filter whitening matched filter structure with synchronous CCI. In Section 2.5, a one symbol correlating received structure is considered. A fractional correlator receiver structure is considered in Section 2.6. Our numerical results and discussion are presented in Section 2.7. Finally our conclusions and summary of the chapter are drawn in Section 2.8.

## 2.2 System Model

Consider a BPSK system with CCI in a slowly fading environment. We adopt the system model presented in [45]. The transmitted signal for the desired user is

$$S_d(t) = \sqrt{2P_s T} s_d(t) \cos \omega_c t \quad (2.1)$$

where  $P_s$  is the transmitted power,  $\omega_c$  is the carrier frequency and  $s_d(t)$  is the baseband signal given by

$$s_d(t) = \sum_{k=-\infty}^{+\infty} a[k] g_T(t - kT) \quad (2.2)$$

where  $\frac{1}{T}$  is the symbol transmission rate and  $g_T(\cdot)$  is the transmitter signal baseband pulse and its energy is normalized according to  $\int_{-\infty}^{+\infty} g_T^2(t) dt = 1$ . In the case of equally likely transmitter symbols and BPSK modulation,  $a[k] \in \{+1, -1\}$  with equal probabilities and the average power of  $s_d(t)$  is  $\frac{1}{T}$  [7]. When  $S_d(t)$  is transmitted, it

is subject to fading, as well as interference caused by other user signals occupying the same channel. We assume that all the interfering user signals have the same modulation format as the desired signal. Therefore, the transmitted signal for the  $i$ -th interfering user's signal is

$$S_i(t) = \sqrt{2P_iT} s_i(t) \cos \omega_c t \quad (2.3)$$

where  $P_i$  is the transmitted power of the  $i$ -th interfering user signal and  $s_i(t)$  is the  $i$ -th interferer baseband signal given by

$$s_i(t) = \sum_{k=-\infty}^{+\infty} b_i[k] g_T(t - kT) \quad (2.4)$$

where the  $i$ -th interfering user's information bit  $b_i[k] \in \{+1, -1\}$  with equal probabilities. We assume that both the desired and  $K$  interfering user signals are transmitted over a slow, frequency non-selective fading channel. The received signal becomes

$$R(t) = \sqrt{2P_sT} R_s s_d(t) \cos(\omega_c t + \theta_s) + \sum_{i=1}^K \sqrt{2P_iT} R_i s_i(t - \tau_i) \cos(\omega_c(t - \tau_i) + \theta_i) + n(t) \quad (2.5)$$

where  $\tau_i$  represents the symbol timing offset of the  $i$ -th interfering user signal with respect to the desired user signal, and it is assumed to be uniform over  $[0, T)$ . The background noise  $n(t)$  is a zero-mean, white Gaussian process with two-sided power spectral density  $N_0/2$ ; the phases  $\theta_s$  and  $\theta_i$ , respectively, for the desired user and the  $i$ -th interferer, represent the random phases introduced by the fading channels, and are assumed to be mutually independent and uniformly distributed over  $[0, 2\pi)$ . The random variables  $R_s$  and  $R_i$  represent the fading channel gains. We assume that the desired user's fading channel gain follows the Nakagami- $m$  distribution with parameters  $(m_s, \Omega_s)$  and its PDF is given in eq. (1.11). We further assume that all  $K$

interfering users' fading gains follow the Rayleigh distribution with PDF given in eq. (1.8). The fading of the desired user and interferers are assumed to be independent. This Nakagami/Rayleigh desired/interference signal model can represent general fading scenarios where the desired signal experiences different fading than the interfering signals. This may, for example, arise in micro-cellular systems [4].

As the fading is slow, coherent reception is feasible. In the conventional coherent receiver design, we assume the desired user's signal phase is estimated perfectly, and the receiver maintains perfect synchronization with the desired user's signal. Then, without loss of generality, we can assume  $\theta_s = 0$ . After demodulation, and matched filtering the received signal becomes

$$Z(t) = \sqrt{\frac{P_s T}{2}} R_s \sum_{k=-\infty}^{\infty} a[k] g(t - kT) + \sum_{i=1}^K \sqrt{\frac{P_i T}{2}} R_i \cos(\theta_i - \omega_c \tau_i) \sum_{k=-\infty}^{\infty} b_i[k] g(t - kT - \tau_i) + n_f(t) \quad (2.6)$$

where  $g(t)$  is the pulse shape at the matched filter output and  $n_f(t)$  is the filtered background noise. Sampling at the symbol time, the decision statistic for the 0-th data symbol,  $a[0]$ , becomes,

$$Z[0] = \sqrt{\frac{P_s T}{2}} R_s a[0] + \sum_{i=1}^K \sqrt{\frac{P_i T}{2}} R_i \cos(\phi_i) \rho_i + n_0 \quad (2.7)$$

where  $\phi_i = \theta_i - \omega_c \tau_i$  is assumed to be uniformly distributed over  $[0, 2\pi)$ ,  $n_0 = n_f(0)$  and

$$\rho_i = \sum_{k=-\infty}^{\infty} b_i[k] g(-kT - \tau_i). \quad (2.8)$$

The first term in (2.7) represents the desired signal component; the second term represents the undesired CCI which contains cross-signal ISI terms from each interferer; the third term represents the background noise component. The background noise

component,  $n_0$ , is a zero-mean Gaussian random variable and without loss of generality, we can assume its variance to be unity ( $\text{VAR}[n_0] = 1$ ), i.e. the output noise power is 1. Therefore, the average SNR and the average SIR for our system model can be expressed, respectively as,

$$\text{SNR (dB)} = 10 \log_{10} \left( \frac{P_s T \Omega_s}{2} \right) \quad (2.9)$$

and,

$$\text{SIR (dB)} = 10 \log_{10} \left( \frac{P_s \Omega_s}{\sum_{i=1}^K \Omega_i P_i} \right). \quad (2.10)$$

Here, we consider the rectangular pulse and two Nyquist pulses namely, spectrum raised-cosine (SRC) pulse and a new pulse shape recently reported in [30], which we denote as Beaulieu-Tan-Damen (BTD) pulse. For the rectangular pulse-shaping,  $g_T(t)$  is  $1/\sqrt{T}$  in  $0 \leq t \leq T$ . The bandlimited raised-cosine spectrum is

$$H_{RC}(f) = \begin{cases} T & 0 \leq |f| \leq \frac{1-\beta}{2T} \\ \frac{T}{2} \left\{ 1 + \cos \left( \frac{\pi T}{\beta} \left( |f| - \frac{1-\beta}{T} \right) \right) \right\} & \frac{1-\beta}{2T} \leq |f| \leq \frac{1+\beta}{2T} \\ 0 & |f| > \frac{1+\beta}{2T} \end{cases} \quad (2.11)$$

with corresponding time pulse,  $g(t)$

$$g(t) = \frac{\sin(\pi t/T)}{\pi t/T} \cdot \frac{\cos(\pi \beta t/T)}{1 - 4\beta^2 t^2/T^2}. \quad (2.12)$$

The bandlimited BTD pulse spectrum is

$$H_{BTD}(f) = \begin{cases} T & 0 \leq |f| \leq B(1-\beta) \\ T \exp \left\{ \frac{\ln[2]}{\beta B} [B(1-\beta) - |f|] \right\} & B(1-\beta) \leq |f| \leq B \\ T - T \exp \left\{ \frac{\ln[2]}{\beta B} [|f| - B(1+\beta)] \right\} & B \leq |f| \leq B(1+\beta) \\ 0 & |f| > B(1+\beta) \end{cases} \quad (2.13)$$

and the time domain pulse is

$$g(t) = \frac{\sin(2\pi Bt)}{2\pi Bt} \cdot \frac{4A\pi t \sin(2\pi B\beta t) + 2A^2 \cos(2\pi B\beta t) - A^2}{A^2 + 4\pi^2 t^2} \quad (2.14)$$

where  $\beta \in [0, 1]$  is the excess bandwidth of the pulse,  $B = \frac{1}{2T}$  and  $A = \frac{\ln[2]}{\beta B}$ .

The conventional MF receiver is optimum for detection of signals only in AWGN. When the CCI is present, it is not optimum and its performance is generally poor. We propose several receiver structures to improve the performance of the conventional MF receiver. The coherently demodulated  $i$ -th interferer signal component is written as

$$I_i(t) = \sqrt{\frac{P_i T}{2}} R_i \cos(\phi_i) s_i(t - \tau_i). \quad (2.15)$$

Double frequency terms arising from the coherent demodulation are ignored in the analysis because they will be cancelled by the receiver filters. In this chapter, we consider three cases, the BPSK system with SRC pulse-shaping, BTD pulse-shaping and rectangular pulse-shaping. It is easily shown that  $I_i(t)$  is stationary and Gaussian for synchronous interferers at sampling instants  $t = 0, \pm T, \pm 2T \dots$  with bandlimited pulse shapes. But,  $I_i(t)$  is first order Gaussian at any time instant  $t \in [0, T]$  with rectangular pulse shapes. Then the signal detection problem in this case is analogous to the classical problem of signal detection in colored Gaussian interference and white Gaussian background noise. Some optimal and suboptimal detection schemes have been proposed in the literature [29], [27] for signal detection in colored Gaussian noise using interference whitening. In this chapter, we use an interference whitening matched filter (WMF) to mitigate the effects of cochannel interference. The WMF maximizes the SNIR. If the total noise component is Gaussian, it gives optimum performance. Otherwise, it may give better performance but not optimum. The WMF introduces ISI in the decision statistic when the desired user transmits a train of symbols. The MLSE equalizer using the Viterbi algorithm is an optimum method to combat the ISI. However, due to complexity, we use a linear fractionally spaced MMSE equalizer. In the following sections, we consider different types of WMF

structures.

## 2.3 Whitening Matched Filter Receivers

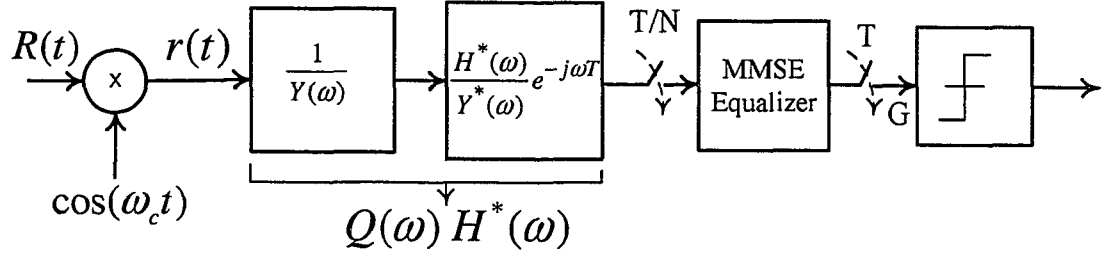


Fig. 2.1. The desired user receiver with whitening matched filter and MMSE equalizer.

In this section, we consider a BPSK system with SRC and BTD pulse-shaping in the presence of synchronous and asynchronous interferers. The synchronous CCI component is Gaussian distributed after demodulation and the background noise is also Gaussian distributed. Since they are independent, their sum is also Gaussian. Here, we design a WMF to whiten the spectrum of the interference and maximize the SNIR using the filter  $Q(\omega)$ , for a single transmitted symbol as in Fig. 2.1. For the time being, we assume the desired user transmits only one symbol while the interferers transmit infinitely long data streams. Now,  $a[0]g_T(t)$  is to be received in noise plus interference with PSD  $S_n(\omega)$ , where the shape of  $g_T(t)$  is known to the receiver and  $a[0]$  is to be detected. As in Chapter 2 of [27] and [23], the WMF receiver can be realized by accepting reasonably long delay with  $Q(\omega) = 1/S_n(\omega)$ . The filter  $1/S_n(\omega)$  can be broken into  $1/Y(\omega)$  that whitens the interference followed by  $1/Y^*(\omega)$ . The filter  $Y(\omega)$  can be chosen to contain all causal poles and zeros of  $S_n(\omega)$ . The filter

$1/Y^*(\omega)$  is combined with  $H^*(\omega)$  to obtain the filter  $(e^{-j\omega T}H^*(\omega)/Y^*(\omega))$  matched to the signal that emerges from the whitening filter  $1/Y(\omega)$ . Using a minimum probability of error criterion for the detection,  $\hat{a}[0] = \text{sgn}\{G_1\}$  where the sampled sufficient statistic is  $G_1$ . The receiver structure maximizes the instantaneous SNIR and it is given as  $\{\mathbb{E}[G_1|a[0]]\}^2/\text{VAR}[G_1|a[0]]$ . As in eq. (2.80) of [27], it is given by

$$SNIR = \frac{P_s T}{2} R_s^2 \int_{-\infty}^{+\infty} \frac{|H(\omega)|^2 d\omega}{S_n(\omega) 2\pi}. \quad (2.16)$$

The maximum SNIR does not depend on any statistics of the interference except its PSD of background noise plus CCI. For synchronous CCI, this receiver maximizes the SNIR and the sufficient statistic is a Gaussian random variable. Thus, it results in optimum performance. From (2.15), for an arbitrary pulse-shaping filter  $H(f)$ , the PSD of CCI is written as

$$S_{CCI}(f) = \frac{P_i \Omega_i K}{4} |H(f)|^2 \quad (2.17)$$

then,  $S_n(f)$  becomes

$$S_n(f) = 1 + \frac{P_i \Omega_i K}{4} |H(f)|^2. \quad (2.18)$$

Now, the instantaneous SNIR is

$$SNIR = \frac{P_s T}{2} R_s^2 \int_{-\infty}^{+\infty} \frac{|H(f)|^2}{1 + P |H(f)|^2} df \quad (2.19)$$

where  $P = \frac{P_i \Omega_i K}{4}$ . As there is no ISI for the desired user, eq. (2.19) is an upper bound to the achievable instantaneous SNIR.

### 2.3.1 Bandlimited Pulse-Shaping

As mentioned in [23], with the flat spectrum pulse-shaping with no excess bandwidth ( $\beta = 0$ ) in (2.11) and (2.13), the whitening filters wouldn't affect the SNIR or BER



performance. Because, for flat spectrum pulse-shaping the CCI spectrum is flat thus, it is white. Then, the whitening filter is a constant value. So, it doesn't have any effect on SNIR and BER. In practice, the flat spectrum pulse shaping is not desirable because of the slow decaying rate in the time domain. When using excess bandwidth increases the performance, the improvement achieved by using a whitening filter also increases, so, in this section we assume 100% excess bandwidth ( $\beta = 1$ ) in eqs. (2.11) and (2.13). For SRC pulse-shaping, as in (2.19), the maximum instantaneous SNIR now becomes

$$SNIR = \frac{P_s T}{4\pi} R_s^2 \int_{-\pi}^{+\pi} \frac{(1 + \cos x)}{1 + \frac{PT}{2}(1 + \cos x)} dx. \quad (2.20)$$

For BTD pulse-shaping the maximum instantaneous SNIR is

$$SNIR = P_s T R_s^2 \left\{ \frac{\ln \left[ \frac{1+PT}{1+PT/2} \right]}{2PT \ln[2]} + \frac{\ln[2] - \frac{\ln[1+PT/2]}{PT}}{2 \ln[2](1+PT)} \right\}. \quad (2.21)$$

For notational convenience we denote  $SNIR = R_s^2 \gamma^2$  in eqs. (2.20) and (2.21). The sufficient statistic,  $G_1$ , is Gaussian for synchronous CCI; then, with one desired user transmitted symbol the average probability of detection error (BER) is written as

$$P_{e1} = \int_0^{+\infty} \mathbf{Q}(\gamma r) \frac{2}{\Gamma(m_s)} \left( \frac{m_s}{\Omega_s} \right)^{m_s} r^{2m_s-1} e^{-\frac{m_s r^2}{\Omega_s}} dr. \quad (2.22)$$

For arbitrary values of  $m_s \in [0.5, \infty)$ , as in eq. (4.3.9) of [48], the integral (2.22) has a closed-form expression. That is given as

$$P_{e1} = \frac{\Gamma(m_s + \frac{1}{2})}{2\sqrt{\pi} m_s \Gamma(m_s)} \left( \frac{2m_s}{\gamma^2 \Omega_s} \right)^{m_s} {}_2F_1 \left( m_s, m_s + \frac{1}{2}; m_s + 1, \frac{-2m_s}{\Omega_s \gamma^2} \right) \quad (2.23)$$

where  ${}_2F_1(\cdot, \cdot; \cdot; \cdot)$  is Gauss hypergeometric function. For the case of asynchronous CCI, with the one desired user transmitted symbol, the exact BER expression is derived in Appendix A. That is

$$P_{e2} = \frac{1}{2} - \frac{\Gamma(m_s + \frac{1}{2})}{\pi \Gamma(m_s)} \sqrt{\frac{P_s T \Omega_s}{2m_s}} \int_0^{+\infty} \Phi_T(\omega) {}_1F_1 \left( m_s + \frac{1}{2}; \frac{3}{2}; \frac{-P_s T \Omega_s \omega^2}{8m_s} \right) d\omega \quad (2.24)$$

where  ${}_1F_1(\cdot)$  is confluent hypergeometric function and  $\Phi_T(\cdot)$  is the characteristic function of the CCI plus noise.

Now, If we let the desired user transmit an infinitely long data stream, there will be ISI in the sufficient statistic  $G_1$ . It is interesting to note that from eqs. (2.18) and (2.19), the ISI is negligible when the total CCI power is negligible compared with background noise power for any  $\beta \in [0, 1]$  and the background noise power is negligible compared with the total CCI power for  $\beta = 1$ . Now, we derive an exact BER expression accounting for ISI with synchronous CCI using the approximate Fourier series method proposed in [31]. The signal emerging from the whitening matched filter consists of the desired signal component, ISI and white Gaussian noise. The desired user signal with frequency domain pulse  $Q(\omega)|H(\omega)|^2$ ,  $q(t)$  is transmitted in white a Gaussian noise channel. Then, the conditional probability of detection error is given by [31]

$$P_{e3|R_s} = \frac{1}{2} - \frac{2}{\pi} \sum_{\substack{v=1 \\ v \text{ odd}}}^M \left\{ \frac{1}{v} \exp \left[ -\frac{v^2 \omega_0^2}{2} \right] \sin(v\omega_0 \gamma R_s q_0) \prod_{\substack{k=N_1 \\ k \neq 0}}^{N_2} \cos(v\omega_0 \gamma R_s q_k) \right\}, \quad (2.25)$$

where  $\omega_0 = 2\pi/T_0$  and  $q_i = q(iT)$ . The parameters  $T_0, M, N_1, N_2$  are chosen to give the required computational accuracy. The unconditional average BER for arbitrary values of desired user fading parameter,  $m_s$ , is written as

$$P_{e3} = \frac{1}{2} - \frac{4}{\pi \Gamma(m_s)} \left( \frac{m_s}{\Omega_s} \right)^{m_s} \sum_{\substack{m=1 \\ m \text{ odd}}}^M \left\{ \frac{1}{m} \exp \left[ -\frac{m^2 \omega_0^2}{2} \right] \times \int_0^\infty r^{2m_s-1} \exp \left[ -\frac{m_s r^2}{\Omega_s} \right] \sin(m\omega_0 \gamma r q_0) \prod_{\substack{k=N_1 \\ k \neq 0}}^{N_2} \cos(m\omega_0 \gamma r q_k) dr \right\}. \quad (2.26)$$

The BER expression (2.26) has to be evaluated numerically. When the CCI is asynchronous, the signal emerging from the whitening matched filter contains desired

signal component, ISI, residual CCI and white Gaussian noise. We employed Monte Carlo computer simulation to obtain the BER performance of this case. In this chapter, we consider a fractionally spaced simple discrete linear MMSE equalizer for simplicity. However, any sophisticated type of equalizer can be used with more complexity. We assume the equalizer is  $T/N_e$  spaced and has  $2K_e + 1$  taps. The optimum coefficients of the MMSE equalizer are the solutions of the linear equation [7]

$$\mathbf{\Gamma}\mathbf{C} = \boldsymbol{\xi} \quad (2.27)$$

where  $\mathbf{C}$  denotes the column vector of  $2K_e + 1$  tap weight coefficients,  $\boldsymbol{\xi}$  is a  $2K_e + 1$  length column vector written as

$$\boldsymbol{\xi} = \begin{bmatrix} q(-K_e T/N_e) \\ q(-(K_e - 1)T/N_e) \\ \vdots \\ q((K_e - 1)T/N_e) \\ q(K_e T/N_e) \end{bmatrix}_{(2K_e+1) \times 1} \quad (2.28)$$

and  $\mathbf{\Gamma}$  denotes the  $(2K_e + 1) \times (2K_e + 1)$  Hermitian covariance matrix which is given by [49]

$$\mathbf{\Gamma} = \gamma^2 \Omega_s \mathbf{X}^T \mathbf{X} + \mathbf{I} \quad (2.29)$$

and

$$\mathbf{X} = \begin{bmatrix} q(-\frac{K_e T}{N_e}) & q(-\frac{(K_e+1)T}{N_e}) & \dots & q(-\frac{(3K_e-1)T}{N_e}) & q(-\frac{3K_e T}{N_e}) \\ q(-\frac{(K_e-N_e)T}{N_e}) & q(-\frac{(K_e-N_e+1)T}{N_e}) & \dots & q(-\frac{(3K_e-N_e-1)T}{N_e}) & q(-\frac{(3K_e-N_e)T}{N_e}) \\ \vdots & & \ddots & & \vdots \\ q(\frac{(3K_e-N_e)T}{N_e}) & q(\frac{(3K_e-N_e-1)T}{N_e}) & \dots & q(\frac{(K_e-N_e+1)T}{N_e}) & q(\frac{(K_e-N_e)T}{N_e}) \\ q(\frac{3K_e T}{N_e}) & q(\frac{(3K_e-1)T}{N_e}) & \dots & q(\frac{(K_e+1)T}{N_e}) & q(\frac{K_e T}{N_e}) \end{bmatrix}. \quad (2.30)$$

Then, the optimum coefficients are given by

$$\mathbf{C}_{\text{opt}} = \mathbf{\Gamma}^{-1}\boldsymbol{\xi}. \quad (2.31)$$

Thus, the  $T/N_e$  sampled output pulse of the MMSE equalizer is  $\boldsymbol{\xi} * \mathbf{C}_{\text{opt}}$ , where  $*$  denotes the convolution operation, and it contains the residual ISI. Then, again we can calculate the average BER using eq. (2.26) for the synchronous CCI case. The derivation of the BER expression when the CCI is asynchronous and a MMSE equalizer is used is very complex. Thus, we employ Monte Carlo computer simulation to obtain the BER performance in this case.

### 2.3.2 NRZ Pulse-Shaping

We consider rectangular pulse-shaping in this section. As the spectrum of the rectangular pulse spreads to infinity in both directions of the frequency axis, a reasonably long delay has to be given to implement the WMF. Here, we neglect the aliasing effect when we design the WMF. This is justified because we sample at higher rate than the symbol rate [24]. From (2.18), for the rectangular pulse-shaping filter  $H(f)$ , the PSD of CCI plus noise is

$$S_n(f) = 1 + \frac{P_i \Omega_i L}{4} |H(f)|^2 \quad (2.32)$$

where

$$H(f) = \sqrt{T} \frac{\sin(\pi f T)}{\pi f T} e^{-j\pi f T} \quad -\infty < f < +\infty. \quad (2.33)$$

Assuming there is no ISI for the desired user, the upper bound of the achievable instantaneous SNIR with the rectangular pulse-shaping, becomes

$$SNIR = \frac{P_s T}{2} R_s^2 T \int_{-\infty}^{+\infty} \frac{\text{sinc}^2(fT)}{1 + \frac{P_i \Omega_i K}{4} T \text{sinc}^2(fT)} df \quad (2.34)$$

where  $\text{sinc}(x) = \sin(\pi x)/(\pi x)$ . As there is no closed-form expression for (2.34), it is calculated numerically. As the CCI component in (2.15) is Gaussian for synchronous and asynchronous interferers, the BER for one transmitted symbol can be given as in eq. (2.23). When the desired user transmits an infinitely long data sequence the BER can be evaluated using eq. (2.26). Then, the fractionally spaced MMSE equalizer is designed as in eq. (2.31). At the output of the MMSE equalizer, the BER is again calculated as in eq. (2.26).

## 2.4 Conventional Matched Filter and Transversal Filter Receiver

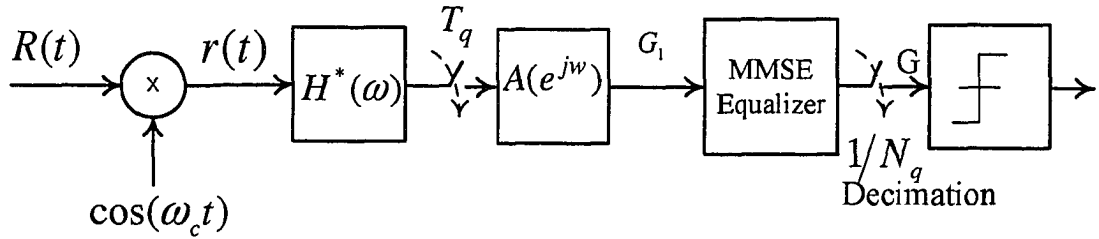


Fig. 2.2. The desired user receiver with transversal filter and MMSE equalizer.

The receiver structure in Section 2.3 employed continuous time whitening matched filters. A conventional matched filter and a discrete transversal filter can be used instead of continuous time WMF [24], [27]. In this section, as shown in Fig. 2.2, we consider a modified system with a conventional matched filter cascaded with a fractionally spaced discrete transversal filter as the SNIR maximizing filter and MMSE equalizer for systems with any pulse-shaping. The received signal after coherent demodulation  $r(t)$  is passed through a matched filter. The matched filter output is

sampled at time  $T_q(= T/N_q)$  and passed through the fractionally spaced transversal filter to maximize the SNIR and then passed through a MMSE equalizer which is again implemented as a fractionally spaced transversal filter to combat the ISI introduced by the SNIR maximizing filter. As the SNIR maximizing filter and the MMSE equalizer have the same tap spacing, they can be convolved to obtain a single transversal filter. The number of taps of the new filter is the sum of the tap spacings of the filters minus one. For the purpose of designing the filter, it is convenient to work with two separate filters. The output is then  $(1/N_q)$  decimated and the transmitted bit is detected. In this section, we only consider synchronous CCI. Thus, the CCI component is Gaussian distributed. The transversal filter is two sided and written as

$$A(e^{j\omega}) = \sum_{n=-K_t}^{+K_t} \alpha_n e^{j\omega n}, \quad (2.35)$$

where there are  $2K_t + 1$  taps,  $\alpha_n$  are the filter coefficients and  $j = \sqrt{-1}$ . The decision statistic after the SNIR maximizing filter can be written as

$$\begin{aligned} G_1 &= \sum_{u=-K_t}^{K_t} \alpha_u y_{-u} \\ &= \mathbf{y}^T \boldsymbol{\alpha} \end{aligned} \quad (2.36)$$

$$= \sqrt{\frac{P_s T}{2}} R_s \mathbf{x}^T \boldsymbol{\alpha} + \mathbf{v}^T \boldsymbol{\alpha} \quad (2.37)$$

where  $\mathbf{x}^T = [h_2(-K_t T_q), \dots, h_2(0), \dots, h_2(K_t T_q)]$  and  $h_2(t)$  is the inverse Fourier transform of  $|H(\omega)|^2$ . Then, the SNIR is written as

$$SNIR = \frac{P_s T R_s^2 (\mathbf{x}^T \boldsymbol{\alpha})^2}{2 \boldsymbol{\alpha}^T \mathbf{R}_v \boldsymbol{\alpha}} \quad (2.38)$$

where the correlation matrix,  $\mathbf{R}_v = \mathbb{E}[\mathbf{v}\mathbf{v}^T]$  is a positive definite matrix. The SNIR in (2.38) is maximized in Appendix B to obtain the optimal tap coefficients. The optimal tap coefficients are solutions to the system of linear equations

$$\mathbf{R}_v \boldsymbol{\alpha} = \mathbf{x}. \quad (2.39)$$

The maximum  $SNIR$  is written as

$$\begin{aligned} SNIR_{max} &= \frac{P_s T R_s^2}{2} \mathbf{x}^T \mathbf{R}_v^{-1} \mathbf{x} \\ &= \Xi^2 R_s^2 \end{aligned} \quad (2.40)$$

where  $\Xi^2 = \frac{P_s T}{2} \mathbf{x}^T \mathbf{R}_v^{-1} \mathbf{x}$ . The power spectral density of the CCI and background noise can be written as

$$S_v(\omega) = |H(\omega)|^2 + \frac{P_i T K \Omega_i}{4} |H(\omega)|^4, \quad (2.41)$$

where  $H(\omega)$  is the frequency response of transmitter filter. Thus, the autocorrelation of the process  $v(t)$  is given by the inverse Fourier transform of (2.41), and is written as

$$R_v[n] = h_2(nT_q) + \frac{P_i T K \Omega_i}{4} h_4(nT_q), \quad (2.42)$$

where  $R_v[n]$  is the autocorrelation at  $nT_q$ , and  $h_2(t)$  and  $h_4(t)$  are the inverse Fourier transform of  $|H(\omega)|^2$  and  $|H(\omega)|^4$ , respectively. The filters  $h_2(t)$  and  $h_4(t)$  are derived for SRC and BTD pulses in Appendix B. The elements of the correlation matrix  $(\mathbf{R}_v)_{i,j} = R_v[n]$  where  $n = |i - j|$ . Then, as in (2.23), for one desired user transmitted symbol, the average probability of detection error can be written as

$$P_{e4} = \frac{\Gamma(m_s + \frac{1}{2})}{2\sqrt{\pi} m_s \Gamma(m_s)} \left( \frac{2m_s}{\Xi^2 \Omega_s} \right)^{m_s} {}_2F_1 \left( m_s, m_s + \frac{1}{2}; m_s + 1, \frac{-2m_s}{\Omega_s \Xi^2} \right) \quad (2.43)$$

when the desired user transmits an infinitely long data stream. Now, the SNIR maximizing filter introduces ISI to the decision statistic  $G_1$ . As in Section 2.3, we use a fractionally spaced ( $T_q$ ) MMSE equalizer. The input signal vector of the MMSE equalizer is denoted as  $\mathbf{u}$ , ( $= \mathbf{y}^T \boldsymbol{\alpha}$ ). The optimum equalizer tap coefficients are given by equation (2.31). The equalizer output is written as  $\mathbf{u} * \mathbf{C}_{opt}$ . The average BER can also be calculated using (2.26).

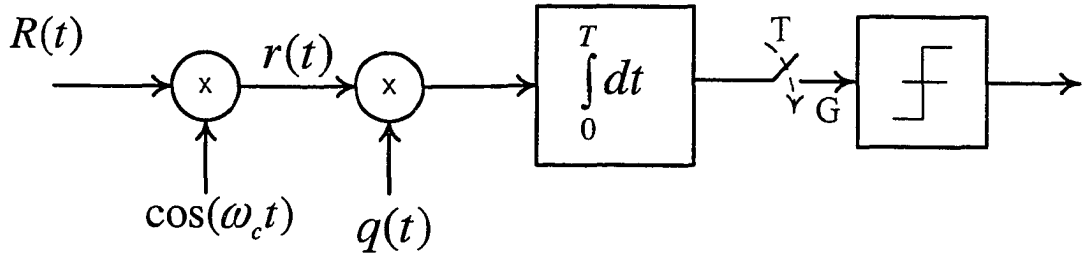


Fig. 2.3. The desired user receiver with correlator.

## 2.5 Correlating Receiver Structure

In this section, we consider a coherent correlating receiver structure to combat the CCI. The long delay for the WMF receiver in Section 2.3.2 may not be desirable for many applications. This receiver makes decision based on the observation over a single symbol duration  $[0, T]$ . We need to derive a correlating waveform to correlate with the received signal to maximize the SNIR. This receiver structure does not introduce ISI as does the WMF receiver. As shown in Chapter 2.2 of [27], the signal  $a[0]g_T(t)$  is to be received in the presence of stationary colored Gaussian noise of autocorrelation  $K_n(\tau)$ , and the receiver is constrained to observe the receive waveform only for  $t \in [0, T]$ . Then using the minimum probability of error criterion, the decision is  $\hat{a}[0] = \text{sgn}\{G\}$ , where

$$G = \int_0^T r(t)q(t)dt. \quad (2.44)$$

The receiver structure is shown in Fig. 2.3 and the demodulated received signal is denoted as  $r(t)$ . The correlating waveform  $q(t)$  is the solution to the integral equation

$$g_T(t) = \int_0^T K_n(t-u)q(u)du. \quad (2.45)$$



As shown in eq. (2.67) of [27], the instantaneous SNIR =  $\text{VAR}[G]$  and is given by

$$SNIR = \int_0^T g_T(t)q(t)dt. \quad (2.46)$$

The sufficient statistic,  $G$  in  $SNIR = \int_0^T g_T(t)q(t)dt$ , the linear time invariant (LTI) filter whose impulse response which is limited to  $T$ , is given by  $q(T-t)$  [27, eq. 2.81]. The filtering operation can be implemented as a correlator receiver structure as shown in Fig. 2.3. The receiver structure maximizes the SNIR for  $a[0]g_T(t)$  in any stationary noise of autocorrelation  $K_n(\tau)$ , when the impulse response of the LTI filter is of duration  $T$ . The CCI is Gaussian and, thus, the receiver provides the corresponding optimum performance. For the rectangular pulse-shaping, the autocorrelation of the background noise plus CCI becomes

$$K_n(\tau) = \delta(\tau) + \frac{P_i\Omega_i K}{4} \phi(\tau) \quad (2.47)$$

where  $\phi(\tau)$  is the autocorrelation of rectangular pulses. That is given by

$$\phi(\tau) = \begin{cases} 1 - \frac{|\tau|}{T} & \text{if } |\tau| \leq T \\ 0 & \text{otherwise} \end{cases}. \quad (2.48)$$

Substituting (2.47) and (2.48) into (2.45) yields

$$g_T(t) = q(t) + P \int_0^T \phi(t-u)q(u)du \quad (2.49)$$

where  $P = \frac{P_i\Omega_i K}{4}$ . Eq. (2.45) is in the form of the Fredholm integral equation of the second kind whose kernel is the autocorrelation function of the rectangular pulses. The derivation of the exact solution of (2.49) is presented in Appendix C. The solution  $q(t)$ , is written as

$$q(t) = C_1 e^{\sqrt{\frac{2P}{T}}t} + C_2 e^{-\sqrt{\frac{2P}{T}}t}, \quad 0 \leq t \leq T \quad (2.50)$$

where  $C_1$  and  $C_2$  are derived in Appendix C. Now, eq. (2.46) becomes

$$SNIR = \frac{P_s T R_s^2}{2} \sqrt{\frac{T}{2P}} \left\{ C_1 \left[ e^{\sqrt{2PT}} - 1 \right] + C_2 \left[ 1 - e^{-\sqrt{2PT}} \right] \right\}. \quad (2.51)$$

For notational convenience, we write it as  $SNIR = \gamma^2 R_s^2$ . As shown in eq. (2.23), the average BER for arbitrary values of  $m_s \in [0.5, \infty)$ , can be written as

$$P_{er5} = \frac{\Gamma(m_s + \frac{1}{2})}{2\sqrt{\pi} m_s \Gamma(m_s)} \left( \frac{2m_s}{\gamma^2 \Omega_s} \right)^{m_s} {}_2F_1 \left( m_s, m_s + \frac{1}{2}; m_s + 1; \frac{-2m_s}{\Omega_s \gamma^2} \right). \quad (2.52)$$

The correlating waveform for different average SNR and SIR values and the BER performance curves are presented in Section 2.7.

## 2.6 Fractionally Spaced Correlator and Transversal Filter Receivers

As the WMF receiver structure in Section 2.3.2 requires a long delay before the decision is made, we consider a similar receiver structure [50] only for systems with rectangular pulse-shaping as shown in Fig. 2.4 with fractionally spaced correlator and transversal filter in this section. Since the spectrum of the CCI is colored, if we take samples at a fraction of a symbol time ( $T$ ), they are highly correlated, and thus, CCI may be rejected effectively. Here, we investigate the use of a transversal filter as whitening filter with taps spaced at a fraction of a symbol duration. Assume that there are  $K$  interfering users in the system and the fraction of the symbol time is denoted as  $T_q (= T/N_q)$  for some integer  $N_q$ . The transversal filter is two sided and written as

$$A(e^{j\omega}) = \sum_{n=-K_t}^{+K_t} \alpha_n e^{j\omega n}, \quad (2.53)$$

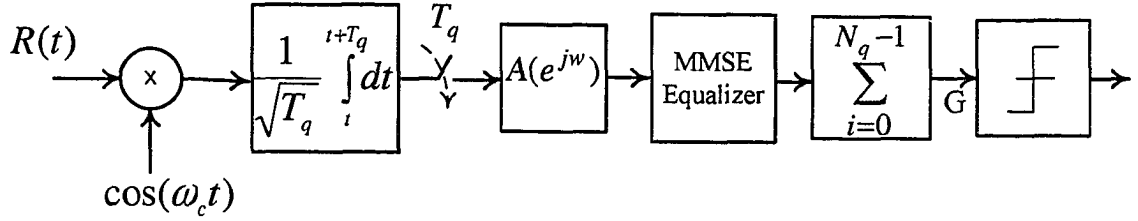


Fig. 2.4. The desired user fractional correlator receiver with transversal filter and MMSE equalizer.

where  $K_t$  is the number of taps per side,  $\alpha_n$  are the filter coefficients and  $j = \sqrt{-1}$ . All other discrete quantities also defined on a  $T_q$  time base. By assuming the transmitted desired user symbol is  $+1 \in [0, T]$ , the output of the discrete correlator is written as

$$\begin{aligned} r_i &= \frac{1}{T_q} \int_{(i-1)T_q}^{iT_q} r(t) dt \\ &= s_i + \sum_{l=1}^K I_i^l + n_i \end{aligned} \quad (2.54)$$

where, ignoring double frequency terms,

$$\begin{aligned} s_i &= \sqrt{\frac{P_s T}{2}} R_s c_i, \\ I_i^l &= \sqrt{\frac{P_l T}{2}} R_l \cos(\phi_l) \frac{1}{\sqrt{T_q}} \int_{(i-1)T_q}^{iT_q} s_l(t - \tau_l) dt \end{aligned} \quad (2.55)$$

and

$$n_i = \frac{1}{\sqrt{T_q}} \int_{(i-1)T_q}^{iT_q} n_c(t) dt \quad (2.56)$$

where in discrete notation  $c_i$  are the values of the desired input signal,  $s_d(t)$  for the interval  $(i-1)T_q < t < iT_q$ . Thus, the  $c_i$  is repeated  $N_q$  times. We define  $J_i$  as

$$J_i = \sum_{l=1}^K I_i^l + n_i. \quad (2.57)$$

Then, the decision statistic can be written as

$$G' = \sum_{i=1}^{N_q} s_i \sum_{j=-K_t}^{K_t} \alpha_j r_{i-j} \quad (2.58)$$

$$= \sum_{k=-(K_t-1)}^{N_q+K_t} r_k q_k \quad (2.59)$$

where

$$q_k = \sum_{i=-K_t}^{K_t} \alpha_i s_{k-i} p_{k-i} \quad (2.60)$$

and  $p_i = 1$  when  $i \in [1 \dots N_q]$  and  $p_i = 0$  elsewhere. Now, we want to write the decision statistic in matrix notation.

$$\begin{aligned} G' &= \mathbf{r}^T \mathbf{q}, \\ &= \mathbf{s}^T \mathbf{q} + \mathbf{J}^T \mathbf{q} \end{aligned} \quad (2.61)$$

where  $\mathbf{q} = [q_{-(K_t-1)} \dots q_{N_q+K_t}]^T$  and the column vectors  $\mathbf{r}, \mathbf{J}$  are also defined over the same time span  $[-(K_t-1) \dots (N_q+K_t)]$  with elements  $r_i$  and  $J_i$ , respectively. The vector  $\mathbf{s}$  is defined as  $[\mathbf{0}_j^T, s_1, \dots, s_{N_q}, \mathbf{0}_j^T]^T$  where  $\mathbf{0}_j$  is a column vector of  $j$  zeros. Then

$$\mathbf{q} = \mathbf{C} \boldsymbol{\alpha} \quad (2.62)$$

where  $\mathbf{C} = [\gamma_0, \dots, \gamma_{2K}]$ ,  $\gamma_j = [\mathbf{0}_{2K_t-j}^T, c_1, \dots, c_{N_q}, \mathbf{0}_j^T]^T$  and the vector  $\boldsymbol{\alpha} = [\alpha_{-K_t}, \dots, \alpha_{K_t}]^T$ . The covariance matrix of the CCI plus background noise is written as

$$\Phi_J = \mathbb{E}[\mathbf{J}\mathbf{J}^T]. \quad (2.63)$$

The SNIR is written in matrix notation as

$$\begin{aligned} SNIR &= \frac{(\mathbf{s}^T \mathbf{q})^2}{\mathbf{q}^T \Phi_J \mathbf{q}} \\ &= \frac{(\mathbf{s}^T \mathbf{C} \boldsymbol{\alpha})^2}{\boldsymbol{\alpha}^T \mathbf{C}^T \Phi_J \mathbf{C} \boldsymbol{\alpha}}. \end{aligned} \quad (2.64)$$

It can be shown that the vector  $\alpha$  which maximizes (2.64) is the solution to

$$\mathbf{C}^T \Phi_J \mathbf{C} \alpha = \mathbf{C}^T \mathbf{s}. \quad (2.65)$$

The maximum SNIR is written as

$$\begin{aligned} SNIR_{max} &= \mathbf{s}^T \Phi_J^{-1} \mathbf{s} \\ &= \frac{P_s T R_s^2}{2} \mathbf{C}^T \Phi_J^{-1} \mathbf{C} \\ &= R_s^2 \Delta^2 \end{aligned} \quad (2.66)$$

where  $\Delta^2 = \frac{P_s T}{2} \mathbf{C}^T \Phi_J^{-1} \mathbf{C}$ . The covariance matrix of the CCI and background noise in (2.63) can be written as

$$\Phi_J = \mathbf{I} + \frac{P_i T K \Omega_i T_q}{4} \phi_{cci}, \quad (2.67)$$

where  $\phi_{cci}$  is correlation matrix of the random rectangular pulses. As shown in [51], [50], [52], it can be given by

$$\phi_{cci_{i,j}} = \begin{cases} \left[ \frac{3N_q - 1}{3N_q} \right], & n = 0 \\ \left[ \frac{N_q - n}{N_q} \right], & 1 \leq n \leq N_q - 1 \\ \left[ \frac{1}{6N_q} \right], & n = N_q \\ 0, & n > N_q \end{cases} \quad (2.68)$$

where  $n = |i - j|$ . Then, assuming one desired user transmitted symbol and the desired user undergoes Nakagami-m fading, the average probability of detection error becomes, as in (2.23)

$$P_{er6} = \frac{\Gamma(m_s + \frac{1}{2})}{2\sqrt{\pi} m_s \Gamma(m_s)} \left( \frac{2m_s}{\Delta^2 \Omega_s} \right)^{m_s} {}_2F_1 \left( m_s, m_s + \frac{1}{2}; m_s + 1, \frac{-2m_s}{\Omega_s \Delta^2} \right). \quad (2.69)$$

As mentioned in Section 2.3, when the desired user transmits an infinitely long data stream, the WMF introduces ISI in the decision statistic. Again, a linear fractionally

spaced MMSE equalizer is employed to combat ISI. The BER before and after the MMSE equalizer and optimum equalizer tap coefficients are obtained using eqns. (2.26) and (2.31), respectively.

## 2.7 Numerical Results and Discussion

In this section, we present our numerical results and discussion. Some of our results are published in [53] and [54]. For comparison, we derive the BER of the conventional matched filter receiver using the Gaussian approximation for the CCI.

### 2.7.1 Bandlimited Pulse-Shaping

The BER of the bandlimited BPSK system with CCI is extensively studied using the Gaussian approximation for CCI and precise analysis using the Fourier series and CF methods [31], [43], [45]. Synchronous CCI with SRC and BTD pulse-shaping is Gaussian distributed at the sampling instants; then, the Gaussian approximation becomes exact. From eq. (2.7), the total CCI component is written as

$$I_{CCI} = \sum_{i=1}^K \sqrt{\frac{P_i T}{2}} R_i \cos(\phi_i) \rho_i, \quad (2.70)$$

where  $\rho_i$  is defined in (2.8). For synchronous interferers, the variance of  $I_{CCI}$  with SRC and BTD pulse-shaping is given by

$$\text{VAR}[I_{CCI}] = \frac{\Omega_i T \sum_{i=1}^K P_i}{4}. \quad (2.71)$$

Then, the total equivalent noise power becomes  $\sigma_t^2 = 1 + \text{VAR}[I_{CCI}]$ . The BER conditioned on  $R_s$ , is given by

$$P_{e|R_s} = Q \left( \sqrt{\frac{P_s T}{2\sigma_t^2}} R_s \right). \quad (2.72)$$

Then, as shown in eqn. (2.23), for arbitrary values of  $m_s$ , the average BER is given by

$$P_{eg} = \frac{\Gamma(m_s + \frac{1}{2})}{2\sqrt{\pi}m_s\Gamma(m_s)} \left( \frac{2m_s}{\Lambda^2\Omega_s} \right)^{m_s} {}_2F_1 \left( m_s, m_s + \frac{1}{2}; m_s + 1, \frac{-2m_s}{\Omega_s\Lambda^2} \right) \quad (2.73)$$

where  $\Lambda^2 = P_s T / (2\sigma_t^2)$ . If we put  $\sigma_t^2 = 1$  in (2.72), the corresponding eq. (2.73) gives the average BER of a BPSK system without CCI and this performance is a lower bound of the ML receiver performance [19]. When the CCI is asynchronous the exact BER of the conventional matched filter receiver can be obtained by substituting the appropriate sampled effective pulse shapes derived in Appendix A.

We assume the transmitted powers of the desired and interfering users are the same and  $P_s = P_i = 1$ , except the case when there is no fading for the desired user. When there is no fading for the desired user, we assume the interfering user transmitted powers are the same. However, we can also consider the dissimilar power users. Our numerical results are obtained for average SIR = 10 dB. Desired user and interfering users undergo Nakagami- $m$  fading and Rayleigh fading, respectively and the fading is assumed to be slow. The SRC and a recently introduced novel BTD pulse-shaping are used with excess bandwidth 100%. A  $T/4$  spaced and 41 taps MMSE equalizer are considered. The  $T/4$  tap spacing is selected to obtain better performance with reasonable complexity. An extensive performance comparison of the proposed receiver structure over different fading environments for the desired user is presented.

In the WMF receiver structure in Section 2.3, the effective pulse shape is

$$X(f) = \frac{|H(f)|^2}{1 + \frac{P_i\Omega_i K}{4}|H(f)|^2}. \quad (2.74)$$

It is interesting to note that, when the CCI power is negligible compared with background noise, there is no ISI and when the background noise is negligible compared with CCI, there is no ISI. This phenomenon is depicted in Fig. 2.5 - 2.8.

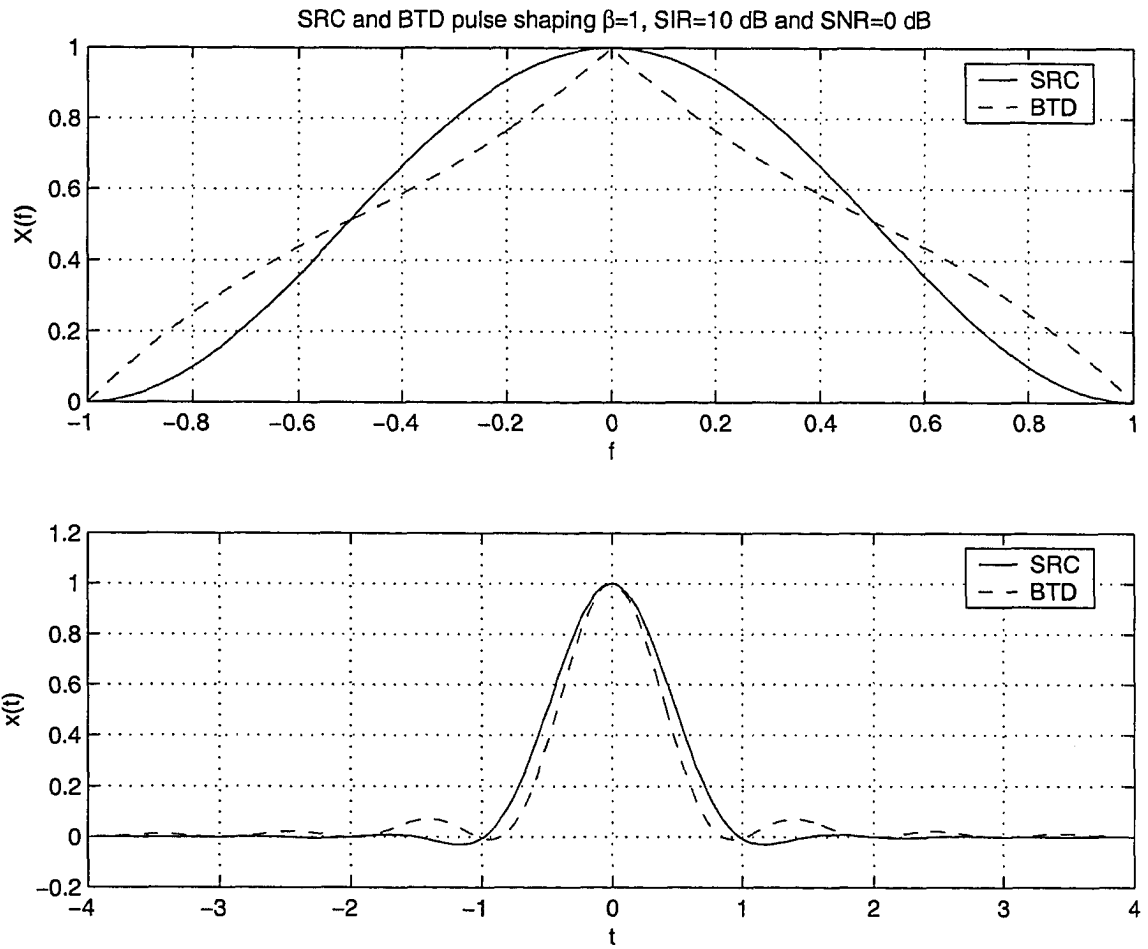


Fig. 2.5. Effective pulse shape of the WMF for SNR= 0 dB and SIR = 10 dB.



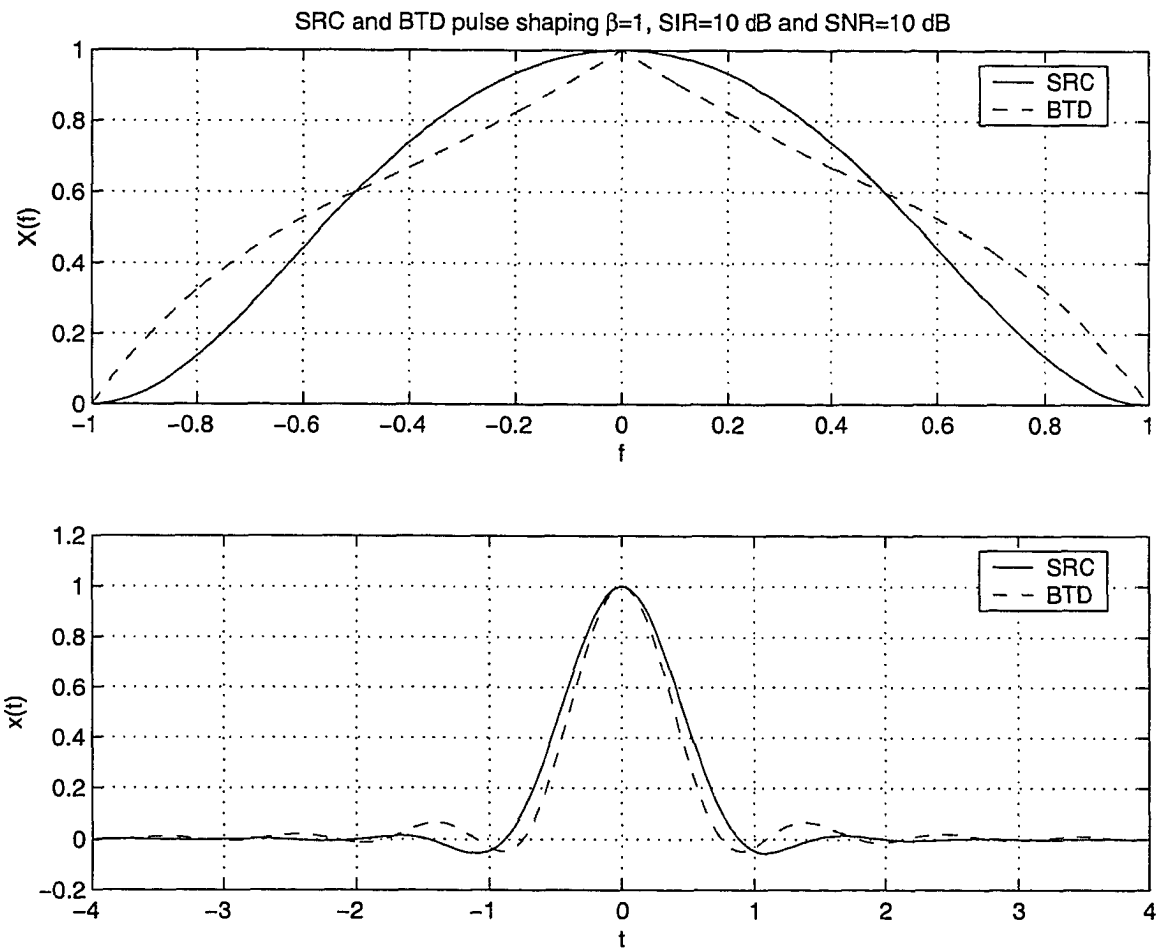


Fig. 2.6. Effective pulse shape of the WMF for SNR= 10 dB and SIR = 10 dB.

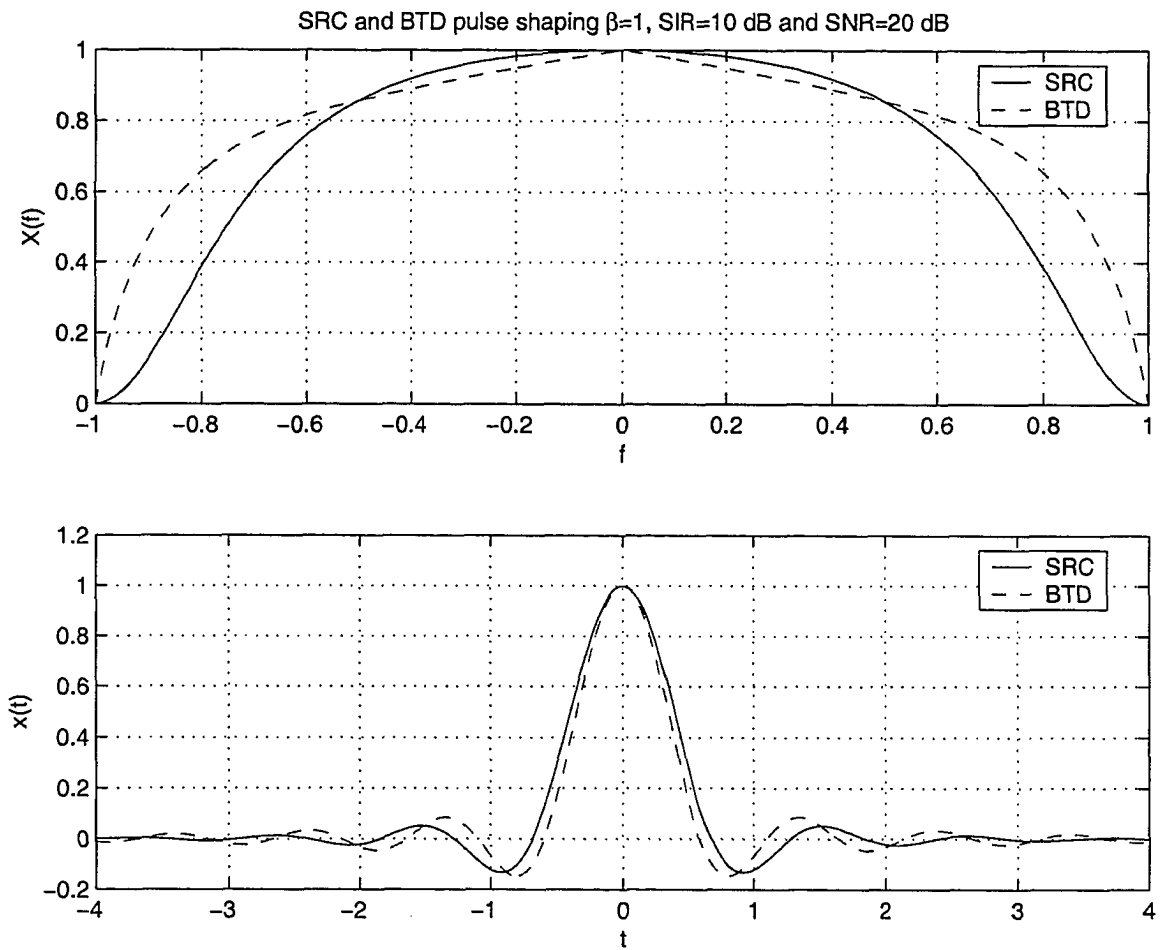


Fig. 2.7. Effective pulse shape of the WMF for SNR= 20 dB and SIR = 10 dB.

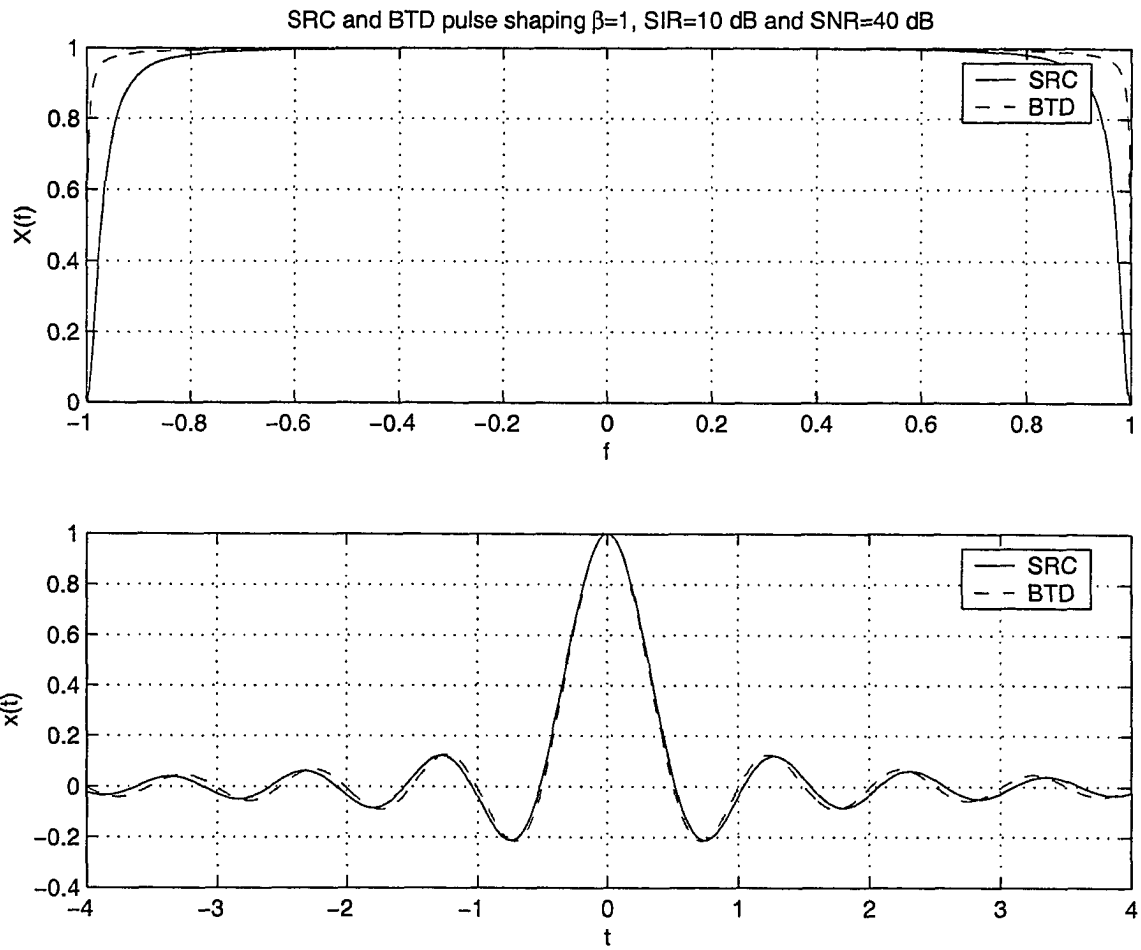


Fig. 2.8. Effective pulse shape of the WMF for SNR= 40 dB and SIR = 10 dB.

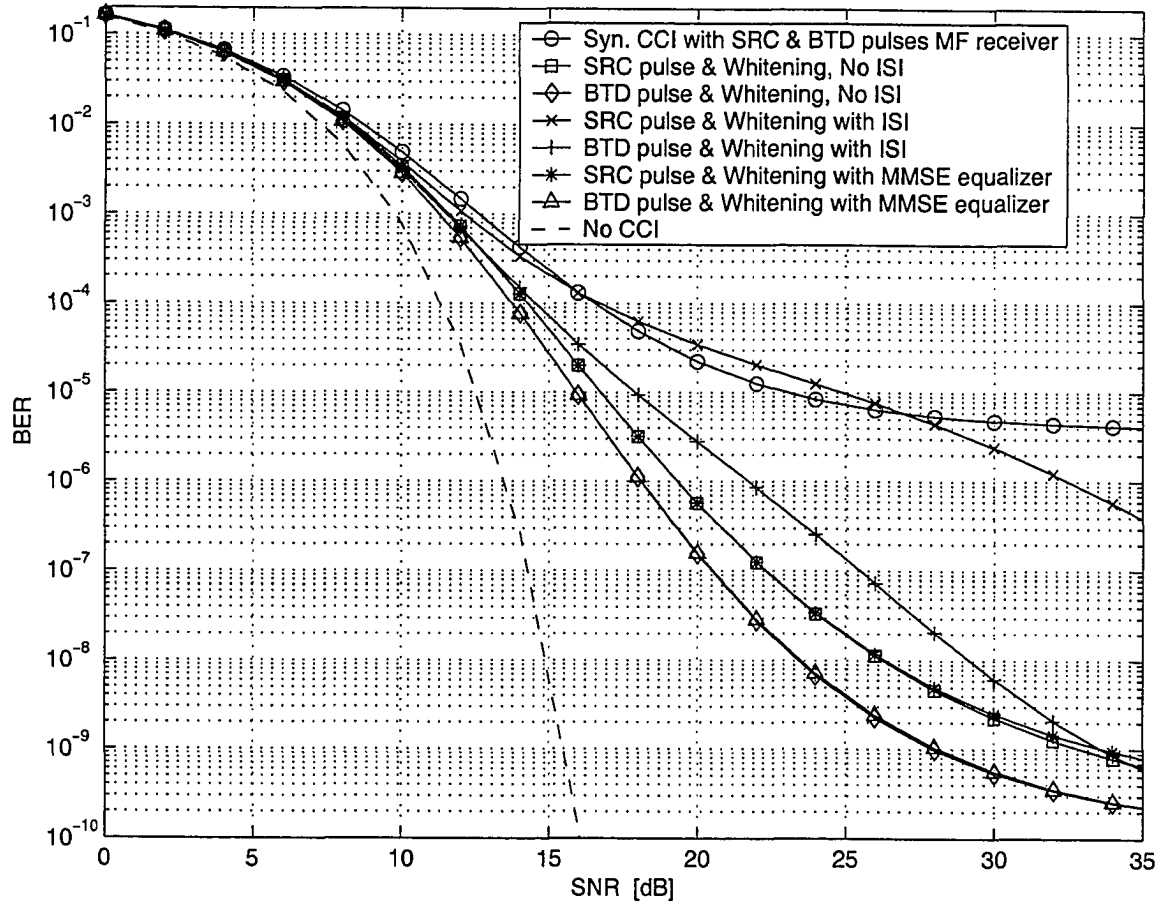


Fig. 2.9. Performance of continuous time WMF with SRC and BTD pulse-shaping, no fading for the desired user,  $SIR = 10$  dB,  $T/4$  spaced MMSE equalizer with 41 taps,  $K = 9$  and synchronous CCI.

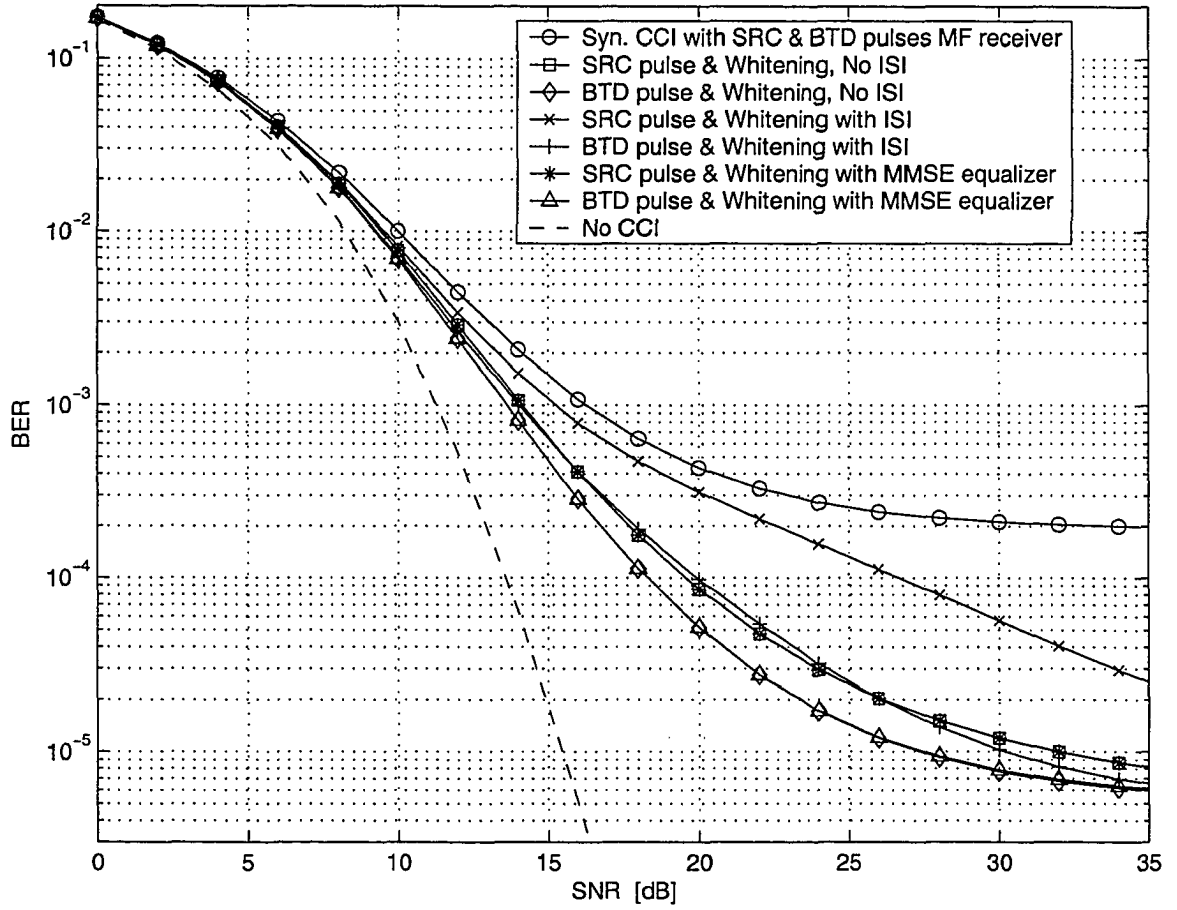


Fig. 2.10. Performance of continuous time WMF with SRC and BTB pulse-shaping,  $m_s = 8$  for the desired user, SIR = 10 dB,  $T/4$  spaced MMSE equalizer with 41 taps,  $K = 9$  and synchronous CCI

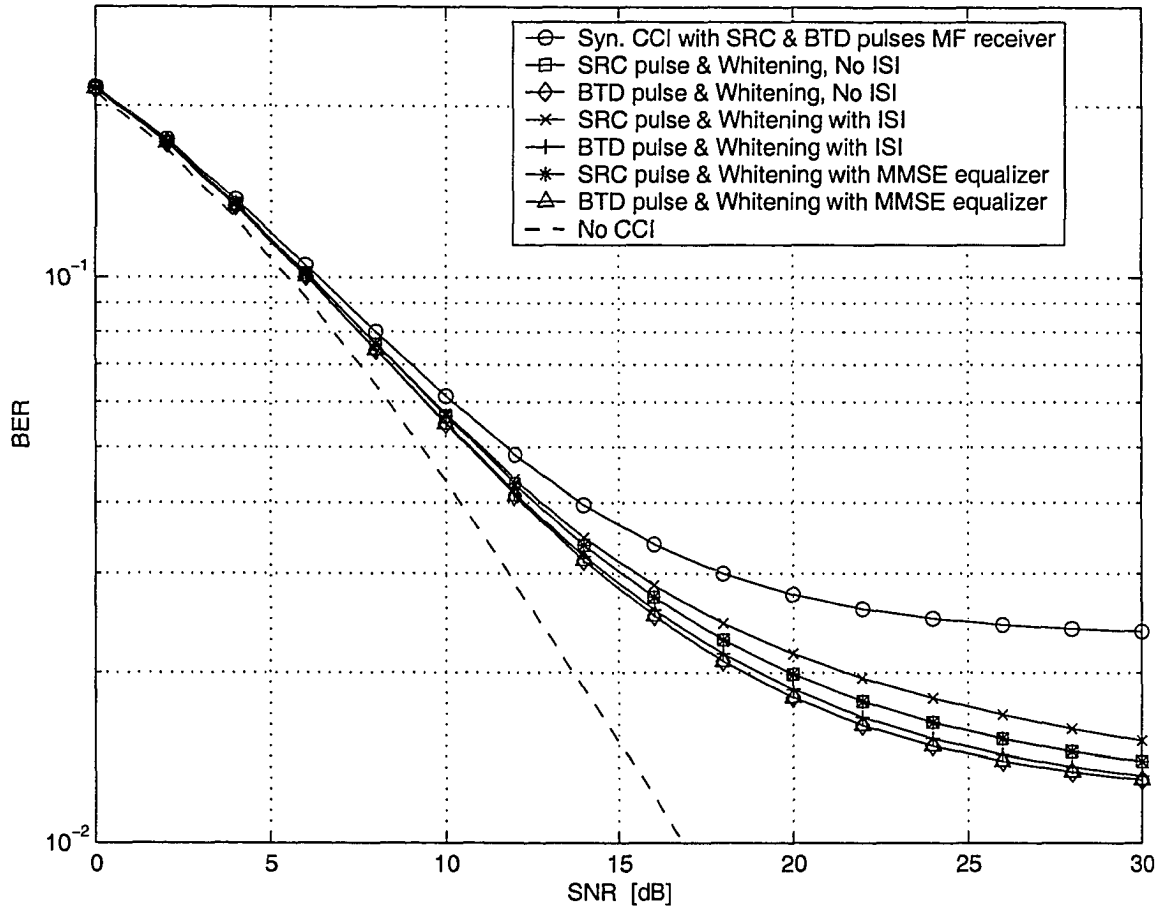


Fig. 2.11. Performance of continuous time WMF with SRC and BTM pulse-shaping, Rayleigh fading for the desired user,  $SIR = 10$  dB and  $T/4$  spaced MMSE equalizer with 41 taps,  $K = 9$  and synchronous CCI.

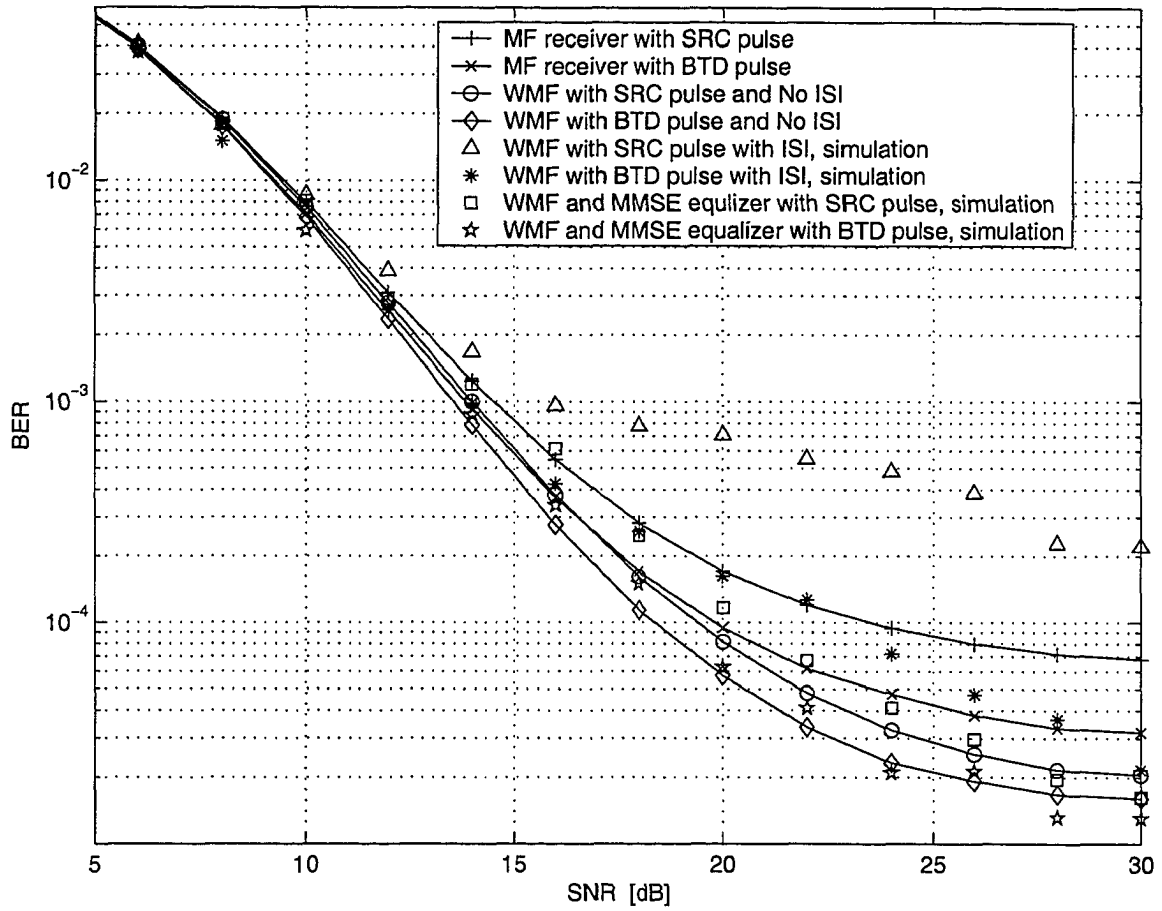


Fig. 2.12. Performance of continuous time WMF with SRC and BTD pulse-shaping,  $m_s = 8$  for the desired user,  $SIR = 10$  dB,  $T/4$  spaced MMSE equalizer with 41 taps and asynchronous CCI.

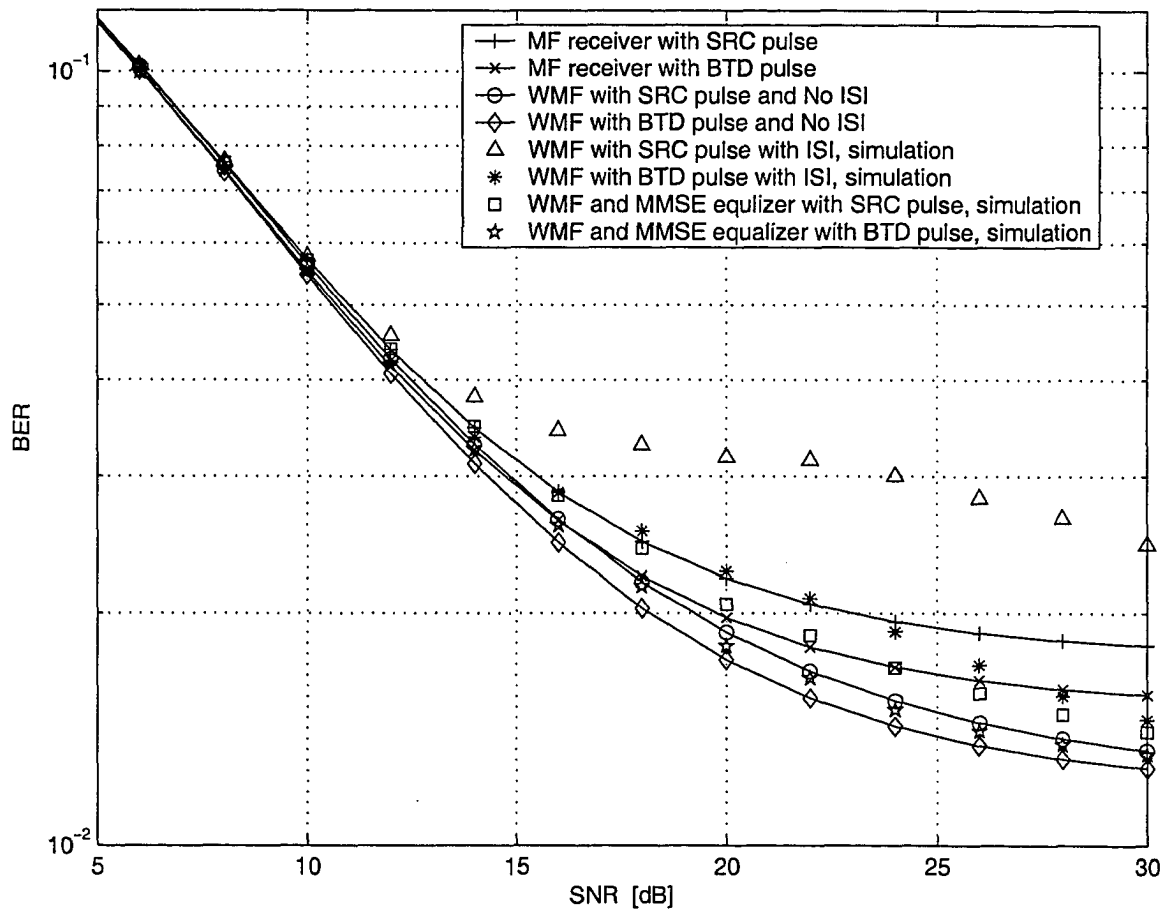


Fig. 2.13. Performance of continuous time WMF with SRC and BTD pulse-shaping, Rayleigh fading for the desired user,  $SIR = 10$  dB,  $T/4$  spaced MMSE equalizer with 41 taps,  $K = 9$  and asynchronous CCI.



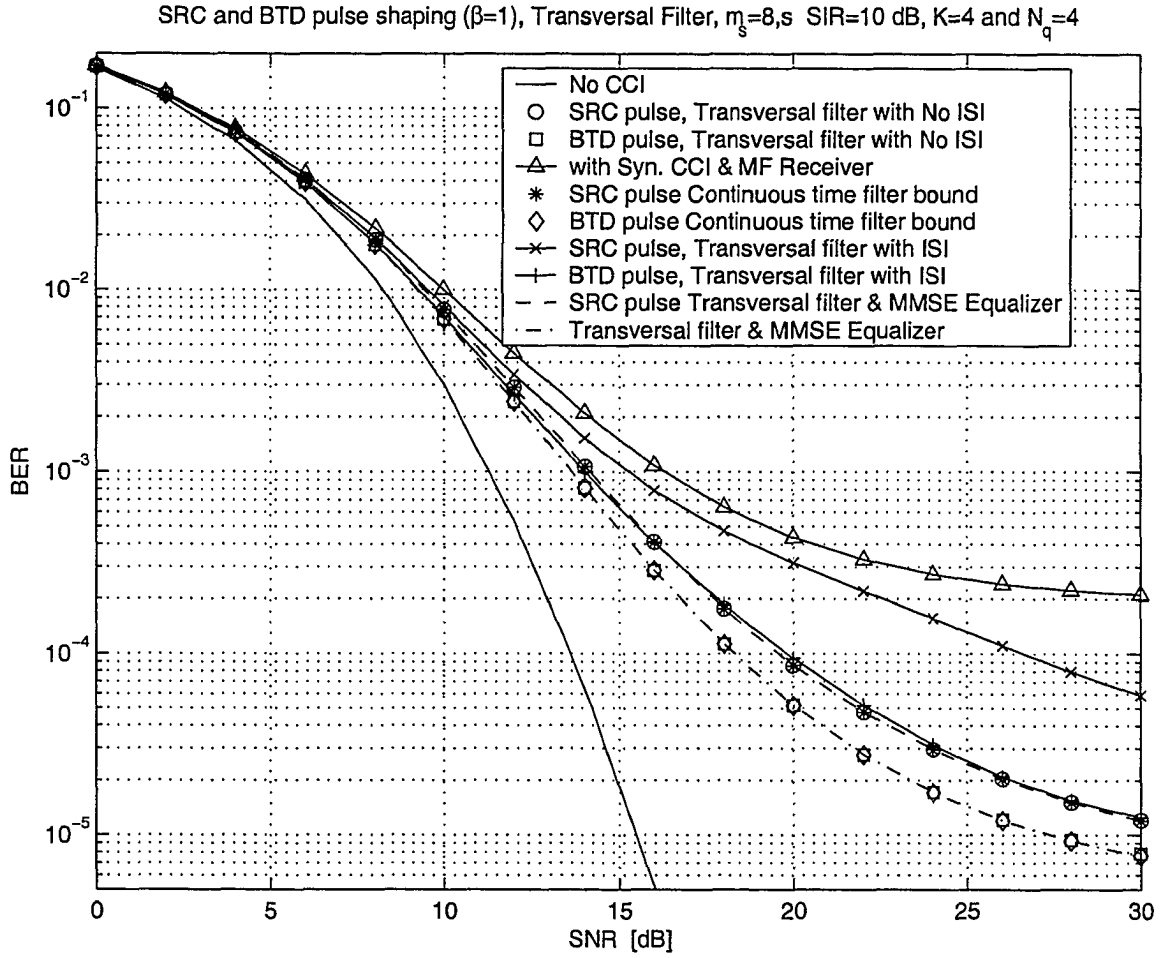


Fig. 2.14. Performance of transversal filter receiver ( $K_e = 4, N_q = 4$ ) with SRC and BTD pulse-shaping,  $m_s = 8$  for the desired user,  $SIR = 10$  dB,  $K = 9$  and synchronous CCI.

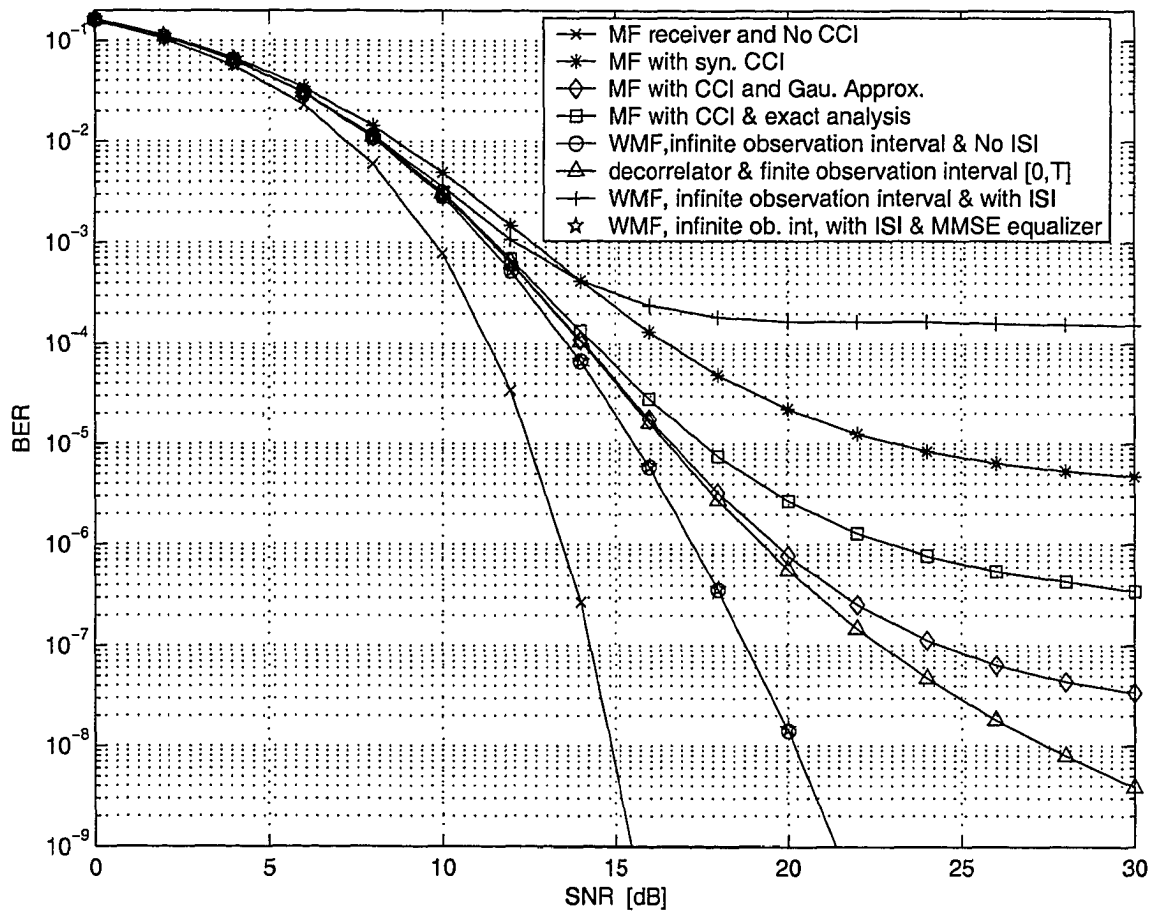


Fig. 2.15. Performance with rectangular pulse-shaping, no fading for the desired user,  $SIR = 10$  dB,  $K = 6$  and  $T/4$  spaced MMSE equalizer with 41 taps

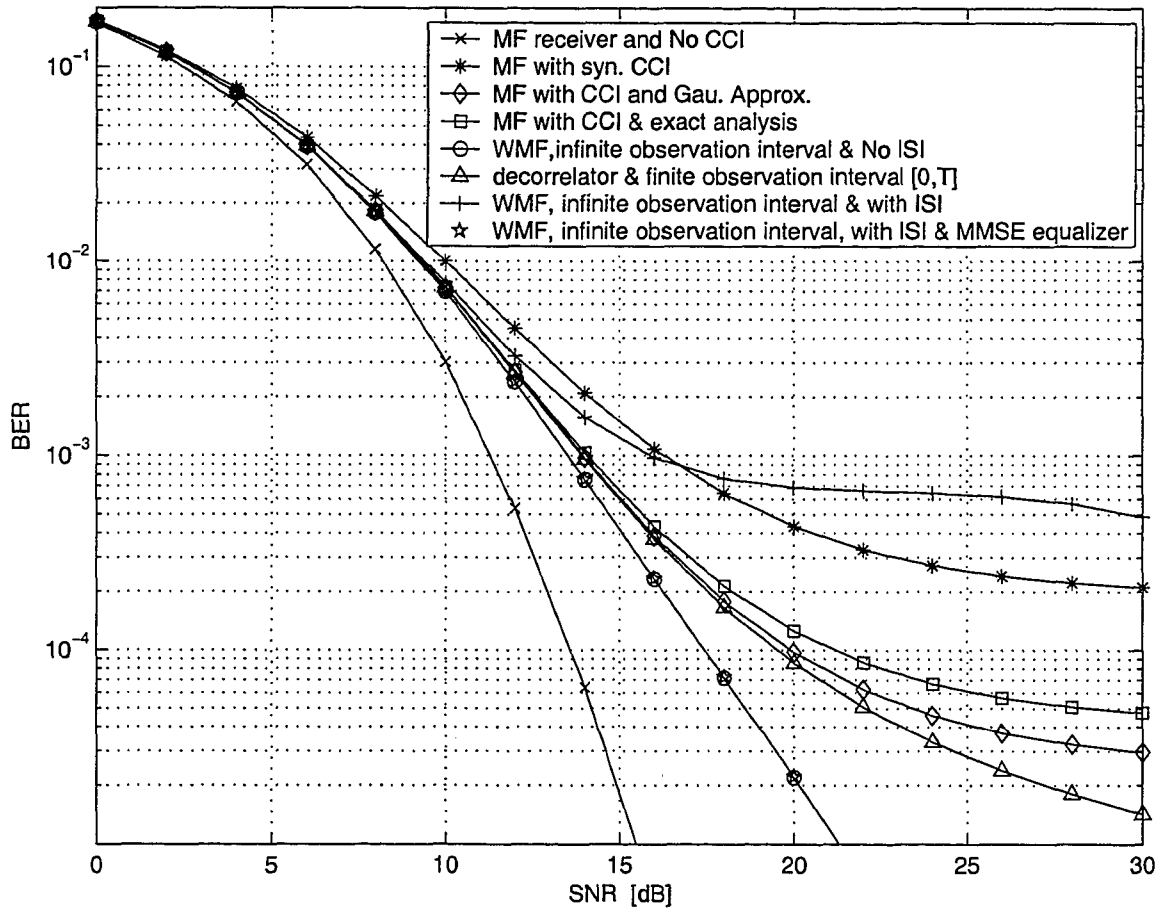


Fig. 2.16. Performance with rectangular pulse-shaping,  $m_s = 8$  for the desired user,  $SIR = 10$  dB,  $K = 6$  and  $T/4$  spaced MMSE equalizer with 41 taps.

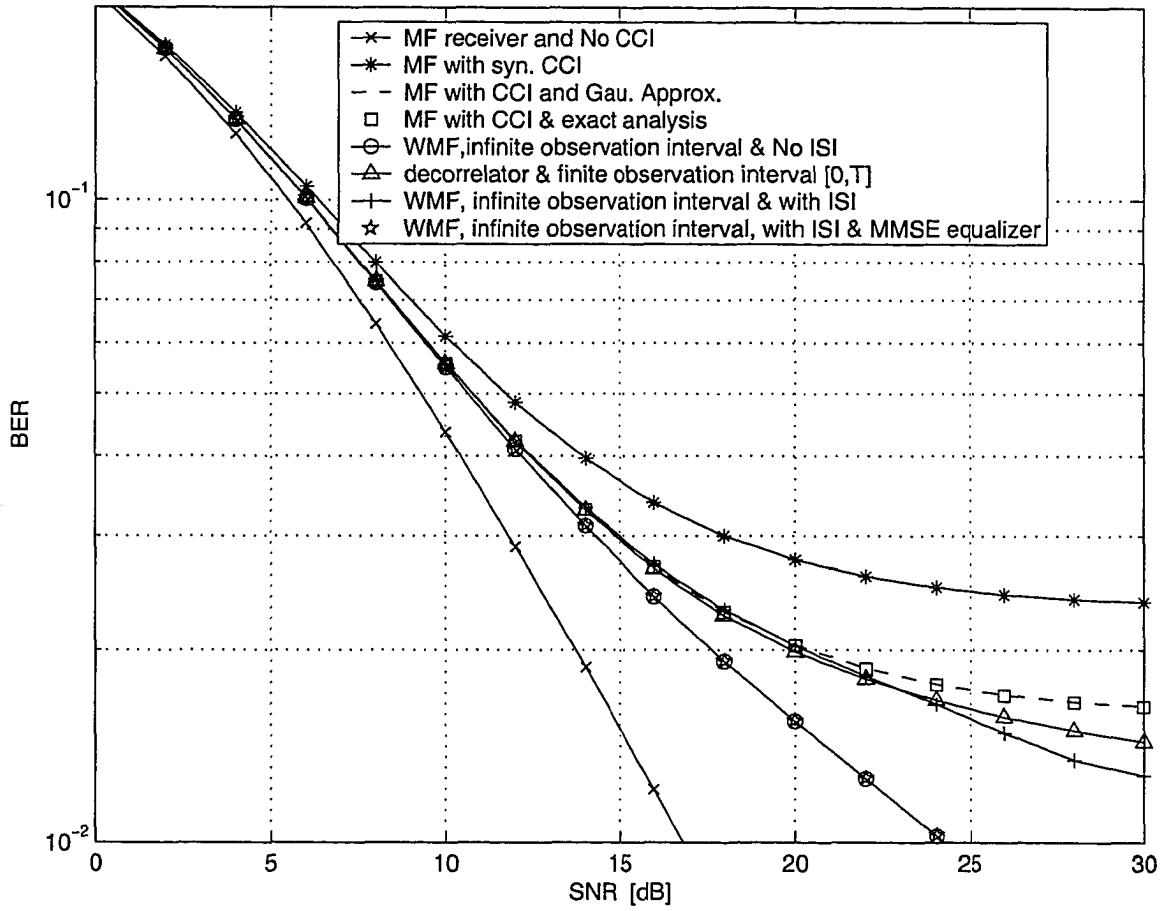


Fig. 2.17. Performance with rectangular pulse-shaping, Rayleigh fading for the desired user,  $SIR = 10$  dB,  $K = 6$  and  $T/4$  spaced MMSE equalizer with 41 taps.

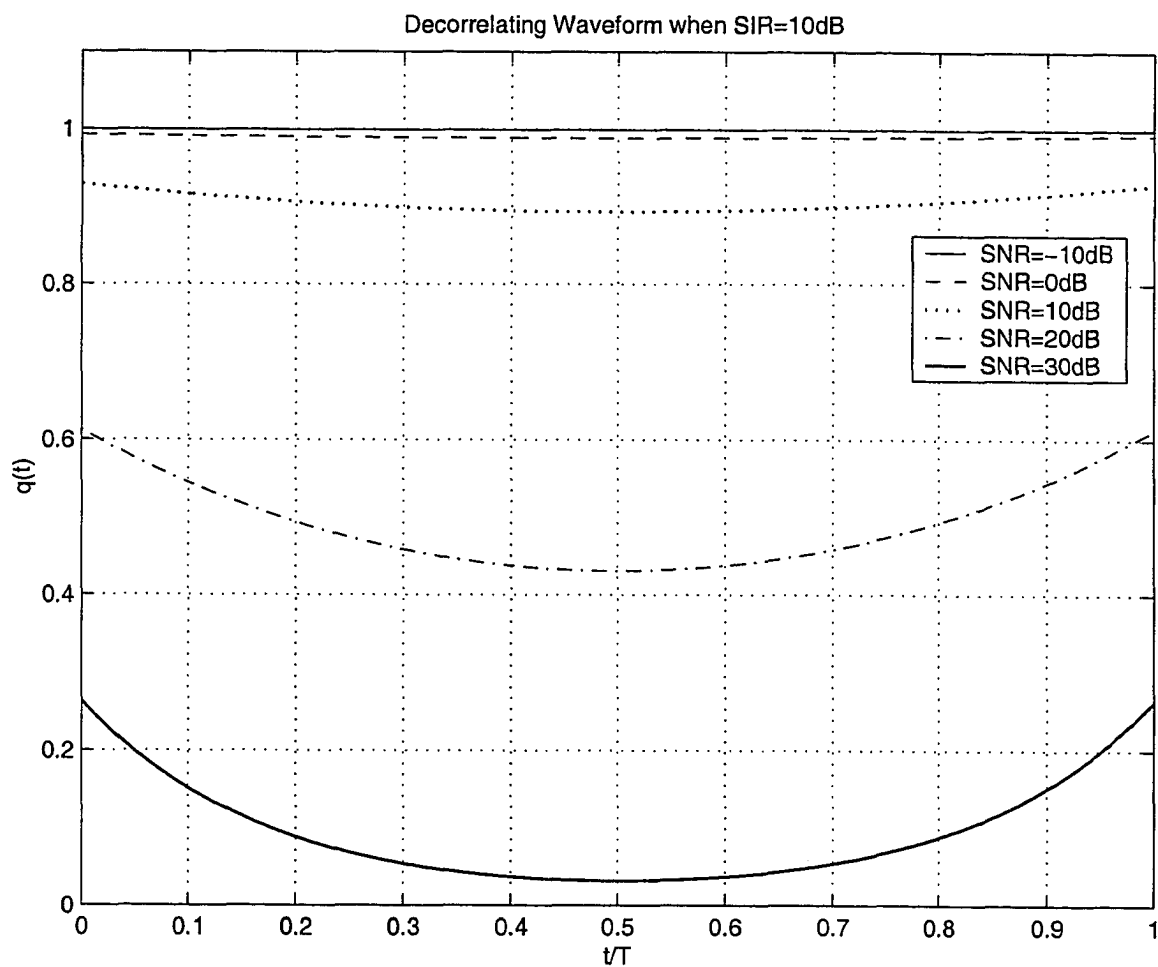


Fig. 2.18. The correlating waveform for finite observation interval  $[0, T]$ ,  $K = 6$  and  $SIR = 10$  dB.

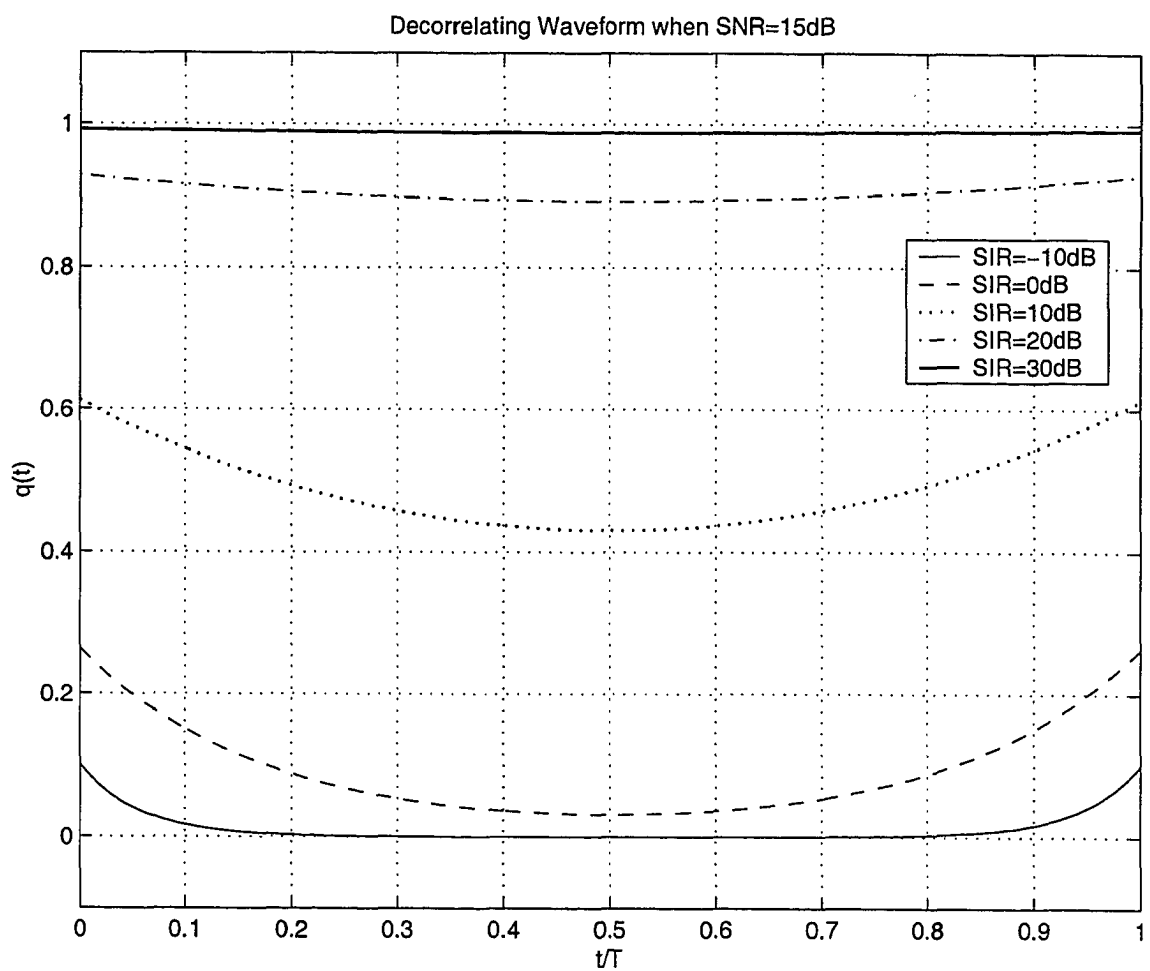


Fig. 2.19. The correlating waveform for finite observation interval  $[0, T]$ ,  $K = 6$  and  $\text{SNR} = 15 \text{ dB}$ .

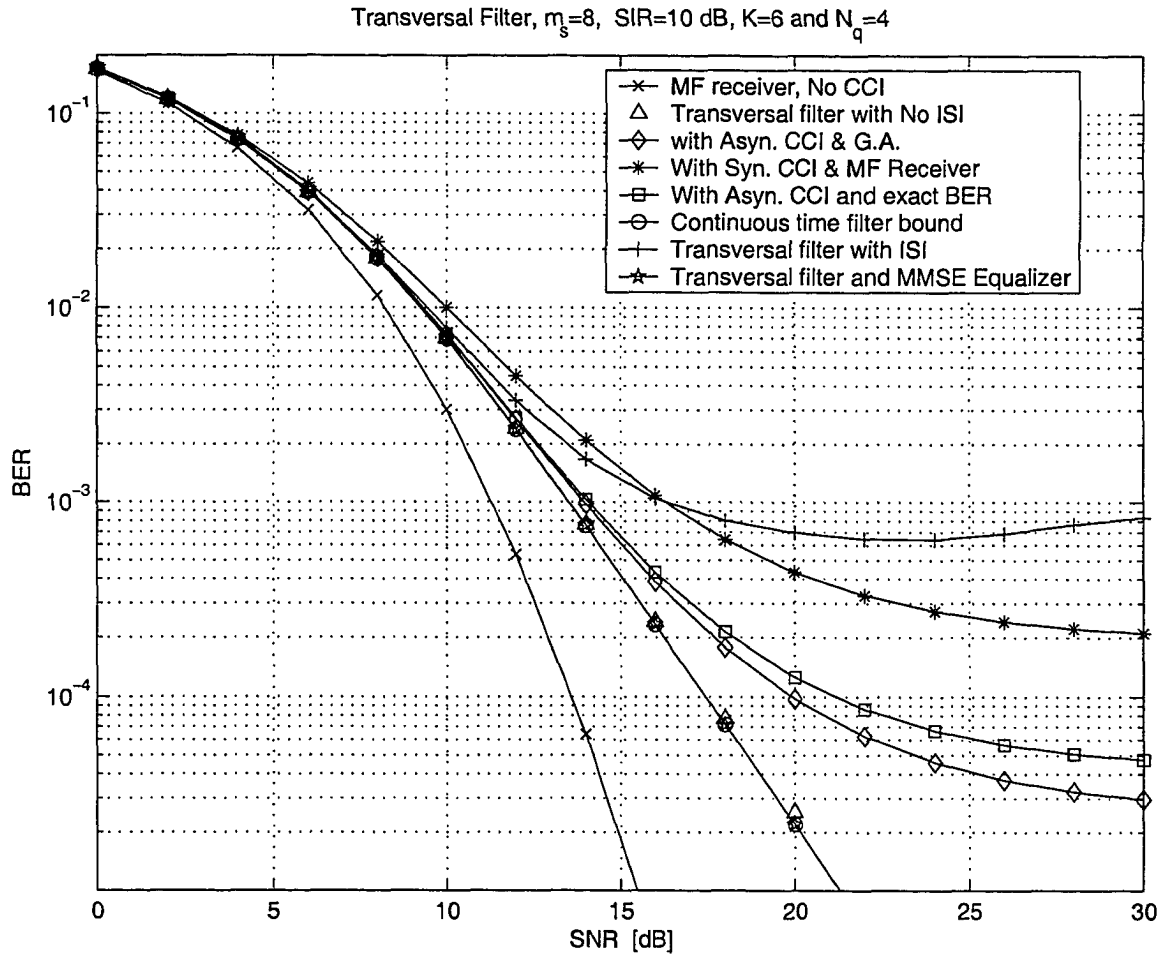


Fig. 2.20. Performance of fractional correlator ( $n_q = 4$ ) and transversal filter ( $K_e = 6$ ) receiver,  $m_s = 8$ , SIR = 10 dB,  $K = 6$  and  $T/4$  spaced linear MMSE equalizer with 41 taps.

Figs. 2.9, 2.10 and 2.11 depict the performance of the BPSK system in the presence of synchronous interferers with no fading,  $m_s = 8$  and Rayleigh fading ( $m_s = 1$ ), respectively for the desired user. The average BER curves presented are as follows: performance of conventional MF receiver with SRC and BTD pulse-shaping; performance of WMF with SRC pulse-shaping for one transmitted symbol; performance of WMF with BTD pulse-shaping for one transmitted symbol; performance of WMF with SRC pulse-shaping for infinitely long transmitted symbols; performance of WMF with BTD pulse-shaping for infinitely long transmitted symbols; performance of WMF and MMSE equalizer receiver structure with SRC pulse-shaping; performance of WMF and MMSE equalizer receiver structure with BTD pulse-shaping; performance of conventional MF receiver without CCI. We make several interesting observations. In a CCI environment, the proposed receiver structure with BTD pulse-shaping performs considerably better than with SRC pulse-shaping. The severity of the ISI introduced by the WMF reduces with the severity of the fading for the desired user. The performance of the WMF and the MMSE equalizer almost attain the optimum performance in all cases considered.

Figs. 2.12 and 2.13 show the performances of the BPSK system in the presence of asynchronous interferers with  $m_s = 8$  and Rayleigh fading ( $m_s = 1$ ), respectively for the desired user. The average BER curves were obtained for the following cases: exact BER performance of conventional MF receiver with SRC and BTD pulse-shaping and of the WMF receiver with one transmitted symbol with SRC and BTD pulse-shaping; BER performance of the WMF and MMSE equalizer with both pulse-shapings using Monte-Carlo computer simulation. We observe that the performance of the receiver with BTD pulse-shaping is considerably better than that with SRC pulse-shaping. The results show that the MMSE equalizer almost removes all the ISI introduced by



the WMF.

Fig. 2.14 presents the performance of the transversal filter (with  $K = 4$  and  $N_q = 4$ ) SNIR maximizing filter and MMSE equalizer receiver structure with synchronous CCI for  $m_s = 8$  for the desired user. The performance of approximate transversal filter receiver structure very closely resembles the performance of the continuous time WMF structure in Fig. 2.9.

### 2.7.2 NRZ Pulse-Shaping

The CCI component in the decision statistic from synchronous slow Rayleigh faded-interferers with the rectangular pulse-shaping is Gaussian distributed. Thus, the Gaussian approximation becomes exact. For the synchronous interferers, the variance of  $I_{CCI}$  with rectangular pulse-shaping is given by

$$\text{VAR}[I_{CCI}] = \frac{T \sum_{i=1}^L \Omega_i P_i}{4}. \quad (2.75)$$

When the asynchronous interferers' signals, with rectangular pulse-shaping, undergo slow Rayleigh fading, the CCI component after the matched filter is not Gaussian distributed due to the nonlinearity introduced by the time offsets. The exact BER expression is derived using the CF method as in Appendix A. Using the Gaussian approximation, the variance of  $I_{CCI}$  is written as

$$\text{VAR}[I_{CCI}] = \mathbb{E}[I_{CCI}^2] = \frac{T \sum_{i=1}^L \Omega_i P_i}{6}. \quad (2.76)$$

Then the total equivalent noise power becomes  $\sigma_t^2 = 1 + \text{VAR}[I_{CCI}]$  and the BER conditioned on  $R_s$ , is given by

$$P_{e|R_s} = \mathbf{Q} \left( \sqrt{\frac{P_s T}{2\sigma_t^2}} R_s \right) \quad (2.77)$$

Then, as shown in eq. (2.23), for arbitrary values of  $m_s$ , the average BER is given by

$$P_{eg} = \frac{\Gamma(m_s + \frac{1}{2})}{2\sqrt{\pi}m_s\Gamma(m_s)} \left( \frac{2m_s}{\Lambda^2\Omega_s} \right)^{m_s} {}_2F_1 \left( m_s, m_s + \frac{1}{2}; m_s + 1, \frac{-2m_s}{\Omega_s\Lambda^2} \right), \quad (2.78)$$

where  $\Lambda^2 = P_s T / (2\sigma_t^2)$ . If we put  $\sigma_t^2 = 1$  in (2.77), the corresponding eq. (6.23) gives the average BER of a BPSK system without CCI.

Again, we assume the transmitted power of the desired and interfering users are equal and  $P_s = P_i = 1$ . However, we can also consider the case of dissimilar powers. Our numerical results are obtained for average SIR = 10 dB.

Figs. 2.15, 2.16 and 2.17 depict the performance of the BPSK system with six interferers and rectangular pulse-shaping, with no fading,  $m_s = 8$  and Rayleigh fading ( $m_s = 1$ ), respectively for the desired user. The average BER curves presented are as follows: MF receiver without CCI; MF receiver with synchronous CCI; Gaussian approximation for the MF receiver with asynchronous CCI; precise BER expression for the MF receiver with asynchronous CCI; WMF with infinite observation interval; correlator with finite observation interval  $[0, T]$ ; WMF with infinite observation interval and ISI and WMF with infinite observation interval and  $T/4$  spaced and 41 taps MMSE equalizer. The lower bound of the BER performance is given by the curve for the WMF with infinite observation interval and one desired user transmitted symbol. We observe that the WMF receiver with MMSE equalizer almost attains the lower bound and, furthermore, the error floor introduced by the fading and CCI is almost removed. In practice, it is not possible to implement a receiver structure with infinite observation interval but it can be approximately implemented with reasonably long delay. The correlator receiver is slightly better than the conventional MF receiver in the large SNR region and the performance gain reduces with the severity of the desired user fading. The correlating waveform  $q(t)$  in (2.50), is dependent on the average SNR and SIR values. Figs. 2.18 and 2.19 show  $q(t)$  for various average SNR

and SIR values. We assume perfect estimates of SNR and SIR are available at the receiver. This is a reasonable assumption because these estimates are also needed for power control and some diversity combining schemes in cellular radio communication. In Fig. 2.18, for fixed SIR, when the average SNR is small, the background noise dominates the CCI and then the receiver becomes a correlation receiver and  $q(t)$  is same as the rectangular pulse. When the SNR is large, the CCI dominates the background noise and then  $1/S_n(\omega)$  is a high pass filter; thus  $q(t)$  becomes a highpass filtered rectangular pulse [27].

Fig. 2.20 presents the performance curves for the approximate WMF receiver structure with fractional correlator and transversal filter. The desired user undergoes Nakagami fading and  $m_s = 8$ . The tap spacing,  $N_q = 4$  and the number of transversal filter taps  $2K_t + 1 = 13$ . The MMSE equalizer is again  $T/4$  spaced and has 41 taps. The average BER curves presented are as follows: MF receiver without CCI; MF receiver with synchronous CCI; transversal filter WMF with no CCI; Gaussian approximation for the MF receiver with asynchronous CCI; exact BER expression for the MF receiver with asynchronous CCI; continuous time WMF with infinite observation interval; transversal filter WMF with ISI; and transversal filter WMF with  $T/4$  spaced and 41 taps MMSE equalizer. We observe that this type of receiver needs a relatively very short observation interval and the performance gain is close to the infinite observation interval receivers.

## 2.8 Summary

The CCI mitigation of BPSK systems in micro-cellular fading environments has been considered in this chapter. The desired user and interfering users undergo slow

Nakagami- $m$  and Rayleigh fading, respectively. Several receiver structures to combat CCI were proposed. Two Nyquist pulse shapes namely, SRC and BTD pulse shapes and the NRZ rectangular pulse shape were considered. An extensive performance comparison study was presented using the CF function and approximate Fourier series methods for a variety of fading situations for the desired user. The proposed whitening receiver structures require only the knowledge of total interference power and the pulse-shaping of the interferers. These parameters may be available in conventional receivers for power control and some diversity combining schemes, for example, maximal ratio combining, etc. Thus, this proposed receiver structure is easily implementable.

## Chapter 3

# Performance Analysis of Bandlimited DS-CDMA Systems in Nakagami Fading Channels

### 3.1 Introduction

Direct sequence code division multiple access (DS-CDMA) systems have good ability to combat interference and fading [1]. Further they have the capability of asynchronous access. Due to these attractive features, bandlimited DS-CDMA is proposed as the major access method in the third generation wireless communication standards. The BER performance of DS-CDMA systems have been extensively studied during the last two decades [19], [33], [55], [56], [57], [58], [59], [60], [32], [61], [62], [63], [64], [65], [66], [67], [68], [69], [70], [71], [72] (and references therein). Most of the reported works focused on the DS-CDMA systems with rectangular pulse-shaping. But in practice, for example, in the CDMA IS-95 standard, a bandlimited chip pulse shape

is employed. Therefore, the performance analysis of such systems is of considerable interest.

There are several methods to estimate the average BER in DS-CDMA systems with bandlimited pulse-shaping and random spreading sequences. The simple and computationally efficient methods are based on Gaussian approximation of the MAI. For systems with bandlimited pulse-shaping, the well known standard Gaussian approximation (SGA) proposed by Pursley in [33] was employed in [55], [56], [57] in AWGN channels. The MAI is treated as a Gaussian random process in the analysis. A computationally complex Gaussian approximation method where the MAI conditioned on interfering user phase offsets and timing offsets is Gaussian distributed, was proposed by Morrow and Lehnert in [32]. A Gaussian approximation method employing a central limit theorem (CLT) for  $n$  correlated identically distributed RVs was proposed by Yoon in [58], [59] and [60]. This was used in combination with a CF method to derive the average BER. The accuracy of the Gaussian approximation was justified using a CLT for ‘ $m$ -dependent sequences’<sup>1</sup>. As observed in [59], the method proposed in [58], [59] and the improved Gaussian approximation (IGA) [32] method give the same results. Simplified improved Gaussian approximation methods were considered by Zang and Ling [61] and Cho *et al.* [62]. In [61], the method proposed by Holtzman in [63] was used for bandlimited signalling. The method proposed in [63] was further improved by using exact derivatives of the Gaussian Q-function in the Taylor series expansion in [62]. The accuracy of the method was discussed using conditional Gaussian approximation of cross-correlation between desired and interfering user spreading sequences. An exact average BER analysis was presented by Yoon in [64] using a CF method. This method is suitable only for systems with

---

<sup>1</sup> $m$ -dependent or weakly dependent sequences and their CLT are discussed in [73], [74]

very short random spreading sequences. In all the above mentioned works with bandlimited pulse shaping, only the AWGN channel was considered. But in practice, fading and MAI are the major factors affecting the performance of the DS-CDMA systems. To the best of our knowledge, there are no reported works investigating the BER performance analysis of the bandlimited DS-CDMA systems in fading channels.

The average BER performance of the DS-CDMA system with rectangular pulse-shaping in frequency selective Nakagami- $m$  fading was investigated in [65] and [66] using the SGA. A coherent RAKE receiver with a BPSK modulation was considered in [65] and a noncoherent RAKE receiver with DPSK modulation was examined in [66]. Cheng and Beaulieu presented an exact evaluation of the average BER using a CF method in flat Rayleigh fading in [67] and in flat Nakagami- $m$  fading with integer  $m$  values in [68].

In this chapter, we study the average BER performance of bandlimited asynchronous binary DS-CDMA systems in Nakagami- $m$  fading. The fading is assumed to be flat and slow. Two types of Nyquist pulse-shapings, namely, SRC and BTD [30] pulse-shapings are considered. The performance of these two pulse shapings are compared under identical system conditions. A new accurate method for computing the BER bandlimited DS-CDMA systems employing random spreading sequences is proposed by incorporating CF method into IGA [32]. A substantial computational complexity reduction is achieved. The results of the proposed method are compared with that obtained using the SGA, Holtzman's simplified improved Gaussian approximation and the improved Holtzman's Gaussian approximation. The accuracies of the results are assessed using Monte Carlo computer simulation. The CF method proposed in [64] is extended to derive the exact average BER expressions for a system with a deterministic desired user spreading sequence and random interfering user

spreading sequences.

The remainder of this chapter is organized as follows. In Section 3.2, the system and channel model are introduced and the receiver decision statistic is presented. The average BER analysis using the Gaussian approximation is presented in Section 3.3. The BER analysis using the CF method is considered in Section 3.4. The numerical results are provided in Section 3.5. A summary of this chapter is presented in Section 3.6.

## 3.2 System and Channel Model

A general asynchronous bandlimited binary DS-CDMA system with  $K + 1$  active users in Nakagami- $m$  fading is considered. We adopt the system model presented in [59], [60] with some modifications to incorporate the fading. Using the complex baseband representation, the received signal is written as

$$r(t) = \sum_{k=0}^K s_k(t) + w(t) \quad (3.1)$$

where  $-\infty < t < +\infty$  and  $w(t)$  is a complex, circularly symmetric [75], zero-mean white Gaussian process with power spectral density  $N_0$ . The  $k$ -th user received signal  $s_k(t)$  is given by

$$s_k(t) = \sqrt{P_k} R_k e^{j\theta_k} \sum_{i=-\infty}^{\infty} b_i^{(k)} a_i^{(k)}(t - \tau_k - iT_b) \quad (3.2)$$

where  $b_i^{(k)} \in [+1, -1]$  are the equiprobable  $k$ -th user bits transmitted at rate  $1/T_b$ ,  $P_k$  is the transmitted signal power of  $k$ -th user and  $\tau_k \sim \mathcal{U}[0, T_b]$  is the timing offset with respect to (wrt) the desired user. The phase offset wrt to the desired user is denoted as  $\theta_k \sim \mathcal{U}[0, 2\pi]$ . The  $k$ -th user fading amplitude  $R_k$ , is assumed to be Nakagami- $m$  distributed with parameters  $[m, \Omega]$  and its PDF is given in eq. (1.11). The fading



is assumed to be slow; thus, coherent reception is feasible. The desired user received signal is denoted as  $s_0(t)$  and without loss of generality, we can assume  $\tau_0 = 0$  and  $\theta_0 = 0$ . The spreading waveform  $a_i^{(k)}(t)$  for  $b_i^{(k)}$ , is

$$a_i^{(k)}(t) = \sum_{n=0}^{N-1} a_{n+iN}^{(k)} q(t - nT_c) \quad (3.3)$$

where the  $n$ -th chip of the  $k$ -th user PN sequence is  $a_n^{(k)} \in [+1, -1]$ . The rate of PN sequence is  $1/T_c$ . The processing gain or spreading factor is given by  $T_b/T_c = N$ . The random variable sets  $\{\tau_k\}$ ,  $\{\theta_k\}$ ,  $\{b_i^{(k)}\}$  and  $\{R_k\}$  are mutually independent and the elements of each set are assumed to be independent and identically-distributed (iid). The received baseband chip pulse is denoted as  $q(t)$  and it satisfies  $\int_{-\infty}^{\infty} |q(t)|^2 dt = T_c$ . We consider two types of Nyquist pulses in this chapter namely, the SRC [7] and the BTD pulse shapes [30]. They are given in eqs. (2.11), (2.12), (2.13) and (2.14). We assume the excess bandwidth of the pulse shape,  $\beta = 1$  in this chapter. However, our analysis is applicable to a system with any  $\beta \in [0, 1]$ . For notational convenience when  $k \neq 0$ , eq. (3.2) is written as

$$s_k(t) = \sqrt{P_k} R_k e^{j\theta_k} \sum_{n=-\infty}^{\infty} d_n^{(k)} q(t - T_k - nT_c) \quad (3.4)$$

where  $d_n^{(k)} \in [+1, -1]$  and  $T_k = \text{mod}(\tau_k, T_c)$ . The  $d_n^{(k)}$  and  $T_k$  can be modeled as iid equiprobable RV's and iid uniform RV's in  $[0, T_c]$ , respectively [59].

In the coherent receiver [59], the received signal is passed through matched filter  $Q^*(f)$ , a sampler, a despreader, a summer and a real operator function to generate the decision statistic. The bit decision statistic is then written as

$$y_i^{(0)} = \mathcal{Re} \left( \sum_{l=iN}^{(i+1)N-1} a_l^{(0)} \int_{-\infty}^{\infty} r(lT_c - u) q(-u) du \right). \quad (3.5)$$

The estimate of the transmitted bit is then obtained by  $\hat{b}_i^{(0)} = \text{sgn}(y_i^{(0)})$ . Then, the

decision statistic is written as

$$y_i^{(0)} = \sqrt{P_0} R_0 T_b b_i^{(0)} + \mathcal{M} + \eta \quad (3.6)$$

where  $\eta$  is a zero-mean Gaussian process with variance  $N_0 T_b/2$ . The MAI component is given by

$$\mathcal{M} = \sum_{k=1}^K \mathcal{M}_k \quad (3.7)$$

$$\mathcal{M}_k = \sqrt{P_k} R_k \cos(\theta_k) T_c \sum_{l=0}^{N-1} \sum_{n=-\infty}^{\infty} a_l^{(0)} d_n^{(k)} g((l-n)T_c - T_k) \quad (3.8)$$

where  $g(t) = \mathcal{F}^{-1}[|Q(f)|^2/T_c]$  and is given by (2.12) and (2.14). The average signal-to-noise ratio is defined as

$$SNR = \frac{P_0 T_b \Omega}{N_0 T_b/2} = \frac{2P_0 \Omega}{N_0}. \quad (3.9)$$

### 3.3 BER Analysis Using Gaussian Approximations

In this section, we consider four Gaussian approximation methods. They are the characteristic function improved Gaussian approximation (CFIGA) method, the standard Gaussian approximation (SGA) [33], Holtzman's simplified improved Gaussian approximation (HSIGA) [63], and the improved Holtzman's Gaussian approximation (IHGA) [62].

#### 3.3.1 Characteristic Function Improved Gaussian Approximation (CFIGA)

A new characteristic function improved Gaussian approximation method is presented in this subsection by incorporating the CF method into the IGA proposed by Morrow and Lehnert [32].

In the improved Gaussian approximation method [32], the MAI conditioned on interferer chip delays,  $\mathbf{T} = \{T_1, \dots, T_k\}$  and  $\mathbf{\mathcal{X}} = \{R_1 \cos(\theta_1), \dots, R_K \cos(\theta_K)\}$  is assumed to be a zero-mean Gaussian random variable. Now, the average BER conditioned on  $\mathbf{T}$ ,  $\mathbf{\mathcal{X}}$ , and  $R_0$  is written as

$$P_{IGA|\mathbf{T}, \mathbf{\mathcal{X}}, R_0} = \mathbf{Q} \left( \sqrt{\frac{P_0 R_0^2 N^2 T_c^2}{\text{VAR}[\eta] + \text{VAR}[\mathcal{M}|\mathbf{T}, \mathbf{\mathcal{X}}]}} \right) \quad (3.10)$$

where

$$\text{VAR}[\mathcal{M}|\mathbf{T}, \mathbf{\mathcal{X}}] = \sum_{k=1}^K \sigma_{\mathcal{M}a_k|\mathcal{X}_k, T_k}^2 \quad (3.11)$$

and

$$\begin{aligned} \sigma_{\mathcal{M}a_k|\mathcal{X}_k, T_k}^2 &= \Psi_k = NP_k \mathcal{X}_k^2 T_c^2 \sum_{i=-\infty}^{\infty} g^2(iT_c - T_k) \\ &= NP_k \mathcal{X}_k^2 T_c^2 \lim_{M \rightarrow \infty} \sum_{i=-M}^M g^2(iT_c - T_k) \\ &= NP_k \mathcal{X}_k^2 T_c^2 \lim_{M \rightarrow \infty} \sum_{i=-M}^M \int_{-\infty}^{\infty} G(f) e^{j2\pi f(iT_c - T_k)} df \\ &= NP_k \mathcal{X}_k^2 T_c^2 \lim_{M \rightarrow \infty} \int_{-\infty}^{\infty} G(f) e^{-j2\pi f T_k} \sum_{i=-M}^M e^{j2\pi f i T_c} df \\ &= NP_k \mathcal{X}_k^2 T_c^2 \lim_{M \rightarrow \infty} \int_{-\infty}^{\infty} G(f) e^{-j2\pi f T_k} \frac{\sin(\pi(2M+1)f)}{\sin(\pi f)} df. \end{aligned} \quad (3.12)$$

From [62], [7] for bandlimited Nyquist pulse shapes with excess bandwidth  $0 \leq \beta \leq 1$ , eq. (3.13) can be written as

$$\sigma_{\mathcal{M}a_k|\mathcal{X}_k, T_k}^2 = NP_k \mathcal{X}_k^2 T_c^2 \left[ G(0) + 2G\left(\frac{1}{T_c}\right) \cos(2\pi T_k) \right] \quad (3.14)$$

where  $G(f) = \mathcal{F}[g^2(t)]$ . The Nyquist criterion implies  $G(0) + 2G\left(\frac{1}{T_c}\right) = 1$ . Then,

$$\sigma_{\mathcal{M}a_k|\mathcal{X}_k, T_k}^2 = NP_k \mathcal{X}_k^2 T_c^2 \left[ 1 - \frac{\zeta\beta}{2} + \frac{\zeta\beta \cos(2\pi T_k)}{2} \right] \quad (3.15)$$

where  $\zeta = 2 \left[ 1 - \frac{1}{T_c^2} \int_{-\infty}^{\infty} |Q(f)|^4 df \right] / \beta$ . The unconditional average BER for arbitrary  $m$  is given by

$$P_{IGA} = \frac{2}{\Gamma(m)} \left( \frac{m}{\Omega} \right)^m \int_0^\infty \int_0^\infty \mathbf{Q} \left( \sqrt{\frac{P_0 r^2 N^2 T_c^2}{\text{VAR}[\eta] + \text{VAR}[\mathcal{M}|\mathbf{T}, \mathcal{X}]}} \right) \times \\ r^{2m-1} e^{-\frac{m r^2}{\Omega}} f_J(y) dy dr \quad (3.16)$$

where  $f_J(y)$  is joint PDF of random variables  $\mathbf{T}$  and  $\mathcal{X}$  and its derivation is given in [59] and [32]. The evaluation of the joint PDF  $f_J(y)$  requires  $(K-1)$ -fold convolution. Thus, (3.16) needs  $(K+1)$ -fold numerical integration. It is computationally very complex.

Now, we propose a new CF improved Gaussian approximation method by incorporating the CF method [67] into the IGA [32]. It is interesting to note that this method and the method proposed in [59], [73] using a CLT for  $m$ -dependent random sequences give quite similar results. The CF of the  $k$ -th user MAI,  $\mathcal{M}_k$ , conditioned on  $\mathcal{X}_k$  and  $T_k$  is written as

$$\Phi_{\mathcal{M}_{a_k}}(\omega|\mathcal{X}_k, T_k) = \exp \left( -\frac{\omega^2 \sigma_{\mathcal{M}_{a_k}|\mathcal{X}_k, T_k}^2}{2} \right). \quad (3.17)$$

Then averaging out  $\mathcal{X}_k$  and  $T_k$ , we get [76]

$$\begin{aligned} \Phi_{\mathcal{M}_{a_k}}(\omega) &= \frac{2}{T_c} \int_0^{T_c} \int_0^\infty \exp \left( -\frac{\omega^2 \sigma_{\mathcal{M}_{a_k}|\mathcal{X}_k, T_k}^2}{2} \right) f_{\mathcal{X}_k}(x) dx dT_k \\ &= \frac{2}{T_c} \int_0^\infty \exp \left( \frac{-\omega^2 N P_k x^2 T_c^2}{2} \left[ 1 - \frac{\zeta \beta}{2} \right] \right) I_0 \left( \frac{\omega^2 N P_k x^2 T_c^2 \zeta \beta}{4} \right) f_{\mathcal{X}_k}(x) dx \end{aligned} \quad (3.18)$$

where  $I_0(\cdot)$  is the modified Bessel function of zero order and (3.18) results by assuming the normalized chip duration,  $T_c = 1$ . The PDF,  $f_{\mathcal{X}_k}(x)$ , is the PDF of the in-phase component of the Nakagami random variable. It can be written as [45]

$$f_{\mathcal{X}_k}(x) = \frac{1}{\sqrt{\pi} \Gamma(m)} \left( \frac{m}{\Omega} \right)^m |x|^{2m-1} e^{-\frac{m x^2}{\Omega}} \Psi \left( \frac{1}{2}; m + \frac{1}{2}; \frac{m x^2}{\Omega} \right) \quad (3.19)$$

where  $\Psi(\cdot)$  is Kummer-U function and it can also be written as the weighted sum of two confluent hypergeometric functions [76]

$$f_{\mathcal{X}_k}(x) = \frac{\Gamma(m - \frac{1}{2})}{\pi\Gamma(m)} \sqrt{\frac{m}{\Omega}} {}_1F_1\left(\frac{1}{2}; \frac{3}{2} - m; \frac{-mx^2}{\Omega}\right) + \frac{\Gamma(\frac{1}{2} - m)}{\pi\sqrt{\pi}} \left(\frac{m}{\Omega}\right)^m (x^2)^{m-\frac{1}{2}} \sin(m\pi) {}_1F_1\left(m; m + \frac{1}{2}; \frac{-mx^2}{\Omega}\right) \quad (3.20)$$

where the second term is zero when the fading parameter  $m$  takes on integer values.

The CF of the total MAI is given by

$$\Phi_{\mathcal{M}_a}(\omega) = \prod_{k=1}^K \Phi_{\mathcal{M}_{a_k}}(\omega). \quad (3.21)$$

The average BER conditioned on  $R_0$  for the desired user is [45]

$$\begin{aligned} P_{IGA|R_0} &= \Pr\left[\sqrt{P_0}R_0T_b b_i^{(0)} + \mathcal{M} + \eta < 0 | b_i^{(0)} = +1\right] \\ &= \frac{1}{2} - \frac{1}{\pi} \int_0^\infty \Phi_{\mathcal{M}}(\omega) \Phi_{\eta}(\omega) \frac{\sin(\sqrt{P_0}R_0T_b\omega)}{\omega} d\omega. \end{aligned} \quad (3.22)$$

The unconditional average BER for arbitrary values of fading parameter  $m$  is written as [45], [46]

$$P_{IGA} = \frac{1}{2} - \frac{\Gamma(m + \frac{1}{2})}{\pi\Gamma(m)} \sqrt{\frac{P_0 T_b^2 \Omega}{m}} \int_0^\infty \Phi_{\mathcal{M}_a}(\omega) \Phi_{\eta}(\omega) {}_1F_1\left(m + \frac{1}{2}; \frac{3}{2}; \frac{-P_0 T_b^2 \Omega \omega^2}{4m}\right) d\omega. \quad (3.23)$$

where the CF of the AWGN component,  $\Phi_{\eta}(\omega) = \exp(-\frac{\omega^2 N_0 T_b}{4})$  and  ${}_1F_1(\cdot; \cdot; \cdot)$  is the confluent hypergeometric function. Comparing (3.23) with (3.16) the  $(K + 1)$ -fold numerical integration is reduced to a 2-fold numerical integration.

### 3.3.2 Standard Gaussian Approximation (SGA)

The SGA proposed by Pursley [33] has been widely used for its computational simplicity. However, it overestimates the system performance [32]. In the SGA, the MAI

is modeled as a zero-mean Gaussian random variable with variance,  $\text{VAR}[\mathcal{M}]$  where

$$\text{VAR}[\mathcal{M}] = \frac{\Omega N T_c^2 X_q}{2} \sum_{k=1}^K P_k \quad (3.24)$$

and

$$X_q = \frac{1}{T_c^3} \int_{-1/T_c}^{+1/T_c} |Q(f)|^4 df. \quad (3.25)$$

For SRC and BTD pulse-shapings, the  $X_q$  values are given by  $(1 - \beta/4)$  and  $(1 - \beta/(4\ln\{2\}))$ , respectively for arbitrary excess bandwidth  $\beta$  [45]. The BER conditioned on  $R_0$  can be written as

$$P_{SGA|R_0} = \mathbf{Q} \left( \sqrt{\frac{P_0 R_0^2 N^2 T_c^2}{\text{VAR}[\eta] + \text{VAR}[\mathcal{M}]}} \right) \quad (3.26)$$

where  $\mathbf{Q}(x) = \frac{1}{\sqrt{2\pi}} \int_x^\infty e^{-\frac{y^2}{2}} dy$ . The unconditional average BER for arbitrary values of fading parameter  $m$  is given by [46]

$$P_{SGA} = \frac{\Gamma(m + \frac{1}{2})}{2\sqrt{\pi}m\Gamma(m)} \left( \frac{2m}{\Lambda^2 \Omega} \right)^m {}_2F_1 \left( m, m + \frac{1}{2}; m + 1; \frac{-2m}{\Omega \Lambda^2} \right) \quad (3.27)$$

where  $\Lambda^2 = P_0 N^2 T_c^2 / (\text{VAR}[\eta] + \text{VAR}[\mathcal{M}])$ .

### 3.3.3 Holtzman's Simplified Improved Gaussian Approximation (HSIGA)

In the SIGA, the IGA [32] is simplified by taking only a few terms in the Taylor series expansion of  $f_J(y)$  to average the conditional BER. In [63], the terms involving the first two moments of  $f_J(y)$  are considered. Assume that  $f(x)$  is a real function of variable  $x$  with mean  $\mu$  and variance  $\sigma^2$ . Assuming the derivatives of  $f(x)$  exist, we expand  $f(x)$  around  $\mu$  using the Taylor series. It becomes

$$f(x) = f(\mu) + f'(\mu)(x - \mu) + \frac{f''(\mu)}{2}(x - \mu)^2 + \dots \quad (3.28)$$

Then, the expected value of  $f(x)$  is written as

$$\mathbb{E}[f(x)] = f(\mu) + \frac{f''(\mu)}{2}\sigma^2 + \dots \quad (3.29)$$

Neglecting all terms that do not contain the first two moments, (3.29) becomes

$$\mathbb{E}[f(x)] \approx f(\mu) + \frac{f''(\mu)}{2}\sigma^2. \quad (3.30)$$

Now, writing a central difference formula for the second derivative, yields

$$\begin{aligned} \mathbb{E}[f(x)] &\approx f(\mu) + \frac{f(\mu+h) - 2f(\mu) + f(\mu-h)}{2h^2}\sigma^2 \\ &\approx \frac{2}{3}f(\mu) + \frac{1}{3}f(\mu+\sqrt{3}\sigma) + \frac{1}{3}f(\mu-\sqrt{3}\sigma) \end{aligned} \quad (3.31)$$

where  $h = \sqrt{3}\sigma$  [63]. If we use this result for the BER conditioned on  $R_0$  in the improved Gaussian approximation, it is written as a sum of three weighted Gaussian  $\mathbf{Q}(\cdot)$  functions,

$$P_{HSIGA|R_0} = \frac{2}{3}\mathbf{Q}\left(\sqrt{\frac{P_0 R_0^2 N^2 T_c^2}{\mu}}\right) + \frac{1}{6}\mathbf{Q}\left(\sqrt{\frac{P_0 R_0^2 N^2 T_c^2}{\mu + \sqrt{3}\sigma}}\right) + \frac{1}{6}\mathbf{Q}\left(\sqrt{\frac{P_0 R_0^2 N^2 T_c^2}{\mu - \sqrt{3}\sigma}}\right) \quad (3.32a)$$

where

$$\mu = \sum_{k=1}^K \mathbb{E}[\Psi_k] + \frac{N_0 T_b}{2} \quad (3.32b)$$

$$\sigma^2 = \sum_{k=1}^K \mathbb{E}[\Psi_k^2] - (\mathbb{E}[\Psi_k])^2. \quad (3.32c)$$

The parameters  $\mu$  and  $\sigma^2$  are derived in Appendix D. The unconditional average BER for arbitrary  $m$  is approximated by

$$\begin{aligned} P_{HSIGA} = & \frac{\Gamma(m + \frac{1}{2})}{2\sqrt{\pi}m\Gamma(m)} \left\{ \frac{2}{3} \left( \frac{2m}{\Lambda^2 \Omega} \right)^m {}_2\mathbf{F}_1 \left( m, m + \frac{1}{2}; m + 1; \frac{-2m}{\Omega \Lambda^2} \right) + \right. \\ & \frac{1}{6} \left( \frac{2m}{\Lambda_1^2 \Omega} \right)^m {}_2\mathbf{F}_1 \left( m, m + \frac{1}{2}; m + 1; \frac{-2m}{\Omega \Lambda_1^2} \right) + \\ & \left. I_{[0,\infty)}(\Lambda_2^2) \frac{1}{6} \left( \frac{2m}{\Lambda_2^2 \Omega} \right)^m {}_2\mathbf{F}_1 \left( m, m + \frac{1}{2}; m + 1; \frac{-2m}{\Omega \Lambda_2^2} \right) \right\} \end{aligned} \quad (3.33)$$

where  $\Lambda^2 = P_0 N^2 T_c^2 / \mu$ ,  $\Lambda_1^2 = P_0 N^2 T_c^2 / (\mu + \sqrt{3}\sigma)$ ,  $\Lambda_2^2 = P_0 N^2 T_c^2 / (\mu - \sqrt{3}\sigma)$  and  $I_A(x)$  is the indicator function taking value 1 when  $x \in A$ , otherwise, value 0. The computational complexity of the HSGA is about 3 times greater than that of the SGA (compare (3.27) with (3.33).)

### 3.3.4 Improved Holtzman's Gaussian Approximation (IHGA)

In this subsection, we consider another simplified improved Gaussian approximation method [62] for DS-CDMA systems in Nakagami fading. This method and the method proposed in [63] are very similar except in the way the Taylor series expansion is employed. The MAI conditioned on  $\mathbf{T}$  and  $\mathcal{X}$  is assumed to be Gaussian distributed. The average BER for BPSK spreading is written as

$$P_{IHGA} = \mathbb{E}_{R_0, \mathcal{X}, \mathbf{T}} \left[ \mathbf{Q} \left( \sqrt{\frac{P_0 R_0^2 N^2 T_c^2}{Y}} \right) \right] \quad (3.34)$$

where

$$Y = \frac{N_0 T_b}{2} + \sum_{k=1}^K P_k \mathcal{X}_k^2 T_c^2 N \sum_{i=-\infty}^{+\infty} g^2(iT_c - T_k). \quad (3.35)$$

From the analysis in [77], (3.35) can be written as

$$Y = \frac{N_0 T_b}{2} + \sum_{k=1}^K P_k \mathcal{X}_k^2 T_c^2 N \left[ 1 - \frac{\zeta \beta}{2} + \frac{\zeta \beta}{2} \cos(2\pi T_k) \right] \quad (3.36)$$

where  $\zeta = 2 \left[ 1 - \frac{1}{T_c^3} \int_{-\infty}^{\infty} |Q(f)|^4 df \right] / \beta$ . Then

$$\mathbb{E}_{\mathcal{X}_k, T_k}[Y] = \bar{Y} = \frac{N_0 T_b}{2} + \frac{\Omega T_c^2 N}{2} \left[ 1 - \frac{\zeta \beta}{2} \right] \sum_{k=1}^K P_k. \quad (3.37)$$

We can write  $Y - \bar{Y}$  as

$$Y - \bar{Y} = \sum_{k=1}^K P_k \mathcal{X}_k^2 T_c^2 N \left[ 1 - \frac{\zeta \beta}{2} + \frac{\zeta \beta}{2} \cos(2\pi T_k) \right] - \frac{\Omega T_c^2 N}{2} \left[ 1 - \frac{\zeta \beta}{2} \right] \sum_{k=1}^K P_k. \quad (3.38)$$



Now, let

$$f(Y) = \mathbf{Q} \left( \sqrt{\frac{P_0 R_0^2 N^2 T_c^2}{Y}} \right). \quad (3.39)$$

As in [62], writing the Taylor series expansion for  $f(Y)$  about  $\bar{Y}$ ,

$$\begin{aligned} P_{IHGA|R_0} &= f(\bar{Y}) + \sum_{n=1}^4 \mathbb{E}_{\mathcal{X}_k, T_k} [(Y - \bar{Y})^n] \frac{f^{(n)}(\bar{Y})}{n!} \\ &= \mathbf{Q} \left( \sqrt{\frac{P_0 R_0^2 N^2 T_c^2}{\bar{Y}}} \right) + \sum_{n=1}^4 \frac{\mathbb{E}_{\mathcal{X}_k, T_k} [(Y - \bar{Y})^n]}{n!} \mathbf{Q}^{(n)} \left( \sqrt{\frac{P_0 R_0^2 N^2 T_c^2}{\bar{Y}}} \right). \end{aligned} \quad (3.40)$$

where  $f^{(n)}(x)$  is the  $n$ -th derivative of  $f(x)$ . We consider four non-zero terms in the Taylor series expansion for simplicity. However, by considering more terms, more accurate results can be obtained at the expense of more computational complexity. For arbitrary fading parameter  $m$ , the unconditional average BER is approximated as

$$\begin{aligned} P_{IHGA} &= \frac{\Gamma(m + \frac{1}{2})}{2\sqrt{\pi} m \Gamma(m)} \left( \frac{2m}{\Omega \Delta^2} \right)^m {}_2F_1 \left( m, m + \frac{1}{2}; m + 1; \frac{-2m}{\Omega \Delta^2} \right) + \\ &\quad \sum_{n=1}^4 \frac{\mathbb{E}_{\mathcal{X}_k, T_k} [(Y - \bar{Y})^n]}{n!} A_n \end{aligned} \quad (3.41)$$

where  $\Delta^2 = \frac{P_0 N^2 T_c^2}{Y}$  and  $\{A_n\}_{n=1}^4$ ,  $\{\mathbb{E}_{\mathcal{X}_k, T_k} [(Y - \bar{Y})^n]\}_{n=1}^4$  are derived in Appendix D.

One expects that the IHGA provides more accurate results than the HSIGA, because in the Taylor series expansion two additional terms are considered and the exact derivatives are used rather than approximations.

### 3.4 Exact BER Analysis Using Characteristic Function Method

In this section, we consider a CF method [64] to derive the exact average BER of bandlimited DS-CDMA system with deterministic desired user spreading sequence

and random interfering users spreading sequences. The CF of  $\mathcal{M}_k$  conditioned on desired user spreading sequence,  $\mathbf{a}^{(0)} = \{a_0^{(0)}, \dots, a_{N-1}^{(0)}\}$ ,  $\mathcal{X}_k$  and  $T_k$  is written as [64]

$$\Phi_{\mathcal{M}_k}(\omega|\mathbf{a}^{(0)}, \mathcal{X}_k, T_k) = \prod_{n=-M}^{N+M-1} \cos \left( \sqrt{P_k} \mathcal{X}_k \omega T_c \sum_{l=0}^{N-1} a_l^{(0)} g((l-n)T_c - T_k) \right) \quad (3.42)$$

where  $\mathcal{X}_k = R_k \cos(\theta_k)$ . Now, averaging out  $\mathcal{X}_k$  and  $T_k$ , one gets

$$\begin{aligned} \Phi_{\mathcal{M}_k}(\omega|\mathbf{a}^{(0)}) &= \frac{2}{T_c} \int_0^\infty f_{\mathcal{X}_k}(x) \int_0^{T_c} \prod_{n=-M}^{N+M-1} \\ &\quad \cos \left( \sqrt{P_k} x \omega T_c \sum_{l=0}^{N-1} a_l^{(0)} g((l-n)T_c - T_k) \right) dT_k dx \end{aligned} \quad (3.43)$$

where  $f_{\mathcal{X}_k}(x)$  is the pdf of the in-phase component of a Nakagami random variable. The unconditional CF of  $\mathcal{M}_k$  is obtained by averaging (3.43) over all possible  $\mathbf{a}^{(0)}$ . Let's assume there are  $L_a$  possible sequences available. Thus, the unconditional CF is given by

$$\Phi_{\mathcal{M}_k}(\omega) = \frac{1}{L_a} \sum_{p=1}^{L_a} \Phi_{\mathcal{M}_k}(\omega|\mathbf{a}_p^{(0)}). \quad (3.44)$$

The CF for the total MAI is given by

$$\Phi_{\mathcal{M}}(\omega) = \prod_{k=1}^K \Phi_{\mathcal{M}_k}(\omega). \quad (3.45)$$

As in (3.23), the unconditional average BER for arbitrary values of Nakagami fading parameter can be written as

$$P_e = \frac{1}{2} - \frac{\Gamma(m + \frac{1}{2})}{\pi \Gamma(m)} \sqrt{\frac{P_0 T_b^2 \Omega}{m}} \int_0^\infty \Phi_{\mathcal{M}}(\omega) \Phi_\eta(\omega) {}_1F_1 \left( m + \frac{1}{2}; \frac{3}{2}; \frac{-P_0 T_b^2 \Omega \omega^2}{4m} \right) d\omega \quad (3.46)$$

where the CF of the AWGN component,  $\Phi_\eta(\omega) = \exp(-\frac{\omega^2 N_0 T_b}{4})$ . In (3.44), generally  $L_a = N$  for deterministic sequences but for random sequences  $L_a = 2^N$ . The computational complexity of this method increases exponentially with the length of the random desired user spreading sequence. Thus, this method is good only for systems with deterministic sequences and short random spreading sequences. However,

in practice deterministic sequences (Gold,  $m$ -sequence, Hadamard) are employed in DS-CDMA systems. Their lengths and the number of sequences are approximately equal. Thus, this method can be employed to study the performance of such systems.

### 3.5 Numerical Results and Discussion

In this section, we present the numerical results. Some of our results are published in [78]. The BER performance of the DS-CDMA system with SRC and BTD pulse shapes are compared under identical system parameters. The excess bandwidth of the pulse-shapings are assumed to be 100 %. We also assume uniform power conditions i.e., perfect power control, in the system, however our results can also be applied to nonuniform power conditions.

Fig. 3.1 depicts the BER performance versus the number of active interferers  $K$  for average SNR = 10 dB of the asynchronous bandlimited DS-CDMA system over slow, flat Nakagami fading channels using the CFIGA, SGA, HSIGA, IHGA and MC simulation. The processing gain,  $N = 64$  and random spreading sequences are assumed. The BER performance versus average SNR is presented in Fig. 3.2 for 10 active interfering users. Some interesting observations are made here. The performance with BTD pulse-shaping is always better than with SRC pulse-shaping. The results obtained using the CFIGA approximation are very close to the results of MC simulation. Thus, the CFIGA provides the most accurate results. The computational complexity of the IGA method was substantially reduced by employing the CF method and the complexity remains the same for faded and unfaded systems. The IHGA method is accurate when the average SNR is high but can be inaccurate for small and moderate values of the average SNR. As observed in many previous research

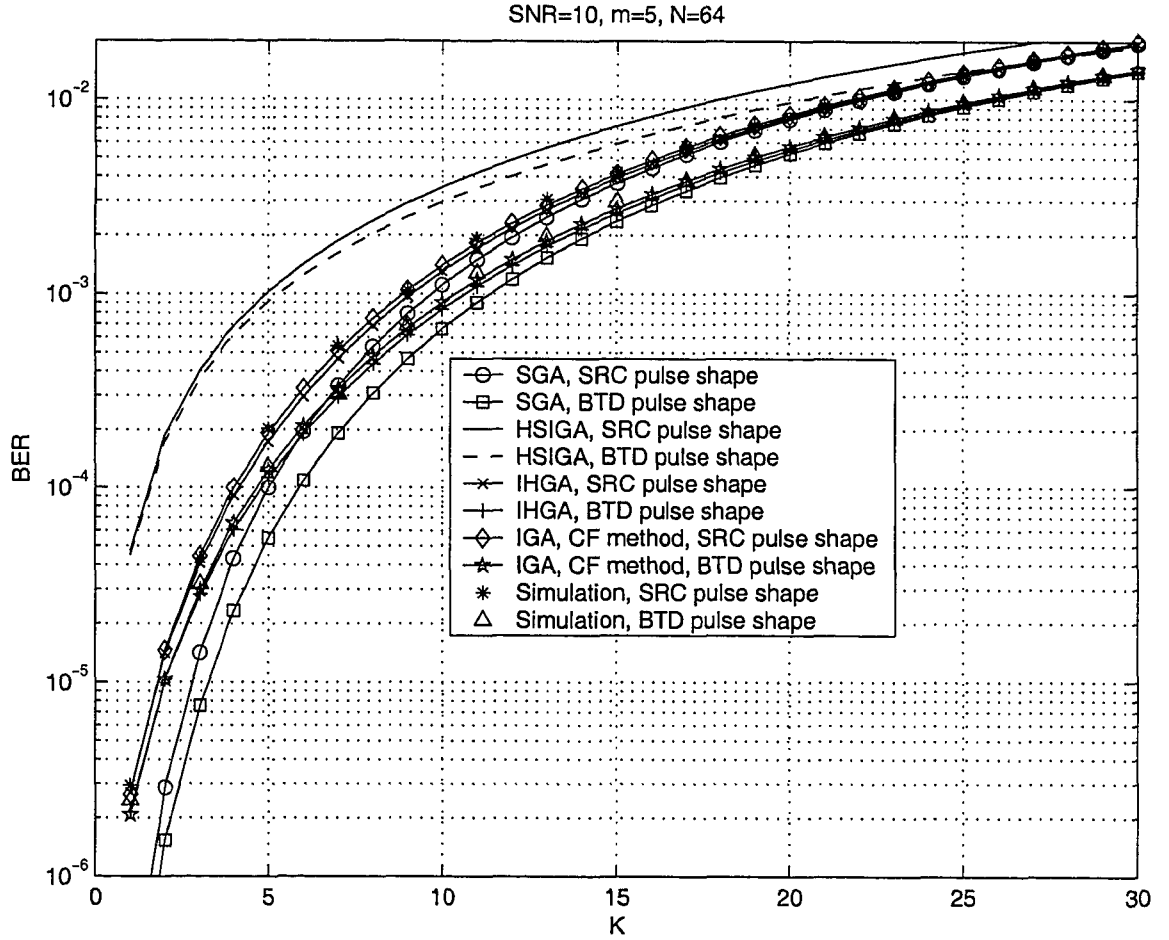


Fig. 3.1. The performance of a bandlimited DS/CDMA system in Nakagami fading ( $m = 5$ ) with random spreading ( $N = 64$ ) and  $SNR = 10$  dB.

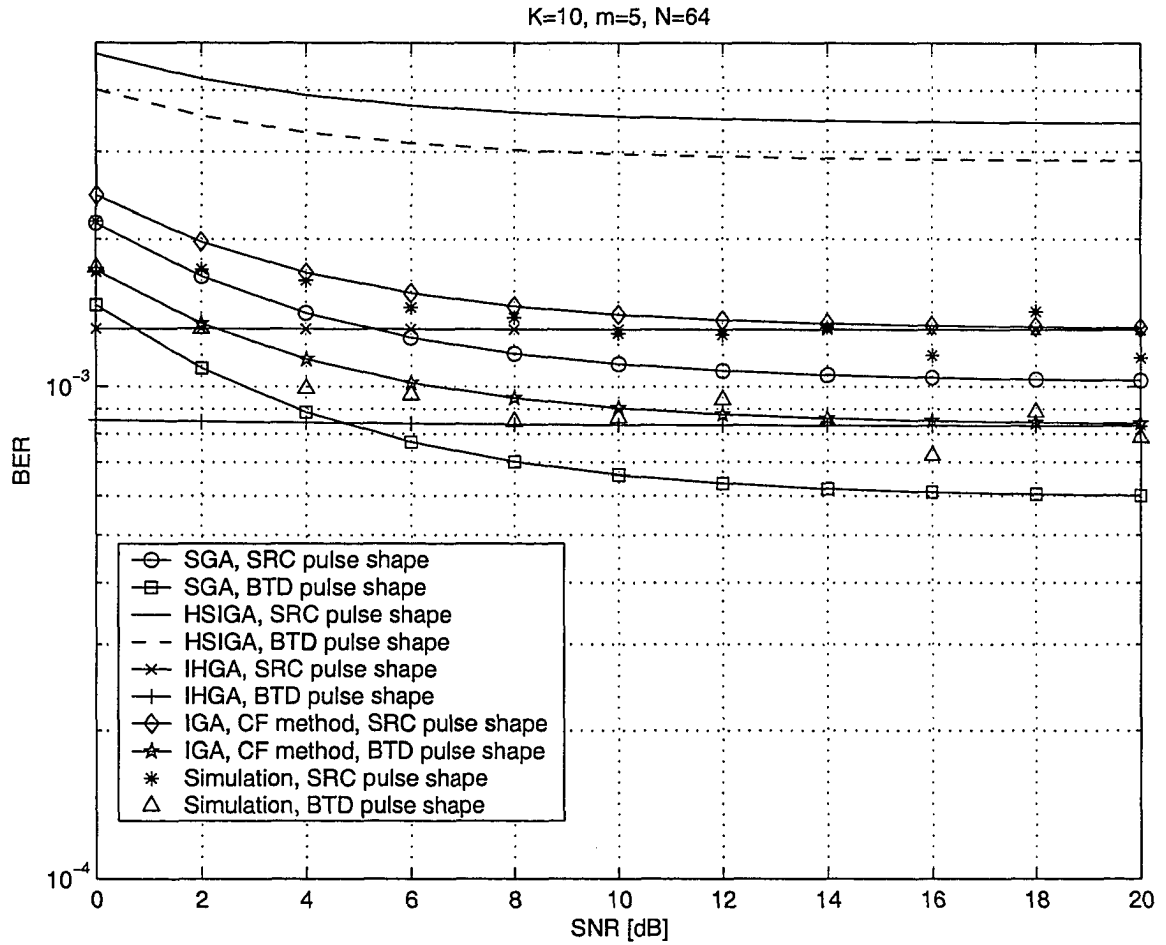


Fig. 3.2. The performance of a bandlimited DS/CDMA system in Nakagami fading ( $m = 5$ ) with random spreading ( $N = 64$ ) and  $K = 10$ .

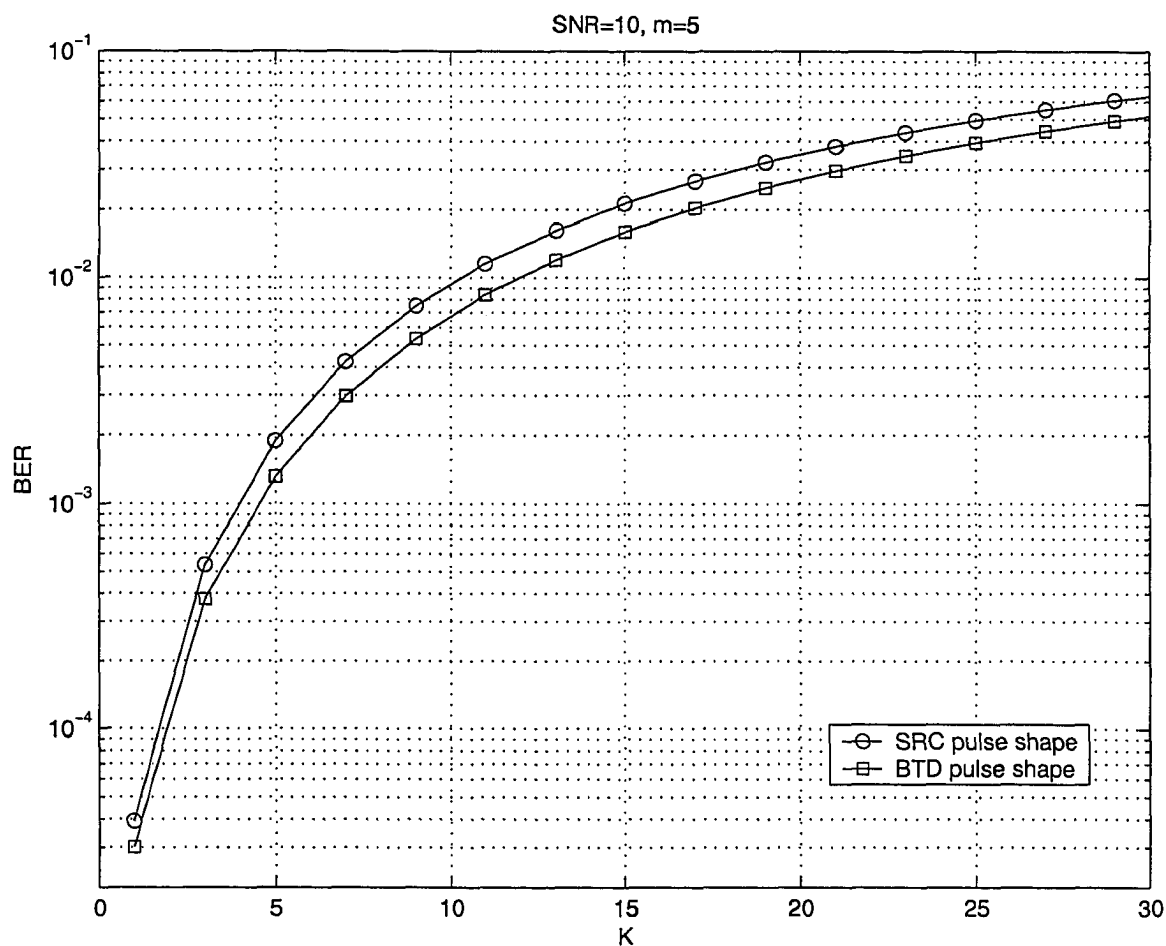


Fig. 3.3. The performance of bandlimited DS/CDMA system using a Gold sequence ( $N = 31$ ) for the desired user and random sequences for the interferers in Nakagami fading ( $m = 5$ ) with  $SNR = 10$  dB.

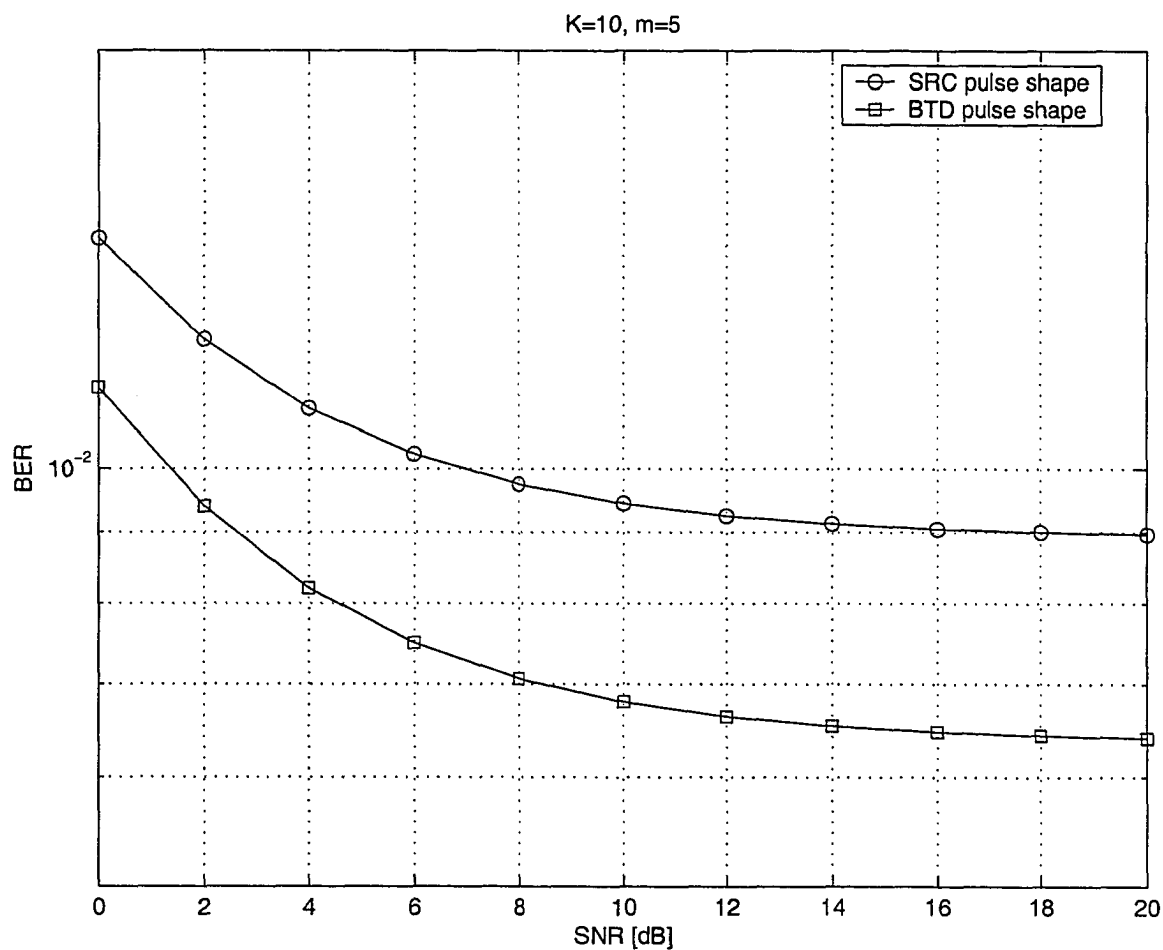


Fig. 3.4. The performance of bandlimited DS/CDMA system using a Gold sequence ( $N = 31$ ) for the desired user and random sequences for the interferers in Nakagami fading ( $m = 5$ ) with  $K = 10$ .

results, the SGA underestimates the BER. It is observed that the SGA provides more accurate results than the HSIGA for bandlimited DS-CDMA systems in Nakagami fading.

The exact average BER versus the number of active interferers,  $K$  and versus the average SNR for an asynchronous bandlimited DS-CDMA system over a slow, flat Nakagami fading channel are presented in Figs. 3.3 and 3.4, respectively, for average SNR = 10 dB and 10 interfering users. A deterministic desired user spreading sequence and random interferers' spreading sequences are considered. The Gold sequence of length 31 is considered as the desired user sequence and  $M = 10$ . The computational complexity of the system grows exponentially with the length of the desired user spreading sequence. As observed before the performance with BTD pulse-shaping is always better than that of SRC pulse-shaping.

### 3.6 Summary

The BER performance analysis of bandlimited DS-CDMA systems in slow, flat Nakagami fading channels have been considered. Several computationally efficient Gaussian approximation methods and an exact CF method were studied. The Gaussian approximation methods were validated using MC computer simulation. The SRC and BTD pulse-shapings were employed. The performance with BTD pulse-shaping is always better than that with SRC pulse-shaping. For systems with random spreading, a BER expression was derived for the IGA method using the CF provides the most accurate results with reasonable computational complexity. The  $(K + 1)$ -fold numerical integration was reduced to 2-fold iterated numerical integration. The IHGA provides accurate results only at high average SNR values. The HIGA performs poorer than



the SGA for bandlimited DS-CDMA systems in Nakagami fading.

# Chapter 4

## Performance Analysis of Bandlimited DS-CDMA Systems with Space Diversity Receivers in Nakagami Fading Channels

### 4.1 Introduction

The optimum and suboptimum joint detection (multiuser) receivers for DS-CDMA systems perform poorly in severe fading conditions. Meanwhile, the single-user conventional matched filter receiver is optimum for single bit decisions when a synchronous bandlimited random binary DS-CDMA system operates in slow flat Rayleigh fading channels with zero excess bandwidth Nyquist chip pulse shape. As conventional space diversity schemes combat fading and MAI simultaneously, they are of practical interest for DS-CDMA systems operating in severe fading conditions. The

commonly used space diversity schemes are maximal ratio combining (MRC), equal gain combining (EGC) and selection combining (SC) [6].

The performance of the diversity receivers in wireless channels without interference was extensively studied in [6] and the references therein. The performance of DS-CDMA systems with BPSK, QPSK and OQPSK modulation schemes and diversity reception was initially studied by Lehnert and Pursley in [79]; multipath Rake diversity combining was employed. In [80], Kchao and Stuber considered the performance of differential DS-CDMA systems with diversity receivers over frequency selective Rayleigh fading channels with lognormal shadowing. A Rake receiver with postdetection EGC and predetection SC was employed. Eng and Milstein studied the performance of a binary, coherent DS-CDMA system in frequency selective Nakagami fading in [65] with a multipath Rake combining receiver. The MAI was treated as a Gaussian RV in the analysis. In [81], Annamalai analyzed the performance of two predetection SC schemes for binary coherent DS-CDMA systems in Nakagami fading channels. Signal plus total interference power selection and SNIR selection schemes were employed. the performance of SC in a coherent DS-CDMA system employing BPSK and BFSK modulations in Nakagami fading was also studied by Ugweje in [82]. Frequency selective fading, Rake reception and maximum SNR selection criteria were considered. The performance of a binary DS-CDMA system with diversity combining and system imperfections such as power control error, path amplitude estimation error and phase estimation error was reported by Panicker and Kumar in [83]. Frequency selective Rayleigh fading was considered. In [84], the performance of a coherent binary DS-CDMA system with synchronization errors in diversity combining receivers was studied by Sunay and McLane. The MRC, EGC, and SC schemes were considered. The Fourier series method [31], [85] was employed for the performance analysis

and the computational complexity grew linearly with the diversity order. The NRZ rectangular pulse-shaping was employed in [79], [80], [65], [81], [82], [83], [84], and the SGA [33] of the MAI was used in the BER analysis in [79], [80], [65], [81], [82], [83]. The performance of coherent bandlimited binary DS-CDMA systems was considered in [59], [73], [62], [61]. Recently, we extended the works in [59], [73], [62], [61] to coherent DS-CDMA system in Nakagami fading in [78]. An exact analysis using a CF method, and approximate analyzes using the SGA [33] and the IGA [32] were presented.

In this chapter, we study the BER performance of space diversity receivers in bandlimited coherent binary DS-CDMA systems in Nakagami fading channels. Specifically, MRC, predetection EGC and predetection SC are considered. Random spreading, flat slow fading, asynchronous timing and independent identically distributed diversity branch fading gains are assumed. Nyquist chip pulse-shapings, namely, SRC and BTD [30] pulses are considered. The performance of these two pulse-shapings are compared under identical system conditions. The SGA [33] for the MAI is employed for all three combining schemes, but the CFIGA [78] is applied for EGC and SC only. A closed-form BER approximation is derived for the MRC scheme. The BER performance analysis is done using the CF [78] and Fourier series methods [31]. Our results are valid for arbitrary diversity orders and arbitrary Nakagami fading parameters, and the computational complexity does not grow with diversity order.

The remainder of this chapter is organized as follows. The system and channel models are introduced in Section 4.2. A closed-form BER expression is derived for the MRC scheme in Section 4.3. The average BER analysis using a CF method for the EGC scheme is presented in Section 4.4. The performance of the SC scheme is examined using a Fourier series method in Section 4.5. Numerical results are provided

in Section 4.6. Our conclusions and a summary of this chapter are drawn in Section 4.7.

## 4.2 System and Channel Model

A general asynchronous bandlimited binary DS-CDMA system with  $L$  independent space diversity branches and  $K + 1$  active users in Nakagami- $m$  fading channels is considered. The system model in [78], [59] is modified to adopt the space diversity reception. Using complex baseband signal representation, the  $l$ -th branch received signal is written as

$$r_l(t) = \sum_{k=0}^K s_{kl}(t) + w_l(t) \quad (4.1)$$

where  $-\infty < t < +\infty$  and  $w_l(t)$  is a complex circularly symmetric zero-mean white Gaussian process with power spectral density  $N_0$ . The  $l$ -th branch  $k$ -th user received signal  $s_{kl}(t)$  is given by

$$s_{kl}(t) = \sqrt{P_k} R_{kl} e^{j\theta_{kl}} \sum_{i=-\infty}^{\infty} b_i^{(k)} a_i^{(k)}(t - \tau_k - iT_b) \quad (4.2)$$

where the transmitted signal power of the  $k$ -th user is  $P_k$ ,  $b_i^{(k)} \in [+1, -1]$  are the equiprobable  $k$ -th user bits transmitted at rate  $1/T_b$  and the  $k$ -th user timing offset wrt the desired user is  $\tau_k \sim \mathcal{U}[0, T_b]$ . The phase offset wrt to the desired user is denoted as  $\theta_{kl} \sim \mathcal{U}[0, 2\pi]$ . The  $l$ -th path  $k$ -th user fading amplitude  $R_{kl}$ , is assumed to be Nakagami- $m$  distributed with parameters  $[m, \Omega]$  and its PDF is given in eq. (1.11). The  $l$ -th branch desired user received signal is denoted as  $s_{0l}(t)$  and without loss of generality,  $\tau_0 = 0$  and  $\theta_{0l} = 0$  are assumed. The spreading waveform  $a_i^{(k)}(t)$  for  $b_i^{(k)}$ , is

$$a_i^{(k)}(t) = \sum_{n=0}^{N-1} a_{n+iN}^{(k)} q(t - nT_c) \quad (4.3)$$

where  $a_n^{(k)} \in [+1, -1]$  is the  $n$ -th chip of the  $k$ -th user PN sequence. The rate of a PN sequence is  $1/T_c$  and the processing gain or spreading factor is given by  $T_b/T_c = N$ . The elements of random variable sets  $\{\tau_k\}$ ,  $\{\theta_{kl}\}$ ,  $\{b_i^{(k)}\}$  and  $\{R_{kl}\}$  are assumed to be iid and all these RV's in these sets are mutually independent. The received baseband chip pulse is denoted as  $q(t)$  and it satisfies  $\int_{-\infty}^{\infty} |q(t)|^2 dt = T_c$ . Two types of Nyquist pulses are considered namely, the SRC pulse and the BTD pulse [30]. They are defined in time and frequency domains in eqs. (2.11), (2.12), (2.13) and (2.14). The excess bandwidth of the chip pulse shape  $\beta \in [0, 1]$  and we assume  $\beta = 1$  in this chapter. However, our analysis is applicable to systems with any  $\beta \in [0, 1]$ . For notational convenience when  $k \neq 0$ , eq. (4.2) is written as

$$s_{kl}(t) = \sqrt{P_k} R_{kl} e^{j\theta_{kl}} \sum_{n=-\infty}^{\infty} d_n^{(k)} q(t - T_k - nT_c) \quad (4.4)$$

where  $T_k = \tau_k \bmod T_c$  and  $d_n^{(k)} \in [+1, -1]$ . The  $d_n^{(k)}$  and  $T_k$  can be modeled as iid equiprobable random variables ( $d_n^{(k)} \in [+1, -1]$ ) and iid uniform RVs in  $[0, T_c]$ , respectively [59]. The average SNR is defined as

$$SNR = \frac{P_0 T_b \Omega}{N_0 T_b / 2} = \frac{2 P_0 \Omega}{N_0}. \quad (4.5)$$

### 4.3 Performance of Maximal Ratio Combining (MRC)

In this section, a closed-form average BER expression for a bandlimited DS-CDMA system with  $L$  branch MRC in Nakagami fading is derived using a SGA [33]. After the matched filtering by  $Q^*(f)$ , cophasing, weighting by the conjugate fading gain, sampling, despreading and  $N$  chip summing the received signal is passed through a

real operator function to generate the receiver decision statistic. The  $i$ -th bit decision statistic of the 0-th (desired) user on the  $l$ -th path can then be written as

$$y_{il}^{(0)} = \mathcal{R}e \left( R_{0l} \sum_{v=iN}^{(i+1)N-1} a_v^{(0)} \int_{-\infty}^{\infty} r_l(vT_c - u) q(-u) du \right). \quad (4.6)$$

After the combining, the decision statistic is given by

$$y_i^{(0)} = \sqrt{P_0} T_b b_i^{(0)} R_M + \mathcal{M}_M + \eta_M \quad (4.7)$$

where  $R_M = \sum_{l=1}^L R_{0l}^2$ ,  $\eta_M = \sum_{l=1}^L R_{0l} \eta_l$  and

$$\mathcal{M}_M = \sum_{l=1}^L \sum_{k=1}^K \mathcal{M}_{kl}^M \quad (4.8)$$

$$\mathcal{M}_{kl}^M = \sqrt{P_k} R_{0l} R_{kl} \cos(\theta_{kl}) T_c \sum_{v=0}^{N-1} \sum_{n=-\infty}^{\infty} a_v^{(0)} d_n^{(k)} g((v-n)T_c - T_k) \quad (4.9)$$

where  $g(t) = \mathcal{F}^{-1}[|Q(f)|^2/T_c]$ , and is given as (2.12) and (2.14). The estimate of the transmitted bit is then obtained by  $\hat{b}_i^{(0)} = \text{sgn}(y_i^{(0)})$ . The variance of the  $\mathcal{M}_{kl}^M$  conditioned on  $R_{0l}$  and  $T_k$  is written as [78]

$$\sigma_{\mathcal{M}_{kl}^M | R_{0l}, T_k}^2 = \frac{1}{2} N P_k R_{0l}^2 \Omega T_c^2 \sum_{i=-\infty}^{\infty} g^2(iT_c - T_k) \quad (4.10)$$

$$= \frac{1}{2} N P_k R_{0l}^2 \Omega T_c^2 \left[ 1 - \frac{\zeta \beta}{2} + \frac{\zeta \beta \cos(2\pi T_k)}{2} \right] \quad (4.11)$$

where  $\zeta = 2 \left[ 1 - \frac{1}{T_c^3} \int_{-\infty}^{\infty} |Q(f)|^4 df \right] / \beta$ . Using the SGA of the MAI, the variance of  $\mathcal{M}_{kl}^M$  conditioned on  $R_{0l}$  is written as [78]

$$\sigma_{\mathcal{M}_{kl}^M | R_{0l}}^2 = \frac{1}{2} P_k R_{0l}^2 \Omega T_c^2 N \left[ 1 - \frac{\zeta \beta}{2} \right]. \quad (4.12)$$

Then, the variance of the MAI,  $\mathcal{M}_M$  conditioned on  $R_M$  is given by

$$\sigma_{\mathcal{M}_M | R_M}^2 = \frac{1}{2} \mathcal{P} R_M \Omega T_c^2 N \left[ 1 - \frac{\zeta \beta}{2} \right] \quad (4.13)$$

where  $\mathcal{P} = \sum_{k=1}^K P_k$ . The variance of the  $\eta_M$  conditioned on  $R_M$  is given by

$$\sigma_{\eta_M|R_M}^2 = \frac{N_0 T_b R_M}{2}. \quad (4.14)$$

Now, using the SGA, the sum of MAI plus background noise is Gaussian distributed conditioned on  $R_M$ . Then, the BER conditioned on  $R_M$  is written as

$$P_{M|R_M} = \mathbf{Q} \left( \sqrt{\frac{2P_0 T_b R_M}{\mathcal{P} \Omega T_c [1 - \frac{\zeta\beta}{2}] + N_0}} \right) \quad (4.15)$$

where  $\mathbf{Q}(\cdot)$  is the area under the tail of the Gaussian PDF. The PDF of  $U = R_{0,l}^2$  can be written as [86]

$$f_U(u) = \frac{1}{\Gamma(m)} \left( \frac{m}{\Omega} \right)^m e^{-(\frac{m}{\Omega})u} u^{m-1}, \quad u > 0 \quad (4.16)$$

where the PDF in (4.16) is the gamma PDF and is closed under convolution. Thus, the PDF of  $R_M$  is also a gamma PDF and is given by [86]

$$f_{R_M}(r) = \frac{1}{\Gamma(mL)} \left( \frac{m}{\Omega} \right)^{mL} e^{-(\frac{m}{\Omega})r} r^{mL-1}, \quad r > 0. \quad (4.17)$$

If the fading gains are not identically distributed the PDF of  $R_M$  is given in [87].

Now, by averaging out  $R_M$  from (4.15), the unconditional BER is given by [48]

$$\begin{aligned} P_M &= \int_0^\infty \mathbf{Q} \left( \sqrt{\frac{2P_0 T_b r}{N_0 + \mathcal{P} T_c \Omega Y}} \right) f_{R_M}(r) dr \\ &= \frac{\Gamma(mL + \frac{1}{2})}{2\sqrt{\pi} mL \Gamma(mL)} \left( \frac{m(N_0 + \mathcal{P} T_c \Omega Y)}{P_0 T_b \Omega} \right)^{mL} \times \\ &\quad {}_2\mathbf{F}_1 \left( mL, mL + \frac{1}{2}; mL + 1; \frac{-m(N_0 + \mathcal{P} T_c \Omega Y)}{\Omega P_0 T_b} \right) \end{aligned} \quad (4.18)$$

where  $Y = [1 - \zeta\beta/2]$ . The closed-form approximation in (4.18) is valid for arbitrary diversity order and arbitrary Nakagami fading parameter.



## 4.4 Performance of Equal Gain Combining (EGC)

The BER performance of a bandlimited DS-CDMA system with  $L$  branch predetection EGC in Nakagami fading is considered in this section. The SGA and IGA of the MAI is employed with a CF method [78]. After the matched filtering by  $Q^*(f)$ , cophasing, sampling, despreading and  $N$  chip summing the received signal is passed through a real operator function to generate the receiver decision statistic. The  $i$ -th bit decision statistic of the 0-th user on the  $l$ -th path is written as

$$y_{il}^{(0)} = \mathcal{R}e \left( \sum_{v=iN}^{(i+1)N-1} a_v^{(0)} \int_{-\infty}^{\infty} r_l(vT_c - u)q(-u)du \right). \quad (4.19)$$

After the combining, the decision statistic becomes

$$y_i^{(0)} = \sum_{l=1}^L y_{il}^{(0)} = \sqrt{P_0}T_b b_i^{(0)} R_E + \mathcal{M}_E + \eta_E \quad (4.20)$$

where  $R_E = \sum_{l=1}^L R_{0l}$ ,  $\eta_E = \sum_{l=1}^L \eta_l$  and  $\eta_l$  is a zero-mean, Gaussian process with variance  $N_0 T_b / 2$ . The estimate of the transmitted bit is then obtained as  $\hat{b}_i^{(0)} = \text{sgn}(y_i^{(0)})$ . The MAI component is given by

$$\mathcal{M}_E = \sum_{l=1}^L \sum_{k=1}^K \mathcal{M}_{kl} \quad (4.21)$$

$$\mathcal{M}_{kl} = \sqrt{P_k} R_{kl} \cos(\theta_{kl}) T_c \sum_{v=0}^{N-1} \sum_{n=-\infty}^{\infty} a_v^{(0)} d_n^{(k)} g((v-n)T_c - T_k). \quad (4.22)$$

Using the SGA, the variance of the MAI,  $\sigma_{\mathcal{M}_E}^2$  is written as

$$\sigma_{\mathcal{M}_E}^2 = \frac{1}{2} N P L \Omega T_c^2 \left[ 1 - \frac{\zeta \beta}{2} \right]. \quad (4.23)$$

Then, the CF of the MAI is given by

$$\Phi_{\mathcal{M}_E}(\omega) = \exp \left( -\frac{\omega^2 \sigma_{\mathcal{M}_E}^2}{2} \right). \quad (4.24)$$

In the IGA method [32], the MAI conditioned on interferer chip delays,  $\mathbf{T} = \{T_1, \dots, T_k\}$  and  $\mathcal{X} = \{R_{11} \cos(\theta_{11}), \dots, R_{KL} \cos(\theta_{KL})\}$  is assumed to be a zero-mean, Gaussian RV. Thus, the variance of  $\mathcal{M}_{kl}$  conditioned on  $\mathcal{X}_{kl}, T_k$  is written as

$$\sigma_{\mathcal{M}_{kl}|\mathcal{X}_{kl}, T_k}^2 = NP_k \mathcal{X}_{kl}^2 T_c^2 \sum_{i=-\infty}^{\infty} g^2(iT_c - T_k) \quad (4.25)$$

$$= NP_k \mathcal{X}_{kl}^2 T_c^2 \left[ 1 - \frac{\zeta\beta}{2} + \frac{\zeta\beta \cos(2\pi T_k)}{2} \right] \quad (4.26)$$

where  $\zeta = 2 \left[ 1 - \frac{1}{T_c^2} \int_{-\infty}^{\infty} |Q(f)|^4 df \right] / \beta$ . Then, the CF of the  $l$ -th branch  $k$ -th user MAI,  $\mathcal{M}_{kl}$  conditioned on  $\mathcal{X}_{kl}$  and  $T_k$  is written as

$$\Phi_{\mathcal{M}_{kl}}(\omega|\mathcal{X}_{kl}, T_k) = \exp \left( -\frac{\omega^2 \sigma_{\mathcal{M}_{kl}|\mathcal{X}_{kl}, T_k}^2}{2} \right). \quad (4.27)$$

Averaging out  $\mathcal{X}_{kl}$  and  $T_k$ , the unconditional CF of  $\mathcal{M}_E$  becomes

$$\Phi_{\mathcal{M}_E}(\omega) = \prod_{k=1}^K \frac{1}{T_c} \int_0^{T_c} \left[ \prod_{l=1}^L 2 \int_0^{\infty} \exp \left( -\frac{\omega^2 \sigma_{\mathcal{M}_{kl}|\mathcal{X}_{kl}, T_k}^2}{2} \right) f_{\mathcal{X}_{kl}}(x) dx \right] dT_k \quad (4.28)$$

where  $f_{\mathcal{X}_{kl}}(x)$ , is the pdf of RV  $\mathcal{X}_{kl}$  and is given in eq. (3.20). The average BER conditioned on  $R_E$  is

$$\begin{aligned} P_{EGC|R_E} &= \Pr \left[ \sqrt{P_0} R_E T_b b_i^{(0)} + \mathcal{M}_E + \eta_E < 0 | b_i^{(0)} = +1 \right] \\ &= \frac{1}{2} - \frac{1}{\pi} \int_0^{\infty} \Phi_{\mathcal{M}_E}(\omega) \Phi_{\eta_E}(\omega) \frac{\sin(\sqrt{P_0} R_E T_b \omega)}{\omega} d\omega \end{aligned} \quad (4.29)$$

where the CF of the AWGN component,  $\Phi_{\eta_E}(\omega) = \exp(-\frac{\omega^2 N_0 T_b L}{4})$ . Several methods have been used in the literature [6], [88], [89] to obtain the unconditional average BER from (4.29). Eq. (4.29) has the required format to apply the Parseval's theorem based method proposed in [89]. Then, averaging out  $R_E$ , the unconditional average BER is written as

$$P_{EGC} = \frac{1}{2} - \frac{1}{\pi} \int_0^{\infty} \int_0^{\infty} \Phi_{\mathcal{M}_E}(u) \Phi_{\eta_E}(u) \frac{\sin(\sqrt{P_0} r T_b u)}{u} f_{R_E}(r) du dr. \quad (4.30)$$

Now, by employing the method proposed in [89], eq. (4.30) becomes,

$$\begin{aligned}
P_{EGC} &= \frac{1}{2} - \int_0^\infty \frac{\Phi_T(u)}{\pi^2 u} \times \\
&\quad \int_0^\infty \Re \left[ \left[ j\pi\delta(\omega + \sqrt{P_0}T_b u) - j\pi\delta(\omega - \sqrt{P_0}T_b u) \right] \Phi_{R_E}^*(\omega) \right] d\omega du \\
&= \frac{1}{2} - \frac{1}{\pi} \int_0^\infty \frac{\Phi_T(u)}{u} \Im \left[ \Phi_{R_E}(\sqrt{P_0}T_b u) \right] du
\end{aligned} \tag{4.31}$$

where  $\Re[x]$  and  $\Im[x]$  is the real and imaginary part of  $x$ , respectively,  $\Phi_T(\omega) = \Phi_{\mathcal{M}_E}(\omega)\Phi_{\eta_E}(\omega)$ ,  $\Phi_{R_E}^*(\omega)$  is the complex conjugate of the CF of  $R_E$  ( $\Phi_{R_E}(\omega)$ ),  $\delta(\cdot)$  is the Dirac delta function and  $j = \sqrt{-1}$ . Eq. (4.31) with eq.(4.24) provides an approximation to the unconditional average BER accounting for the pulse-shaping. A single numerical integration is required, but the computational complexity does not grow with diversity order. The CF of  $R_{0j}$  is written as [88], [13]

$$\Phi_{R_{0j}}(\omega) = {}_1F_1 \left( m; \frac{1}{2}; \frac{-\Omega\omega^2}{4m} \right) + j\omega \frac{\Gamma(m + \frac{1}{2})}{\Gamma(m)} \sqrt{\frac{\Omega}{m}} {}_1F_1 \left( m + \frac{1}{2}; \frac{3}{2}; \frac{-\Omega\omega^2}{4m} \right). \tag{4.32}$$

Then, the CF of  $R_E$  is  $\Phi_{R_E}(\omega) = (\Phi_{R_{0j}}(\omega))^L$ .

## 4.5 Performance of Selection Combining (SC)

In this section, the average BER of  $L$  branch predetection SC of a bandlimited DS-SS-CDMA system is derived using a Fourier series method [78], [31]. A maximum desired signal power selection scheme is considered. The SGA and IGA of the MAI are employed for the performance analysis. As in Section 4.4, the decision statistic is written as

$$y_i^{(0)} = \sqrt{P_0} T_b b_i^{(0)} R_s + \mathcal{M}_s + \eta_l \tag{4.33}$$

where  $R_s = \max_{j \in [1 \dots L]} R_{0j}$ ,

$$\mathcal{M}_s = \sum_{k=1}^K \mathcal{M}_{kl} \tag{4.34}$$

and  $\mathcal{M}_{kl}$  is given in eq. (4.22). Using the SGA, the variance of the MAI,  $\mathcal{M}_s$  is written as

$$\sigma_{\mathcal{M}_s}^2 = \frac{1}{2} N \mathcal{P} \Omega T_c^2 \left[ 1 - \frac{\zeta \beta}{2} \right]. \quad (4.35)$$

Then, the CF of the MAI is given by

$$\Phi_{\mathcal{M}_s}(\omega) = \exp \left( -\frac{\omega^2 \sigma_{\mathcal{M}_s}^2}{2} \right). \quad (4.36)$$

Now, we employ the IGA by substituting  $L = 1$  in (4.28), and the CF of  $\mathcal{M}_{kl}$  is written as

$$\Phi_{\mathcal{M}_s}(\omega) = \prod_{k=1}^K \frac{2}{T_c} \int_0^{T_c} \int_0^\infty \exp \left( -\frac{\omega^2 \sigma_{\mathcal{M}_{kl}|\mathcal{X}_s, T_k}^2}{2} \right) f_{\mathcal{X}_{kl}}(x) dx dT_k. \quad (4.37)$$

As in [78], (4.37) can be written as

$$\Phi_{\mathcal{M}_s}(\omega) = \prod_{k=1}^K 2 \int_0^\infty \exp \left( -\frac{\omega^2 N P_k x^2 \left[ 1 - \frac{\zeta \beta}{2} \right]}{2} \right) I_0 \left( \frac{\omega^2 N P_k x^2 \zeta \beta}{4} \right) f_{\mathcal{X}_{kl}}(x) dx \quad (4.38)$$

where  $I_0(\cdot)$  is the modified Bessel function of zero order and (4.38) is derived by assuming the normalized chip duration,  $T_c = 1$ . Using the Fourier series method of [31], the BER conditioned on  $R_S$  is given by

$$P_{s|R_s} = \frac{1}{2} - \frac{2}{\pi} \sum_{\substack{v=1 \\ v \text{ odd}}}^\infty \frac{e^{-\frac{v^2 \omega_0^2}{2}} \Phi_{\mathcal{M}_s} \left( \frac{v \omega_0}{\sqrt{N_0 T_b/2}} \right)}{v} \sin \left( \frac{\sqrt{P_0} T_b R_s v \omega_0}{\sqrt{N_0 T_b/2}} \right) \quad (4.39)$$

where  $\omega_0 = 2\pi/T_0$  and  $T_0$  is selected to obtain the required numerical accuracy. By averaging out  $R_s$ , the unconditional average BER is given by

$$P_s = \frac{1}{2} - \frac{2}{\pi} \sum_{\substack{v=1 \\ v \text{ odd}}}^\infty \frac{e^{-\frac{v^2 \omega_0^2}{2}} \Phi_{\mathcal{M}_s} \left( \frac{v \omega_0}{\sqrt{N_0 T_b/2}} \right)}{v} \int_0^\infty \sin \left( \frac{\sqrt{P_0} T_b r v \omega_0}{\sqrt{N_0 T_b/2}} \right) f_{R_S}(r) dr \quad (4.40)$$

where  $f_{R_S}(r)$  is the PDF of  $R_S$  and  $R_S = \max_{j \in [1, \dots, L]} R_{0j}$ . Using order statistics [74], [6] the PDF of the RV  $R_S$  is given by

$$f_{R_S}(r) = \left( \frac{\partial [F_{R_S}(s)]^L}{\partial s} \right)_{s=r} \quad (4.41)$$

where  $F_{R_S}(s)$  is the cumulative probability distribution function (CDF) of RV  $R_S$ . Then, (4.41) becomes [76]

$$f_{R_S}(r) = \frac{2L \left[ \gamma(m, \frac{mr^2}{\Omega}) \right]^{L-1}}{[\Gamma(m)]^L} \left( \frac{m}{\Omega} \right)^m e^{-\frac{mr^2}{\Omega}} r^{2m-1}, \quad r > 0 \quad (4.42)$$

where  $\gamma(\cdot, \cdot)$  is the lower incomplete gamma function [76].

## 4.6 Numerical Results and Discussion

Some of our numerical results are presented in this section. We published part of the results obtained in this chapter in [90]. The BER performance of the diversity receivers for bandlimited DS-CDMA system with SRC and BTD pulse shapes are compared under identical system conditions. Random spreading sequences of length 64 ( $N = 64$ ) are employed. The excess bandwidth of the chip pulse shape is assumed to be 100%. Perfect power control is assumed in the system. However, our analysis can also be applied to nonuniform power conditions.

Fig. 4.1 shows the BER performance versus the average SNR of an asynchronous bandlimited DS-CDMA system with MRC, EGC and SC diversity over slow, flat Nakagami fading channels for a number of active interferers,  $K = 10$ . Figs. 4.2 and 4.3 depict the BER performance versus the number of active interferers,  $K$ , for average  $SNR = 10$  dB with BTD and SRC chip pulse shapes, respectively. The SGA method was considered for Figs. 4.1-4.3. The Nakagami fading parameter  $m = 2$  and diversity orders  $L = 1, 2$  and 3 are considered. At average  $SNR = 10$  dB and  $K = 10$ , the average BER is reduced by about 10, 25 and 35 times and the capacity is increased by 9, 15 and 16 users at  $BER = 10^{-3}$  by increasing  $L$  from 1 to 2 in SC, EGC and MRC schemes with BTD pulse-shaping, respectively.

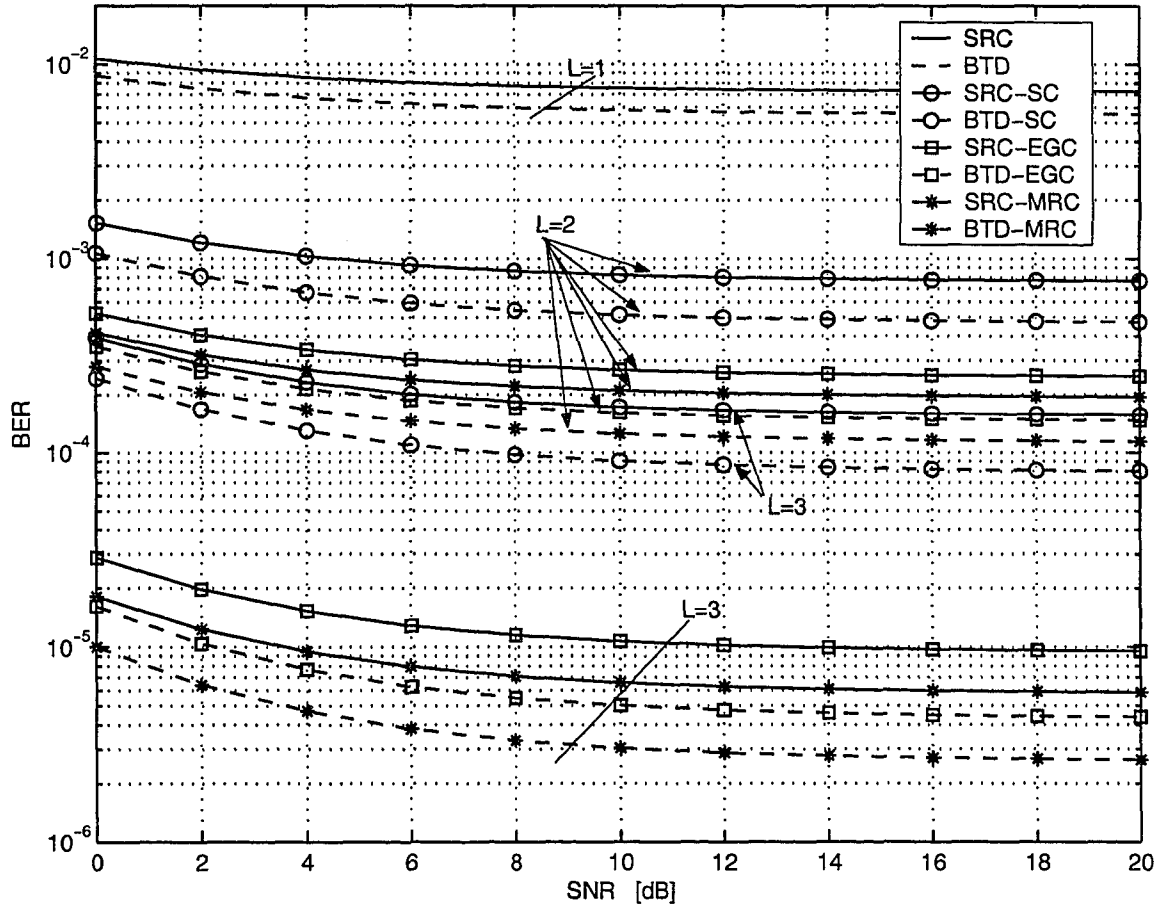


Fig. 4.1. The BER performance of a bandlimited DS-CDMA system estimated using the SGA for MRC, EGC and SC diversity in Nakagami fading ( $m = 2$ ) with random spreading ( $N = 64$ ) and  $K = 10$ .

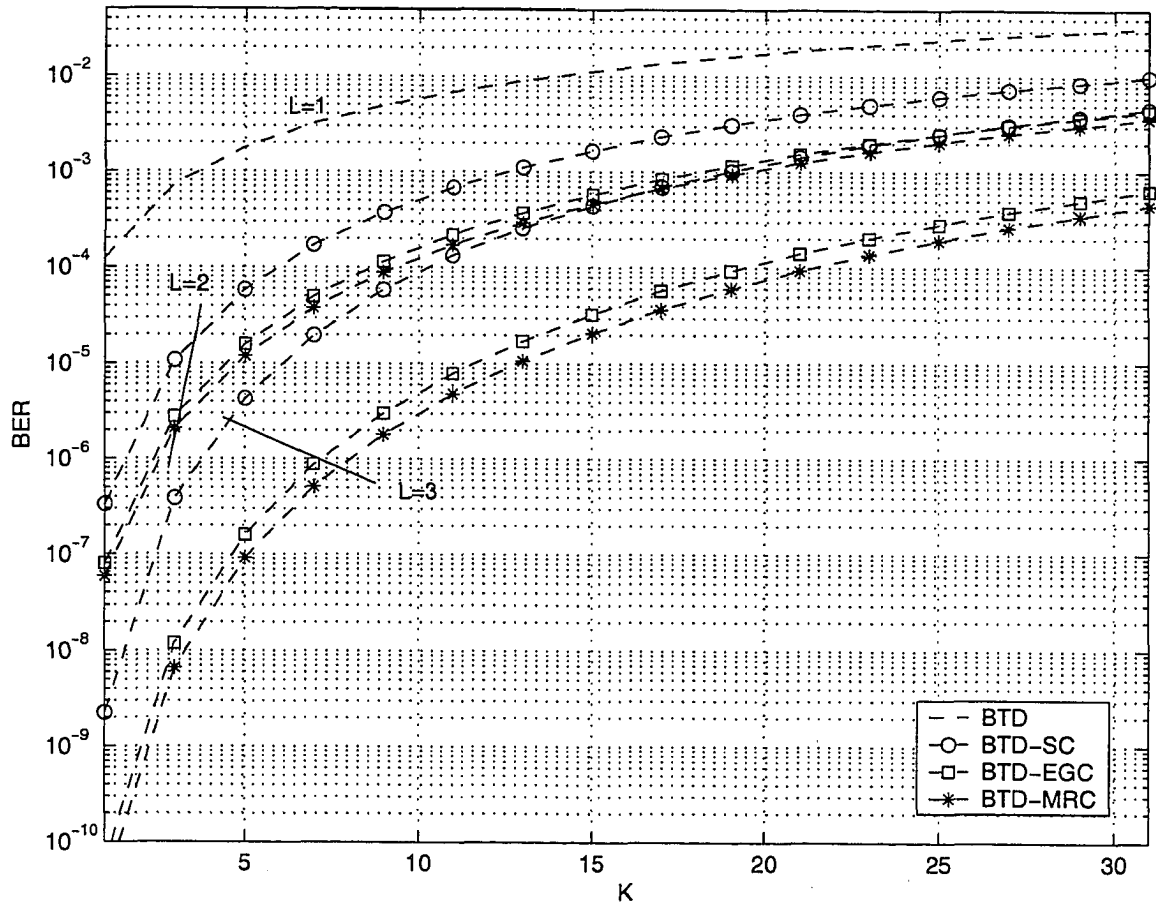


Fig. 4.2. The BER performance of a bandlimited DS-CDMA system estimated using the SGA for MRC, EGC and SC diversity in Nakagami fading ( $m = 2$ ) with random spreading ( $N = 64$ ) and  $SNR = 10$  dB.

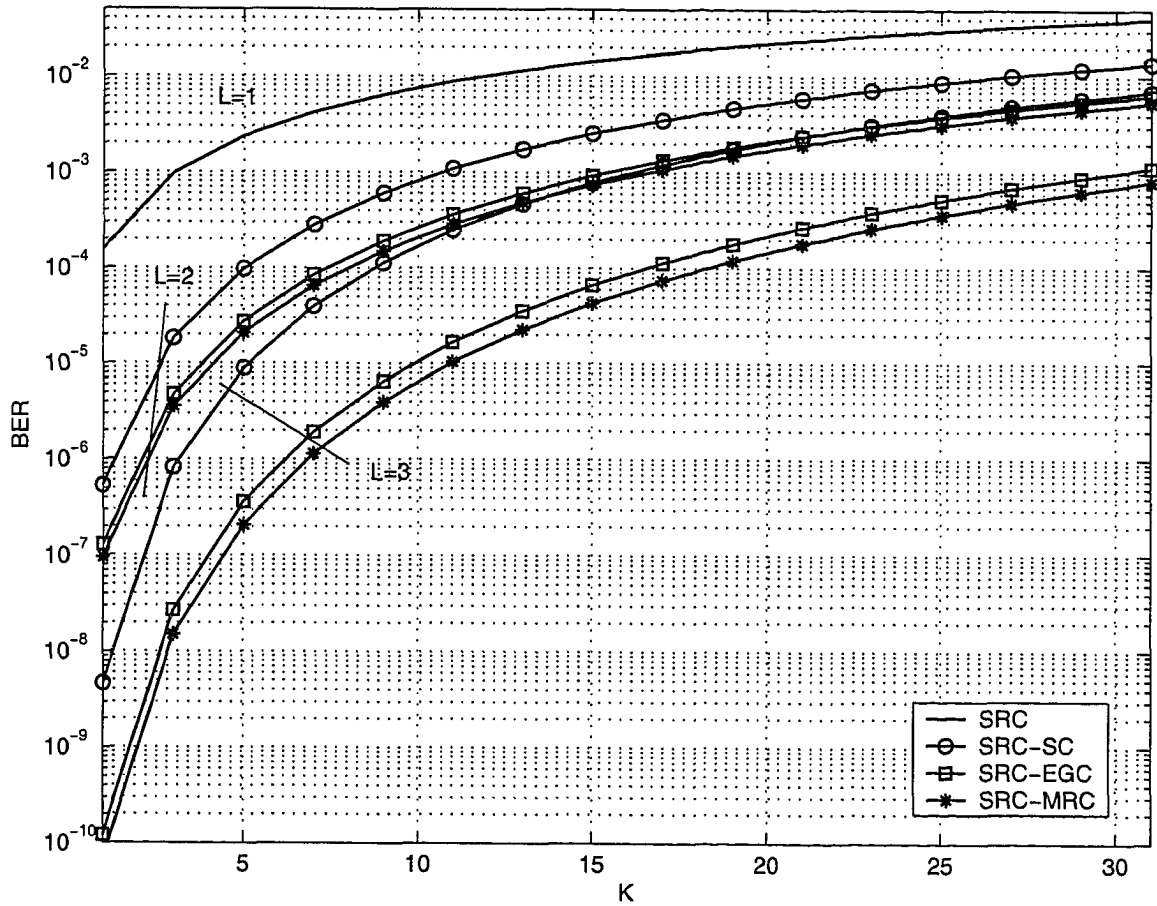


Fig. 4.3. The BER performance of a bandlimited DS-CDMA system estimated using the SGA for MRC, EGC and SC diversity in Nakagami fading ( $m = 2$ ), with random spreading ( $N = 64$ ) and  $SNR = 10$  dB.



Fig. 4.4 depicts the BER versus the average SNR of an asynchronous bandlimited DS-CDMA system with EGC and SC diversity when the number of active interferers  $K = 15$  over a slow, flat Nakagami fading channel for diversity orders,  $L = 1, 2$  and 3. The CF and Fourier series methods were used with the IGA of MAI to obtain the results. The BER versus the number of active interferers  $K$  for average SNR = 5 dB is presented in Fig. 4.5 for  $L = 1, 2$  and 3. As mentioned in the literature performance analysis of DS-CDMA systems with the IGA is very accurate [78]. Some interesting observations are made here. The performance with BTD pulse-shaping is always better than that with SRC pulse-shaping and the superiority increases with the diversity order. The EGC and SC space diversity receivers provide substantial SNR and capacity gains as seen in Fig. 4.1 - 4.5.

## 4.7 Summary

Average BER performance analysis of three diversity receivers for a bandlimited DS-CDMA system in slow, flat Nakagami fading channel was presented. Three well known combining schemes, MRC, EGC and SC were considered. The bandlimited Nyquist pulse-shapings, namely, SRC and BTD pulse-shapings were employed. A closed-form BER approximation was derived for the MRC using the SGA and the BER approximation for the EGC and SC schemes were derived using the SGA and IGA entail numerical integrations. The computational complexity does not increase with the number of users or the diversity order. These results are valid for arbitrary diversity order and arbitrary Nakagami fading parameter. The performance with BTD pulse-shaping is better than that with SRC pulse-shaping in all cases examined.

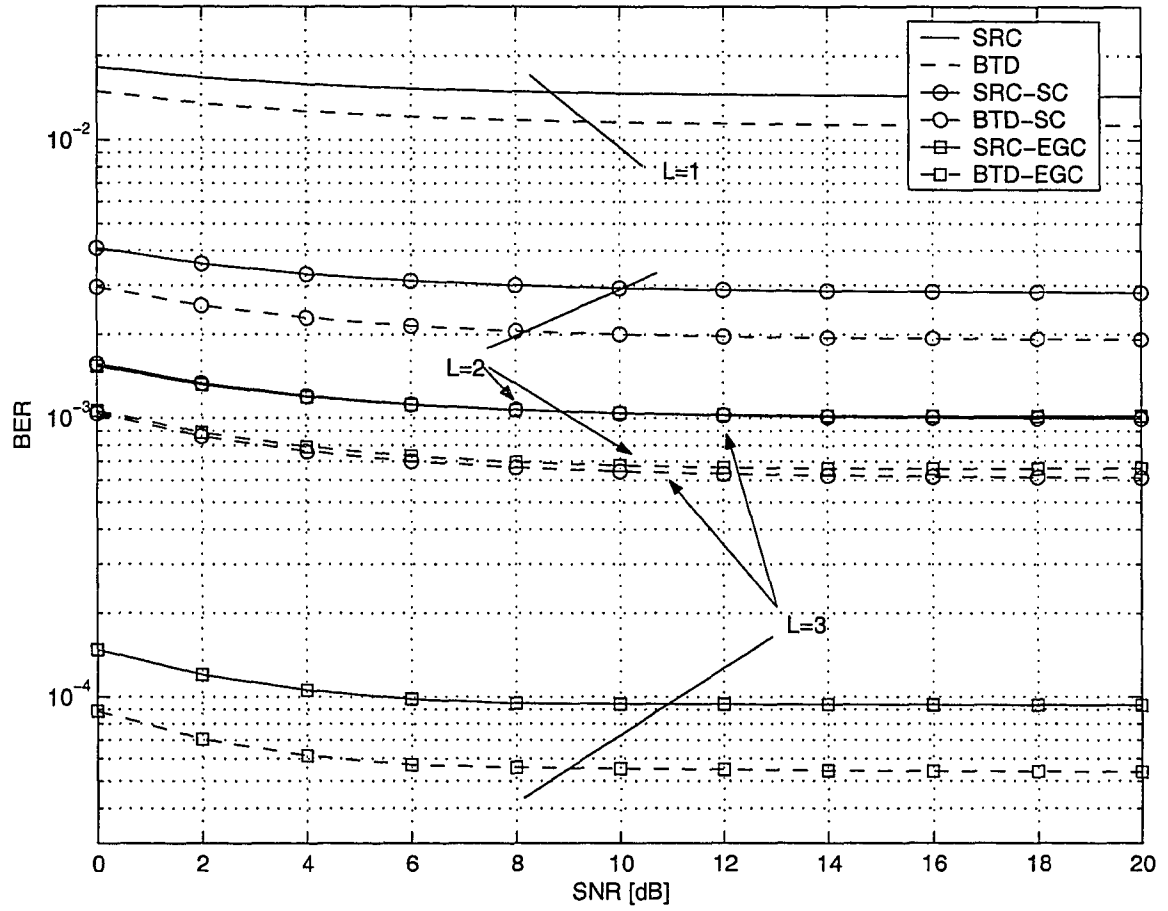


Fig. 4.4. The BER performance of a bandlimited DS-CDMA system estimated using the IGA for EGC and SC diversity in Nakagami fading ( $m = 2$ ) with random spreading ( $N = 64$ ) and  $K = 15$ .

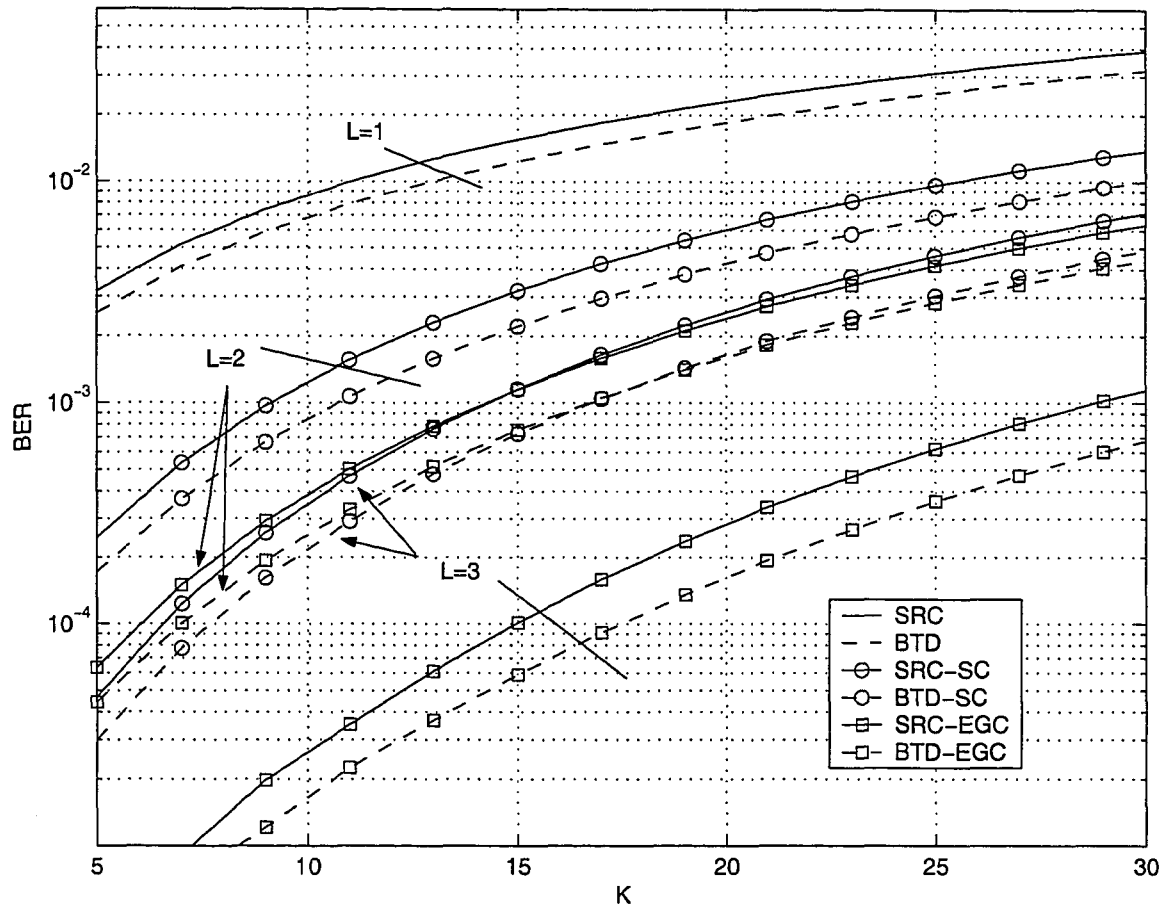


Fig. 4.5. The BER performance of a bandlimited DS-CDMA system estimated using the IGA for EGC and SC diversity in Nakagami fading ( $m = 2$ ) with random spreading ( $N = 64$ ) and  $SNR = 5$  dB.

# Chapter 5

## Interference Whitening Receivers for Bandlimited DS-CDMA Systems in Nakagami Fading Channels

### 5.1 Introduction

Multipath fading and MAI are the major limitations of DS-CDMA systems in wireless environments. The conventional MF or single-user receiver is not optimum when MAI is present. Both jointly optimum and sub-optimum detection schemes have been extensively studied in the literature; see [19] and the references therein. Most of these schemes require knowledge of timing offset, phase offset, spreading sequence, etc. for all the active users in the system. These receiver structures are generally near-far resistant and provide small error rate with high computational complexity.

The high computational complexity makes these schemes less viable for some practical systems, particularly in the down-link. Thus, improved single-user receiver structures were considered by several authors in the literature [23], [24], [42], [91], [92], [93], [94], [95], [96], [97]. These schemes do not require any information about the interfering users's signals . Generally, improved single-user receivers are not near-far resistant and provide poor BER performances compared to joint detection schemes.

A WMF receiver structure studied in [27] was introduced to suppress MAI in DS-CDMA systems in [23] and [24]. Multipath fading was not considered in this work and several assumptions were made in the performance analysis. While whitening maximizes the SNIR, the WMF introduces ISI and the ISI was ignored in the analysis of [23] and [24]. The MAI was assumed to be Gaussian distributed in order to derive the average BER. NRZ rectangular and bandlimited chip pulse shapes were considered. The WMF was generalized to improper complex noise in [42] for an application in DS-CDMA. In [91], [92], the WMF receiver structure was modified to obtain near-far resistance using the knowledge of the timing offsets and powers of all interfering users. A one-shot receiver was considered and, thus, the ISI was neglected. Variations of the receiver structure in [23] were considered in [93] and [94]. In [93], low-pass filtered rectangular pulses and a weighted despreading function were employed. A single-user adaptive MMSE receiver and chip waveform selection were considered for MAI rejection in [94]. The WMF receiver structure in [23] was generalized as a space-time matched filter for asynchronous DS-CDMA with antenna arrays in [95] and [96]. The receiver structure proposed in [92] was extended to DS-CDMA systems with antenna arrays in [97]. An exact performance analysis of a bandlimited DS-CDMA system using a CF method was proposed in [64] and was extended to DS-CDMA systems in Nakagami fading channels in [78].

In this chapter, we derive the accurate BER performance of a WMF receiver structure for a bandlimited asynchronous DS-CDMA system in Nakagami fading without using a Gaussian approximation for the MAI and without neglecting the ISI as in [23]. We introduce a linear fractionally spaced MMSE equalizer [49] to combat the ISI introduced by the WMF. Two Nyquist chip pulse shapes, the SRC and the BTD pulse shapes are employed [30]. The CF [64], [78] and approximate Fourier series [31] methods are used to derive the average BERs. As in [23], we assume the desired and interfering users are spread using Gold and random sequences, respectively.

The remainder of this chapter is organized as follows. In Section 5.2, the system and channel models are introduced. A fractionally spaced MMSE equalizer is designed and the receiver decision statistic is derived. A performance analysis of the proposed WMF receiver is presented in Section 5.3. Numerical results are provided in Section 5.4. Our conclusions for this chapter are drawn in Section 5.5.

## 5.2 System and Channel Model

An asynchronous bandlimited binary DS-CDMA system with  $K + 1$  active users in a Nakagami- $m$  fading channel is considered. In this chapter, the WMF receiver structure is considered for bandlimited DS-CDMA systems in Nakagami fading channels. Therefore, the system model and the definitions in Chapter 3 hold in this chapter also. Now, we consider the interference WMF receiver structure [27], [23], [24] as shown in Fig. 5.1. The real operator and decision device follow the receiver structure in Fig.5.1. The filter  $Q(\omega)H_T^*(\omega)$  is a WMF which whitens the spectrum of the interference and maximizes the SNIR. While maximizing the SNIR, the WMF introduces ISI in the desired samples. A fractionally spaced linear MMSE equalizer is

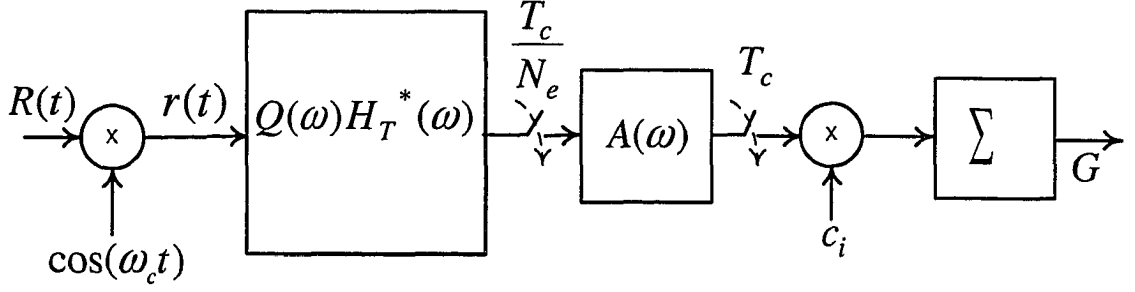


Fig. 5.1. The interference whitening receiver structure for the DS-CDMA system.

employed to combat the ISI introduced by the WMF and it is denoted as  $A(\omega)$ . The filter  $Q(\omega) = 1/S_n(\omega)$  where  $S_n(\omega)$  is the power spectral density of the total multiple access interference plus background noise. The maximum SNIR after the WMF is given by [27], [23]

$$SNIR = \frac{1}{2\pi} \int_{-\infty}^{\infty} \frac{|S(\omega)|^2}{S_n(\omega)} d\omega \quad (5.1)$$

where  $S(\omega)$  is the Fourier transform of the received desired signal component. In this paper, we assume the desired user and interfering user signals are spread using Gold and random sequences, respectively. The desired user signal component in the received signal is

$$s(t) = \sqrt{P_0} R_0 T_c b_i^{(0)} \sum_{i=0}^{N-1} a_i^{(0)} g_T(t - iT_c) \quad (5.2)$$

and its Fourier transform is

$$S(\omega) = \sqrt{P_0} R_0 T_c b_i^{(0)} \sum_{i=0}^{N-1} a_i^{(0)} H_T(\omega) \exp(-j\omega iT_c). \quad (5.3)$$

The PSD of the MAI plus background noise is given by [98]

$$S_n(\omega) = N_0 + \frac{K P_k \Omega T_c^2}{2} H(\omega) \quad (5.4)$$

where static fading and perfect power control (i.e. the interfering users transmit the data at the same power level) are assumed. The average SNIR is written as

$$SNIR = \frac{P_0 \Omega T_c^2}{2\pi} \int_{-\infty}^{\infty} \frac{H(\omega) |C^{(0)}(\omega)|^2}{N_0 + \frac{K P_k \Omega T_c^2}{2} H(\omega)} d\omega \quad (5.5a)$$

where

$$C^{(0)}(\omega) = \sum_{i=0}^{N-1} a_i^{(0)} \exp(-j\omega i T_c). \quad (5.5b)$$

Now, (5.5a) is written as

$$SNIR = \sum_{i=0}^{N-1} \sum_{n=0}^{N-1} a_i^{(0)} a_n^{(0)} f(n-i) \quad (5.6)$$

where

$$\begin{aligned} f(l) &= P_0 \Omega T_c^2 \int_{-\infty}^{+\infty} \frac{H(f) \exp(-j2\pi f l T_c)}{N_0 + \frac{K P_k \Omega T_c^2}{2} H(f)} df \\ &= P_0 \Omega T_c^2 g_w(-l T_c) \end{aligned} \quad (5.7)$$

and  $g_w(t)$  is the inverse Fourier transform of  $H(f)/Q(f)$ . Then, the SNIR can be written as [23]

$$SNIR = N f(0) + 2 \sum_{l=1}^{N-1} R(l) f(l) \quad (5.8a)$$

where

$$R(l) = \sum_{i=0}^{N-1-l} a_i^{(0)} a_{i+l}^{(0)} \quad (5.8b)$$

and is averaged over all possible desired user spreading sequences. The fractionally spaced MMSE equalizer [49] is  $T_c/N_e$  spaced and has  $2K_e + 1$  taps. The optimum coefficients of the MMSE equalizer are the solutions of the system of linear equations [7]

$$\Gamma \mathbf{C} = \boldsymbol{\xi} \quad (5.9)$$



where  $\mathbf{C}$  denotes the column vector of  $2K_e + 1$  tap weight coefficients,  $\boldsymbol{\xi}$  is a  $2K_e + 1$  length column vector written as

$$\boldsymbol{\xi} = \begin{bmatrix} g_w(-K_e T/N_e) \\ g_w(-(K_e - 1)T/N_e) \\ \vdots \\ g_w((K_e - 1)T/N_e) \\ g_w(K_e T/N_e) \end{bmatrix}_{(2K_e+1) \times 1} \quad (5.10)$$

and  $\boldsymbol{\Gamma}$  denotes a  $(2K_e + 1) \times (2K_e + 1)$  Hermitian covariance matrix which is given by [49]

$$\boldsymbol{\Gamma} = \gamma^2 \boldsymbol{\Omega} \mathbf{X}^T \mathbf{X} + \mathbf{I} \quad (5.11)$$

and

$$\mathbf{X} = \begin{bmatrix} g_w(-\frac{K_e T}{N_e}) & g_w(-\frac{(K_e+1)T}{N_e}) & \dots & g_w(-\frac{(3K_e-1)T}{N_e}) & g_w(-\frac{3K_e T}{N_e}) \\ g_w(-\frac{(K_e-N_e)T}{N_e}) & g_w(-\frac{(K_e-N_e+1)T}{N_e}) & \dots & g_w(-\frac{(3K_e-N_e-1)T}{N_e}) & g_w(-\frac{(3K_e-N_e)T}{N_e}) \\ \vdots & \vdots & & \vdots & \vdots \\ g_w(\frac{(3K_e-N_e)T}{N_e}) & g_w(\frac{(3K_e-N_e-1)T}{N_e}) & \dots & g_w(\frac{(K_e-N_e+1)T}{N_e}) & g_w(\frac{(K_e-N_e)T}{N_e}) \\ g_w(\frac{3K_e T}{N_e}) & g_w(\frac{(3K_e-1)T}{N_e}) & \dots & g_w(\frac{(K_e+1)T}{N_e}) & g_w(\frac{K_e T}{N_e}) \end{bmatrix}. \quad (5.12)$$

The average  $SNIR = \gamma^2 \Omega$ . Then, the optimum coefficients are given by

$$\mathbf{C}_{\text{opt}} = \boldsymbol{\Gamma}^{-1} \boldsymbol{\xi}. \quad (5.13)$$

Thus, the sampled output pulse of the MMSE equalizer sampled at  $T_c/N_e$  intervals is obtained as  $\boldsymbol{\xi} * \mathbf{C}_{\text{opt}}$ , where  $*$  denotes the convolution operation. The output contains residual ISI. Now, we derive the decision statistic of this receiver structure. The decision statistic is written as

$$y_i^{(0)} = \sqrt{P_0} R_0 T_b b_i^{(0)} + \mathcal{M}^w + I_c + I_s + \eta_w \quad (5.14)$$

where  $\eta_w$  is a zero-mean Gaussian process with variance  $N_0 T_b / 2$ . The MAI component is given by

$$\mathcal{M}^w = \sum_{k=1}^K \mathcal{M}_k^w \quad (5.15)$$

$$\mathcal{M}_k^w = \sqrt{P_k} R_k \cos(\theta_k) T_c \sum_{l=0}^{N-1} \sum_{n=-\infty}^{\infty} a_l^{(0)} d_n^{(k)} w((l-n)T_c - T_k) \quad (5.16)$$

where  $w(t)$  is the effective pulse-shaping of the receiver structure. The interchip interference  $I_c$ , is written as

$$I_c = \sqrt{P_0} R_0 T_b b_i^{(0)} \sum_{l=0}^{N-1} \sum_{\substack{n \neq l \\ n=0}}^{N-1} a_l^{(0)} a_n^{(0)} w((l-n)T_c) \quad (5.17)$$

and the intersymbol interference  $I_s$ , is given by

$$I_s = \sqrt{P_0} R_0 T_b \sum_{l=0}^{N-1} \sum_{\substack{n \notin [0, N-1] \\ n=-\infty}}^{+\infty} b_{\lfloor \frac{n}{N} \rfloor}^{(0)} a_l^{(0)} a_n^{(0)} w((l-n)T_c). \quad (5.18)$$

In the following section, we consider the performance of the whitening matched filter receiver structure with a fractionally spaced MMSE equalizer.

### 5.3 Performance Analysis of Whitening Matched Filter Receiver Structure

Accurate BER performance analysis of the WMF receiver structure is studied using an approximate Fourier series method [31]. As shown in Section 3.4, the conditional CF of the MAI is given by

$$\Phi_{\mathcal{M}_k^w}(\omega | \mathbf{a}^{(0)}) = \frac{2}{T_c} \int_0^\infty f_{\mathcal{X}_k}(x) \times \int_0^{T_c} \prod_{n=-M}^{N+M-1} \cos \left( \sqrt{P_k} x \omega T_c \sum_{l=0}^{N-1} a_l^{(0)} w((l-n)T_c - T_k) \right) dT_k dx \quad (5.19)$$

where  $f_{\mathcal{X}_k}(x)$  is given in eq. (3.20). The CF of the total conditional MAI is then written as

$$\Phi_{\mathcal{M}^w}(\omega|\mathbf{a}^{(0)}) = \prod_{k=1}^K \Phi_{\mathcal{M}_k^w}(\omega|\mathbf{a}^{(0)}) \quad (5.20)$$

and the conditional CF of the intersymbol interference is written as

$$\begin{aligned} \Phi_{I_s}(\omega|\mathbf{a}^{(0)}, R_0) &= \cos \left( \omega \sqrt{P_0} R_0 T_b \sum_{l=0}^{N-1} \sum_{n=-M}^{-1} a_l^{(0)} a_n^{(0)} w((l-n)T_c) \right) \times \\ &\quad \cos \left( \omega \sqrt{P_0} R_0 T_b \sum_{l=0}^{N-1} \sum_{n=N}^{N+M-1} a_l^{(0)} a_n^{(0)} w((l-n)T_c) \right). \end{aligned} \quad (5.21)$$

Now, we use the Fourier series method proposed in [31] to derive a precise BER expression. The probability of error conditioned on  $\mathcal{M}^w, \mathbf{a}^{(0)}, R_0, b_i^{(1)}, b_i^{(-1)}$ , is

$$\begin{aligned} P(e|\mathcal{M}^w, \mathbf{a}^{(0)}, R_0, b_i^{(1)}, b_i^{(-1)}) &= P(-\sqrt{P_0} R_0 T_b + \mathcal{M}^w + I_{c|b_i^{(0)}=-1} + I_s + \eta_w > 0) \\ &= \mathbf{Q} \left( \frac{\sqrt{P_0} R_0 T_b - \mathcal{M}^w - I_{c|b_i^{(0)}=-1} - I_s}{\sqrt{\text{VAR}[\eta_w]}} \right) \end{aligned} \quad (5.22)$$

where without loss of generality we assume  $b_i^{(0)} = -1$ . The Gaussian tail probability function is denoted as  $\mathbf{Q}(\cdot)$  and it can be written as an infinite series [31]

$$\mathbf{Q}(x) = \frac{1}{2} - \sum_{\substack{v=1 \\ v \text{ odd}}}^{\infty} \frac{\exp(-v^2 \omega_0^2 / 2) \sin(v \omega_0 x)}{v} \quad (5.23)$$

where  $\omega_0 = \frac{2\pi}{T_0}$  and the sampling time,  $T_0$  is appropriately chosen to give the required accuracy. As  $I_s$ ,  $I_c$  and  $\mathcal{M}^w$  are independent random variables conditioned on  $\mathbf{a}^{(0)}$ , the conditional probability of error conditioned on  $\mathbf{a}^{(0)}$  and  $R_0$  is given by

$$\begin{aligned} P(e|\mathbf{a}^{(0)}, R_0) &= \frac{1}{2} - \frac{2}{\pi} \sum_{\substack{v=1 \\ v \text{ odd}}}^{\infty} \frac{\exp(-v^2 \omega_0^2 / 2) \sin \left( v \omega_0 \frac{\sqrt{P_0} R_0 T_b - I_{c|b_i^{(0)}=-1}}{\sqrt{N_0 T_b / 2}} \right)}{v} \times \\ &\quad \Phi_{I_s} \left( -\frac{v \omega_0}{\sqrt{N_0 T_b / 2}} | \mathbf{a}^{(0)}, R_0 \right) \Phi_{\mathcal{M}^w} \left( -\frac{v \omega_0}{\sqrt{N_0 T_b / 2}} | \mathbf{a}^{(0)} \right). \end{aligned} \quad (5.24)$$

If there are  $L_a$  possible desired user spreading sequences, the unconditional probability of error is given by

$$P(e) = \frac{1}{2} - \frac{2}{\pi} \sum_{\substack{v=1 \\ v \text{ odd}}}^{\infty} \frac{\exp(-v^2 \omega_0^2 / 2)}{v L_a} \sum_{l=1}^{L_a} \Phi_{\mathcal{M}^w} \left( -\frac{v \omega_0}{\sqrt{N_0 T_b / 2}} |a^{(0)}| \right) \times \\ \int_0^{\infty} \sin \left( v \omega_0 \frac{\sqrt{P_0} r T_b - I_{c|b_i^{(0)}=-1}}{\sqrt{N_0 T_b / 2}} \right) \Phi_{I_s} \left( -\frac{v \omega_0}{\sqrt{N_0 T_b / 2}} |a^{(0)}, R_0 = r \right) f_{R_0}(r) dr. \quad (5.25)$$

where  $f_{R_0}(r)$  is given by eq. (1.11). The unconditional average BER in eq. (5.25) is evaluated numerically.

## 5.4 Numerical Results and Discussion

In this section, we present some numerical results. The BER performance of the receiver structure with SRC and BTD pulse shapes are compared under identical system parameters. The excess bandwidth of the chip pulse-shapings are assumed to be 100%. We also assume uniform power conditions, i.e. perfect power control in the system is assumed. However, our results can also be applied to nonuniform power conditions. The processing gain,  $N = 31$ . The desired user and interfering users are spread using Gold and random sequences, respectively. The Gold sequences are generated using the primitive polynomials  $1 + x^2 + x^5$  and  $1 + x + x^2 + x^4 + x^5$ . The MMSE equalizer is  $T_c/8$  spaced ( $N_e = 8$ ) and has 81 taps ( $K_e = 40$ ).

Fig. 5.2 depicts the average BER performance versus the average SNR with 10 active interfering users ( $K = 10$ ) for the conventional matched filter and the proposed receiver for an asynchronous bandlimited DS-CDMA system over a slow, flat Nakagami fading channel. The average BER of the WMF receiver structure without the equalizer remains at 0.5 for all SNR values and it is not shown in the

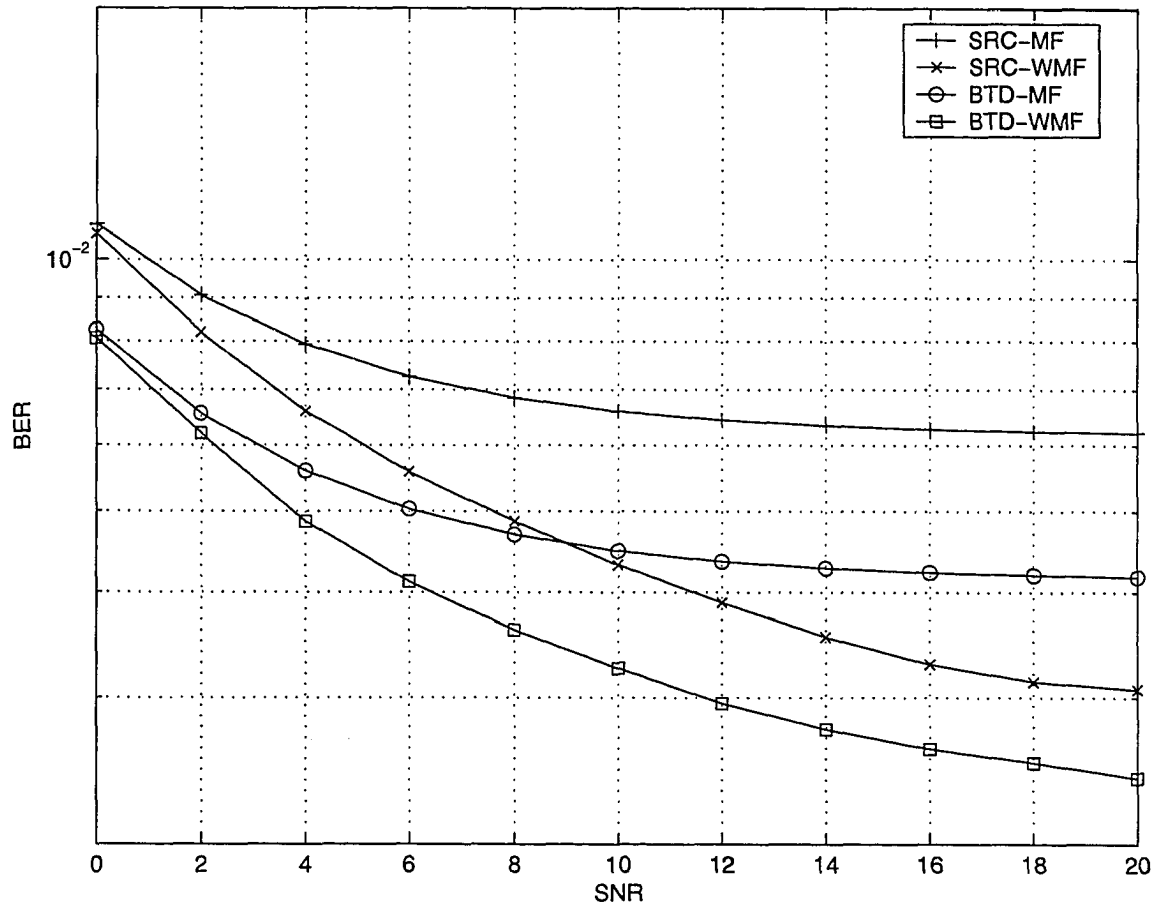


Fig. 5.2. The performance of the whitening matched filter with MMSE equalizer receiver for a bandlimited DS/CDMA system in Nakagami fading ( $m = 8$ ) with Gold/random spreading for desired/interfering users ( $N = 31$ ) and  $K = 10$ .

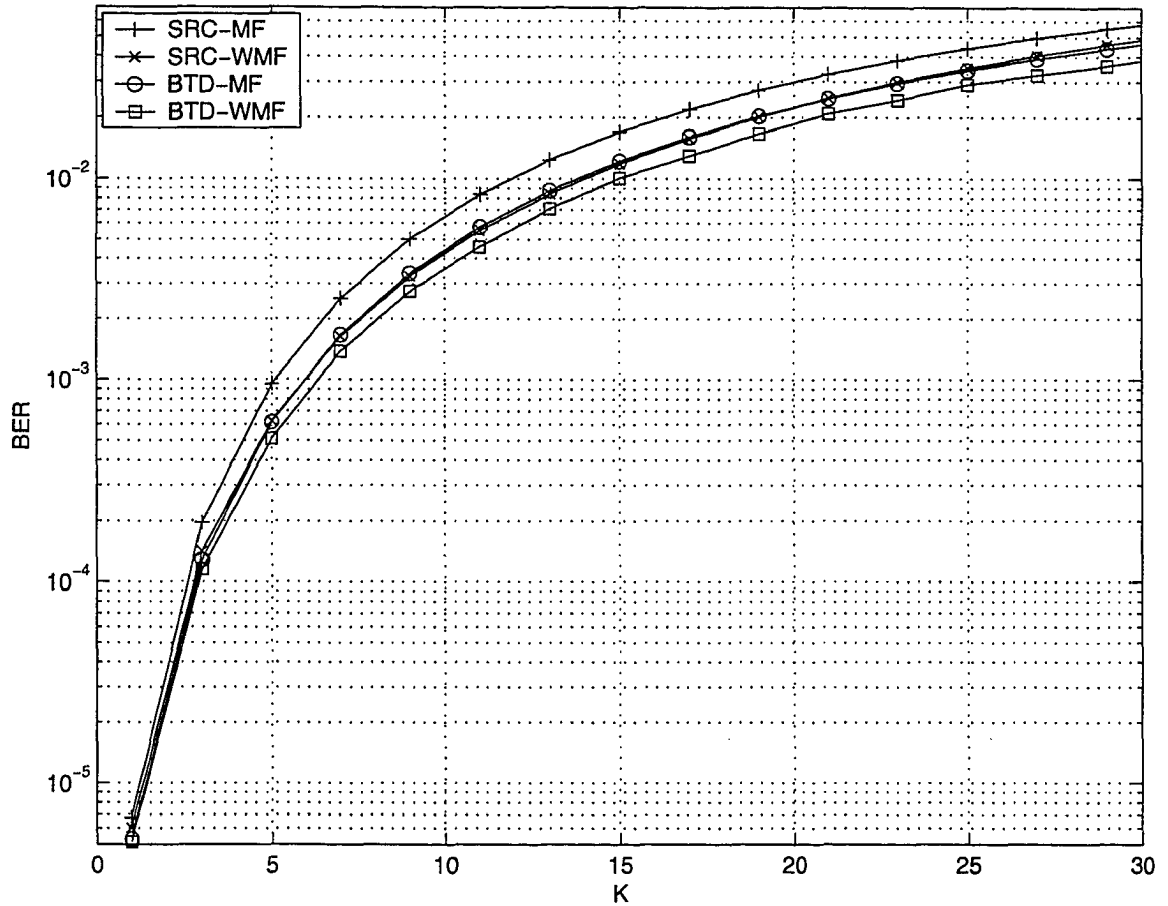


Fig. 5.3. The performance of the whitening matched filter receiver for a bandlimited DS/CDMA system in Nakagami fading ( $m = 8$ ) with Gold/random spreading for desired/interfering users ( $N = 31$ ) and  $SNR = 10$  dB.

figure. This is due to the ISI generated by the WMF. By using the WMF receiver with a fractionally spaced MMSE equalizer, the average BER is halved at  $SNR = 20$  dB. The average BER versus the number of active interferers ( $K$ ) is presented in Fig. 5.3 for average  $SNR = 10$  dB. As observed in [78], the performance with BTM pulse-shaping is always better than that with SRC pulse-shaping.

## 5.5 Summary

A multiple access interference suppression method for a bandlimited DS-CDMA system in slow, flat Nakagami fading was considered. The whitening matched filter receiver proposed in [23] was employed with a fractionally spaced MMSE equalizer to combat the intersymbol interference created by the WMF. The precise BER performance was derived using the CF and Fourier series methods. Without the equalizer the average BER is 0.5 for all values of average SNR and numbers of interferers. When a linear MMSE equalizer is used with the WMF the BER is halved relative to the BER of a conventional MF receiver. The system employing the new BTM pulse outperforms the system using SRC pulse when the same system parameters are considered.

# Chapter 6

## Performance Analysis of Space Diversity Receivers in Cochannel Interference and Fading Channels

### 6.1 Introduction

Performance analysis of wireless communication systems is normally based on average BER and/or outage probability [4]. Normally the BER analysis of diversity systems is much more involved than outage probability analysis. The mathematical modeling and treatment of CCI is usually difficult. Thus, performance analyzes are restricted to approximate analysis or exact analysis of specialized cases. Recently, the BER of BPSK with NRZ rectangular pulse shaping in a Rayleigh/Rayleigh desired/interfering user flat fading environment with asynchronous interferers was published by Hamdi in [44]. Exact analytical results for some probability distributions involved in NRZ BPSK were given by Chiani in [40] and for the error rate of NRZ BPSK in CCI on an



AWGN channel in [16]. General solutions for QPSK error rates in Nakagami/Rayleigh fading were presented by Beaulieu and Abu-Dayya in [43], but these involve three-fold iterated integrations. Furthermore, the case of BPSK in Nakagami/Nakagami fading was not considered. In reference [99], Aalo and Zhang considered the BER of BPSK and BFSK in CCI limited Nakagami/Nakagami fading environments. Gaussian approximation of the CCI was employed through the invocation of [99, eq.(9)]. Recently, the BER performance of bandlimited BPSK systems with CCI in Nakagami fading was investigated using a CF method by Beaulieu and Cheng in [45].

Conventional space diversity schemes combat fading and cochannel interference simultaneously. Among space diversity schemes, EGC and SC are of practical interest because of their simple implementations. The BER performances of EGC and SC in fading channels without CCI were well studied in [88], [89], [10], [6] and the references therein. In [88], a series method was proposed for the computation of the PDF of the sum of independent RV to analyze BER performance of the EGC in Nakagami fading by Beaulieu and Abu-Dayya. A numerical method based on Parseval's theorem was proposed by Annamalai *et al.* in [89] for EGC in wireless channels. A method based on an alternate representation of the Gaussian  $Q$ -function was proposed by Simon and Alouini and is given in [6]. Two types of SC schemes were studied in [10] for CPSK and NCFSK in Rayleigh fading channels. A unified integral solution treatment of fading channels and diversity schemes was presented in [6]. In [100], the BER performance of dual branch EGC and SC in bandlimited BPSK, QPSK and 8PSK systems with CCI in Nakagami/Rayleigh fading was analyzed by Abu-Dayya and Beaulieu using an approximate Fourier series method.

Calculation of the BER and outage probability of MRC with CCI in fading channels is quite complicated. The BER and outage performance of MRC diversity with-

out CCI is discussed in depth in [6] and the references therein. However, the BER and outage performance when CCI is present has been considered by very few authors [101] [102], [103], [104], [105]. The outage probability for a constant envelope modulation scheme with CCI in Rayleigh fading was studied by Cui and Sheikh in [101]; one and three interferers were considered in the analysis. In [102], Shah and Haimovich derived an outage probability expression for an interference limited BPSK system with an arbitrary number of interferers in Rayleigh fading. The BER expression was derived using a Gaussian approximation for the CCI. Equal interferer powers were assumed. In [103], the performances of BPSK and DPSK over independent Nakagami fading diversity channels was studied by Aalo and Zhang. Some assumptions were made in the analysis without being explicitly stated. The SNIR expression in [103, eq.(1)] was written by assuming the interferers' phase and timing offsets were zero. The sum of the CCI and background noise was assumed to be Gaussian distributed conditioned on the instantaneous SNIR by invoking [103, eqs. (12), (20)]. Then, the BER and outage probability expressions were derived only for integer values of the Nakagami fading parameter. The performance of MPSK in a Rician/Rayleigh fading model was considered in [104] with the same assumptions made in [103]. The BER of BPSK with MRC in correlated and independent Rician fading channels was considered by Ma *et al.* in [105] but only synchronous interferers were considered. An exact BER computation was done using saddle point integration techniques [106], but the method of [105] has complexity increasing exponentially with the number of interferers. An approximate analysis was performed by invoking a CLT. Recently, in [107] the outage analysis for Rician/Rayleigh and Nakagami/Rayleigh models was considered for unequal power interferers. In references [101], [103], [104], [105], pulse-shaping was not considered.

In this chapter, we first derive the exact BER of coherent NRZ BPSK in asynchronous CCI with Nakagami/Nakagami flat fading and of coherent NRZ QPSK in asynchronous CCI with Nakagami/Rayleigh flat fading using a characteristic function method. The fading is assumed to be slow and the fading gains of the user signals are assumed independent. Our results are more general than those of [44] in that [44] considers only NRZ BPSK in Rayleigh/Rayleigh fading. We examine NRZ BPSK and QPSK in Nakagami/Nakagami and Nakagami/Rayleigh fading, respectively. Our analysis differs from that of [44]; we use a CF method while [44] uses a Hermite polynomial approach. Our results also establish the limitations of accuracy of the Gaussian approximation invoked in [99]. In some cases, the accurate error rates are different by a factor of 5.3 from the error rates predicted by the results of [99].

Then, we derive the exact BER of coherent bandlimited BPSK in asynchronous CCI and Nakagami flat fading with EGC using a CF method and with SC using a Fourier series method for arbitrary diversity orders and Nakagami fading parameters. The SRC and BTD [30] pulse shapes are employed. Again slow fading and independent fading gains are assumed. The BER analysis of [45] is extended to EGC with CCI using the method based on Parseval's theorem presented in [89]. The Fourier series method of [100] applied for a Nakagami/Rayleigh fading model with dual branch SC is extended to iid Nakagami fading with arbitrary diversity order. Thus, our results are more general than those obtained in [100].

Finally, we consider outage and BER analyzes of coherent bandlimited BPSK with MRC diversity and asynchronous CCI in micro-cellular systems. A Nakagami/Rayleigh fading model is assumed. Again SRC and BTD [30] pulse shapes are employed. Slow fading and independent fading gains are assumed. Exact closed-form expressions for outage probability with equal and distinct interferer powers are derived. An average

BER expression is derived using a Gaussian approximation for the CCI. The accuracy of the Gaussian approximation is validated using Monte Carlo simulation. Our expressions are valid for arbitrary diversity order, number of interferers and desired user Nakagami fading parameter. For BPSK, our results are more general than those obtained in [101], [102], [103], [104], [105] and in particular our outage probability expressions are much simpler than those obtained in [107].

The remainder of this chapter is organized as follows. The system and channel models are presented in Section 6.2. The BER analyzes of BPSK and QPSK systems in CCI and fading with NRZ pulse shapes are considered in Section 6.3. In Section 6.4, the BER analyzes of EGC and SC diversities in CCI and Nakagami fading are presented. The outage and BER of MRC diversity with CCI and fading is studied in Section 6.5. Some interesting numerical results and discussion are given in Section 6.6. Finally our conclusions and summary for this chapter are drawn in Section 6.7.

## 6.2 System and Channel Model

Consider a coherent bandlimited BPSK system with cochannel interference in a slowly fading environment. We adopt the system model of Chapter 2 for the diversity receiver structure. There are  $L$  space diversity branches and  $K + 1$  active users in the system. The  $j$ -th branch received signal of the desired (0-th) user is

$$R_j(t) = \sqrt{2P_0T} R_{0,j} s_d(t) \cos(\omega_c t) + \sum_{i=1}^K \sqrt{2P_iT} R_{i,j} s_i(t - \tau_i) \cos(\omega_c(t - \tau_i) + \theta_{i,j}) + n(t) \quad (6.1)$$

where  $P_i$  is the transmitted power of the  $i$ -th user,  $\omega_c$  is the carrier frequency,  $s_d(t) = \sum_{k=-\infty}^{+\infty} a[k]g_T(t - kT)$ ,  $s_i(t) = \sum_{k=-\infty}^{+\infty} b_i[k]g_T(t - kT)$ ,  $\frac{1}{T}$  is the symbol transmission rate and  $g_T(\cdot)$  is the transmitter signal baseband pulse with its energy

normalized according to  $\int_{-\infty}^{+\infty} g_T^2(t)dt = 1$ ,  $a[k] \in \{+1, -1\}$  with equal probabilities and  $\tau_i$  represents the symbol timing offset of the  $i$ -th user signal with respect to the desired user signal, assumed to be uniform over  $[0, T)$ . The background noise  $n(t)$  is a zero-mean, white Gaussian process with two-sided power spectral density  $N_0/2$ ; the phases  $\theta_{i,j}$ , are assumed to be mutually independent and uniformly distributed over  $[0, 2\pi)$ . The fading gains are assumed to be independent and identically distributed. The received signal for the coherent QPSK system is given by

$$\begin{aligned}
R_j(t) = & \sqrt{P_0 T} R_{0,j} [s_{Id}(t) \cos(\omega_c t) + s_{Qd}(t) \sin(\omega_c t)] + \\
& \sum_{i=1}^K \sqrt{P_i T} R_{i,j} \left[ s_{Ii}(t - \tau_i) \cos(\omega_c(t - \tau_i) + \theta_i) + \right. \\
& \left. s_{Qi}(t - \tau_i) \sin(\omega_c(t - \tau_i) + \theta_i) \right] + n(t).
\end{aligned} \tag{6.2}$$

The common symbols in (6.1) and (6.2) denote the same parameters. The desired user in-phase and quadrature symbol sequences are  $s_{Id}(t)$  and  $s_{Qd}(t)$ ;  $s_{Ii}(t)$  and  $s_{Qi}(t)$  are  $i$ -th interferer in-phase and quadrature symbol sequences. The desired user average signal-to-noise ratio and signal-to-interference ratio are defined as  $\text{SNR}(\text{dB}) = 10 \log_{10} (P_0 T \Omega_0 / 2)$ , and  $\text{SIR}(\text{dB}) = 10 \log_{10} \left( P_0 \Omega_0 / (\sum_{i=1}^K P_i \Omega_i) \right)$ , where  $\Omega_i = \mathbb{E}[R_{i,j}^2]$  and without loss of generality, we assume the noise variance is one.

### 6.3 BER Analysis of BPSK and QPSK in CCI and Fading with NRZ Pulse-Shaping

In this section, exact BER expressions are derived for a BPSK system with a Nakagami/Nakagami fading model and QPSK with Nakagami/Rayleigh fading model in the presence of CCI. The rectangular pulse-shaping,  $g_T(t)$  is  $1/\sqrt{T}$  in  $0 \leq t \leq T$ .

### 6.3.1 BPSK Analysis

For a BPSK system, we assume the fading amplitude  $R_{i,j}$  follows the Nakagami- $m$  distribution with parameters  $(m_i, \Omega_i)$  and is given in eq. (1.11). The fading gains  $R_{i,j}$  are assumed to be independent. After demodulation and matched filtering, the decision statistic for desired user data symbol  $a[0]$  is

$$Z[0] = \sqrt{\frac{P_0 T}{2}} R_{0,j} a[0] + \sum_{i=1}^K \sqrt{\frac{P_i T}{2}} R_{i,j} \cos(\phi_{i,j}) \rho_i + n_f, \quad (6.3)$$

where  $\phi_{i,j} = (\theta_{i,j} - \omega_i \tau_i) \sim \mathcal{U}[0, 2\pi]$ ,

$$\rho_i = b_i[-1] \frac{\tau_i}{T} + b_i[0] \left[1 - \frac{\tau_i}{T}\right], \quad (6.4)$$

and  $n_f$  is zero-mean Gaussian noise with variance one. The total CCI,  $I_{CCI} = \sum_{i=1}^K I_i$ , where

$$I_i = \sqrt{\frac{P_i T}{2}} R_{i,j} \cos(\phi_{i,j}) \left[ b_i[-1] \frac{\tau_i}{T} + b_i[0] \left[1 - \frac{\tau_i}{T}\right] \right]. \quad (6.5)$$

If  $b_i[-1] = b_i[0]$ , the conditional CF of  $I_i$ , derived in [45] is

$$\Phi_{I_i|b_i[-1]=b_i[0]}(\omega) = {}_1F_1 \left( m_i; 1; -\frac{P_i T \Omega_i \omega^2}{8m_i} \right). \quad (6.6)$$

When  $b_i[-1] \neq b_i[0]$ ,  $I_i$  becomes

$$I_i = \sqrt{\frac{P_i T}{2}} R_{i,j} \cos(\phi_{i,j}) u, \quad (6.7)$$

where  $u \sim \mathcal{U}[-1, 1]$ . Then, the CF of  $I_i$  conditioned on  $u$  is

$$\Phi_{I_i|b_i[-1] \neq b_i[0], u}(\omega) = {}_1F_1 \left( m_i; 1; -\frac{P_i T \Omega_i u^2 \omega^2}{8m_i} \right). \quad (6.8)$$

Averaging out  $u$  in (6.8) one obtains [76]

$$\Phi_{I_i|b_i[-1] \neq b_i[0]}(\omega) = {}_2F_2 \left( \frac{1}{2}, m_i; 1, \frac{3}{2}; -\frac{P_i T \Omega_i \omega^2}{8m_i} \right) \quad (6.9)$$

where  ${}_2F_2(\cdot)$  was defined in [99]. Then, the unconditional CF becomes

$$\Phi_{I_i}(\omega) = \frac{1}{2}\Phi_{I_i|b_i[-1]=b_i[0]}(\omega) + \frac{1}{2}\Phi_{I_i|b_i[-1]\neq b_i[0]}(\omega). \quad (6.10)$$

Since the interferer signals are independent, the CF of  $I_{CCI}$  is  $\Phi_{I_{CCI}}(\omega) = \prod_{i=1}^K \Phi_{I_i}(\omega)$ , and the CF of the noise component is,  $\Phi_{n_f}(\omega) = e^{-\frac{\omega^2}{2}}$ . The CF of the total CCI plus background noise is given by

$$\Phi_T(\omega) = \Phi_{I_{CCI}}(\omega)\Phi_{n_f}(\omega). \quad (6.11)$$

The average BER, conditioned on  $R_{0,j}$  is written as [67]

$$\begin{aligned} P_{e|R_{0,j}} &= \Pr \left[ \sqrt{\frac{P_0 T}{2}} R_{0,j} a[0] + I_{CCI} + n_f < 0 \mid a[0] = +1 \right] \\ &= \frac{1}{2} - \frac{1}{\pi} \int_0^{+\infty} \frac{\sin \left( \sqrt{\frac{P_0 T}{2}} R_{0,j} \omega \right)}{\omega} \Phi_T(\omega) d\omega. \end{aligned} \quad (6.12)$$

When the desired user undergoes Nakagami fading, the average BER becomes

$$P_e = \frac{1}{2} - \frac{\Gamma(m_0 + \frac{1}{2})}{\pi \Gamma(m_0)} \sqrt{\frac{P_0 T \Omega_0}{2m_0}} \int_0^{+\infty} \Phi_T(\omega) {}_1F_1 \left( m_0 + \frac{1}{2}; \frac{3}{2}; \frac{-P_0 T \Omega_0 \omega^2}{8m_0} \right) d\omega. \quad (6.13)$$

The single integral in (6.13) can be readily evaluated numerically.

### 6.3.2 QPSK Analysis

Assuming Gray-code bit-mapping and symmetric I and Q branches, the decision statistic for the desired user data symbol  $a_I[0]$  in the in-phase branch after coherent demodulation and matched filtering, is written as

$$Z_I[0] = \frac{\sqrt{P_0 T}}{2} R_{0,j} a_I[0] + \sum_{i=1}^K \frac{\sqrt{P_i T}}{2} R_{i,j} [r_I \cos(\phi_{i,j}) + r_Q \sin(\phi_{i,j})] + n_c, \quad (6.14)$$

where  $n_c$  is complex background noise and

$$r_I = b_{Ii}[-1] \frac{\tau_i}{T} + b_{Ii}[0] [1 - \frac{\tau_i}{T}], \quad (6.15a)$$

$$r_Q = b_{Qi}[-1] \frac{\tau_i}{T} + b_{Qi}[0] [1 - \frac{\tau_i}{T}]. \quad (6.15b)$$

The total CCI,  $I_{CCI} = \sum_{i=1}^K I_i$ , where

$$I_i = \frac{\sqrt{P_i T}}{2} R_{i,j} [r_I \cos(\phi_{i,j}) + r_Q \sin(\phi_{i,j})]. \quad (6.16)$$

The conditional CF when  $b_{Ii}[-1] = b_{Ii}[0]$  and  $b_{Qi}[-1] = b_{Qi}[0]$ , becomes

$$\Phi_{I_i|b_{Ii}[-1]=b_{Ii}[0], b_{Qi}[-1]=b_{Qi}[0]}(\omega) = e^{-\frac{P_i T \Omega_i \omega^2}{8}}. \quad (6.17)$$

When  $b_{Ii}[-1] \neq b_{Ii}[0]$  and  $b_{Qi}[-1] \neq b_{Qi}[0]$ , the conditional CF is

$$\Phi_{I_i|b_{Ii}[-1] \neq b_{Ii}[0], b_{Qi}[-1] \neq b_{Qi}[0], u}(\omega) = e^{-\frac{P_i T \Omega_i u^2 \omega^2}{8}}, \quad (6.18)$$

where  $u \sim U[-1, 1]$  as in Section 6.3.1. After averaging out  $u$ , (6.18) becomes

$$\Phi_{I_i|b_{Ii}[-1] \neq b_{Ii}[0], b_{Qi}[-1] \neq b_{Qi}[0]}(\omega) = \sqrt{\frac{2\pi}{P_i T \Omega_i \omega^2}} \left[ 1 - 2Q \left( \sqrt{\frac{P_i T \Omega_i}{4}} \omega \right) \right]. \quad (6.19)$$

If  $b_{Ii}[-1] \neq b_{Ii}[0]$  and  $b_{Qi}[-1] = b_{Qi}[0]$  or  $b_{Ii}[-1] = b_{Ii}[0]$  and  $b_{Qi}[-1] \neq b_{Qi}[0]$ , the conditional CF becomes

$$\Phi_{I_i|b_{Ii}[-1]=b_{Ii}[0], b_{Qi}[-1] \neq b_{Qi}[0], u}(\omega) = \Phi_{I_i|b_{Ii}[-1] \neq b_{Ii}[0], b_{Qi}[-1]=b_{Qi}[0], u}(\omega) = e^{-\frac{P_i T \Omega_i [1+u^2] \omega^2}{16}}. \quad (6.20)$$

After averaging out  $u$ , (6.20) becomes

$$\Phi_{I_i|b_{Ii}[-1] \neq b_{Ii}[0], b_{Qi}[-1]=b_{Qi}[0]}(\omega) = \sqrt{\frac{4\pi}{P_i T \Omega_i \omega^2}} e^{-\frac{P_i T \Omega_i \omega^2}{16}} \left[ 1 - 2Q \left( \sqrt{\frac{P_i T \Omega_i}{8}} \omega \right) \right]. \quad (6.21)$$

Then, the unconditional CF of  $I_i$  becomes

$$\begin{aligned} \Phi_{I_i}(\omega) &= \frac{1}{4} \Phi_{I_i|b_{Ii}[-1]=b_{Ii}[0], b_{Qi}[-1]=b_{Qi}[0]}(\omega) + \frac{1}{4} \Phi_{I_i|b_{Ii}[-1] \neq b_{Ii}[0], b_{Qi}[-1] \neq b_{Qi}[0]}(\omega) + \\ &\quad \frac{1}{2} \Phi_{I_i|b_{Ii}[-1] \neq b_{Ii}[0], b_{Qi}[-1]=b_{Qi}[0]}(\omega). \end{aligned} \quad (6.22)$$

Now the CFs  $\Phi_{I_{CCI}}(\omega)$ , and  $\Phi_T(\omega)$  can be written as in Section 6.3.1 and the average BER can be calculated according to (6.13).



### 6.3.3 BER Analysis Using Gaussian Approximation

Here, we derive a BER expression using the Gaussian approximation for the CCI to compare with our exact results. The variance of  $I_{CCI}$  is given by  $\text{VAR}[I_{CCI}] = T \sum_{i=1}^K \Omega_i P_i / 6$  for BPSK and QPSK systems. Then, using a Gaussian approximation the BER conditioned on  $R_0$  is  $\mathcal{Q}(\sqrt{P_0 T R_{0,j}^2 / 2\sigma_t^2})$  where  $\sigma_t^2 = 1 + \text{VAR}[I_{CCI}]$ . The unconditional average BER approximation for an arbitrary value of  $m_0$ , is obtained by averaging the conditional BER over the Nakagami fading as

$$P_{eg} = \frac{\Gamma(m_0 + \frac{1}{2})}{2\sqrt{\pi}m_0\Gamma(m_0)} \left( \frac{2m_0}{\Lambda^2\Omega_0} \right)^{m_0} {}_2F_1 \left( m_0, m_0 + \frac{1}{2}; m_0 + 1; \frac{-2m_0}{\Omega_0\Lambda^2} \right), \quad (6.23)$$

where  $\Lambda^2 = P_0 T / (2\sigma_t^2)$ .

## 6.4 BER Analysis of Bandlimited BPSK with EGC and SC Diversity in CCI and Nakagami Fading

In this section, the fading gains,  $R_{i,j}$  are Nakagami- $m$  distributed with parameters  $(m, \Omega)$ . The fading gains are iid. As in [45], two types of bandlimited Nyquist pulse shapes the spectrum SRC and the BTD [30] pulse shapes are considered,. We assume 100 % excess bandwidth pulse shapes in this section.

### 6.4.1 Equal Gain Combining (EGC)

In this subsection, the performance of a BPSK system with  $L$  branch predetection EGC in Nakagami fading is considered. Since the fading is slow, coherent reception is possible. After demodulation, matched filtering and cophasing, the decision statistic

for the desired user data symbol  $a[0]$ , on the  $j$ -th branch, is given by

$$Z_j[0] = \sqrt{\frac{P_0 T}{2}} R_{0,j} a[0] + \sum_{i=1}^K \sqrt{\frac{P_i T}{2}} R_{i,j} \cos(\phi_{i,j}) \rho_i + n_j, \quad (6.24)$$

where  $\phi_{i,j} = (\theta_{ij} - \omega_c \tau_i) \sim \mathcal{U}[0, 2\pi]$ ,  $n_j$  is zero-mean Gaussian noise with variance one,

$$\rho_i = \sum_{k=-\infty}^{+\infty} b_i[k] g(-kT - \tau_i) \quad (6.25)$$

and  $g(\cdot)$  is the pulse shape at the receiver. After the EGC, the decision statistic is given by

$$Z[0] = \sqrt{\frac{P_0 T}{2}} a[0] \sum_{j=1}^L R_{0,j} + \sum_{j=1}^L \sum_{i=1}^K \sqrt{\frac{P_i T}{2}} R_{i,j} \cos(\phi_{i,j}) \rho_i + \sum_{j=1}^L n_j. \quad (6.26)$$

The third term of (6.26) is the CCI component usefully rewritten as  $I_C = \sum_{j=1}^L \sum_{i=1}^K I_{i,j}$ , where

$$I_{i,j} = \sqrt{\frac{P_i T}{2}} R_{i,j} \cos(\phi_{i,j}) \rho_i. \quad (6.27)$$

Now, as shown in [100], [45], the conditional CF of the  $I_{i,j}$  conditioned on  $\tau_i$  and  $X_{i,j}$ , ( $X_{i,j} = R_{i,j} \cos \phi_{i,j}$ ) is written as

$$\Phi_{I_{i,j}|X_{i,j},\tau_i}(\omega) = \prod_{k=-M}^M \cos \left( \sqrt{\frac{P_i T}{2}} X_{i,j} \omega g(-kT - \tau_i) \right) \quad (6.28)$$

where the cross ISI contribution is assumed to be from  $2M + 1$  symbols only. The PDF of the  $f_{X_{i,j}}(x)$  is given in eq. (3.20). Now, forming the double product over  $i$  and  $j$  from (6.28) and then averaging out  $\tau_i$  and  $X_{i,j}$ ,

$$\Phi_{I_C}(\omega) = \prod_{i=1}^K \frac{1}{T} \int_0^T \left[ \prod_{j=1}^L 2 \int_0^\infty f_{X_{i,j}}(x) \prod_{k=-M}^M \cos \left( \sqrt{\frac{P_i T}{2}} x \omega g(-kT - u) \right) dx \right] du. \quad (6.29)$$

As the  $n_j$ s are independent zero-mean Gaussian RVs with unit variance, the background noise term  $n = \sum_{j=1}^L n_j$ , in (6.26) is zero-mean Gaussian distributed with

variance  $L$ . The CF of  $n$  is  $\Phi_n(\omega) = e^{-\frac{\omega^2 L}{2}}$ . The CF of the total CCI plus background noise is given by

$$\Phi_T(\omega) = \Phi_{I_C}(\omega)\Phi_n(\omega). \quad (6.30)$$

The average BER, conditioned on  $R_E$  is written as [67]

$$\begin{aligned} P_{e1|R_E} &= \Pr \left[ \sqrt{\frac{P_0 T}{2}} R_E + I_C + n < 0 \middle| a[0] = +1 \right] \\ &= \frac{1}{2} - \frac{1}{\pi} \int_0^{+\infty} \frac{\sin \left( \sqrt{\frac{P_0 T}{2}} R_E u \right)}{u} \Phi_T(u) du \end{aligned} \quad (6.31)$$

where  $R_E = \sum_{j=1}^L R_{0,j}$ . The unconditional BER can be obtained using several methods. One approach is to average out the  $R_{0,j}$ s one by one or similarly, using  $L - 1$  fold convolution find the PDF of  $R_E$  and then average it out. This method is computationally very complex when  $L$  is large. Another approach is to find the PDF of  $R_E$  using the series method proposed in [88] and average it out. A method based on an alternate representation of the Gaussian  $Q$  function is given in [6]. A fourth approach uses the Parseval's theorem based method proposed in [89]. Eq. (6.31) has the desired format to apply the latter method. Now, the unconditional BER is given by

$$P_{e1} = \frac{1}{2} - \frac{1}{\pi} \int_0^\infty \int_0^\infty \frac{\sin \left( \sqrt{\frac{P_0 T}{2}} r u \right) \Phi_T(u) f_{R_E}(r)}{u} du dr. \quad (6.32)$$

By applying the method proposed in [89], (6.32) becomes

$$\begin{aligned} P_{e1} &= \frac{1}{2} - \int_0^\infty \frac{\Phi_T(u)}{\pi^2 u} \int_0^\infty \Re \left[ \left[ j\pi\delta \left( \omega + \sqrt{\frac{P_0 T}{2}} u \right) - \right. \right. \\ &\quad \left. \left. j\pi\delta \left( \omega - \sqrt{\frac{P_0 T}{2}} u \right) \right] \Phi_{R_E}^*(\omega) \right] d\omega du \\ &= \frac{1}{2} - \frac{1}{\pi} \int_0^\infty \frac{\Phi_T(u)}{u} \Im \left[ \Phi_{R_E} \left( \sqrt{\frac{P_0 T}{2}} u \right) \right] du \end{aligned} \quad (6.33)$$

where  $\Re[x]$  and  $\Im[x]$  is the real and imaginary part of  $x$ , respectively,  $\Phi_{R_E}^*(\omega)$  is the complex conjugate of the CF of  $R_E$  ( $\Phi_{R_E}(\omega)$ ),  $j = \sqrt{-1}$  and  $\delta(\cdot)$  is the Dirac delta function. Eq. (6.33) with eq.(6.30) is an exact solution for the general case including pulse-shaping. A triple numerical integration is required, but the computational complexity does not grow with  $L$ . The CF of  $R_{0,j}$  is written as [88], [13]

$$\Phi_{R_{0,j}}(\omega) = {}_1F_1\left(m; \frac{1}{2}; \frac{-\Omega\omega^2}{4m}\right) + j\omega \frac{\Gamma(m + \frac{1}{2})}{\Gamma(m)} \sqrt{\frac{\Omega}{m}} {}_1F_1\left(m + \frac{1}{2}; \frac{3}{2}; \frac{-\Omega\omega^2}{4m}\right). \quad (6.34)$$

Then, the CF of  $R_E$  is  $\Phi_{R_E}(\omega) = (\Phi_{R_{0,j}}(\omega))^L$ .

### 6.4.2 Selection Combining (SC)

In this subsection, the performance of  $L$ -branch predetection SC in Nakagami fading is considered. The decision statistic for the desired user data symbol  $a[0]$  after coherent demodulation and matched filtering in all branches, is written as

$$Z[0] = \sqrt{\frac{P_0 T}{2}} a[0] R_S + \sum_{i=1}^K \sqrt{\frac{P_i T}{2}} R_{i,j} \cos(\phi_{i,j}) \rho_i + n_j \quad (6.35)$$

where  $R_S = \max_{j \in [1 \dots L]} R_{0,j}$ . The CF of the total CCI,  $\Phi_{I_C}^s(\omega)$  is then obtained by substituting  $L = 1$  in (6.29). As in [100], using an approximate Fourier series method [31], the unconditional BER is given by

$$P_{e2} = \frac{1}{2} - \frac{2}{\pi} \sum_{\substack{l=1 \\ l \text{ odd}}}^{\infty} \frac{e^{-\frac{l^2 \omega_0^2}{2}} \Phi_{I_C}^s(l\omega_0)}{l} \int_0^{\infty} \sin\left(\sqrt{\frac{P_0 T}{2}} r l \omega_0\right) f_{R_S}(r) dr \quad (6.36)$$

where  $f_{R_S}(r)$  is the PDF of  $R_S$ ,  $\omega_0 = 2\pi/T_0$  and  $T_0$  is selected to obtain the required accuracy. Now, the PDF of  $R_S$  can be obtained using order statistics [6], [4]. For  $L$  independent branch SC in Nakagami fading, the PDF of  $R_S$  is [76]

$$f_{R_S}(r) = \frac{2L \left[ \gamma(m, \frac{mr^2}{\Omega}) \right]^{L-1}}{[\Gamma(m)]^L} \left( \frac{m}{\Omega} \right)^m e^{-\frac{mr^2}{\Omega}} r^{2m-1} \quad (6.37)$$

where  $\gamma(\cdot, \cdot)$  is the lower incomplete gamma function [76].

## 6.5 Outage and BER Analysis of Bandlimited BPSK with MRC Diversity in CCI and Fading

In this section, the performance of a BPSK system with  $L$ -branch MRC in a Nakagami-Rayleigh fading model is considered. The desired user fading parameters are  $(m, \Omega_0)$  and for interferers  $\mathbb{E}[R_{i,j}^2] = \Omega$ ,  $i \neq 0$ . Again, SRC and BTD pulse shapes are employed with 100 % excess bandwidth. After demodulation, matched filtering, cophasing and weighting by the conjugate fading gain, the decision statistic for the desired user data symbol  $a[0]$ , on the  $j$ -th branch, is given by

$$Z_j[0] = \sqrt{\frac{P_0 T}{2}} R_{0,j}^2 a[0] + n_j R_{0,j} + \sum_{i=1}^K \sqrt{\frac{P_i T}{2}} R_{i,j} R_{0,j} \cos(\phi_{i,j}) \rho_i \quad (6.38)$$

where  $\phi_{i,j} = (\theta_{ij} - \omega_c \tau_i) \sim \mathcal{U}[0, 2\pi]$ ,  $n_j$  is zero-mean Gaussian noise with variance one,  $\rho_i = \sum_{k=-\infty}^{+\infty} b_i[k] g(-kT - \tau_i)$  and  $g(\cdot)$  is the pulse shape at the receiver. After the combining, the decision statistic is given by

$$Z[0] = \sqrt{\frac{P_0 T}{2}} a[0] \mathbf{c}_s^T \mathbf{c}_s + \sum_{i=1}^K \sqrt{\frac{P_i T}{2}} \rho_i \mathbf{c}_s^T \mathbf{c}_i + \mathbf{c}_s^T \mathbf{n} \quad (6.39)$$

where  $\mathbf{c}_s = [R_{01}, \dots, R_{0L}]^T$ ,  $\mathbf{n} = [n_1, \dots, n_L]^T$  and  $\mathbf{c}_i = [R_{i1} \cos(\phi_{i1}), \dots, R_{iL} \cos(\phi_{iL})]^T$ .

### 6.5.1 Outage Probability Analysis

Now, we study the exact outage probability for an interference limited system. The instantaneous SIR is

$$SIR = \frac{P_0 |\mathbf{c}_s|^4}{\sum_{i=1}^K P_i Y |\mathbf{c}_s^T \mathbf{c}_i|^2} = \frac{P_0 |\mathbf{c}_s|^2}{Y \sum_{i=1}^K P_i \frac{|\mathbf{c}_s^T \mathbf{c}_i|^2}{|\mathbf{c}_s|^2}} \quad (6.40)$$

where  $Y = \mathbb{E}[\rho_i^2]$ ,  $Y = 1 - \beta/4$  for the SRC pulse,  $Y = 1 - \beta/(4 \ln[2])$  for the BTD pulse [45] and  $\beta$  is the excess bandwidth. As in [102], the RV  $a_i = \mathbf{c}_s^T \mathbf{c}_i / |\mathbf{c}_s|$  is

independent of  $\mathbf{c}_s$  and zero-mean Gaussian distributed with variance  $\Omega/2$ . Thus, the PDF of  $A_i = P_i a_i^2$  is [74]

$$f_{A_i}(y) = \frac{1}{\sqrt{\pi P_i \Omega}} y^{-\frac{1}{2}} e^{-\frac{y}{P_i \Omega}}, \quad y > 0 \quad (6.41)$$

which is a gamma PDF with parameters  $(\frac{1}{2}, P_i \Omega)$ . For the case of distinct interferer powers, the PDF of  $B = \sum_{i=1}^K A_i$  is given by [87]

$$f_B(y) = \left[ \prod_{i=1}^K \sqrt{\frac{P_1}{P_i}} \right] \sum_{k=0}^{\infty} \frac{\delta_k y^{\frac{K}{2}+k-1} e^{-\frac{y}{P_1 \Omega}}}{\Gamma(\frac{K}{2} + k) (P_1 \Omega)^{\frac{K}{2}+k}}, \quad y > 0 \quad (6.42)$$

where without loss of generality  $P_1 = \min_j \{P_j\}$  and

$$\delta_{k+1} = \frac{1}{k+1} \sum_{u=1}^{k+1} \left[ \sum_{v=1}^K \frac{1}{2} \left( 1 - \frac{P_1}{P_v} \right)^u \right] \delta_{k+1-u} \quad (6.43)$$

with  $\delta_0 = 1$ . The PDF of  $R_M = |\mathbf{c}_s|^2$  is given by [103]

$$f_{R_M}(r) = \frac{1}{\Gamma(mL)} \left( \frac{m}{\Omega_0} \right)^{mL} e^{-\left(\frac{m}{\Omega_0}\right)r} r^{mL-1}, \quad r > 0. \quad (6.44)$$

The outage probability is defined as the probability that the instantaneous SIR falls below a specified SIR threshold value  $q$ . It is written as

$$\begin{aligned} P_O &= \Pr \left( \frac{P_0 R_M}{YB} < q \right) \\ &= \int_0^{\infty} f_{R_M}(r) \int_{\frac{P_0 R_M}{Yq}}^{\infty} f_B(y) dy dr. \end{aligned} \quad (6.45)$$

Substituting (6.42) and (6.44) in (6.45), it becomes [108]

$$P_O = \left[ \prod_{i=1}^K \sqrt{\frac{P_1}{P_i}} \right] \sum_{k=0}^{\infty} \delta_k \mathbf{I}_{\Xi} \left( mL, \frac{K}{2} + k \right) \quad (6.46)$$

where  $\Xi = m / \left( m + \frac{P_0 \Omega_s}{\Omega P_1 q Y} \right)$  and  $\mathbf{I}_x(\cdot, \cdot)$  is the normalized incomplete beta function [108], [109]. It is interesting to note that when the interferers' powers are equal,  $P_O$  becomes

$$P_O = \mathbf{I}_{\Xi} \left( mL, \frac{K}{2} \right). \quad (6.47)$$

### 6.5.2 BER Analysis

Now, we derive a BER expression using a Gaussian assumption for the CCI. The second term of (6.39) is the cochannel interference component usefully rewritten as

$I_C = \sum_{i=1}^K I_i$ , where

$$I_i = \sum_{j=1}^L \sqrt{\frac{P_i T}{2}} R_{i,j} R_{0,j} \cos(\phi_{i,j}) \rho_i. \quad (6.48)$$

Then, the variance of the  $I_i$  conditioned on the  $R_{0,j}$ 's,  $\text{VAR}[I_i|\{R_{0,j}\}] = P_i \Omega T Y R_M / 4$ .

As in [102], [110] using Cramer's CLT, we assume  $I_C$  conditioned on  $R_M$  is Gaussian distributed. The variance of the total CCI conditioned on  $R_M$  is then written as  $\text{VAR}[I_C|R_M] = \mathcal{P} \Omega T Y R_M / 4$  where  $\mathcal{P} = \sum_{i=1}^K P_i$ . Then, the unconditional BER is given by [48]

$$\begin{aligned} P_{eg} &= \int_0^\infty \mathbf{Q} \left( \sqrt{\frac{2P_0 T r}{4 + \mathcal{P} T \Omega Y}} \right) f_{R_M}(r) dr \\ &= \frac{\Gamma(mL + \frac{1}{2})}{2\sqrt{\pi} mL \Gamma(mL)} \left( \frac{m(4 + \mathcal{P} T \Omega Y)}{P_0 T \Omega_0} \right)^{mL} \times \\ &\quad {}_2\mathbf{F}_1 \left( mL, mL + \frac{1}{2}; mL + 1; \frac{-m(4 + \mathcal{P} T \Omega Y)}{\Omega_0 P_0 T} \right). \end{aligned} \quad (6.49)$$

## 6.6 Numerical Results and Discussion

In this section, we present some of our numerical results. Our results are also published in [46], [111], [112], [113], [114].

Fig. 6.1 depicts the BER performance of the BPSK system with a Nakagami/Nakagami fading model and NRZ rectangular pulse-shaping. We assume that the desired user average SIR= 10 dB, the desired user Nakagami fading parameter,  $m_0 = 8$  and the interferers' Nakagami fading parameter,  $m_i = 5$ ,  $i \neq 0$ . Fig. 6.2 gives the BER performances of the QPSK system with a Nakagami/Rayleigh fading model and NRZ

rectangular pulse-shaping. We observe that the Gaussian approximation overestimates the error rate of a BPSK system and underestimates the error rate of a QPSK system at large SNR values. As expected, the average BER depends only on the average SIR, not on the number of interferers when the CCI is assumed Gaussian. In Fig. 6.1, at SNR=30 dB, the BER for six interferers is 5.1 times that for one interferer while in Fig. 6.2, the BER for one interferer is 2 times that for six interferers, also at 30 dB. This behavior is not predicted by the approximate results given in [99].

Figs. 6.3 and 6.4 depict the BER performances of bandlimited BPSK with CCI in Nakagami ( $m = 5$ ) and Rayleigh ( $m = 1$ ) fading, respectively for EGC and SC with diversity orders  $L = 1, 2$  and 4 with SRC and BTD pulse shapes. We assume there are 6 interfering users ( $K = 6$ ) with equal powers and  $M = 10$ . The excess bandwidth is assumed to be 100 %, however, our analysis is valid for any arbitrary value of excess bandwidth.

Figs. 6.5 and 6.6 depict the outage performance versus threshold SIR for different  $L$  and  $K$  values, respectively. The average SIR is assumed to be 5 dB. In the case of unequal interferer powers, the normalized power distributions [0.1, 0.9] and [0.05, 0.1, 0.15, 0.22, 0.23, 0.25] are assumed for  $K = 2$  and  $K = 6$ , respectively [115]. It is observed that the equal interferer powers assumption underestimates the outage probability. The outage performance with the BTD pulse is about 0.8 dB better than that of the SRC pulse at outage probability  $10^{-3}$  and the superiority does not change with  $L$  under the equal interferer powers assumption. Fig. 6.7 shows the BER performance versus average SNR for average SIR=2 dB using the Gaussian approximation for the CCI. The BER results using the Gaussian approximation are compared with those obtained from Monte-Carlo simulation and very good agreement is seen.



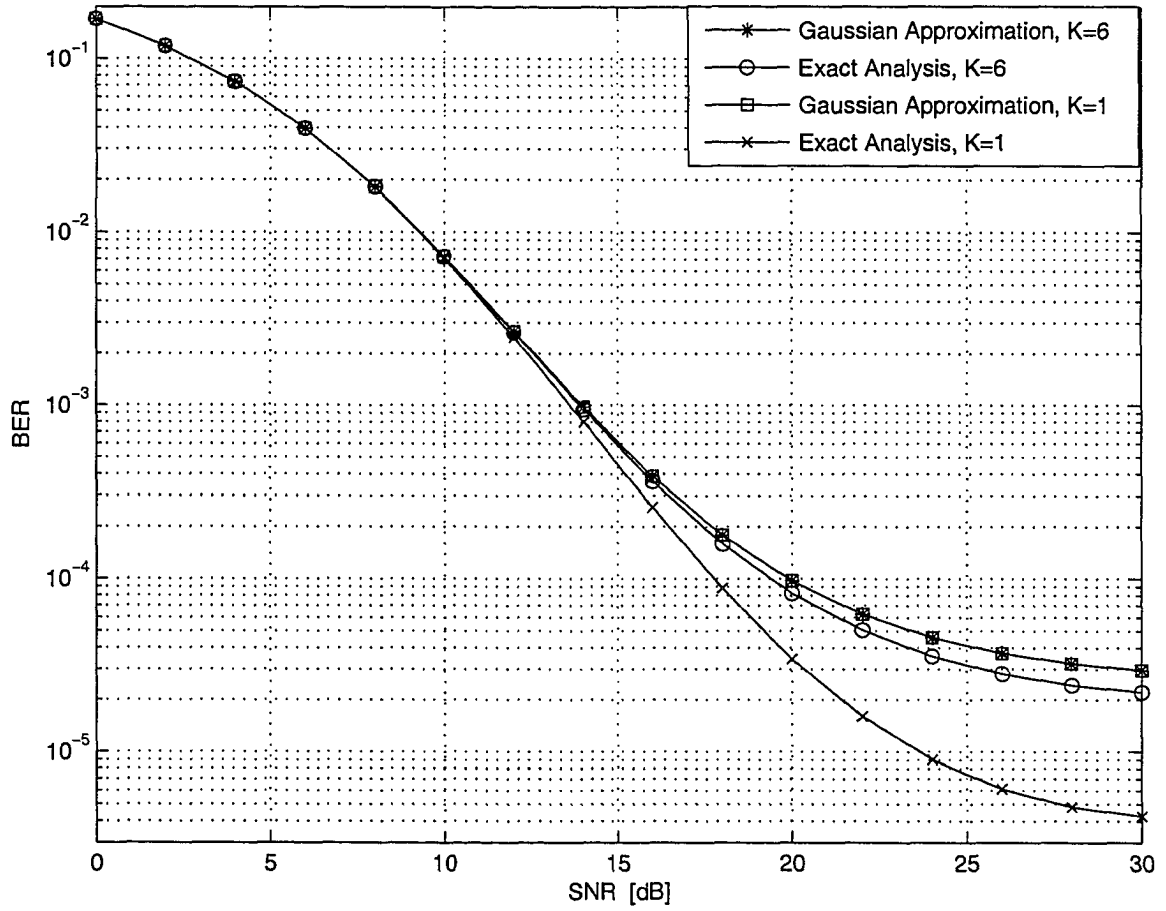


Fig. 6.1. The performance of the BPSK system with the Nakagami/Nakagami model, for  $m_0 = 8$ ,  $m_i = 5$ , and SIR=10 dB.

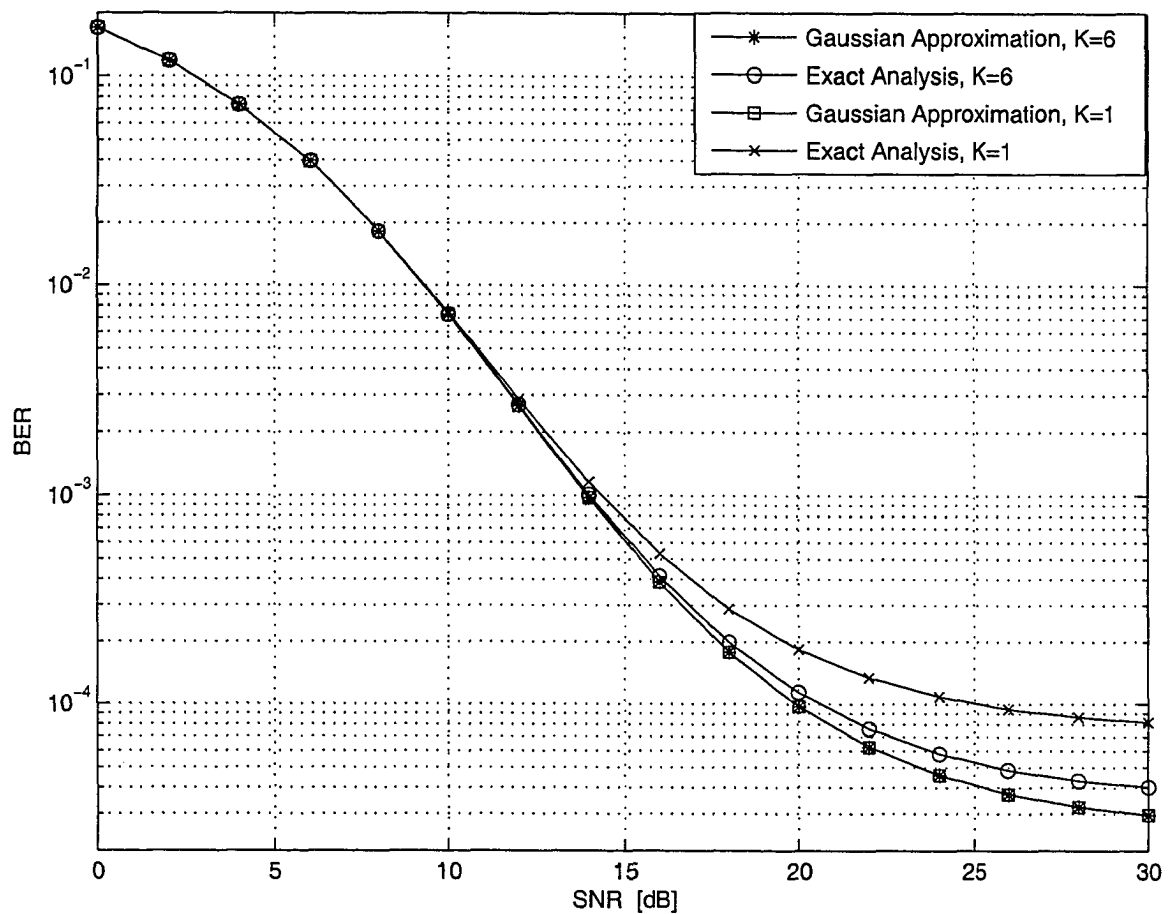


Fig. 6.2. The performance of the QPSK system with the Nakagami/Rayleigh model, for  $m_0 = 8$ , and  $SIR=10$  dB.

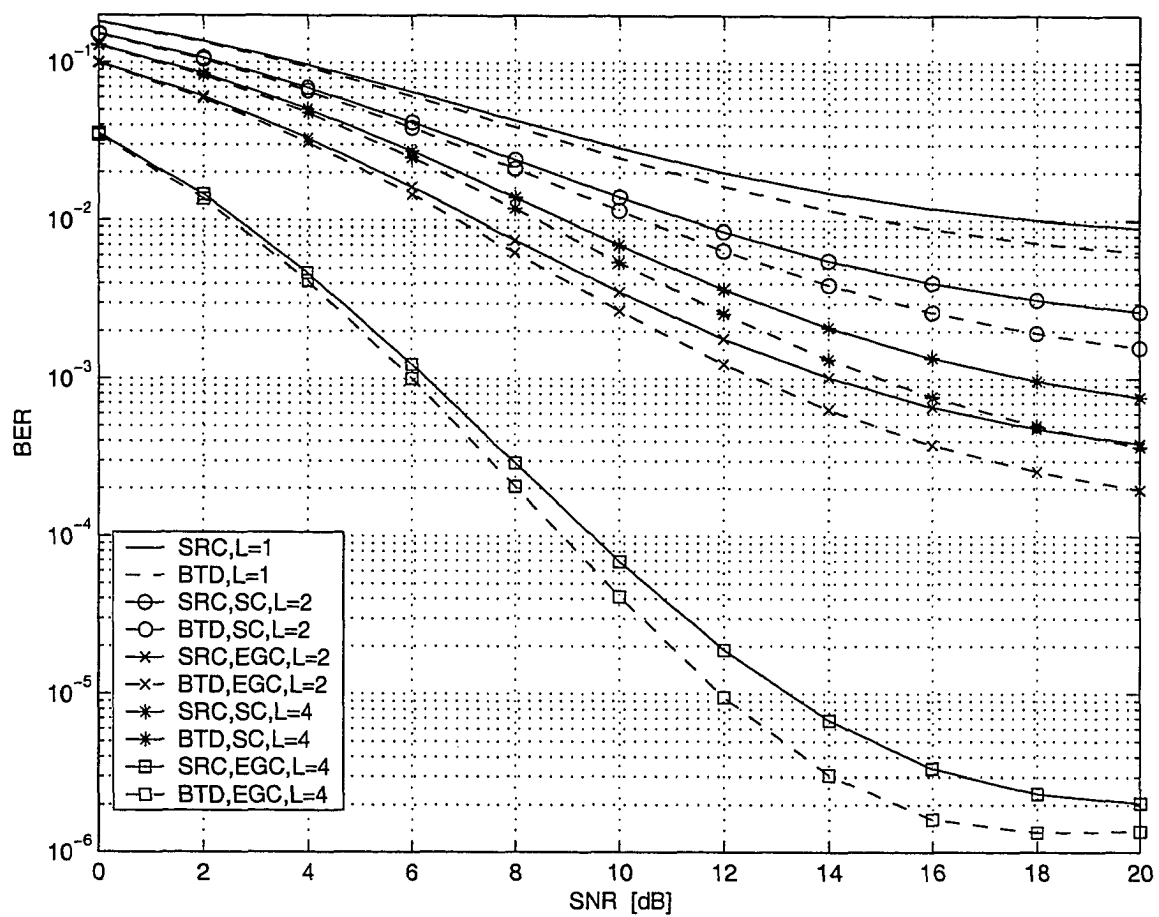


Fig. 6.3. The performance of the bandlimited BPSK system with EGC and SC in Nakagami fading ( $m = 5$ ), with CCI,  $K = 6$ , and SIR=5 dB.

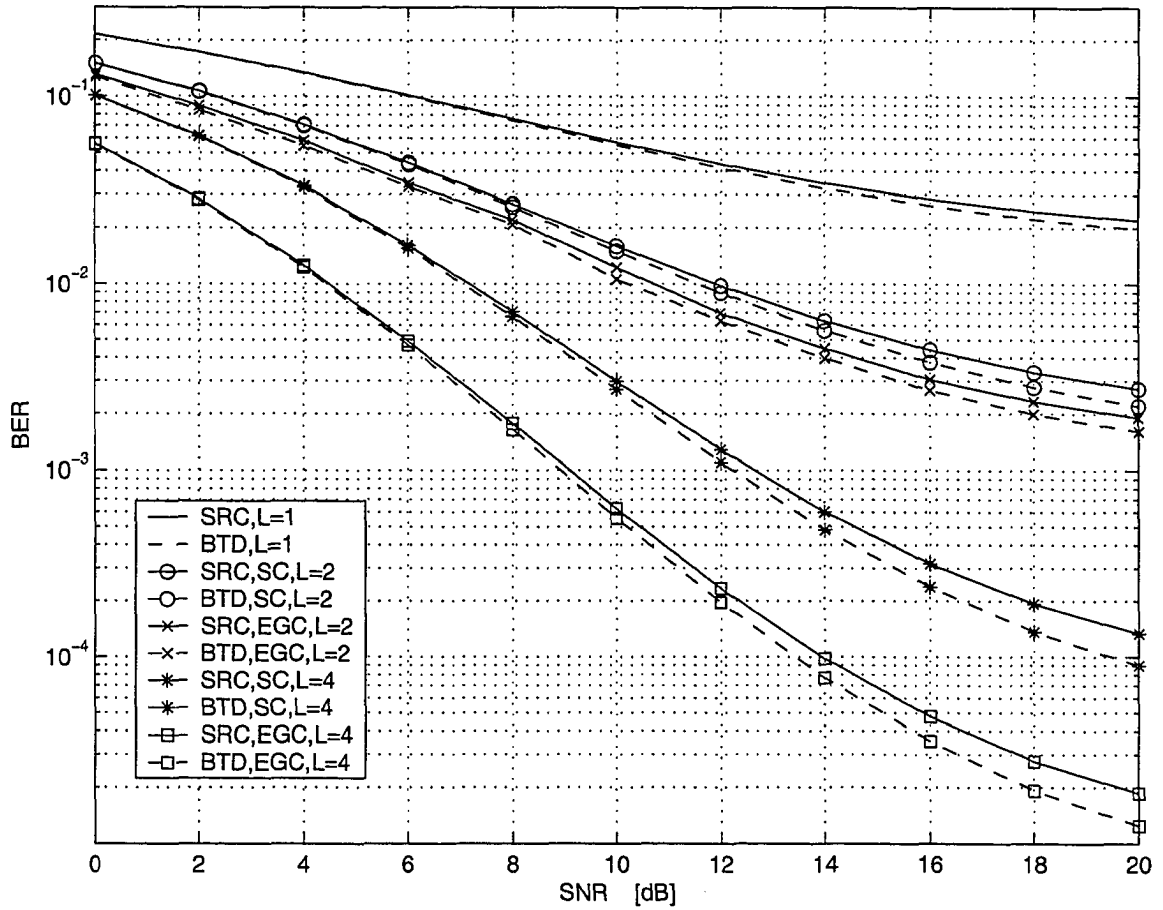


Fig. 6.4. The performance of the bandlimited BPSK system with EGC and SC in Rayleigh fading ( $m = 1$ ), with CCI,  $K = 6$ , and SIR=10 dB.

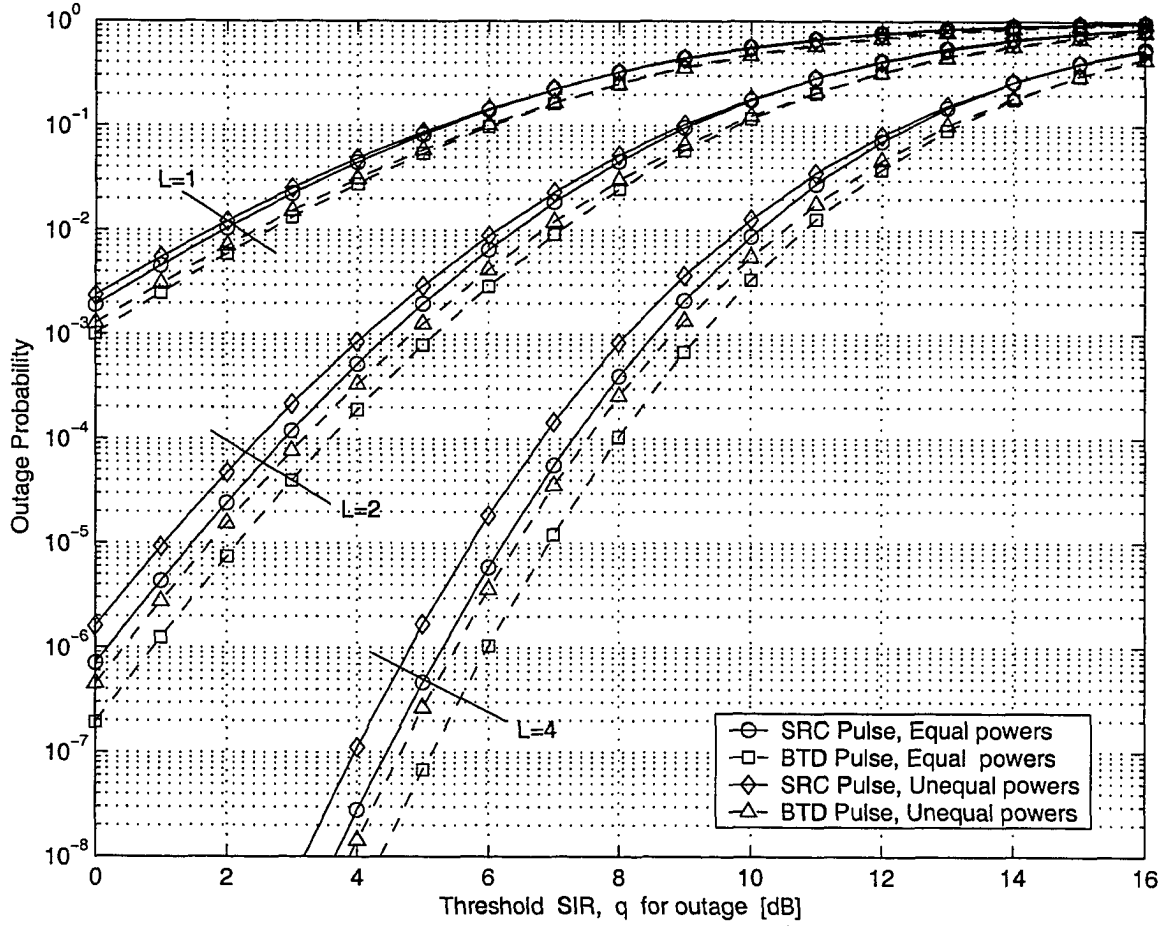


Fig. 6.5. The outage performance of the bandlimited BPSK system with MRC in CCI with  $m = 5$ ,  $K = 6$ , and average SIR=5 dB. In the case of unequal interferer powers, the normalized power distribution  $[0.05, 0.1, 0.15, 0.22, 0.23, 0.25]$  is assumed for  $K = 6$ .

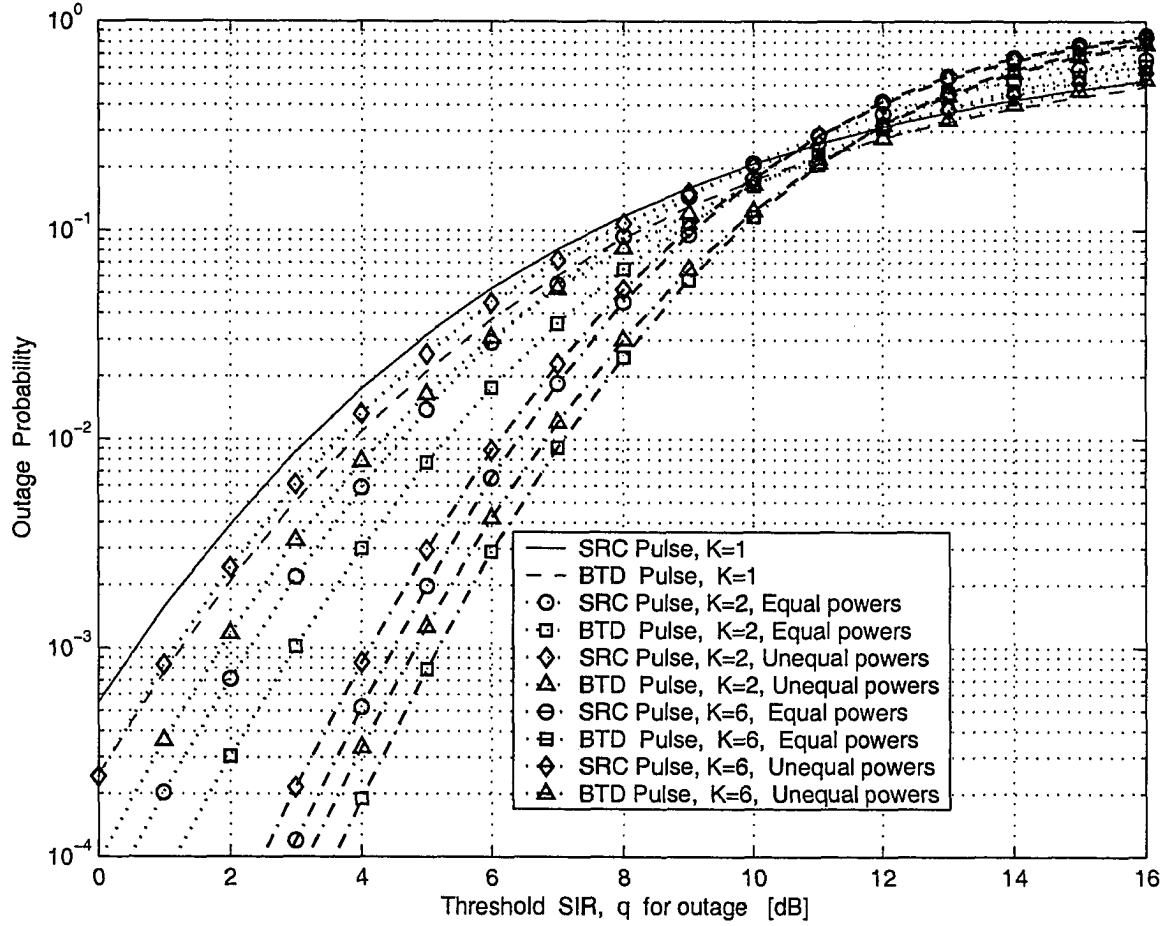


Fig. 6.6. The outage performance of the bandlimited BPSK system with MRC in CCI with  $m = 5$ ,  $L = 2$ , and average SIR=5 dB. In the case of unequal interferer powers, the normalized power distributions  $[0.1, 0.9]$  and  $[0.05, 0.1, 0.15, 0.22, 0.23, 0.25]$  are assumed for  $K = 2$  and  $K = 6$ , respectively.

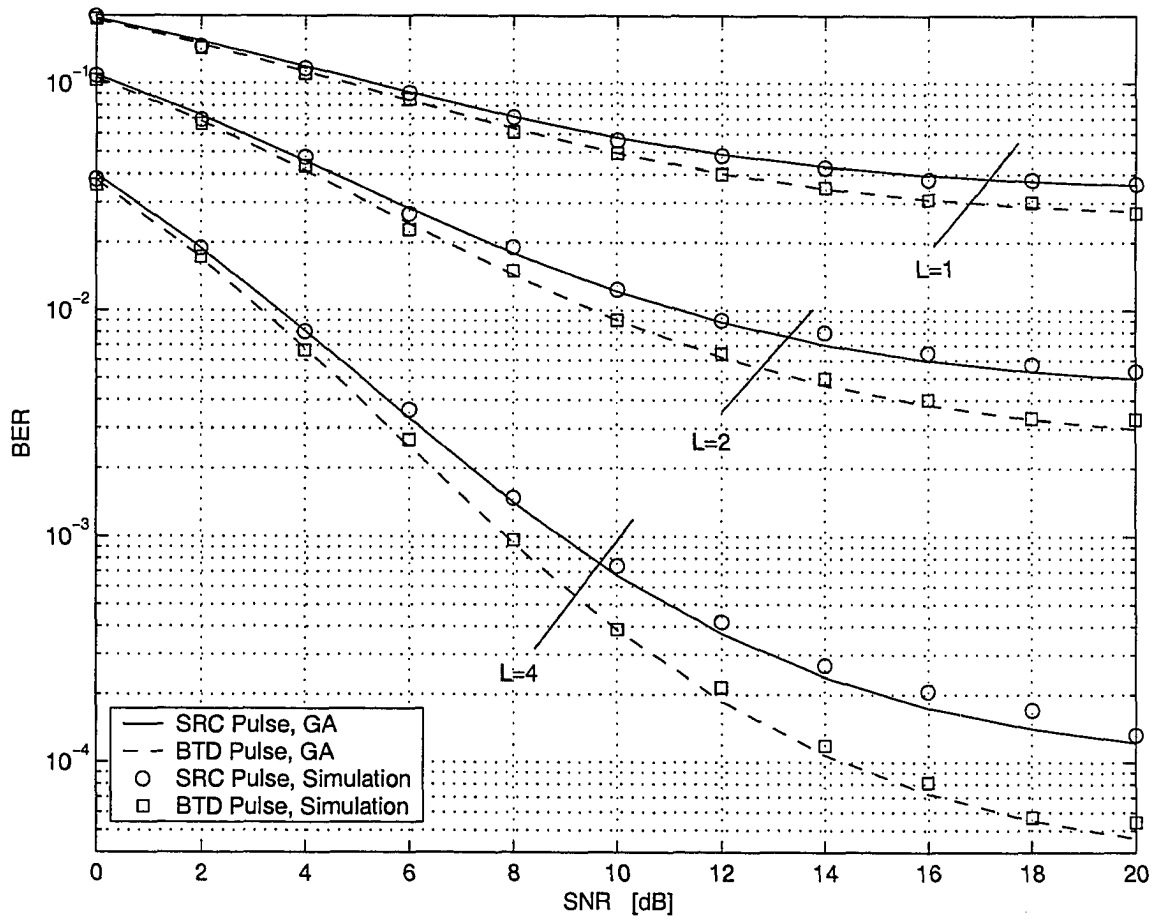


Fig. 6.7. The BER performance of the bandlimited BPSK system with MRC in CCI with  $m = 5$ ,  $K = 6$ , and average SIR=2 dB.

## 6.7 Summary

The exact BER performance of coherent BPSK and QPSK systems with CCI and fading have been investigated. Closed-form expressions for the characteristic functions of CCI for a BPSK system with independent Nakagami faded interferers and a QPSK system with independent Rayleigh faded interferers have been obtained. The average BER expression was derived in single integral form and is readily evaluated numerically. The accuracy of the Gaussian approximation for the CCI is assessed and it is found to be accurate in the presence of large number of interferers or the interferers undergo Rayleigh fading.

The accurate performances of coherent bandlimited BPSK systems with EGC and SC in CCI and fading have been investigated. Exact integral results were obtained for arbitrary diversity orders and Nakagami fading parameters. The computational complexity does not increase either with diversity order or number of interferers. The superiority of the BTD pulse over the SRC pulse is once again observed and the superiority increases with the diversity order.

The outage and BER performances of coherent bandlimited BPSK with MRC in CCI micro-cellular systems have been determined. The Gaussian approximation is quite accurate for BER estimation for six or more interferers. The superiority of the BTD pulse over the SRC pulse is once again observed. While the superiority in BER performance increases with diversity order, the superiority in outage performance remains approximately the same for different diversity orders.



# Chapter 7

## Precise Outage Analysis of SC Diversity and SWC Diversity in Micro-cellular Systems with CCI

### 7.1 Introduction

Conventional space diversity schemes combat fading and CCI simultaneously. Among space diversity schemes, SWC diversity and SC diversity are of great practical interest because of their simple implementations. The CCI and fading are due to the frequency reuse and the multipath propagation of the radio waves, respectively. As the demand for wireless channels increases, frequency reuse increases, and the cells are made smaller giving rise to micro-cellular systems [4]. In a micro-cellular system only the desired user has a LOS propagation path. Thus, the fading model employs different distributions for the desired and interfering users. Micro-cellular systems are normally interference limited systems [4]. The outage probability is defined as the probability

that the instantaneous SIR falls below a specified threshold value [116]. The proper design of micro-cellular systems requires the knowledge of the average BER and the outage probability.

The outage performance of wireless communication systems without CCI has been well studied in [6] and the references therein. In [117], Sowerby and Williamson studied the outage performance of wireless systems with multiple cochannel interferers in a Rayleigh fading environment. The same authors extended their work to Rayleigh fading with lognormal shadowing in [118], [119]. A micro-cellular system described by a Rician/Rayleigh fading model and multiple interferers was considered by Yao and Sheikh [120]. Then, the outage performance for a Nakagami/Nakagami fading model with integer-valued fading parameters was studied by Abu-Dayya and Beaulieu [86]. The outage probability of a single lognormally shadowed Nakagami interferer was also derived analytically and the case of multiple interferers was studied using MC computer simulations. Zhang extended the work in [86] to Nakagami fading with arbitrary parameters in [121], [122] and to lognormally shadowed Nakagami fading with multiple interferers by using a CF method in [123]. Outage analyzes for Rician/Nakagami and Nakagami/Nakagami fading models were also considered by Karagiannidis *et al.* in [124] and [125]. Outage analysis for a Rician/Rician fading model with lognormal shadowing for both desired and interfering users was considered by Wang and Lea in [126]. Tellambura in [127] studied the outage performance of Nakagami/Nakagami fading models with arbitrary fading parameters using a Fourier series method.

Outage studies have also been carried out for wireless communication systems with diversity receivers. Jakes [116] derived the outage probability for selection combining using a maximum desired signal power algorithm over Rayleigh fading channels

with a single interferer. Based on a total output power algorithm, Schiff [14] derive the CDF of the SIR for SC and SWC diversities in Rayleigh fading. Sowerby and Williamson [128] studied the outage performance of SC diversity in Rayleigh fading channels with arbitrary diversity orders and arbitrary numbers of interferers. Both the maximum output power selection and SIR selection schemes were considered. The outage performance of a correlated dual-branch SC diversity scheme over Nakagami fading channels was studied by Okui in [129], [130] using maximum desired power [129] and maximum carrier-to-interference ratio (CIR) [130] selection schemes. Yao and Sheikh [131] considered a micro-cellular system with a Nakagami/Nakagami fading model; signal-plus-interference power and SIR selection diversities were employed. The results were derived for an arbitrary number of interferers and integer values of fading parameter. The EGC, SC and SWC diversity schemes with a Nakagami/Nakagami fading model were studied by Abu-Dayya and Beaulieu [13] for arbitrary numbers of interferers and integer values of the fading parameter. Desired signal power selection, total power selection and SIR power selection schemes were considered and an output power switching criterion was employed for the switched diversity receiver. Yang and Alouini [132] studied the outage performance of dual-branch selection and switch and stay combining in Rayleigh fading for a single interferer. Correlated and uncorrelated branches were considered and a maximum desired signal power algorithm was employed for both diversity schemes. In all the works [117], [118], [119], [120], [86], [121], [122], [123], [124], [125], [126], [127], [14], [128], [129], [130], [131], [13] and [132] interference limited systems were considered and the interferers were assumed to be time synchronous with the desired user and their phase offsets wrt the desired user were assumed to be zero. These assumptions do not hold in practical wireless communication systems. Hence, the results obtained

in [117], [118], [119], [120], [86], [121], [122], [123], [124], [125], [126], [127], [14], [128], [129], [130], [131], [13] and [132] are only approximations.

In this chapter, we derive the exact outage probabilities of predetection SC and SWC diversities in a micro-cellular fading environment. A widely accepted Nakagami-Rayleigh fading model for micro-cellular systems is employed. A more practical system model [45] which takes account of the pulse-shaping and phase offsets and time delays of the interfering users is considered. Flat slow fading is assumed. Two Nyquist pulse shapes, namely, SRC and BTD pulse shapes [30] are examined. In both diversity schemes, maximum desired signal power, SIR power and total output power criteria are considered. The results are valid for arbitrary numbers of interferers, arbitrary fading parameter of the desired user and arbitrary diversity order. It is found that in selection diversity, the maximum SIR and total output power selection criterions provide the smallest and largest outage probabilities, respectively for the same system conditions. Optimum switching thresholds are derived for all cases of switched diversity.

The remainder of this chapter is organized as follows. The system and channel models are presented in Section 7.2. The outage analysis of a selection diversity receiver is given in Section 7.3. Three selection criteria, namely, maximum desired signal power, SIR power and total output power are considered. In Section 7.4, switched diversity schemes with desired signal power, SIR and total output power switching criteria are presented. The optimum switching threshold for each system is quantified. Some interesting numerical results are given in Section 7.5. The outage performances of the systems with different pulse shapes are compared under the same system conditions. Finally our conclusions are drawn in Section 7.6.

## 7.2 System Model

A coherent bandlimited BPSK system is considered in a slowly fading micro-cellular environment. We adopt the system model of [45] for the diversity receiver structures. There are  $L$  space diversity branches and  $K + 1$  active users in the system. The  $j$ -th branch received signal of the desired (0-th) user is

$$R_j(t) = \sqrt{2P_0T} R_{0,j} s_d(t) \cos(\omega_c t) + \sum_{i=1}^K \sqrt{2P_iT} R_{i,j} s_i(t - \tau_i) \cos(\omega_c(t - \tau_i) + \theta_{i,j}) \quad (7.1)$$

where  $s_d(t) = \sum_{k=-\infty}^{+\infty} a[k]g_T(t - kT)$ ,  $s_i(t) = \sum_{k=-\infty}^{+\infty} b_i[k]g_T(t - kT)$ ,  $P_i$  is the transmitted power of the  $i$ -th user,  $\omega_c$  is the carrier frequency, and  $\frac{1}{T}$  is the symbol transmission rate. The transmitter signal baseband pulse is denoted as  $g_T(\cdot)$  and its energy is normalized according to  $\int_{-\infty}^{+\infty} g_T^2(t)dt = 1$ ,  $a[k], b_i[k] \in \{+1, -1\}$  with equal probabilities and  $\tau_i$  represents the symbol timing offset of the  $i$ -th user signal with respect to the desired user signal, assumed to be uniform over  $[0, T)$ . The phases  $\theta_{i,j}$ , are assumed to be mutually independent and uniformly distributed over  $[0, 2\pi)$ . The random variables  $R_{0,j}, j \in [1, \dots, L]$  represent the desired user fading channel gains and each follows the Nakagami- $m$  distribution with parameters  $(m, \Omega_s)$  [4]. The interfering users' fading gains  $R_{i,j}, i \in [1, \dots, K], j \in [1, \dots, L]$  follow a Rayleigh distribution with parameter  $\Omega$ , i.e.  $\mathbb{E}[R_{i,j}^2] = \Omega$ . The fading gains are assumed to be mutually independent. The Nakagami/Rayleigh desired /interfering user fading scenario arises in the micro-cellular environment [4], and the micro-cellular systems are interference limited systems. Thus, we neglect the effects of background noise in this chapter. The desired user average SIR is defined as  $\text{SIR}(\text{dB}) = 10 \log_{10} \left( P_0 \Omega_s / (\Omega \sum_{i=1}^K P_i) \right)$ . As in [45], two types of bandlimited Nyquist pulse shapes, SRC and BTD [30] pulse shapes are considered. We assume 100% excess bandwidth pulse shapes in this chap-

ter. However, our analysis is valid for arbitrary excess bandwidth.

### 7.3 Selection Diversity

Few studies in the literature have examined the performance of predetection selection diversity schemes when cochannel interference is present [116], [13]. In this section, we derive the exact outage probabilities for the Nakagami-Rayleigh fading scenario with arbitrary Nakagami fading parameter and arbitrary diversity order. We consider maximum desired signal power selection, maximum SIR selection and maximum total power selection criteria. The decision statistic for the desired user (0-th) data symbol  $a[0]$  on the  $j$ -th branch after coherent demodulation and matched filtering, is written as

$$Z_j[0] = \sqrt{\frac{P_0 T}{2}} a[0] R_{0j} + \sum_{i=1}^K \sqrt{\frac{P_i T}{2}} R_{i,j} \cos(\phi_{i,j}) \rho_i \quad (7.2)$$

where  $\phi_{i,j} = (\theta_{ij} - \omega_c \tau_i) \sim \mathcal{U}[0, 2\pi]$ ,

$$\rho_i = \sum_{k=-\infty}^{+\infty} b_i[k] g(-kT - \tau_i) \quad (7.3)$$

and  $g(\cdot)$  is the pulse shape at the receiver. The outage probability is defined as the probability that the instantaneous SIR falls below a specified SIR value  $q$ . It is written as

$$P_O = \Pr(\text{SIR} < q). \quad (7.4)$$

The  $j$ -th branch instantaneous SIR is given by

$$\text{SIR}_j = \frac{P_0 R_{0,j}^2}{Y \sum_{i=1}^K P_i X_{i,j}^2} \quad (7.5)$$

where  $X_{i,j} = R_{i,j} \cos(\phi_{i,j})$  is a zero-mean Gaussian RV with variance  $\frac{\Omega}{2}$ ,

$$Y = \mathbb{E}[\rho_i^2] = \begin{cases} 1 - \frac{\beta}{4} & \text{SRC pulse} \\ 1 - \frac{\beta}{4 \ln[2]} & \text{BTD pulse} \end{cases} \quad (7.6)$$

and  $\beta$  is the excess bandwidth [45].

### 7.3.1 Maximum Desired Signal Power Selection

In this algorithm, the branch with the maximum desired signal power is selected. Thus, a branch is selected with  $A = \max_{j \in [1, \dots, L]} R_{0j}^2$ . The random variable  $S = R_{0j}^2$  is gamma distributed and is given by [86]

$$f_S(s) = \frac{1}{\Gamma(m)} \left( \frac{m}{\Omega_s} \right)^m \exp \left( -\frac{m}{\Omega_s} s \right) s^{m-1}, \quad s > 0. \quad (7.7)$$

Using order statistics [74], the PDF of the RV  $A$  is given by

$$f_A(r) = \left( \frac{\partial [F_S(s)]^L}{\partial s} \right)_{s=r} \quad (7.8)$$

where  $F_S(s)$  is the CDF of RV  $S$ . Then, (7.8) becomes [76]

$$f_A(r) = \frac{L[\gamma(m, \frac{mr}{\Omega_s})]^{L-1}}{[\Gamma(m)]^L} \left( \frac{m}{\Omega_s} \right)^m \exp \left( -\frac{mr}{\Omega_s} \right) r^{m-1}, \quad r > 0 \quad (7.9)$$

where  $\gamma(\cdot, \cdot)$  is the lower incomplete gamma function. It was observed in [115] that, for practical values of the number of interferers, the different interferer's power and equal interferer's power assumptions give almost the same outage probability. Thus, for the case of equal interferer powers  $P = P_i$ , the PDF of  $B = \sum_{i=1}^K X_{ij}^2$  is given by

$$f_B(y) = \frac{1}{\Gamma(\frac{K}{2})\Omega^{\frac{K}{2}}} y^{\frac{K}{2}-1} \exp \left( -\frac{y}{\Omega} \right), \quad y > 0 \quad (7.10)$$

which is a chi-square PDF with  $K$  degrees of freedom or gamma PDF with parameters  $\frac{K}{2}$  and  $\Omega$ . Now, the outage probability is written as

$$\begin{aligned} P_O &= \Pr \left( \frac{P_0 A}{P Y B} < q \right) \\ &= \int_0^\infty f_A(r) \int_{\frac{P_0 r}{P Y q}}^\infty \frac{1}{\Gamma(\frac{K}{2})\Omega^{\frac{K}{2}}} y^{\frac{K}{2}-1} \exp \left( -\frac{y}{\Omega} \right) dy dr. \end{aligned} \quad (7.11)$$

By using [76, eq. 9.6.1], eq. (7.11) becomes

$$P_O = \frac{1}{\Gamma(\frac{K}{2})} \int_0^\infty f_A(r) \Gamma\left(\frac{K}{2}, \frac{P_0 r}{PYq\Omega}\right) dr \quad (7.12)$$

where  $\Gamma(\cdot, \cdot)$  is the upper incomplete gamma function [76]. Substituting (7.9) in (7.12), the outage probability becomes

$$P_O = \frac{L \left(\frac{m}{\Omega_s}\right)^m}{[\Gamma(m)]^L \Gamma(\frac{K}{2})} \int_0^\infty \left[ \gamma\left(m, \frac{mr}{\Omega_s}\right) \right]^{L-1} \Gamma\left(\frac{K}{2}, \frac{P_0 r}{PYq\Omega}\right) \exp\left(-\frac{mr}{\Omega_s}\right) r^{m-1} dr. \quad (7.13)$$

Eq. (7.13) is evaluated numerically<sup>1</sup>

### 7.3.2 Maximum Signal-to-Interference Power Ratio (SIR) Selection

When the maximum SIR selection algorithm is employed, the branch with the maximum instantaneous SIR is selected. The outage probability is written as [86]

$$P_O = (\Pr[SIR_j < q, j = 1])^L. \quad (7.14)$$

Now

$$\Pr[SIR_j < q, j = 1] = \Pr\left[\frac{P_0 S}{PY \sum_{i=1}^K X_{ij}^2} < q\right]. \quad (7.15)$$

For the case of equal interferer powers, using (7.7) and (7.10), eq. (7.15) becomes

$$\begin{aligned} \Pr[SIR_j < q, j = 1] &= \int_0^\infty f_S(s) \int_{\frac{P_0 s}{PYq}}^\infty f_B(y) dy ds \\ &= \frac{1}{\Gamma(\frac{K}{2})} \int_0^\infty f_S(s) \Gamma\left(\frac{K}{2}, \frac{P_0 s}{\Omega PYq}\right) ds. \end{aligned} \quad (7.16)$$

---

<sup>1</sup>There is a closed form expression for (7.13) using the Lauricella function proposed by Aalo *et al.* in a submitted manuscript.



There is a closed-form expression for (2.15) using [108, eq. 16] and it is given by

$$\Pr[SIR_j < q, j = 1] = \mathbf{I}_{\Xi(q)} \left( m, \frac{K}{2} \right) \quad (7.17)$$

where  $\Xi(q) = \frac{m}{m + \frac{P_0 \Omega_s}{\Omega PY q}}$ , and  $\mathbf{I}_x(\cdot, \cdot)$  is the normalized incomplete beta function defined as

$$\mathbf{I}_x(a, b) = \frac{\Gamma(a+b)}{\Gamma(a)\Gamma(b)} \int_0^x t^{a-1} (1-t)^{b-1} dt, \quad 0 < x < 1. \quad (7.18)$$

Then, the outage probability becomes

$$P_O = \left[ \mathbf{I}_{\Xi(q)} \left( m, \frac{K}{2} \right) \right]^L. \quad (7.19)$$

### 7.3.3 Maximum Output Power Selection

In the maximum output power selection algorithm, the branch with maximum instantaneous total output power is selected. Then, the outage probability is given by [86]

$$P_O = L \cdot \Pr \left( \frac{S_1}{B_1} < q, S_1 + B_1 > S_j + B_j, j \neq 1 \right) \quad (7.20)$$

where  $S_j = P_0 R_{0j}^2$  and  $B_j = PY \sum_{i=1}^K X_{ij}^2$ . Now, from (7.7) and (7.10), the PDF of RV  $S_j$  is given by

$$f_{S_j}(s) = \frac{1}{\Gamma(m)} \left( \frac{m}{P_0 \Omega_s} \right)^m \exp \left( -\frac{m}{P_0 \Omega_s} s \right) s^{m-1}, \quad s > 0 \quad (7.21)$$

and the PDF of RV  $B_j$  is

$$f_{B_j}(y) = \frac{1}{\Gamma(\frac{K}{2})(PY\Omega)^{\frac{K}{2}}} y^{\frac{K}{2}-1} \exp \left( -\frac{y}{PY\Omega} \right), \quad y > 0. \quad (7.22)$$

The RVs  $S_1$  and  $B_1$  are independent. Thus, the joint PDF of  $S_1$  and  $B_1$  is written as

$$f_{S_1 B_1}(s, y) = \frac{\left( \frac{m}{P_0 \Omega_s} \right)^m s^{m-1} y^{\frac{K}{2}-1}}{\Gamma(m)\Gamma(\frac{K}{2})(PY\Omega)^{\frac{K}{2}}} \exp \left( -\frac{m}{P_0 \Omega_s} s \right) \exp \left( -\frac{y}{PY\Omega} \right), \quad s > 0, y > 0. \quad (7.23)$$

The RVs  $U_j$  and  $V_j$  are defined as  $U_j = S_j/B_j$  and  $V_j = S_j + B_j$ . Using conventional methods the joint PDF of RVs  $U_1$  and  $V_1$  is given by

$$f_{U_1 V_1}(u, v) = \frac{\left(\frac{m}{P_0 \Omega_s}\right)^m u^{m-1} v^{m+\frac{K}{2}-1} \exp\left[-\frac{v}{1+u} \left(\frac{m u}{P_0 \Omega_s} + \frac{1}{PY \Omega}\right)\right]}{\Gamma(m) \Gamma(\frac{K}{2}) (PY \Omega)^{\frac{K}{2}} (1+u)^{m+\frac{K}{2}}}, \quad u > 0, v > 0. \quad (7.24)$$

The outage probability in (7.20) becomes

$$P_O = L \cdot \Pr(U_1 < q, V_1 > S_j + B_j, j \neq 1). \quad (7.25)$$

The RVs  $S_j$  and  $B_j$  are independent and nonidentically distributed gamma RVs.

Using the method presented in [87], the pdf of RV  $V_j = S_j + B_j$  is given by

$$f_{V_j}(w) = \left(\frac{m \alpha_m}{P_0 \Omega_s}\right)^m \left(\frac{\alpha_m}{\Omega PY}\right)^{\frac{K}{2}} \sum_{k=0}^{\infty} \frac{\delta_k w^{m+\frac{K}{2}+k-1} \exp\left(-\frac{w}{\alpha_m}\right)}{\Gamma(m + \frac{K}{2} + k) \alpha_m^{m+\frac{K}{2}+k}}, \quad w > 0 \quad (7.26)$$

where  $\alpha_m = \min[\frac{P_0 \Omega_s}{m}, \Omega PY]$  and

$$\delta_{k+1} = \frac{1}{k+1} \sum_{l=1}^{k+1} \left[ m \left(1 - \frac{m \alpha_m}{\Omega_s P_0}\right)^l + \frac{K}{2} \left(1 - \frac{\alpha_m}{\Omega PY}\right)^l \right] \delta_{k+1-l}, \quad k = 0, 1, 2, \dots \quad (7.27)$$

with initial condition  $\delta_0 = 1$ . Now, the  $\Pr(S_j + B_j < V_1)$  is

$$\begin{aligned} \Pr(S_j + B_j < V_1) &= \left(\frac{m \alpha_m}{P_0 \Omega_s}\right)^m \left(\frac{\alpha_m}{\Omega PY}\right)^{\frac{K}{2}} \sum_{k=0}^{\infty} \delta_k \int_0^{V_1} \frac{w^{m+\frac{K}{2}+k-1} \exp\left(-\frac{w}{\alpha_m}\right)}{\Gamma(m + \frac{K}{2} + k) \alpha_m^{m+\frac{K}{2}+k}} dw \\ &= \left(\frac{m \alpha_m}{P_0 \Omega_s}\right)^m \left(\frac{\alpha_m}{\Omega PY}\right)^{\frac{K}{2}} \sum_{k=0}^{\infty} \delta_k \left[ 1 - \frac{\Gamma\left(m + \frac{K}{2} + k, \frac{V_1}{\alpha_m}\right)}{\Gamma(m + \frac{K}{2} + k)} \right] \end{aligned} \quad (7.28)$$

Then, the outage probability in (7.25) is written as

$$\begin{aligned} P_O &= L \int_0^q du \int_0^\infty f_{U_1 V_1}(u, v) [\Pr(S_i + B_i < V_1)]^{L-1} dv \\ &= L \int_0^q du \int_0^\infty f_{U_1 V_1}(u, v) \times \\ &\quad \left[ \left(\frac{m \alpha_m}{P_0 \Omega_s}\right)^m \left(\frac{\alpha_m}{\Omega PY}\right)^{\frac{K}{2}} \sum_{k=0}^{\infty} \delta_k \left[ 1 - \frac{\Gamma\left(m + \frac{K}{2} + k, \frac{v}{\alpha_m}\right)}{\Gamma(m + \frac{K}{2} + k)} \right] \right]^{L-1} dv. \end{aligned} \quad (7.29)$$

Eq. (7.29) with (7.24) provides the outage probability for arbitrary diversity order. It involves with a double numerical integration. However, when the diversity order is two, eq. (7.29) can be further simplified. It specializes to

$$\begin{aligned}
P_O &= L \int_0^q \frac{du \left(\frac{m}{P_0 \Omega_s}\right)^{2m} \alpha_m^{m+\frac{K}{2}} u^{m-1}}{\Gamma(m) \Gamma(\frac{K}{2}) (PY\Omega)^K (1+u)^{m+\frac{K}{2}}} \sum_{k=0}^{\infty} \delta_k \\
&\quad \times \int_0^{\infty} v^{m+\frac{K}{2}-1} \exp \left[ -\frac{v}{1+u} \left( \frac{mu}{P_0 \Omega_s} + \frac{1}{PY\Omega} \right) \right] \left[ 1 - \frac{\Gamma \left( m + \frac{K}{2} + k, \frac{v}{\alpha_m} \right)}{\Gamma(m + \frac{K}{2} + k)} \right] dv \\
&= L \int_0^q \frac{\left(\frac{m}{P_0 \Omega_s}\right)^{2m} \Gamma(m + \frac{K}{2}) \alpha_m^{m+\frac{K}{2}} u^{m-1}}{\Gamma(m) \Gamma(\frac{K}{2}) (PY\Omega)^K \left( \frac{mu}{P_0 \Omega_s} + \frac{1}{PY\Omega} \right)^{m+\frac{K}{2}}} \times \\
&\quad \sum_{k=0}^{\infty} \delta_k \left[ 1 - \mathbf{I}_{\frac{1}{1+\frac{\bar{\gamma}}{\alpha_m}}} \left( m + \frac{K}{2}, m + \frac{K}{2} + k \right) \right] du
\end{aligned} \tag{7.30a}$$

where

$$\bar{\gamma} = \frac{1+u}{\left( \frac{mu}{P_0 \Omega_s} + \frac{1}{PY\Omega} \right)}. \tag{7.30b}$$

Eq. (7.30a) provides the outage probability of dual-branch maximum output power selection diversity.

## 7.4 Switched Diversity

In predetection switched diversity, a switching metric of a particular diversity branch is continuously compared with a predetermined threshold value, and if the branch metric is greater than the threshold, the same branch is selected. Otherwise, the output is switched to other branches until a branch with metric greater than the threshold is found [14]. If all the branch metrics are below the threshold, the output switches branches cyclically and never settles to any branch. The switching metrics considered are desired signal power, SIR and total branch power. An expression for

the outage probability of a  $L$ -branch switched diversity scheme in Nakagami-Rayleigh fading is derived and an expression for the optimum switching thresholds is also obtained in this section.

#### 7.4.1 Desired Signal Power Switching

For the desired signal power switching criterion, the outage probability is given by [14], [13]

$$\begin{aligned}
P_O &= \Pr(SIR < q) \\
&= \Pr(SIR_j < q | S_j < \zeta, \text{ for all } j) \Pr(S_j < \zeta \text{ for all } j) \\
&\quad + \Pr(SIR_j < q | S_j > \zeta \text{ for at least one } j) \Pr(S_j > \zeta \text{ for at least one } j) \\
&= 1 \cdot [\Pr(S_1 < \zeta)]^L + \Pr\left(\frac{S_1}{B_1} < q | S_1 > \zeta\right) \cdot (1 - [\Pr(S_1 < \zeta)]^L) \\
&= [\Pr(S_1 < \zeta)]^L + \Pr\left(\frac{S_1}{B_1} < q, S_1 > \zeta\right) \frac{(1 - [\Pr(S_1 < \zeta)]^L)}{\Pr(S_1 > \zeta)} \tag{7.31}
\end{aligned}$$

where  $\zeta$  is the desired signal power threshold, from (7.21)

$$\Pr(S_1 < \zeta) = \frac{\gamma\left(m, \frac{m\zeta}{P_0\Omega_s}\right)}{\Gamma(m)} \tag{7.32}$$

and

$$\Pr(S_1 > \zeta) = \frac{\Gamma\left(m, \frac{m\zeta}{P_0\Omega_s}\right)}{\Gamma(m)}. \tag{7.33}$$

Now, let RVs  $U_1 = S_1/B_1$  and  $W_1 = S_1$ , then the joint PDF of RVs  $U_1$  and  $W_1$  is given by [74], [133]

$$f_{U_1, W_1}(u, w) = \frac{\left(\frac{m}{P_0\Omega_s}\right)^m w^{m+\frac{K}{2}-1} \exp\left(-w\left[\frac{m}{\Omega_s P_0} + \frac{1}{u\Omega P Y}\right]\right)}{\Gamma(m)\Gamma(\frac{K}{2})(\Omega P Y)^{\frac{K}{2}} u^{\frac{K}{2}+1}}, \quad u > 0, w > 0. \tag{7.34}$$

Then, the  $\Pr\left(\frac{S_1}{B_1} < q, S_1 > \zeta\right)$  is

$$\begin{aligned}
\Pr\left(\frac{S_1}{B_1} < q, S_1 > \zeta\right) &= \Pr(U_1 < q, W_1 > \zeta) \\
&= \int_0^q du \int_{\zeta}^{\infty} f_{U_1, W_1}(u, w) dw \\
&= \int_0^q \frac{\left(\frac{m}{P_0 \Omega_s}\right)^m \Gamma\left(m + \frac{K}{2}, \zeta \left[\frac{m}{\Omega_s P_0} + \frac{1}{u \Omega P Y}\right]\right)}{\Gamma(m) \Gamma\left(\frac{K}{2}\right) (\Omega P Y)^{\frac{K}{2}} \left[\frac{m}{\Omega_s P_0} + \frac{1}{u \Omega P Y}\right]^{m + \frac{K}{2}} u^{\frac{K}{2} + 1}} du.
\end{aligned} \tag{7.35}$$

Eq. (7.31) with (7.32), (7.33) and (7.35) provides the outage probability for arbitrary values of  $m$ ,  $K$  and  $L$ . The optimum switching threshold in the minimum outage probability sense is given by

$$\left. \frac{\partial P_O}{\partial \zeta} \right|_{\zeta=\zeta_0} = 0. \tag{7.36}$$

Using the definitions of the lower and upper incomplete gamma functions and Leibniz's rule [76], one has

$$\frac{\partial \gamma(\alpha, bx)}{\partial x} = -b^\alpha \exp(-bx) x^{\alpha-1} \tag{7.37}$$

$$\frac{\partial \Gamma(\alpha, bx)}{\partial x} = b^\alpha \exp(-bx) x^{\alpha-1}. \tag{7.38}$$

Now, from (7.36), the optimum switching threshold is a solution to a nonlinear equation and is given by

$$\begin{aligned}
&LC_1^{L-1}(\Gamma[m] - C_1)^2 - ((\Gamma[m])^L - C_1^L) (\Gamma[m] - C_1) \frac{\Gamma\left(\frac{K}{2}, \frac{\zeta_0}{\Omega P Y q}\right)}{\Gamma\left(\frac{K}{2}\right) \zeta_0^{m + \frac{K}{2} - 1}} \\
&\Pr\left(\frac{S_1}{B_1} < q, S_1 > \zeta_0\right) \Gamma[m] [(\Gamma[m])^L + L\Gamma[m]C_1^{L-1} - (L+1)C_1^L] = 0
\end{aligned} \tag{7.39}$$

where  $C_1 = \gamma\left(m, \frac{m\zeta_0}{P_0 \Omega_s}\right)$ , and thus  $\Gamma\left(m, \frac{m\zeta_0}{P_0 \Omega_s}\right) = \Gamma[m] - C_1$ . Eq. (7.39) is solved numerically to obtain the optimum switching thresholds.

### 7.4.2 Signal-to-Interference Power Ratio (SIR) Switching

For the SIR switching criterion, assuming the first branch is in operation, the outage probability is given by

$$\begin{aligned}
 P_O &= \Pr(SIR < q) \\
 &= \begin{cases} \Pr([SIR_1 < \zeta] \cap [SIR_2 < \zeta] \cap \dots \cap [SIR_L < \zeta]), & q < \zeta \\ \Pr([\zeta < SIR_1 < q] \cup [[SIR_1 < \zeta] \cap [\zeta < SIR_2 < q]] \\ \cup [[SIR_1 < \zeta] \cap [SIR_2 < \zeta] \cap [\zeta < SIR_3 < q]] \cup \dots \\ \cup [[SIR_1 < \zeta] \cap [SIR_2 < \zeta] \cap \dots \\ \cap [SIR_{L-1} < \zeta] \cap [\zeta < SIR_L < q]] \\ \cup [[SIR_1 < \zeta] \cap [SIR_2 < \zeta] \cap \dots \cap [SIR_L < \zeta]]), & q > \zeta \end{cases} \quad (7.40)
 \end{aligned}$$

where  $\zeta$  is the signal-to-interference power ratio threshold. When  $q < \zeta$ , the first branch is not in outage condition; however,  $SIR_j$  is less than the switching threshold and, thus, the receiver cyclically switches branches and never settles to any branch. Hence, this is an outage condition. When  $q > \zeta$ , outage occurs in the following situations: if the  $SIR_1$  satisfies  $\zeta < SIR_1 < q$ , i.e. the receiver does not switch from the first branch or if the first  $j - 1$  branch SIRs are less than  $\zeta$  and the  $j$ -th branch SIR satisfies  $\zeta < SIR_j < q$ ,  $j \in [2, \dots, L]$  or all the branch SIRs are below  $\zeta$ . Assuming the branch SIRs are statistically identical, the outage probability is given

by

$$\begin{aligned}
P_O &= \begin{cases} [\Pr(\frac{P_0 S}{PYB} < \zeta)]^L, & q < \zeta \\ \Pr(\zeta < \frac{P_0 S}{PYB} < q) + [\Pr(\frac{P_0 S}{PYB} < \zeta)]^L + \\ \Pr(\frac{P_0 S}{PYB} < \zeta) \Pr(\zeta < \frac{P_0 S}{PYB} < q) \\ + [\Pr(\frac{P_0 S}{PYB} < \zeta)]^2 \Pr(\zeta < \frac{P_0 S}{PYB} < q) + \dots + \\ \Pr(\frac{P_0 S}{PYB} < \zeta)]^L \Pr(\zeta < \frac{P_0 S}{PYB} < q), & q > \zeta \end{cases} \\
&= \begin{cases} [\Pr(\frac{P_0 S}{PYB} < \zeta)]^L, & q < \zeta \\ \Pr(\zeta < \frac{P_0 S}{PYB} < q) \frac{1 - [\Pr(\frac{P_0 S}{PYB} < \zeta)]^L}{1 - \Pr(\frac{P_0 S}{PYB} < \zeta)} + [\Pr(\frac{P_0 S}{PYB} < \zeta)]^L, & q > \zeta \end{cases}. \quad (7.41)
\end{aligned}$$

From (7.17),

$$\Pr\left(\frac{P_0 S}{PYB} < \zeta\right) = \mathbf{I}_{\Xi(\zeta)}\left(m, \frac{K}{2}\right) \quad (7.42)$$

and

$$\Pr\left(\frac{P_0 S}{PYB} < q\right) = \mathbf{I}_{\Xi(q)}\left(m, \frac{K}{2}\right). \quad (7.43)$$

From (7.42) and (7.43)

$$\Pr\left(\zeta < \frac{P_0 S}{PYB} < q\right) = \mathbf{I}_{\Xi(q)}\left(m, \frac{K}{2}\right) - \mathbf{I}_{\Xi(\zeta)}\left(m, \frac{K}{2}\right). \quad (7.44)$$

Eq. (7.40) with (7.42), (7.43) and (7.44) provides a closed-form expression for the outage probability. Now, it is easy to show the outage probability in (7.41) is a monotonically decreasing and increasing function of  $\zeta$  in  $q > \zeta$  and  $q < \zeta$ , respectively. Thus,  $q$  is the optimum switching threshold for this SIR switching scheme.

### 7.4.3 Total Branch Power Switching

When the total branch power switching criterion is employed, the outage probability is written as [14], [13]

$$\begin{aligned}
 P_O &= \Pr(SIR < q) \\
 &= \Pr(SIR < q | S_j + B_j < \zeta, \text{ for all } j) \Pr(S_j + B_j < \zeta, \text{ for all } j) \\
 &\quad + \Pr(SIR < q | S_j + B_j > \zeta, \text{ for at least one } j) \times \\
 &\quad \Pr(S_j + B_j > \zeta, \text{ for at least one } j)
 \end{aligned} \tag{7.45}$$

where  $\zeta$  is the switching power threshold. Now, (7.31) becomes [14], [13]

$$P_O = [\Pr(S_1 + B_1 < \zeta)]^L + C \frac{1 - [\Pr(S_1 + B_1 < \zeta)]^L}{1 - \Pr(S_1 + B_1 < \zeta)} \tag{7.46}$$

where

$$\begin{aligned}
 C &= \Pr\left(\frac{S_1}{B_1} < q, S_1 + B_1 > \zeta\right) \\
 &= \int_0^q \int_{\zeta}^{\infty} f_{U_1 V_1}(u, v) du dv \\
 &= \int_0^q du \int_{\zeta}^{\infty} \frac{\left(\frac{m}{P_0 \Omega_s}\right)^m u^{m-1} v^{m+\frac{K}{2}-1} \exp\left[-\frac{v}{1+u} \left(\frac{mu}{P_0 \Omega_s} + \frac{1}{PY\Omega}\right)\right]}{\Gamma(m)\Gamma(\frac{K}{2})(PY\Omega)^{\frac{K}{2}}(1+u)^{m+\frac{K}{2}}} dv
 \end{aligned} \tag{7.47}$$

$$= \int_0^q \frac{\left(\frac{m}{P_0 \Omega_s}\right)^m u^{m-1} \Gamma\left(m + \frac{K}{2}, \frac{\zeta}{1+u} \left(\frac{mu}{P_0 \Omega_s} + \frac{1}{PY\Omega}\right)\right)}{\Gamma(m)\Gamma(\frac{K}{2})(PY\Omega)^{\frac{K}{2}} \left(\frac{mu}{P_0 \Omega_s} + \frac{1}{PY\Omega}\right)^{m+\frac{K}{2}}} du \tag{7.48}$$

where (7.48) is derived from (7.47) using the definition of the upper incomplete gamma function [76]. From (7.28),  $\Pr(S_1 + B_1 < \zeta)$  is written as

$$\Pr(S_1 + B_1 < \zeta) = \left(\frac{m\alpha_m}{P_0 \Omega_s}\right)^m \left(\frac{\alpha_m}{\Omega PY}\right)^{\frac{K}{2}} \sum_{k=0}^{\infty} \delta_k \left[1 - \frac{\Gamma\left(m + \frac{K}{2} + k, \frac{\zeta}{\alpha_m}\right)}{\Gamma\left(m + \frac{K}{2} + k\right)}\right]. \tag{7.49}$$

Eq. (7.46) with (7.48) and (7.49) provides the outage probability for arbitrary diversity order in micro-cellular systems and is easily evaluated numerically. The optimum



switching threshold is obtained following a similar analysis to that presented in Section 7.4.1.

## 7.5 Numerical Results and Discussion

In this section, some numerical results are presented. The outage probability analysis is performed with the following system parameters and assumptions. The excess bandwidth of the pulse shapes are assumed to be 100% ( $\beta = 1$ ). However, our analysis holds for arbitrary values of excess bandwidth. There are six interferers in the system. The interferers are assumed to have equal power levels. For practical values of the number of interferers, for e.g. six interferers, the distinct power assumption gives almost the same results as the equal power assumption [115], under the assumption that the total interference power is the same. An interference limited micro-cellular system is considered with a Nakagami-Rayleigh fading model. The desired user fading parameter,  $m = 5$ . The average SIR in all cases is assumed as 5 dB.

Figs. 7.1, 7.2, 7.3 depict the outage probability performance versus the SIR threshold,  $q$  of selection diversity with maximum desired power, SIR and total output power selection criteria, respectively for SRC and BTD pulse shapes and diversity orders 1, 2 and 4. It is interesting to note that the BTD pulse is about 0.8 dB better than the SRC pulse at outage probability  $=10^{-3}$  in all cases and this improvement remains about the same for the different diversity orders. When the diversity order increases from 1 to 2, the outage probability gains are about 2.8 dB, 4.0 dB and 1.8 dB for maximum desired power, SIR and total output power selection criteria, respectively at outage probability  $=10^{-3}$ . For a diversity order increase from 2 to 4, the gains are about 1.7 dB, 3.0 dB and 1.5 dB, showing diminishing returns.

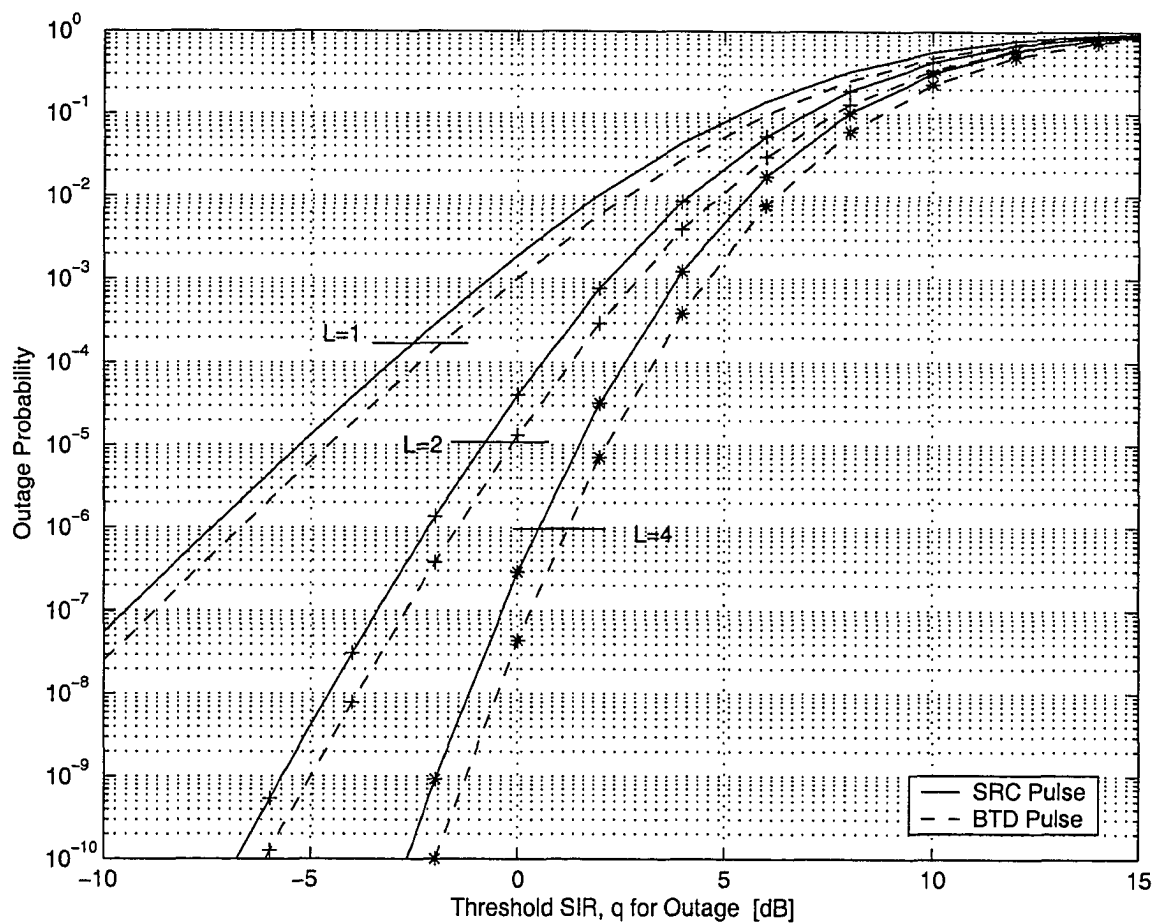


Fig. 7.1. The outage performance of selection diversity with a maximum desired power criterion for average SIR=5 dB.

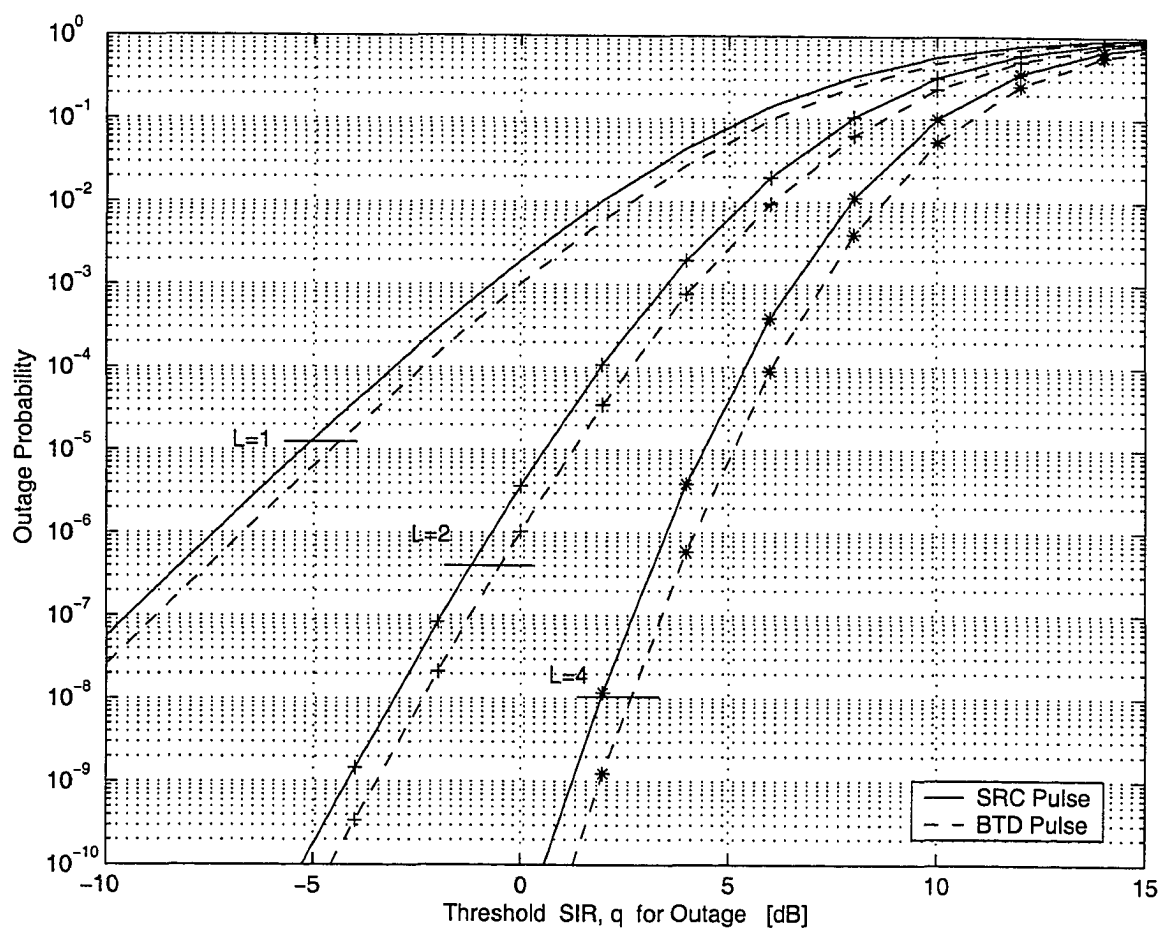


Fig. 7.2. The outage performance of selection diversity with a maximum SIR criterion for average SIR=5 dB.

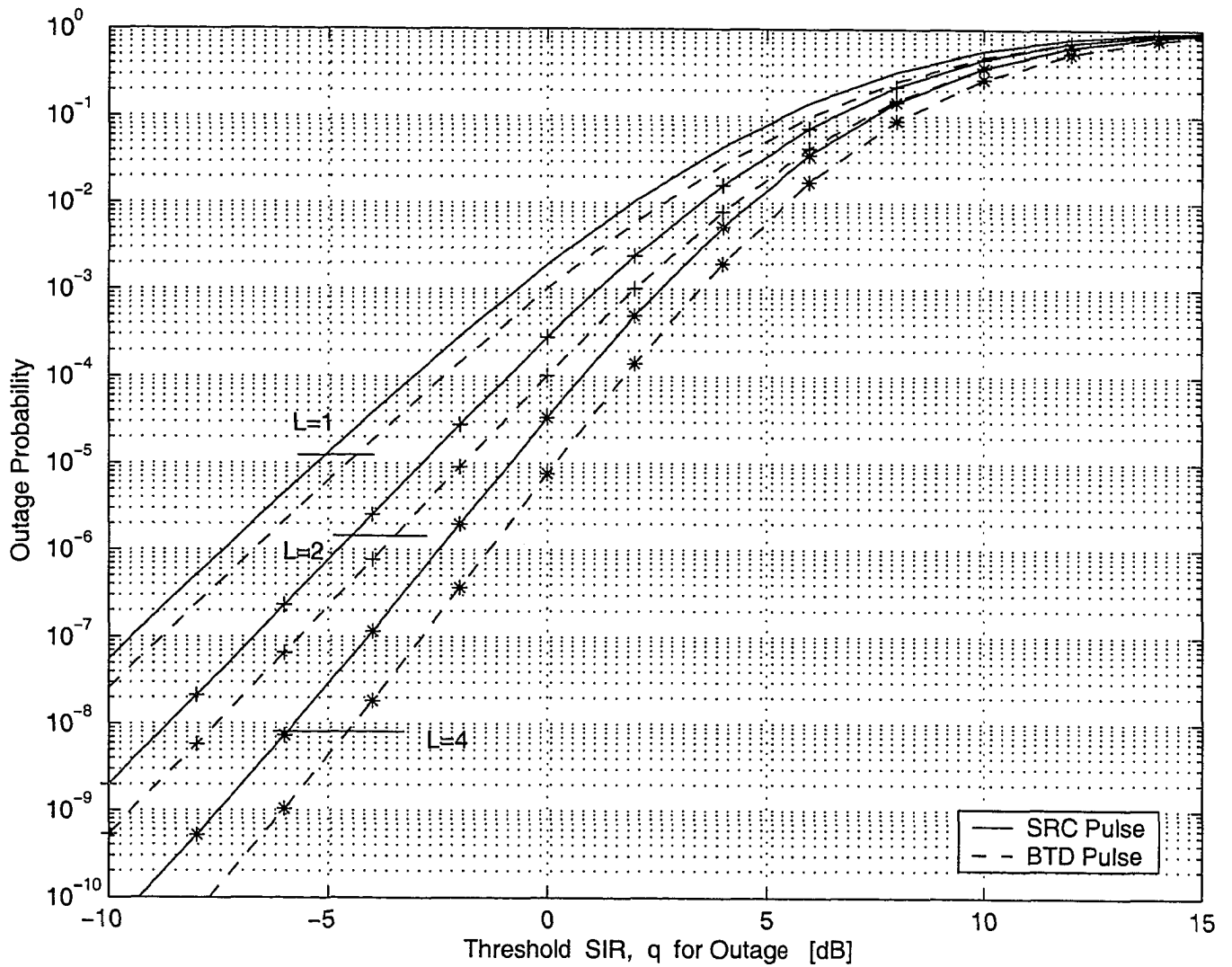


Fig. 7.3. The outage performance of selection diversity with a maximum output power criterion for average SIR=5 dB.

Outage performance comparisons of selection diversity with the three selection criteria and identical system parameters are presented in Figs. 7.4 and 7.5 for SRC and BTM pulse shapes, respectively. In both cases, when the diversity order is 2 the desired signal power selection criterion is about 1 dB better than the total output power criterion and the SIR selection criterion is about 1.2 dB better than desired signal power criterion at outage probability  $10^{-3}$ . The corresponding outage performance gains are 1.2 dB and 2.5 dB for diversity order  $L = 4$ . It is observed that the performance gain increases with the diversity order, as expected.

Fig. 7.6 depicts the outage probability performance versus the desired power switching threshold,  $\zeta$ , for switched diversity with the desired power switching criterion. When  $\zeta$  is less than the optimum switching threshold, the outage probability of the system with the BTM pulse shape is better than that of the systems with the SRC pulse shape but the diversity order does not have any significant effect on the performance. For values of  $\zeta$  greater than the optimum switching threshold, the outage performance of  $L = 4$  is better than that of  $L = 2$  but pulse-shaping does not have any effect. The optimum switching threshold versus the SIR threshold,  $q$  for outage is presented in Fig. 7.7 for SRC and BTM pulse shapes with  $L = 2$  and 4. The outage probability performance versus the SIR switching threshold  $\zeta$  is presented in Fig. 7.8 for switching diversity with the SIR switching criterion. It is observed that the optimum switching threshold,  $\zeta_0 = q$ . The system with BTM pulse-shaping gives better outage performance than that with SRC pulse-shaping. Fig. 7.9 shows the outage probability performance versus the total output power switching threshold,  $\zeta$ , for switched diversity with the total output power switching criterion. A quite similar behavior to the switched diversity with the desired signal power switching criterion is observed. The optimum switching threshold versus the SIR threshold,  $q$ , for outage

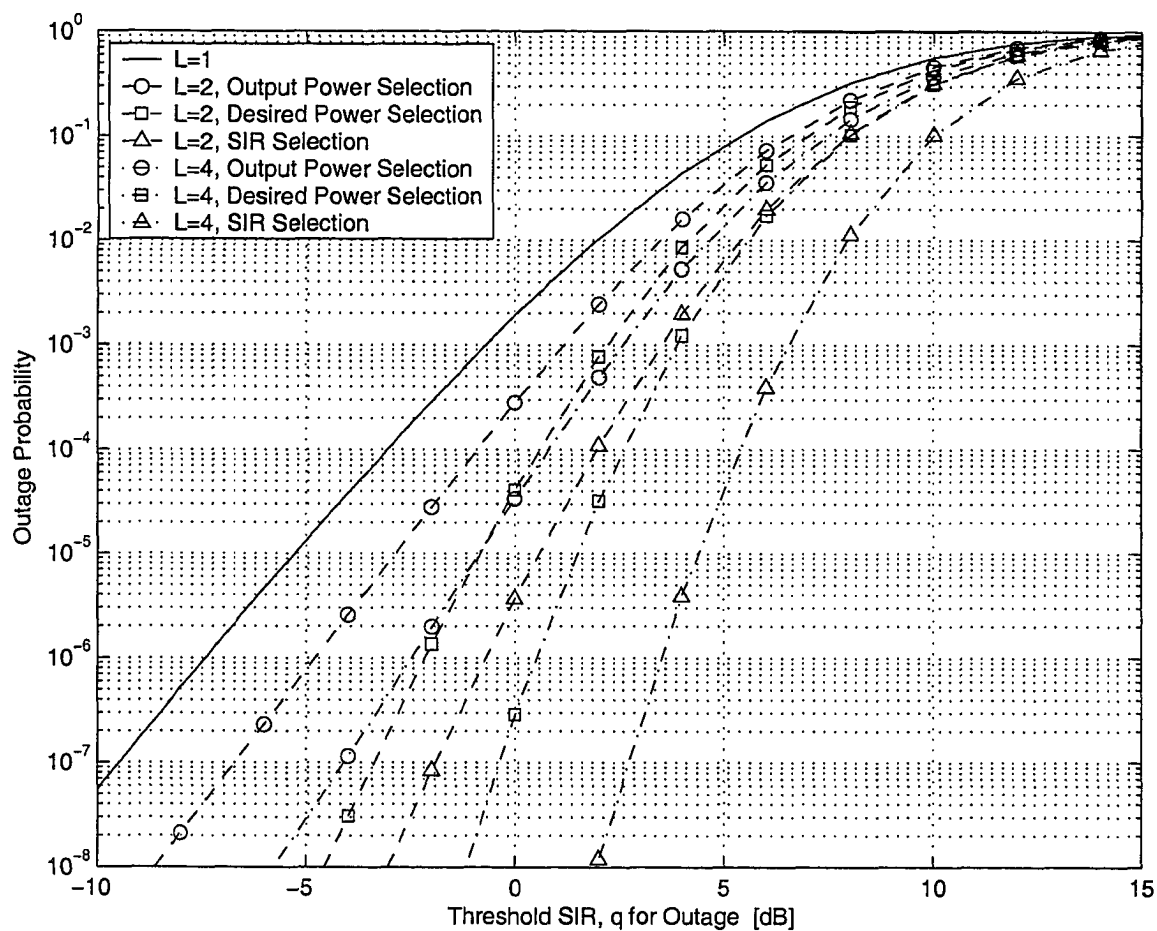


Fig. 7.4. Outage performance comparison of selection diversity with maximum desired power, SIR and output power selection criteria for average SIR=5 dB and SRC pulse shape.

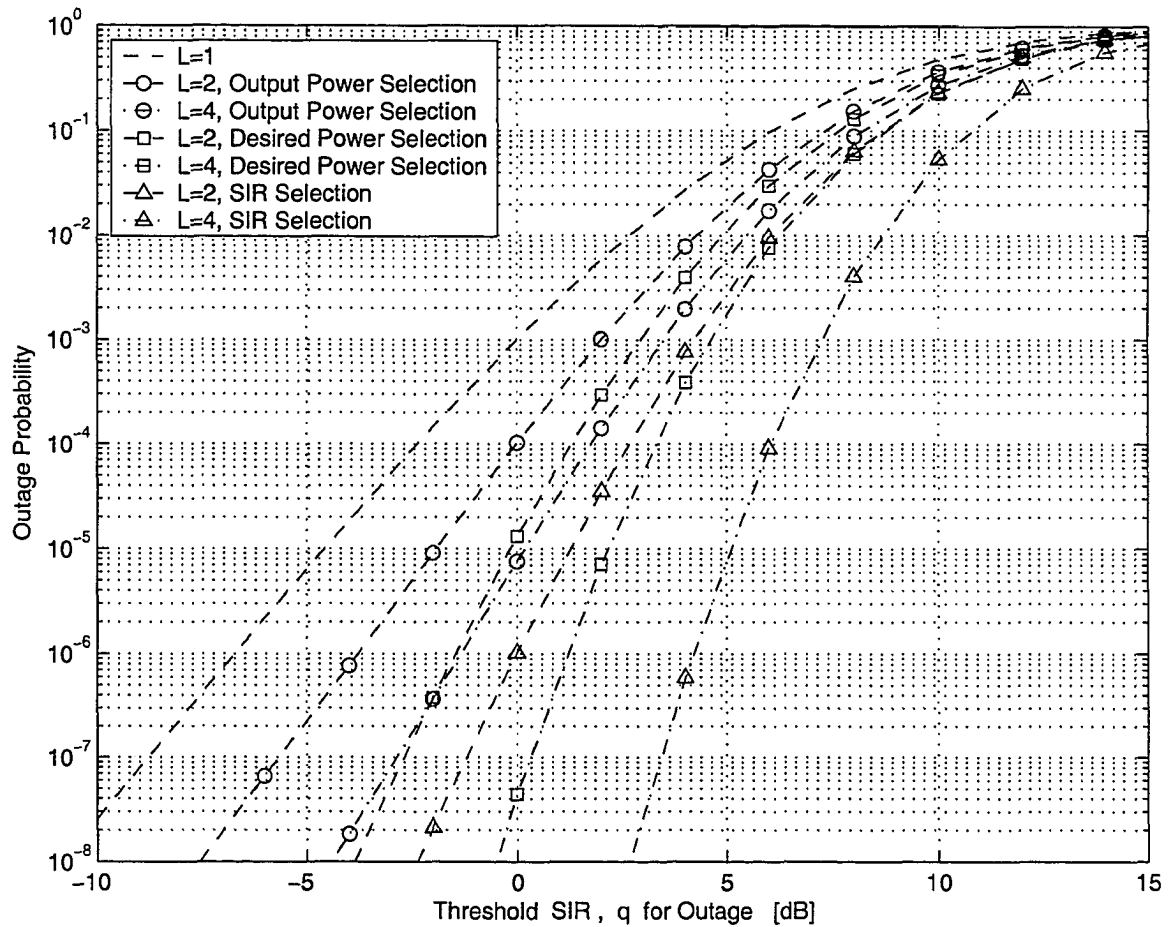


Fig. 7.5. Outage performance comparison of selection diversity with maximum desired power, SIR and output power selection criteria for average SIR=5 dB and BTD pulse shape.

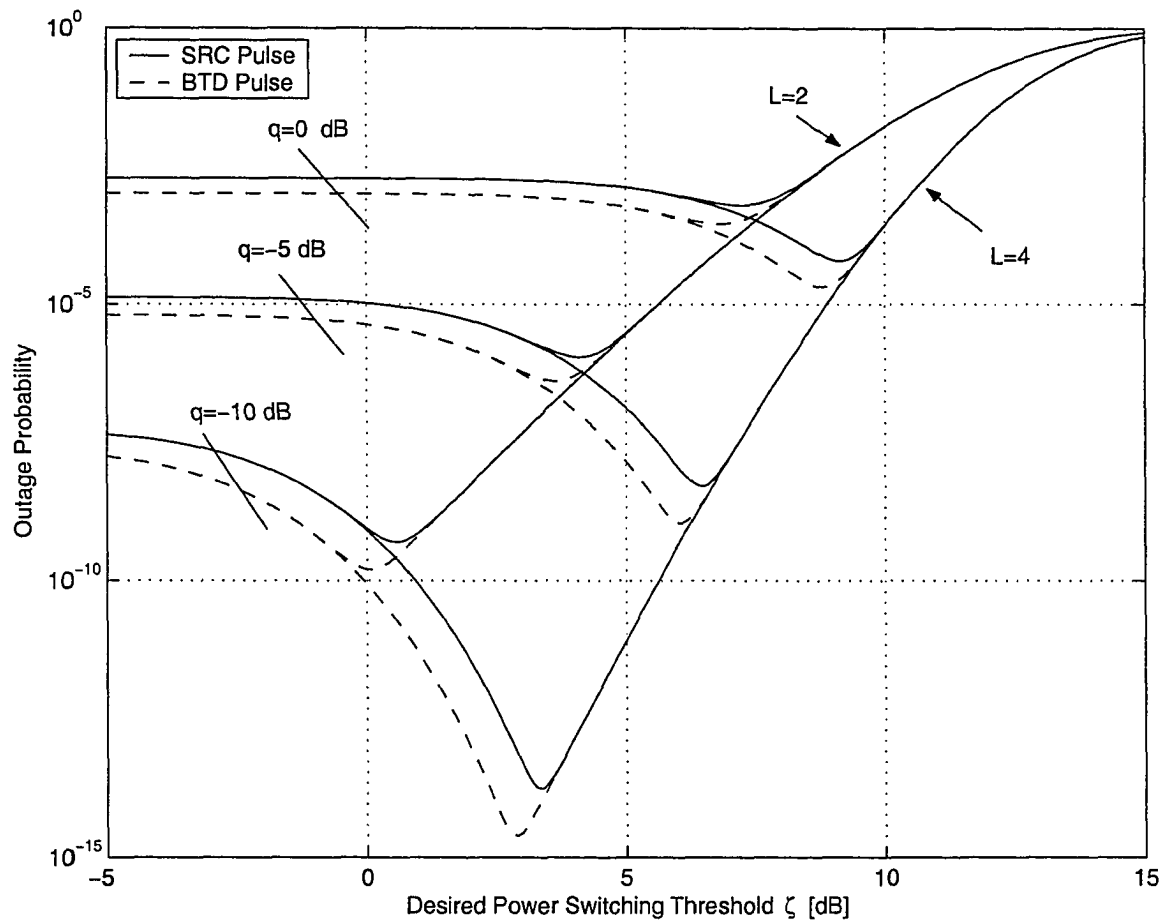


Fig. 7.6. The outage performance of switched diversity with desired power switching criterion for average SIR=5 dB.



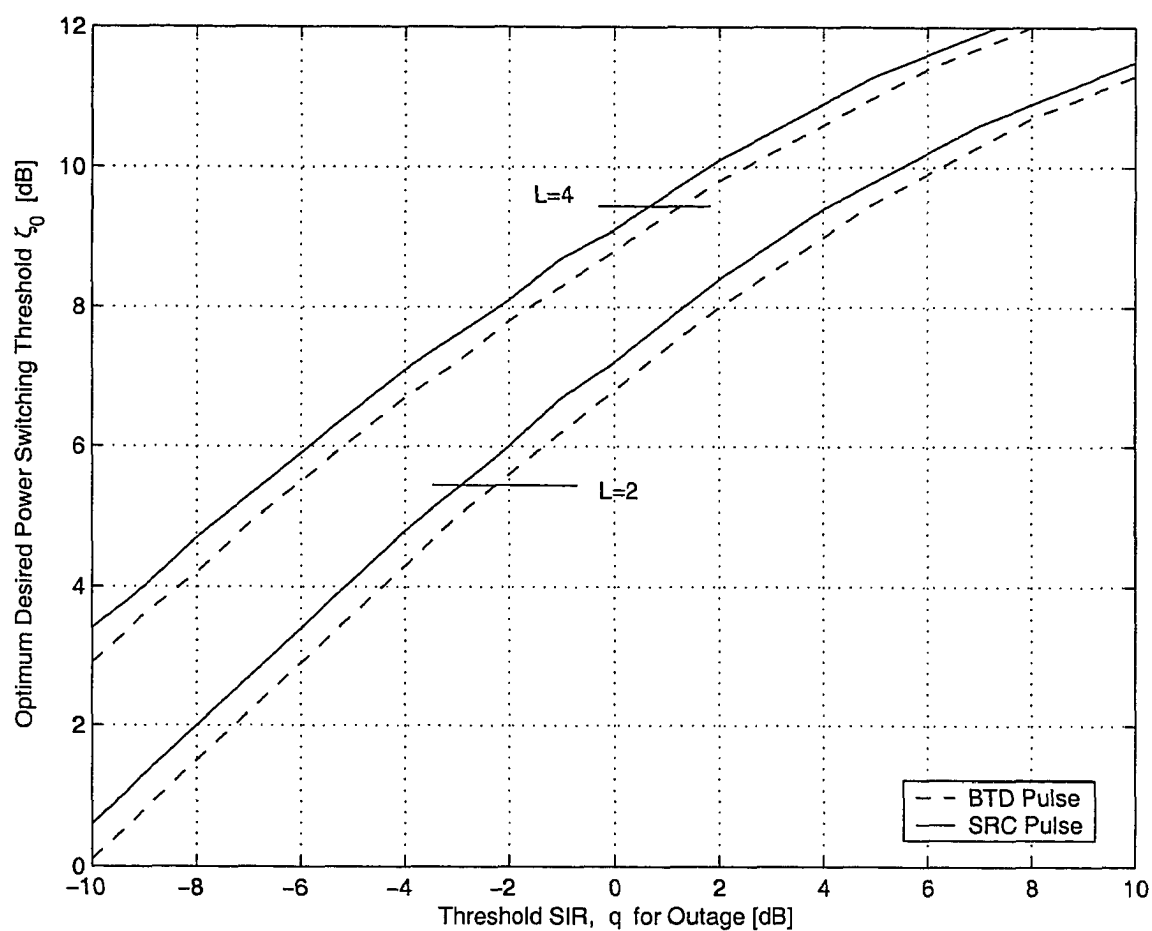


Fig. 7.7. The optimum switching threshold for switched diversity with desired power switching criterion for average SIR=5 dB.

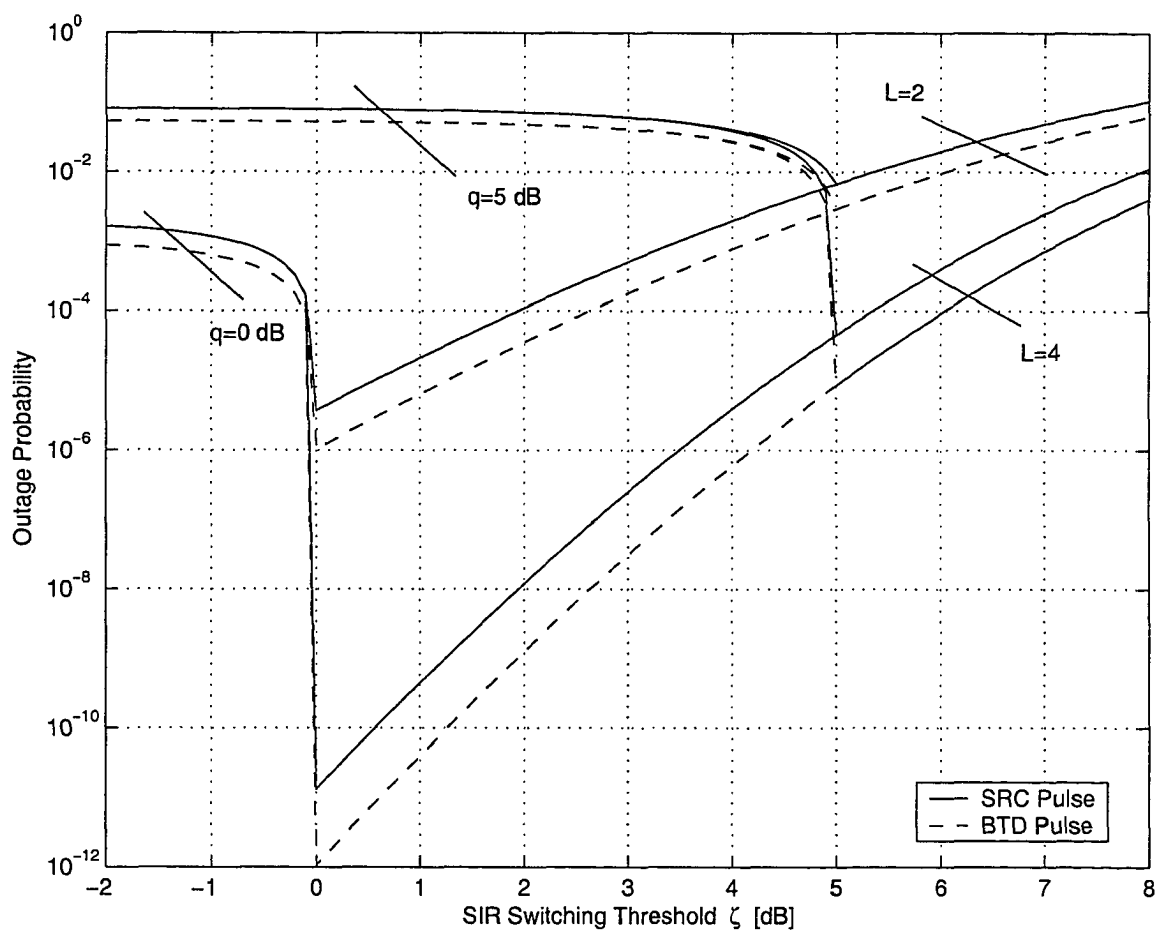


Fig. 7.8. The outage performance of switched diversity with SIR switching criterion for average SIR=5 dB.

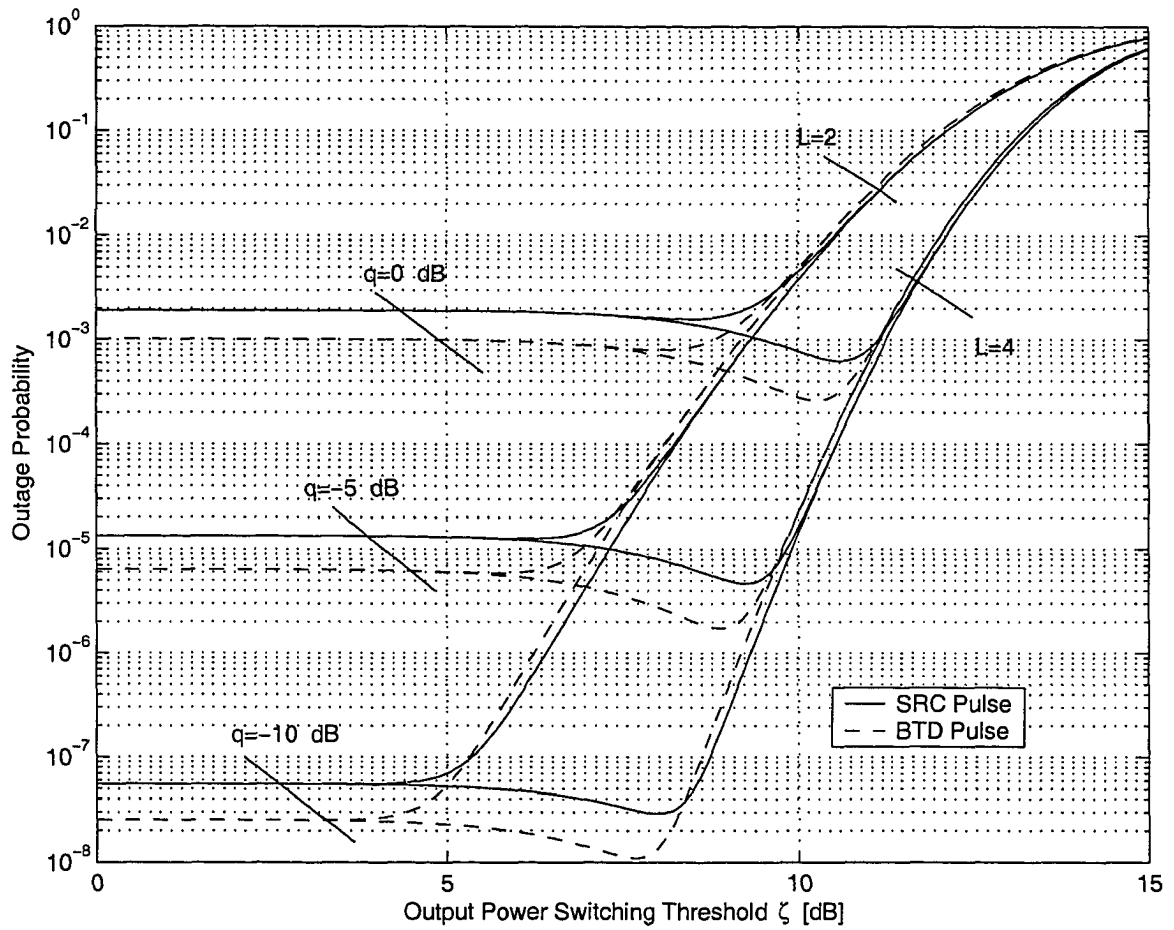


Fig. 7.9. The outage performance of switched diversity with total output power switching criterion for average SIR=5 dB.

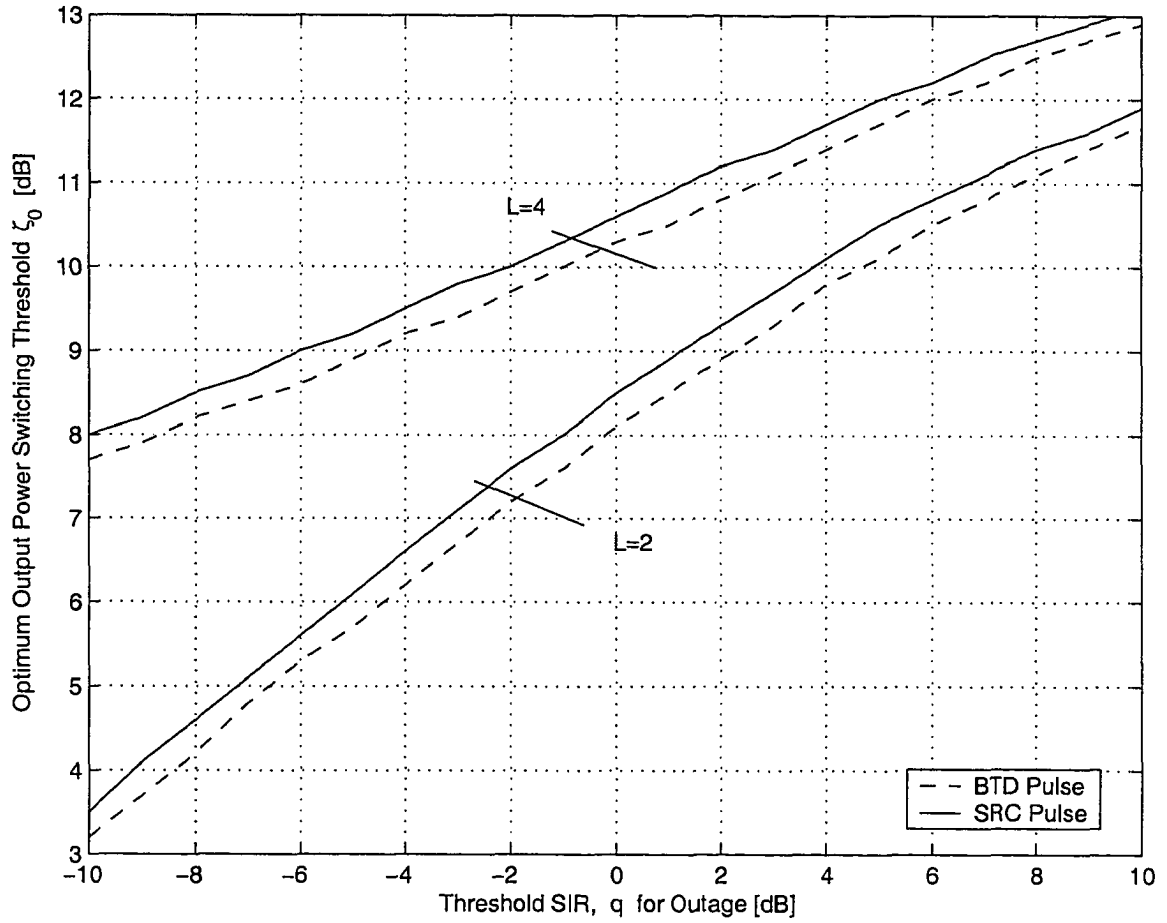


Fig. 7.10. The optimum switching threshold for switched diversity with total output power switching criterion for average SIR=5 dB.

is presented in Fig. 7.10 for SRC and BTD pulse shapes with  $L = 2$  and 4.

## 7.6 Summary

Exact outage probability of the predetection selection and switched diversities has been studied in micro-cellular systems with a Nakagami/Rayleigh fading model. Three selection and switching criteria, namely, desired signal power, SIR and total output power were considered. The outage probability expressions were derived for an arbitrary number of interferers, arbitrary diversity order and arbitrary value of desired user fading parameter. A system with BTD pulse shape gives better outage performance than that with SRC pulse shape for identical system conditions. It was found that the SIR selection criterion provided the best outage performance, and the total output power criterion had the worst. Their outage performance difference increased with the diversity order. The optimum switching thresholds for the three switching criteria were found.

# Chapter 8

## Conclusions and Suggestions for Future Work

In this chapter, we draw our conclusions and present possible directions for future research.

### 8.1 Conclusions

In mature wireless communication systems fading and CCI or MAI degrades the BER performance and they normally cause an error floor in the BER performance. Currently, CDMA and conventional narrowband systems such as TDMA and FDMA are the access methods used in practice and the CDMA takes over as the main access method in third generation wireless communication systems. The topics of interference and fading mitigation have long been studied in the literature. The exact performance evaluation of such systems is often needed but may be difficult. The MC computer simulation method may also suffer due to the long execution time per trial.

This thesis examined the CCI or MAI mitigation in wireless communication systems in fading environments. Several interference whitening receiver structures and conventional receiver diversity schemes were studied. The exact performances of such receivers were studied analytically in most cases. In the other cases, MC computer simulation or approximation methods were invoked for the performance estimation. In summary:

1. The cochannel interference mitigation using interference whitening for BPSK systems in micro-cellular fading environments has been considered. A flat slow Nakagami-Rayleigh desired/interfering user fading model was assumed. Four receiver structures were studied. Two Nyquist pulse shapes namely, SRC and BTD pulse shapes and the NRZ rectangular pulse shape were considered. An extensive performance comparison study was presented using characteristic function and approximate Fourier series methods for a variety of fading situations of the desired user. The proposed receivers require only knowledge of the total interference power and the pulse-shaping of the interferers at the receiver. These parameters may be available in conventional receivers for the power control or diversity combining. As the receiver structure changes with the parameters thus, these receivers are adaptive single-user receivers.
2. The BER performance analysis of bandlimited DS-CDMA system in slow, flat Nakagami- $m$  fading channels has been considered. Several computationally efficient Gaussian approximation methods and an exact CF method were studied. Gaussian approximation methods were validated using MC computer simulation. The SRC and BTD pulse-shapings were employed. The performance with BTD pulse-shaping was always better than that with SRC pulse-shaping. For

systems with random spreading, the BER expression derived using the IGA method with the CF provided the most accurate results with reasonable computational complexity. The  $K + 1$  fold numerical integration was reduced to 2-fold iterated numerical integration. The IHGA provided accurate results only at high average SNR values. The HIGA performed poorer than the SGA for bandlimited DS-CDMA systems in Nakagami fading.

3. Average BER performance analyses of three diversity receivers for a bandlimited DS-CDMA system in slow, flat Nakagami fading channel were presented. The well known combining schemes, such as, MRC, EGC and SC were considered. The bandlimited Nyquist pulse-shapings, namely, SRC and BTD pulse-shapings were employed. A closed-form BER approximation was derived for the MRC using the SGA and BER approximations for the EGC and SC schemes entailing numerical integration were derived using the SGA and the IGA. The computational complexity does not increase with the number of users or the diversity order. These results are valid for arbitrary diversity order and arbitrary Nakagami fading parameter. The performance with BTD pulse-shaping is better than that with SRC pulse-shaping in all cases examined.
4. A multiple access interference suppression method for a bandlimited DS-CDMA system in slow, flat Nakagami fading was considered. The whitening matched filter receiver proposed in [23] was employed with a fractionally spaced MMSE equalizer to combat the ISI created by the WMF. The precise BER performance was derived using CF and approximate Fourier series methods. Without the equalizer the average BER is 0.5 for all values of average SNR and number of interferers. The system employing the new BTD pulse outperformed the system



using the SRC pulse when the same system parameters were considered.

5. The exact BER performances of coherent BPSK and QPSK systems with CCI and fading have been investigated. Closed-form expressions for the characteristic functions of CCI for a BPSK system with independent Nakagami faded interferers and a QPSK system with independent Rayleigh faded interferers have been obtained. The average BER expression was derived in single integral form and is readily evaluated numerically. The accuracy of the Gaussian approximation for the CCI was assessed and found to be more accurate in the presence of large number of interferers, as expected
6. The accurate performances of coherent bandlimited BPSK systems with EGC and SC in CCI and fading have been investigated. Exact integral results were obtained for arbitrary diversity orders and Nakagami fading parameters. The computational complexity does not increase either with diversity order or number of interferers. The superiority of the BTD pulse over the SRC pulse was once again observed and the superiority increases with the diversity order.
7. The outage and BER performances of coherent bandlimited BPSK with MRC in CCI micro-cellular systems have been determined. The Gaussian approximation is quite accurate for BER estimation for six or more interferers. The superiority of the BTD pulse over the SRC pulse was once again observed. While the superiority in BER performance increases with diversity order, the superiority in outage performance remains approximately the same for different diversity orders.
8. The exact outage probability of predetection SC and SWC diversities has been studied in micro-cellular systems with a Nakagami/Rayleigh fading model. Three

selection and switching criteria, namely, desired signal power, SIR and total output power were considered. The outage probability expressions were derived for an arbitrary number of interferers, arbitrary diversity order and arbitrary value of desired user fading parameter. A system with BTD pulse shape gives better outage performance than that with SRC pulse shape for identical system conditions. It was found that the SIR selection criterion provided the best outage performance, and the total output power criterion had the worst. Their outage performance differences increased with the diversity order. The optimum switching thresholds for the three switching criteria were found.

## 8.2 Suggestions for Future Work

1. The results for interference whitening receivers can be extended to linear sub-optimum multiuser receivers. A bank of WMFs can be used instead of bank of conventional MF as the first stage in MMSE and decorrelating multiuser receivers. The conventional matched filter maximizes the SNR in AWGN channels but the WMF maximizes SNIR when the MAI is present with the AWGN. Thus, the new structures may give better performance than multiuser receivers with conventional MFs in multiuser channels. The WMF requires knowledge of the total interference power and the pulse-shaping of the interfering users. As this information is already available in the MMSE receiver, no new information is required for the MMSE receiver with interference whitening. However, decorrelating receiver with interference whitening needs to estimate the total interference power for each user.
2. A jointly optimum combining receiver for space diversity reception was proposed

by Winters [36] to jointly combat both CCI and fading. The SNIR in all diversity branches are jointly maximized using adaptive array techniques. There are some shortcomings with this scheme. The number of antennas should be larger than number of interferers. Otherwise a few dominant interferers are considered and the remainder are treated as background noise. When there is only one antenna this receiver structure neither combats fading nor CCI. This scheme cannot be used with RAKE receivers. An individually optimum combining scheme to combat CCI and fading individually can be considered. The receiver structure consists of a whitening matched filter and a linear MMSE equalizer in each diversity branch and the branches are combined using maximal ratio combining. The whitening matched filters individually maximize the SNIR in each branch. Now, the individually maximum SNIR is always greater than or equal to the jointly maximum SNIR. So the individually optimum combining is better than jointly optimum combining in a SNIR sense. This proposed receiver structure is more general than the structure proposed in [36] and does not have the shortcomings mentioned above. The complexity of this receiver structure is somewhat greater but comparable.

3. The effects of interference whitening receivers in multiple-input-multiple-output (MIMO) channels can be considered. Recently, a simple transmit diversity scheme was proposed by Alamouti in [134] and this scheme drew lot of attention in the literature. The performance of a whitening matched filter and MMSE equalizer structure in independent and correlated fading for simple receiver and transmit diversity schemes in the presence of CCI can be studied. When the fadings of the transmit diversity branches are correlated, the whitening filter should consist of temporal and spatial whitening filters.

4. Performance analysis of bandlimited DS-CDMA in flat fading channel was considered. A more appropriate model for a CDMA system with frequency selective fading channels and a RAKE receiver structure [65] may be considered in the analysis. As the exact analysis is difficult, the Gaussian approximation methods considered in this thesis may be extended to study the BER performance.

# References

- [1] T. S. Rappaport, *Wireless Communications Principles and Practice*, 2nd ed. New Jersey: Prentice Hall PTR, 2002.
- [2] T. S. Rappaport, A. Annamalai, R. M. Buehrer, and W. H. Tranter, "Wireless communications: Past events and a future perspective," *IEEE Communications Magazine*, pp. 148–161, May 2002.
- [3] R. L. Pickholtz, L. B. Milstein, and D. L. Schilling, "Overview of cellular CDMA," *IEEE Transactions on Vehicular Technology*, vol. 40, pp. 291–302, May 1991.
- [4] G. L. Stüber, *Principles of Mobile Communication*, 2nd ed. Boston, MA: Kluwer Academic, 2001.
- [5] B. Sklar, *Digital Communications: Fundamentals and applications*. Upper Saddle River, NJ: Prentice Hall, 2001.
- [6] M. K. Simon and M.-S. Alouini, *Digital Communication over Fading Channels: A Unified Approach to Performance Analysis*. New York: Wiley, 2000.
- [7] J. G. Proakis, *Digital Communications*, 4th ed. New York: McGraw-Hill, 2001.

- [8] J. D. Parsons, *The Mobile Radio Propagation Channel*, 2nd ed. New York: McGraw-Hill, 2000.
- [9] M. Nakagami, "The  $m$  distribution: a general formula of intensity distribution of rapid fading," *Statistical Methods in Radio Wave Propagation*. Oxford: Pergoman Press, pp. 3–36, 1960.
- [10] E. A. Neasmith and N. C. Beaulieu, "New results on selection diversity," *IEEE Transactions on Communications*, vol. 46, no. 11, pp. 695 – 704, May 1998.
- [11] Y. G. Kim and S. W. Kim, "Optimum selection diversity for BPSK signal in rayleigh fading channels," *IEEE Transactions on Communications*, vol. 49, pp. 1715–1718, Oct. 2001.
- [12] A. A. Abu-Dayya and N. C. Beaulieu, "Analysis of switched diversity systems on generalized fading channels," vol. 42, pp. 2959–2966, Nov. 1994.
- [13] A. A. Abu-Dayya and N. C. Beaulieu, "Outage probabilities of diversity cellular systems with cochannel interference in Nakagami fading," *IEEE Transactions on Vehicular Technology*, vol. 41, pp. 343 – 355, Nov. 1992.
- [14] L. Schiff, "Statistical suppression of interference with diversity in a mobile-radio environment," *IEEE Transactions on Vehicular Technology*, vol. 21, pp. 121–128, Nov. 1972.
- [15] S. Verdu, "Minimum probability of error for asynchronous gaussian multiple-access channels," *IEEE Transactions on Information Theory*, vol. 32, pp. 85–96, Jan. 1986.

- [16] M. Chiani, "Performance of BPSK and GMSK with multiple cochannel interferers," in *Proc. of IEEE PIMRC'96*, Taipei, Taiwan, Oct. 1996, pp. 833–837.
- [17] R. Kwan and C. Leung, "Optimal detection of a BPSK signal contaminated by interference and noise," *IEEE Communications Letters*, vol. 6, no. 6, pp. 225–227, June 2002.
- [18] T. V. Poon and N. C. Beaulieu, "Error performance analysis of a jointly optimal single-cochannel-interferer BPSK receiver," *IEEE Transactions on Communications*, vol. 52, pp. 1051–1054, July 2004.
- [19] S. Verdú, *Multiuser Detection*. New York: Cambridge University Press, 1998.
- [20] Z. Xie, R. T. Short, and C. K. Rushforth, "A family of suboptimum detectors for coherent multiuser communications," *IEEE Journal on Selected Areas in Communications*, vol. 8, no. 4, pp. 683–690, May 1990.
- [21] R. Lupas and S. Verdu, "Near-far resistance multiuser detectors in asynchronous channels," *IEEE Transactions on Communications*, vol. 38, no. 4, pp. 496–508, Apr. 1990.
- [22] A. Duel-Hallen, "Decorrelating decision-feedback multiuser detector for synchronous code-division multiple access channels," *IEEE Transactions on Communications*, vol. 2, pp. 285–290, Feb. 1993.
- [23] A. Monk, M. Davis, L. B. Milstein, and C. Helstrom, "A noise whitening approach to multiple-access noise rejection - part I: Theory and background," *IEEE Journal on Selected Areas in Communications*, vol. 12, no. 6, pp. 817–827, June 1994.

- [24] M. Davis, A. Monk, and L. B. Milstein, "A noise whitening approach to multiple-access noise rejection - part II: Implementation issues," *IEEE Journal on Selected Areas in Communications*, vol. 14, no. 10, pp. 1488–1499, Oct. 1996.
- [25] J. H. A. Duel-Hallen and Z. Zvonar, "Multi-user detection for CDMA systems," *IEEE Personal Communications Magazine*, vol. 2, pp. 46–58, Apr. 1995.
- [26] S. Moshavi, "Multi-user detection for DS-CDMA communications," *IEEE Communications Magazine*, vol. 34, no. 10, pp. 124–136, Oct. 1996.
- [27] C. W. Helstrom, *Elements of Signal Detection & Estimation*. Englewood Cliffs, NJ: Prentice Hall PTR, 1995.
- [28] B. M. Dwork, "The detection of a pulse superimposed on fluctuation noise," *Proceedings of the IRE*, vol. 38, pp. 771–774, July 1950.
- [29] H. L. Van-Trees, *Detection, Estimation, and Modulation Theory: Part I*. New York: John Wiley and Sons, 1968.
- [30] N. C. Beaulieu, C. C. Tan, and M. O. Damen, "A "better than" Nyquist pulse," *IEEE Communications Letters*, vol. 5, no. 9, pp. 367–368, Sept. 2001.
- [31] N. C. Beaulieu, "The evaluation of error probabilities for intersymbol and cochannel interference," *IEEE Transactions on Communications*, vol. 39, no. 12, pp. 1740–1749, Dec. 1991.
- [32] R. K. Morrow and J. S. Lehnert, "Bit-to-bit error dependence in slotted DS/SSMA packet systems with random signature sequences," *IEEE Transactions on Communications*, vol. 37, no. 10, pp. 1052–1061, Oct. 1989.



- [33] M. B. Pursley, "Performance evaluation for phase-coded spread-spectrum multiple-access communication-part I: System analysis," *IEEE Transactions on Communications*, vol. 25, no. 8, pp. 795–799, Aug. 1977.
- [34] N. W. K. Lo, D. D. Falconer, and A. U. H. Sheikh, "Adaptive equalization for co-channel interference in a multipath fading environment," *IEEE Transactions on Communications*, vol. 43, no. 2/3/4, pp. 1441–1453, Feb./Mar./Apr. 1995.
- [35] B. C. W. Lo and K. B. Letaief, "Adaptive equalization and interference cancellation for wireless communication," *IEEE Transactions on Communications*, vol. 47, no. 4, pp. 538–545, Apr. 1999.
- [36] J. Winters, "Optimum combining in digital mobile radio with cochannel interference," *IEEE Transactions on Vehicular Technology*, vol. 33, no. 3, pp. 144–155, Aug. 1984.
- [37] J. W. Liang, J. T. Chen, and A. J. Paulraj, "A two-stage hybrid approach for CCI/ISI reduction with space-time processing," *IEEE Communications Letters*, vol. 1, no. 11, pp. 163–165, Nov. 1997.
- [38] M. O. Hazna, M. S. Alouini, A. Bastami, and E. S. Ebbini, "Performance analysis of cellular mobile systems with successive co-channel interference cancellation," *IEEE Transactions on Wireless Communications*, vol. 2, no. 1, pp. 29–40, Jan. 2003.
- [39] H. Arslan and K. Molnar, "Cochannel interference suppression with successive cancellation in narrow-band systems," *IEEE Communications Letters*, vol. 5, no. 2, pp. 367–368, Feb. 2001.

- [40] M. Chiani, "Analytical distribution of linearly modulated cochannel interferers," *IEEE Transactions on Communications*, vol. 45, no. 1, pp. 73–79, Jan. 1997.
- [41] S. W. Wales, "Technique for cochannel interference suppression in TDMA mobile radio systems," *IEE Proceedings-Communications*, vol. 6, pp. 106–114, Apr. 1995.
- [42] Y. C. Yoon and H. Leib, "Maximizing SNR in improper complex noise and applications to CDMA," *IEEE Communications Letters*, vol. 1, no. 1, pp. 5–8, Jan. 1997.
- [43] N. C. Beaulieu and A. A. Abu-Dayya, "Bandwidth efficient QPSK in cochannel interference and fading," *IEEE Transactions on Communications*, vol. 43, no. 9, pp. 2464–2474, Sept. 1995.
- [44] K. A. Hamdi, "Exact probability of error of BPSK communication links subjected to asynchronous interference in Rayleigh fading environment," *IEEE Transactions on Communications*, vol. 50, no. 10, pp. 1577–1579, Oct. 2002.
- [45] N. C. Beaulieu and J. Cheng, "Precise error-rate analysis of bandwidth-efficient BPSK in Nakagami fading and cochannel interference," *IEEE Transactions on Communications*, vol. 52, no. 1, pp. 149–158, Jan. 2004.
- [46] K. Sivanesan and N. C. Beaulieu, "Exact BER analyses of Nakagami/Nakagami CCI BPSK and Nakagami/Rayleigh CCI QPSK system in slow fading," *IEEE Communications Letters*, vol. 1, pp. 45–47, Jan. 2004.

- [47] C. Tellambura and A. Annamalai, "Further results on the Beaulieu series," *IEEE Transactions on Communications*, vol. 48, no. 11, pp. 1774–1777, Nov. 2000.
- [48] E. W. Ng and M. Geller, "Table of integrals of the error functions," *Journal of Research of the National Bureau of Standards*, vol. 73B, pp. 1–20, Jan.-Mar. 1969.
- [49] R. D. Gitlin and S. B. Weinstein, "Fractionally-spaced equalization: An improved digital transversal equalizer," *The Bell System Technical Journal*, vol. 60, pp. 275–297, Feb. 1981.
- [50] M. Davis and L. B. Milstein, "Improved CDMA performance through multiple access noise rejection," in *Proc. of IEEE MILCOM'92*, San Diego, CA, Oct. 1992, pp. 846–850.
- [51] S. Haykin, *Communication Systems*, 4th ed. New York: John Wiley & Sons, 2001.
- [52] M. Davis and L. B. Milstein, "Implementation of a CDMA receiver with multiple access noise rejection," in *Proc. of IEEE PIMRC'92*, Boston, MA, Oct. 1992, pp. 103–107.
- [53] K. Sivanesan and N. C. Beaulieu, "Interference whitening receivers for CCI mitigation in micro-cellular BPSK systems," in *Proc. of IEEE VTC-Fall'2004*, Los Angeles, CA, Sept. 2004.
- [54] K. Sivanesan and N. C. Beaulieu, "CCI mitigation using interference whitening in bandlimited micro-cellular BPSK systems," in *Proc. of IEEE Globecom'2004*, Dallas, TX, Dec. 2004, pp. xxx–yyy.

- [55] Y. Asano, Y. Daido, and J. Holtzman, "Performance evaluation for band-limited DS-CDMA communication systems," in *Proc. of IEEE VTC'93*, New York, USA, May 1993, pp. 464–468.
- [56] T. Shibata and A. Ogawa, "Performance of asynchronous band-limited DS/SSMA systems," *IEICE Transactions on Communication*, vol. E76-B, pp. 921–928, Aug. 1993.
- [57] A. J. Viterbi, *Principles of Spread Spectrum Communication*. Massachusetts: Addison-Wesley, 1995.
- [58] Y. C. Yoon, "Accurate approximation for probability of bit error in asynchronous bandlimited DS-CDMA system with multiple data rates," in *Proc. of 20-th Queens Biennial Symposium on Communications*, Kingston, ON, Canada, May 2000, pp. 326–330.
- [59] Y. C. Yoon, "A simple and accurate method of probability of bit-error analysis for asynchronous band-limited DS-CDMA systems," *IEEE Transactions on Communications*, vol. 50, no. 4, pp. 656–663, Apr. 2002.
- [60] Y. C. Yoon, "Quadriphase DS-CDMA with pulse shaping and the accuracy of the Gaussian approximation for matched filter receiver performance analysis," *IEEE Transactions on Wireless Communications*, vol. 1, no. 3, pp. 761–768, Oct. 2002.
- [61] G. Zang and C. Ling, "Performance evaluation for band-limited DS-CDMA systems based on simplified improved Gaussian approximations," *IEEE Transactions on Communications*, vol. 51, no. 7, pp. 1204–1213, July 2003.

- [62] J. H. Cho, Y. K. Jeong, and J. S. Lehnert, "Average bit-error-rate performance of band-limited DS/SSMA communications," *IEEE Transactions on Communications*, vol. 50, no. 7, pp. 1150–1159, July 2002.
- [63] J. M. Holtzman, "A simple, accurate method to calculate spread-spectrum multiple-access error probabilities," *IEEE Transactions on Communications*, vol. 40, no. 3, pp. 461–464, Mar. 1992.
- [64] Y. C. Yoon, "Probability of bit error and Gaussian approximation in asynchronous DS-CDMA systems with chip pulse shaping," in *Proc. of 20-th Queens Biennial Symposium on Communications*, Kingston, ON, Canada, May 2000, pp. 111–115.
- [65] T. Eng and L. B. Milstein, "Coherent DS-CDMA performance in Nakagami multipath fading," *IEEE Transactions on Communications*, vol. 43, no. 2/3/4, pp. 1134 – 1143, Feb./Mar./Apr. 1995.
- [66] G. P. Efthymoglou, V. Aalo, and H. Helmken, "Performance analysis of coherent DS-CDMA system in Nakagami fading channel with arbitrary parameters," *IEEE Transactions on Vehicular Technology*, vol. 46, pp. 289–297, May 1997.
- [67] J. Cheng and N. C. Beaulieu, "Accurate DS-CDMA bit-error probability calculation in Rayleigh fading," *IEEE Transactions on Wireless Communications*, vol. 1, no. 1, pp. 3–15, Jan. 2002.
- [68] J. Cheng and N. C. Beaulieu, "Precise bit error rate calculation for asynchronous DS-CDMA in Nakagami fading," in *Proc. of IEEE GLOBE-COM'2000*, San Francisco, CA, Nov. 2000, pp. 980–984.

- [69] E. Geranoitis and B. Ghaffari, "Performance of binary and quaternary direct sequence spread-spectrum multiple access systems with random signature sequence," *IEEE Transactions on Communications*, vol. 39, no. 5, pp. 713 – 724, May 1991.
- [70] M. O. Sunay and P. J. McLane, "Calculating error probabilities for DS-CDMA systems: When not to use the Gaussian approximation," in *Proc. of IEEE GLOBECOM'96*, London, U.K, Nov. 1996, pp. 1774–1749.
- [71] R. K. Morrow, "Accurate CDMA BER calculations with low computational complexity," *IEEE Transactions on Communications*, vol. 46, no. 11, pp. 1413 – 1417, Nov. 1998.
- [72] K. B. Letaief, "Efficient evaluation of the error probabilities of spread-spectrum multiple-access communications," *IEEE Transactions on Communications*, vol. 45, no. 2, pp. 239–246, Feb. 1997.
- [73] Y. C. Yoon, "An improved Gaussian approximation for probability of bit-error analysis of asynchronous bandlimited DS-CDMA systems with BPSK spreading," *IEEE Transactions on Wireless Communications*, vol. 1, no. 2, pp. 373–382, July 2002.
- [74] A. Papoulis and S. U. Pillai, *Probability, Random Variables, and Stochastic Processes*, 4th ed. New York: McGraw-Hill, 2002.
- [75] E. A. Lee and D. G. Messerschmitt, *Digital Communication*, 2nd ed. Norwell, MA: Kluwer, 1994.
- [76] I. S. Gradshteyn and I. M. Ryzhik, *Tables of Integrals, Series and Products*, 6th ed. San Diego CA: Academic Press, 2000.

- [77] J. H. Cho and J. S. Lehnert, "An optimal signal design for band-limited asynchronous DS-CDMA communications," *IEEE Transactions on Information Theory*, vol. 48, no. 5, pp. 1172–1185, May 2002.
- [78] K. Sivanesan and N. C. Beaulieu, "Performance analysis of bandlimited DS-CDMA systems in Nakagami fading," in *Proc. of IEEE ICC'2004*, Paris, France, June 2004, pp. 400–404.
- [79] J. S. Lehnert and M. B. Pursley, "Multipath diversity reception of spread-spectrum multiple access communications," *IEEE Transactions on Communications*, vol. 35, no. 11, pp. 1189–1198, Nov. 1987.
- [80] C. Kchao and G. L. Stüber, "Analysis of a direct-sequence spread spectrum cellular radio system," *IEEE Transactions on Communications*, vol. 41, pp. 1507 – 1516, Nov. 1993.
- [81] A. Annamalai, "Microdiversity reception of spread-spectrum signals on Nakagami fading channels," *IEEE Transactions on Communications*, vol. 47, no. 11, pp. 1747 – 1756, Nov. 1999.
- [82] O. C. Ugweje, "Selection diversity for wireless communications in Nakagami-fading with arbitrary parameters," *IEEE Transactions on Vehicular Technology*, vol. 50, pp. 1437–1448, Nov. 2001.
- [83] J. Panicker and S. Kumar, "Effects of the system imperfections on BER performance of a CDMA receiver with multipath diversity combining," *IEEE Transactions on Vehicular Technology*, vol. 45, pp. 622 – 630, Nov. 1996.

- [84] M. O. Sunay and P. J. McLane, "Probability of error for diversity combining in DS-CDMA systems with synchronization errors," *European Transactions on Telecommunication*, vol. 9, pp. 449–463, Sep.-Oct. 1998.
- [85] N. C. Beaulieu, "A investigation of Gaussian tail and Rayleigh tail density functions for importance sampling digital communication system simulation," *IEEE Transactions on Communications*, vol. 38, no. 9, pp. 1288–1292, Sept. 1990.
- [86] A. A. Abu-Dayya and N. C. Beaulieu, "Outage probabilities of cellular mobile radio systems with multiple Nakagami interferers," *IEEE Transactions on Vehicular Technology*, vol. 40, pp. 757–768, Nov. 1991.
- [87] M. S. Alouini, A. Abdi, and M. Kaveh, "Sum of gamma variates and performance of wireless communication systems over Nakagami-fading channels," *IEEE Transactions on Vehicular Technology*, vol. 50, pp. 1471 – 1480, Nov. 2001.
- [88] N. C. Beaulieu and A. A. Abu-Dayya, "Analysis of equal gain diversity on Nakagami fading channels," *IEEE Transactions on Communications*, vol. 39, no. 2, pp. 225 – 234, Feb. 1991.
- [89] A. Annamalai, C. Tellambura, and V. Bhargava, "Equal-gain diversity receiver performance in wireless channels," *IEEE Transactions on Communications*, vol. 48, no. 10, pp. 1732 – 1745, Oct. 2000.
- [90] K. Sivanesan and N. C. Beaulieu, "Performance analysis of bandlimited DS-CDMA systems with diversity receivers over Nakagami fading channels," in *Proc. of IEEE Milcom'2004*, Monterey, CA, Nov. 2004.



- [91] Y. C. Yoon and H. Leib, "Matched filters with interference suppression capabilities for DS-CDMA," *IEEE Journal on Selected Areas in Communications*, vol. 14, pp. 1510–1521, Oct. 1996.
- [92] Y. C. Yoon and H. Leib, "Chip-delay locked matched filter for DS-CDMA systems using long sequence spreading," *IEEE Transactions on Communications*, vol. 49, no. 8, pp. 1468–1478, Aug. 2001.
- [93] Y. Huang and T. S. Ng, "Capacity enhancement of band-limited DS-CDMA systems using weighted despreading function," *IEEE Transactions on Communications*, vol. 47, no. 8, pp. 1218–1226, Aug. 1999.
- [94] T. F. Wong and J. S. Lehnert, "Asynchronous multiple-access interference suppression and chip waveform selection with aperiodic random sequences," *IEEE Transactions on Communications*, vol. 47, no. 1, pp. 103–113, Jan. 1999.
- [95] Y. Huang and H. Leib, "SNIR maximizing space-time filtering for asynchronous DS-CDMA," *IEEE Journal on Selected Areas in Communications*, vol. 18, pp. 1191–1202, July 2000.
- [96] J. H. Cho and J. S. Lehnert, "Performance of a spatio-temporal matched filter receiver for DS/SSMA communications," .
- [97] Y. Huang and H. Leib, "Chip-locked space-time filtering for maximizing SNIR in asynchronous DS-CDMA systems," *IEEE Transactions on Wireless Communications*, vol. 2, pp. 723–735, July 2003.
- [98] F. Xiong, *Digital Modulation Techniques*. Norwood, MA: Artech House Inc., 2000.

- [99] V. A. Aalo and J. Zhang, "On the effect of cochannel interference on average error rates in Nakagami-fading channels," *IEEE Communications Letters*, vol. 3, pp. 136 – 138, May 1999.
- [100] A. A. Abu-Dayya and N. C. Beaulieu, "Diversity MPSK receivers in cochannel interference," *IEEE Transactions on Vehicular Technology*, vol. 48, pp. 1959 – 1965, Nov. 1999.
- [101] J. Cui and A. U. H. Sheikh, "Outage probability of cellular radio systems using maximal ratio combining in the presence of multiple interferers," *IEEE Transactions on Communications*, vol. 47, no. 8, pp. 1121–1124, Aug. 1999.
- [102] A. Shah and A. M. Haimovich, "Performance analysis of maximal ratio combining and comparison with optimum combining for mobile radio communications with cochannel interference," *IEEE Transactions on Vehicular Technology*, vol. 49, pp. 1454–1463, July 2000.
- [103] V. A. Aalo and J. Zhang, "Performance analysis of maximal ratio combining in the presence of multiple equal-power cochannel interferers in a Nakagami fading channel," *IEEE Transactions on Vehicular Technology*, vol. 50, pp. 497–503, Mar. 2001.
- [104] C. Chayawan and V. A. Aalo, "Average error probability of digital cellular radio systems using MRC diversity in the presence of multiple interferers," *IEEE Transactions on Wireless Communications*, vol. 2, pp. 860–864, Sept. 2003.

- [105] Y. Ma, T. J. Lim, and S. Pasupathy, "Error probability for coherent and differential PSK over arbitrary Rician fading with multiple cochannel interferers," *IEEE Transactions on Communications*, vol. 50, no. 3, pp. 429–441, Mar. 2002.
- [106] C. W. Helstrom, "Calculating error probabilities for intersymbol and cochannel interference," *IEEE Transactions on Communications*, vol. COM-34, no. 5, pp. 430–435, May 1986.
- [107] X. W. Cui, Q. T. Zhang, and Z. M. Feng, "Outage performance for maximal ratio combiner in the presence of unequal-power co-channel interferers," *IEEE Communications Letters*, vol. 8, pp. 289–291, May 2004.
- [108] A. H. Wojnar, "Unknown bounds on performance in Nakagami channels," *IEEE Transactions on Communications*, vol. 34, no. 1, pp. 22–24, Jan. 1986.
- [109] M. Abramowitz and I. A. Stegun, Eds., *Handbook of Mathematical Functions*, 10th ed. New York: Dover Publications, 1972.
- [110] H. Cramer, *Elements of Probability Theory*. New York: John Wiley & Sons, 1955.
- [111] K. Sivanesan and N. C. Beaulieu, "Exact BER analysis of bandlimited BPSK with EGC and SC diversity in cochannel interference and Nakagami fading," *IEEE Communications Letters*, vol. 10, pp. 623–625, Oct. 2004.
- [112] K. Sivanesan and N. C. Beaulieu, "Outage and BER of MRC diversity in bandlimited micro-cellular systems with CCI," *to appear in IEEE Communications Letters*.

- [113] K. Sivanesan and N. C. Beaulieu, "Exact performance analysis of bandlimited BPSK with EGC and SC diversity in cochannel interference and Nakagami fading," in *Proc. of IEEE VTC-Fall'2004*, Los Angeles, CA, Sept. 2004.
- [114] K. Sivanesan and N. C. Beaulieu, "Precise performance analysis of MRC diversity in micro-cellular systems with cochannel interference," in *Proc. of Asilomar Conference-2004*, Monterey, CA, Nov. 2004.
- [115] Y. Song, S. D. Blostein, and J. Cheng, "Exact outage probability for equal gain combining with cochannel interference in Rayleigh fading," *IEEE Transactions on Wireless Communications*, vol. 2, pp. 865–870, Sept. 2003.
- [116] W. C. Jakes, *Microwave Mobile Communications*. New York: IEEE press, reprint, 1974.
- [117] K. W. Sowerby and A. G. Williamson, "Outage probability calculations for multiple cochannel interferers in cellular mobile radio systems," *IEE Proceedings-Part-F*, vol. 135, pp. 208–215, June 1988.
- [118] K. W. Sowerby and A. G. Williamson, "Outage probabilities in mobile radio systems suffering cochannel interferers," *IEE Electronics Letters*, vol. 24, pp. 1511–1513, Nov. 1988.
- [119] K. W. Sowerby and A. G. Williamson, "Outage probabilities in mobile radio systems suffering cochannel interferers," *IEEE Journal on Selected Areas in Communications*, vol. 10, pp. 516–522, Apr. 1992.
- [120] Y. D. Yao and A. U. H. Sheikh, "Outage probability analysis for microcell mobile radio systems with cochannel interferers in Rician/Rayleigh fading environment," *IEE Electronics Letters*, vol. 26, pp. 864–866, June 1990.

- [121] Q. T. Zhang, "Outage probability of cellular mobile radio in the presence of multiple Nakagami interferers with arbitrary fading parameters," *IEEE Transactions on Vehicular Technology*, vol. 44, pp. 661–667, Aug. 1995.
- [122] Q. T. Zhang, "Outage probability in cellular mobile radio due to Nakagami signal and interferers with arbitrary parameters," *IEEE Transactions on Vehicular Technology*, vol. 45, pp. 364–372, May 1996.
- [123] Q. T. Zhang, "Co-channel interference analysis for mobile radio suffering log-normal shadowed Nakagami fading," *IEE Proceedings-Communications*, vol. 146, pp. 49–54, Feb. 1999.
- [124] G. Karagiannidis, S. Kostopoulos, and C. Georgopoulos, "Outage probability analysis for a Rician signal in  $l$  Nakagami interferers with arbitrary parameters," *KICS Journal of Communication Networks*, vol. 1, pp. 26–30, Mar. 1999.
- [125] G. Karagiannidis, C. Georgopoulos, and S. Kostopoulos, "Outage probability analysis for a Nakagami signal in  $l$  Nakagami interferers," *European Transactions on Telecommunication*, vol. 12, pp. 145–150, Mar./Apr. 2001.
- [126] L. C. Wang and C. T. Lea, "Co-channel interference analysis of shadowed Rician channels," *IEEE Communications Letters*, vol. 2, no. 3, pp. 67–69, Mar. 1998.
- [127] C. Tellambura, "Cochannel interference computation for arbitrary Nakagami fading," *IEEE Transactions on Vehicular Technology*, vol. 48, pp. 487–489, Mar. 1999.

- [128] K. W. Sowerby and A. G. Williamson, "Outage probability calculation for mobile radio systems with multiple interferers," *IEE Electronics Letters*, vol. 24, pp. 1073–1075, Aug. 1988.
- [129] S. Okui, "Probability of co-channel interference for selection diversity reception in the Nakagami  $m$ -fading channel," *IEE Proceedings - I*, vol. 139, pp. 91–94, Feb. 1992.
- [130] S. Okui, "Effects of CIR selection diversity with two correlated branches in the  $m$ -fading channel," *IEEE Transactions on Communications*, vol. 48, no. 10, pp. 1631–1633, Oct. 2000.
- [131] Y. D. Yao and A. U. H. Sheikh, "Investigations into cochannel interference in microcellular mobile radio systems," *IEEE Transactions on Vehicular Technology*, vol. 41, pp. 114–123, May 1992.
- [132] H. Yang and M. S. Alouini, "Outage probability of dual-branch diversity systems in presence of co-channel interference," *IEEE Transactions on Wireless Communications*, vol. 2, pp. 310–319, Mar. 2003.
- [133] A. Leon-Garcia, *Probability and Random Processes for Electrical Engineering*, 2nd ed. Reading, Massachusetts, USA: Addison Wesley, 1994.
- [134] S. M. Alamouti, "A simple transmit diversity technique for wireless communications," *IEEE Journal on Selected Areas in Communications*, vol. 16, pp. 1451–1458, Oct. 1998.
- [135] R. A. Horn and C. R. Johnson, *Matrix Analysis*. New York: Cambridge University Press, 1985.

- [136] S. M. Kay, *Fundamentals of Statistical Signal Processing: Detection Theory*. Upper Saddle River, NJ: Prentice Hall PTR, 1993.
- [137] E. Kreyszig, *Advanced Engineering Mathematics*, 8th ed. New York: John Wiley & Sons, 1999.
- [138] M. Schwartz, W. R. Bennett, and S. Stein, *Communication Systems and Techniques*, 2nd ed. New York, NY: IEEE Press, 1996.
- [139] M. K. Simon, S. M. Hinedi, and W. C. Lindsey, *Digital Communication Techniques: Signal Design and Detection*. Upper Saddle River, NJ: Prentice Hall, 1995.
- [140] J. M. Wozencraft and I. M. Jacobs, *Principles of Communication Engineering*. New York: John Wiley and Sons, 1965.
- [141] J. Chow and N. C. Beaulieu, "Analysis of cochannel interference in angle modulated systems," in *Proc. of PACRIM'99*, Victoria, BC, Canada, Aug. 1999, pp. 123–127.
- [142] T. Kailath, "Some integral equations with "Nonrational" kernels," *IEEE Transactions on Information Theory*, vol. 12, pp. 442–447, Oct. 1966.
- [143] W. C. Y. Lee, "Spread spectrum for mobile communications," *IEEE Transactions on Vehicular Technology*, vol. 40, pp. 313–322, May 1991.

# Appendix A

In this appendix, we derive the exact BER expression for the whitening and SNIR maximizing filter receiver with Nakagami-Rayleigh fading model and SRC and BTD pulse-shaping using the CF method [45], [46]. The total CCI component at the output of the WMF or SNIR maximizing filter is

$$I_{CCI} = \sum_{i=1}^K \sqrt{\frac{P_i T}{2}} R_i \cos(\phi_i) \rho_i = \sum_{i=1}^K I_i, \quad (\text{A.1})$$

where

$$I_i \approx \sqrt{\frac{P_i T}{2}} R_i \cos(\phi_i) \left( \sum_{k=-N_I}^{N_I} b_i[k] q_{k,i} \right) \quad (\text{A.2})$$

where  $q_{k,i} = q(-kT - \tau_i)$  and  $q(t)$  is the time domain pulse of  $Q(\omega)|H(\omega)|^2$ . We assume that the cross-term ISI contribution of the  $i$ -th interferer is limited to  $2N_I + 1$  terms. Then, the conditional CF of  $I_i$  given  $X_i$  and  $\tau_i$  is [43], [45]

$$\Phi_{I_i|X_i, \tau_i}(\omega) = \prod_{k=-N_I}^{N_I} \cos \left( \sqrt{\frac{P_i T}{2}} X_i \omega q_{k,i} \right) \quad (\text{A.3})$$

where  $X_i = R_i \cos(\phi_i)$ , which is a zero-mean Gaussian random variable with variance  $\Omega_i/2$ . Averaging out  $X_i$  and  $\tau_i$  in (A.3) gives

$$\Phi_{I_i}(\omega) = \frac{2}{T} \int_0^T \left[ \int_0^{+\infty} f_{X_i}(x) \prod_{k=-N_I}^{N_I} \cos \left( \sqrt{\frac{P_i T}{2}} x \omega q(kT - u) \right) dx \right] du. \quad (\text{A.4})$$



Since the CCI and background noise are independent, the CF of the total CCI and the background noise is

$$\Phi_T(\omega) = \Phi_{I_{CCI}}(\omega)\Phi_{n_0}(\omega), \quad (\text{A.5})$$

where  $\Phi_{I_{CCI}}(\omega)$  and  $\Phi_{n_0}(\omega) (= e^{-\frac{\omega^2}{2}})$  are the CF of the total CCI and background noise, respectively. Assuming the interference from different users are independent, we can write the CF of the total CCI as

$$\Phi_{I_{CCI}}(\omega) = \prod_{i=1}^K \Phi_{I_i}(\omega). \quad (\text{A.6})$$

The average BER, conditioned on  $R_s$  is written as

$$\begin{aligned} P_{e|R_s} &= \Pr \left[ \sqrt{\frac{P_s T}{2}} R_s a[0] + I_{CCI} + n_0 < 0 \middle| a[0] = +1 \right] \\ &= \frac{1}{2} - \frac{1}{\pi} \int_0^{+\infty} \frac{\sin \left( \sqrt{\frac{P_s T}{2}} R_s \omega \right)}{\omega} \Phi_T(\omega) d\omega. \end{aligned} \quad (\text{A.7})$$

The average BER, for the case in which there is no fading for the desired user, can be obtained from (A.7) by substituting  $R_s = 1$ . When the desired user undergoes Nakagami fading, the average BER becomes

$$P_{e2} = \frac{1}{2} - \frac{\Gamma(m_s + \frac{1}{2})}{\pi \Gamma(m_s)} \sqrt{\frac{P_s T \Omega_s}{2m_s}} \int_0^{+\infty} \Phi_T(\omega) {}_1F_1 \left( m_s + \frac{1}{2}; \frac{3}{2}; \frac{-P_s T \Omega_s \omega^2}{8m_s} \right) d\omega, \quad (\text{A.8})$$

where  ${}_1F_1(\cdot)$  is the confluent hypergeometric function. Note that (A.8), through  $\Phi_T(\omega)$  which contains double integral in (A.4) through  $\Phi_{I_i}(\omega)$  and (A.5) and (A.6) is a triple integral. As there is no general closed-form expression for the triple integral in (A.8), it is evaluated using numerical integration.

# Appendix B

In this appendix, we derive the optimal tap coefficients which maximize the signal-to-noise-plus-interference ratio in (2.38). One has

$$\begin{aligned} SNIR &= \frac{P_s T R_S^2}{2} \frac{(x^T \alpha)^2}{\alpha^T \mathbf{R}_v \alpha} \\ &= \frac{P_s T R_S^2}{2} \frac{|x^T \alpha|^2}{\alpha^T \mathbf{U} \mathbf{\Lambda} \mathbf{U}^T \alpha} \end{aligned} \quad (\text{B.1})$$

$$= \frac{P_s T R_S^2}{2} \frac{|x^T \mathbf{U} \mathbf{\Lambda}^{-\frac{1}{2}} \mathbf{\Lambda}^{\frac{1}{2}} \mathbf{U}^T \alpha|^2}{\alpha^T \mathbf{U} \mathbf{\Lambda}^{\frac{1}{2}} \mathbf{\Lambda}^{\frac{1}{2}} \mathbf{U}^T \alpha} \quad (\text{B.2})$$

$$\leq \frac{P_s T R_S^2}{2} \frac{|x^T \mathbf{U} \mathbf{\Lambda}^{-\frac{1}{2}}|^2 |\mathbf{\Lambda}^{\frac{1}{2}} \mathbf{U}^T \alpha|^2}{|\mathbf{\Lambda}^{\frac{1}{2}} \mathbf{U}^T \alpha|^2} \quad (\text{B.3})$$

$$= \frac{P_s T R_S^2}{2} x^T \mathbf{R}_v^{-1} x \quad (\text{B.4})$$

where (B.1) results from eigendecomposition [135] of  $\mathbf{R}_v$  and  $\mathbf{R}_v$  is a positive definite matrix. Matrix  $\mathbf{U}$  is an orthogonal matrix which contains the eigenvectors corresponding to different eigenvalues of  $\mathbf{R}_v$  in columns. Matrix  $\mathbf{\Lambda}$  is a diagonal matrix with the eigenvalues as elements. Eq. (B.3) is written by Cauchy-Schwartz inequality for matrices [135]. The equality in (B.3) holds when

$$\begin{aligned} \mathbf{\Lambda}^{\frac{1}{2}} \mathbf{U}^T \alpha &= \mathbf{\Lambda}^{-\frac{1}{2}} \mathbf{U}^T x \\ \Rightarrow \mathbf{R}_v \alpha &= x. \end{aligned} \quad (\text{B.5})$$

Thus, (B.4) is maximum when  $\alpha$  is the solution to eq. (B.5).

Now, we present the inverse Fourier transform of  $|H(\omega)|^2$  and  $|H(\omega)|^4$  for the SRC and BTB pulses with 100% excess bandwidth ( $\beta = 1$ ). For SRC and BTB pulses with  $\beta = 1$  the inverse Fourier transforms of  $|H(f)|^2$  are obtained by substituting  $\beta = 1$  in (2.12) and (2.14), respectively. For the SRC pulse-shaping,  $|H(f)|^4$  is written as

$$|H(f)|^4 = \frac{T^2}{4} \left( \frac{3}{2} + 2 \cos(\pi T f) + \frac{1}{2} \cos(2\pi T f) \right), \quad -\frac{1}{T} \leq f \leq \frac{1}{T} \quad (\text{B.6})$$

and the inverse Fourier transform is given by

$$h_4(t) = \frac{\frac{3T}{4} \sin(\frac{2\pi t}{T})}{\frac{2\pi t}{T} (1 - \frac{4t^2}{T^2})(1 - \frac{t^2}{T^2})}. \quad (\text{B.7})$$

For the BTB pulse-shaping,

$$|H(f)|^4 = \begin{cases} T^2 \exp(-4T \ln[2]f) & 0 \leq f \leq \frac{1}{2T} \\ T^2 - 2T^2 \exp(2T \ln[2](f - \frac{1}{T})) + \\ T^2 \exp(4T \ln[2](f - \frac{1}{T})) & \frac{1}{2T} \leq f \leq \frac{1}{T} \end{cases} \quad (\text{B.8})$$

and

$$h_4(t) = T^2 \left[ \frac{\sin(\frac{2\pi t}{T}) - \sin(\frac{\pi t}{T})}{\pi t} \right] + T^2 \left[ \frac{T \ln[2][2 - \cos(\frac{\pi t}{T}) + 2 \cos(\frac{2\pi t}{T})] + \pi t \sin(\frac{2\pi t}{T})}{(2T \ln[2])^2 + \pi^2 t^2} \right] - T^2 \left[ \frac{T \ln[2][2 \cos(\frac{2\pi t}{T}) - \cos(\frac{\pi t}{T})] + \pi t [2 \sin(\frac{2\pi t}{T}) - \sin(\frac{\pi t}{T})]}{(T \ln[2])^2 + \pi^2 t^2} \right]. \quad (\text{B.9})$$

# Appendix C

In this appendix, we derive the exact solution  $q(t)$ , to the integral equation in (2.49), given by

$$g_T(t) = q(t) + P \int_0^T \phi(t-u)q(u)du \quad (\text{C.1})$$

where

$$\phi(\tau) = \begin{cases} 1 - \frac{|\tau|}{T}, & \text{if } |\tau| \leq T \\ 0, & \text{Otherwise} \end{cases} \quad (\text{C.2})$$

To solve the integral equation, we use the method proposed in [142] for triangular kernels. Substituting (C.2) in (C.1)

$$g_T(t) = q(t) + P \int_0^t \left(1 - \frac{t}{T} + \frac{u}{T}\right) q(u)du + P \int_t^T \left(1 + \frac{t}{T} - \frac{u}{T}\right) q(u)du, \quad 0 \leq t \leq T. \quad (\text{C.3})$$

On the open interval  $0 < t < T$ , differentiating (C.3), with respect to  $t$  [76], gives

$$g'_T(t) = q'(t) - \frac{P}{T} \int_0^t q(u)du + \frac{P}{T} \int_t^T q(u)du \quad 0 < t < T, \quad (\text{C.4})$$

and differentiating (C.4) again on the open interval  $0 < t < T$ , gives

$$g''_T(t) = q''(t) - \frac{2P}{T}q(t) \quad 0 < t < T. \quad (\text{C.5})$$

In the open interval  $0 < t < T$ ,  $g''_T(t) = 0$ . Thus, eq. (C.5) becomes

$$q''(t) - \frac{2P}{T}q(t) = 0. \quad (\text{C.6})$$

This is a homogeneous differential equation of order 2. Then, the solution is in the form of [137]

$$q(t) = C_1 e^{\sqrt{\frac{2P}{T}}t} + C_2 e^{-\sqrt{\frac{2P}{T}}t} \quad 0 \leq t \leq T, \quad (\text{C.7})$$

with the boundary conditions at  $t = 0$  and  $t = T$ . Now, at the boundary conditions, by substituting (C.7) in (C.3), a pair of simultaneous equations in  $C_1$  and  $C_2$  are obtained as

$$a_1 C_1 + a_2 C_2 = K^2 \sqrt{T} \quad (\text{C.8})$$

$$b_1 C_1 + b_2 C_2 = K^2 \sqrt{T}, \quad (\text{C.9})$$

where

$$K = \sqrt{\frac{2P}{T}}, \quad (\text{C.10})$$

$$a_1 = K^2 T e^{KT} + P[1 + e^{KT}(KT - 1)], \quad (\text{C.11})$$

$$a_2 = K^2 T e^{KT} + P[1 - e^{-KT}(KT + 1)], \quad (\text{C.12})$$

$$b_1 = K^2 T + P[e^{KT} - 1 - KT], \quad (\text{C.13})$$

$$b_2 = K^2 T + P[e^{-KT} - 1 + KT]. \quad (\text{C.14})$$

Now, from (C.8) and (C.9), the constants  $C_1$  and  $C_2$  can be written as

$$C_1 = \frac{K^2 \sqrt{T}(b_2 - a_2)}{(a_1 b_2 - b_1 a_2)}, \quad (\text{C.15})$$

$$C_2 = \frac{K^2 \sqrt{T}(b_1 - a_1)}{(b_1 a_2 - a_1 b_2)}. \quad (\text{C.16})$$

# Appendix D

## Derivation of $\mathbb{E}[\Psi_k]$ and $\mathbb{E}[\Psi_k^2]$

In this appendix, we derive  $\mathbb{E}[\Psi_k]$  and  $\mathbb{E}[\Psi_k^2]$  for the SIGA method. The quantity  $\Psi_k$  is given by

$$\Psi_k = P_k \mathcal{X}_k^2 T_c^2 N \sum_{i=-\infty}^{+\infty} g^2(iT_c - T_k) \quad (\text{D.1})$$

$$= NP_k \mathcal{X}_k^2 T_c^2 \left[ 1 - \frac{\zeta\beta}{2} + \frac{\zeta\beta \cos(2\pi T_k)}{2} \right]. \quad (\text{D.2})$$

Then the mean of  $\Psi_k$  is written as

$$\begin{aligned} \mathbb{E}[\Psi_k] &= P_k T_c^2 N \mathbb{E}[\mathcal{X}_k^2] \mathbb{E} \left[ \sum_{i=-\infty}^{\infty} g^2(iT_c - T_k) \right] \\ &= \frac{P_k T_c^2 N \Omega}{2} \frac{1}{T_c^3} \int_{-1/T_c}^{1/T_c} |Q(f)|^4 df \end{aligned} \quad (\text{D.3})$$

The second moment of  $\Psi_k$  is written as

$$\begin{aligned} \mathbb{E}[\Psi_k^2] &= P_k^2 T_c^4 N^2 \mathbb{E}[\mathcal{X}_k^4] \mathbb{E} \left[ \left[ 1 - \frac{\zeta\beta}{2} + \frac{\zeta\beta \cos(2\pi T_k)}{2} \right]^2 \right] \\ &= \frac{3P_k^2 T_c^4 N^2 \Gamma(m+2)}{8 \Gamma(m)} \left( \frac{\Omega}{m} \right)^2 \left[ \left[ 1 - \frac{\zeta\beta}{2} \right]^2 + \frac{\zeta^2 \beta^2}{8} \right]. \end{aligned} \quad (\text{D.4})$$

## Derivation of $\{A_n\}_{n=1}^4$ , and $\{\mathbb{E}_{\mathcal{X}_k, T_k}[(Y - \bar{Y})^n]\}_{n=1}^4$

The expression  $Y - \bar{Y}$  is written as

$$Y - \bar{Y} = B - C \quad (\text{D.5})$$

where

$$B = \sum_{k=1}^K P_k \mathcal{X}_k^2 T_c^2 N \left[ 1 - \frac{\zeta\beta}{2} + \frac{\zeta\beta}{2} \cos(2\pi T_K) \right] \quad (\text{D.6})$$

and

$$C = \frac{\Omega T_c^2 N}{2} \left[ 1 - \frac{\zeta\beta}{2} \right] \sum_{k=1}^K P_k. \quad (\text{D.7})$$

Then,

$$\mathbb{E}[(Y - \bar{Y})] = 0, \quad (\text{D.8a})$$

$$\mathbb{E}[(Y - \bar{Y})^2] = \mathbb{E}[B^2] - C^2, \quad (\text{D.8b})$$

$$\mathbb{E}[(Y - \bar{Y})^3] = \mathbb{E}[B^3] - 3C\mathbb{E}[B^2] + 3C^2\mathbb{E}[B] - C^3, \quad (\text{D.8c})$$

$$\mathbb{E}[(Y - \bar{Y})^4] = \mathbb{E}[B^4] - 4C\mathbb{E}[B^3] + 6C^2\mathbb{E}[B^2] - 4C^3\mathbb{E}[B] + C^4. \quad (\text{D.8d})$$

Using  $\mathbb{E}[R_k^n] = \frac{\Gamma(m+\frac{n}{2})}{\Gamma(m)} \left(\frac{\Omega}{m}\right)^{\frac{n}{2}}$  and  $\mathbb{E}[\cos^{2l}(\theta_k)] = \frac{\Gamma(l+\frac{1}{2})}{\sqrt{\pi}\Gamma(l+1)}$ , and the fact that  $R_k$ ,  $\theta_k$  and  $T_k$  are iid RVs,  $\mathbb{E}[B] = C$ , and

$$\begin{aligned} \mathbb{E}[B^2] = & \sum_{k=1}^K \frac{3P_k^2 \Gamma(m+2) T_c^4 N^2}{8\Gamma(m)} \left(\frac{\Omega}{m}\right)^2 \left[ 1 - \zeta\beta + \frac{3}{8}(\zeta\beta)^2 \right] + \\ & \sum_{\substack{k \neq j, \\ K(K-1)/2 \text{ terms}}} \frac{P_k P_j \Omega^2 T_c^2 N^2}{2} \left[ 1 - \frac{\zeta\beta}{2} \right]^2. \end{aligned} \quad (\text{D.9a})$$

$$\begin{aligned}
\mathbb{E}[B^3] = & \sum_{k=1}^K \frac{5P_k^3 \Gamma(m+3) T_c^6 N^3}{16 \Gamma(m)} \left( \frac{\Omega}{m} \right)^3 \left[ 1 - \frac{3\zeta\beta}{2} + \frac{9(\zeta\beta)^2}{8} - \frac{5(\zeta\beta)^3}{16} \right] + \\
& \sum_{\substack{k \neq j, \\ K(K-1) \text{ terms}}} \frac{9P_k P_j^2 \Gamma(m+2) T_c^6 N^3 \Omega}{16 \Gamma(m)} \left( \frac{\Omega}{m} \right)^2 \left[ 1 - \zeta\beta + \frac{3(\zeta\beta)^2}{8} \right] \left[ 1 - \frac{\zeta\beta}{2} \right] + \\
& \sum_{\substack{k \neq j \neq l, \\ K(K-1)(K-2)/6 \text{ terms}}} \frac{3P_k P_j P_l \Omega^3 T_c^6 N^3}{4} \left[ 1 - \frac{\zeta\beta}{2} \right]^3. \tag{D.9b}
\end{aligned}$$

$$\begin{aligned}
\mathbb{E}[B^4] = & \sum_{k=1}^K \frac{35P_k^4 \Gamma(m+4) T_c^8 N^4}{128 \Gamma(m)} \left( \frac{\Omega}{m} \right)^4 \left[ 1 - 2\zeta\beta + \frac{9(\zeta\beta)^2}{4} - \frac{5(\zeta\beta)^3}{4} + \frac{35(\zeta\beta)^4}{128} \right] + \\
& \sum_{\substack{k \neq j, \\ K(K-1) \text{ terms}}} \frac{5P_k^3 P_j \Gamma(m+3) T_c^8 N^4 \Omega}{8 \Gamma(m)} \left( \frac{\Omega}{m} \right)^3 \times \\
& \quad \left[ 1 - \frac{3\zeta\beta}{2} + \frac{9(\zeta\beta)^2}{8} - \frac{5(\zeta\beta)^3}{16} \right] \left[ 1 - \frac{\zeta\beta}{2} \right] + \\
& \sum_{\substack{k \neq j, \\ K(K-1)/2 \text{ terms}}} \frac{27P_k^2 P_j^2 \Gamma^2(m+2) T_c^8 N^4}{32 \Gamma^2(m)} \left( \frac{\Omega}{m} \right)^4 \left[ 1 - \zeta\beta + \frac{3(\zeta\beta)^2}{8} \right]^2 + \\
& \sum_{\substack{k \neq j \neq l, \\ K(K-1)(K-2)/2 \text{ terms}}} \frac{9P_k P_j P_l^2 \Gamma(m+2) T_c^8 N^4 \Omega^2}{8 \Gamma(m)} \left( \frac{\Omega}{m} \right)^2 \times \\
& \quad \left[ 1 - \zeta\beta + \frac{3(\zeta\beta)^2}{8} \right] \left[ 1 - \frac{\zeta\beta}{2} \right]^2 + \\
& \sum_{\substack{k \neq j \neq l \neq n, \\ K(K-1)(K-2)(K-3)/24 \text{ terms}}} \frac{3P_k P_j P_l P_n \Omega^4 T_c^8 N^4}{2} \left[ 1 - \frac{\zeta\beta}{2} \right]^4. \tag{D.9c}
\end{aligned}$$

The  $f(\bar{Y})$  in (3.39) is given by

$$f(\bar{Y}) = \mathbf{Q} \left( \sqrt{\frac{P_0 R_0^2 N^2 T_c^2}{\bar{Y}}} \right). \tag{D.10}$$

Using the Leibniz rule [76], the second derivative of  $f(\bar{Y})$  wrt to  $\bar{Y}$  is given by

$$f^{(2)}(\bar{Y}) = \frac{P_0^{3/2} R_0^3 N^3 T_c^3}{4\sqrt{2\pi} \bar{Y}^{7/2}} e^{\frac{-P_0 R_0^2 N^2 T_c^2}{2\bar{Y}}} - \frac{3\sqrt{P_0} R_0 N T_c}{4\sqrt{2\pi} \bar{Y}^{5/2}} e^{\frac{-P_0 R_0^2 N^2 T_c^2}{2\bar{Y}}}. \tag{D.11}$$



Then averaging the (D.11) over the Nakagami PDF,  $A_1$  is written as

$$A_2 = \frac{P_0^{\frac{3}{2}} N^3 T_c^3 \Gamma\left(\frac{2m+3}{2}\right) \left(\frac{m}{\Omega}\right)^m}{4\sqrt{2\pi} \bar{Y}^{\frac{7}{2}} \Gamma(m) \left[\frac{m}{\Omega} + \frac{P_0 N^2 T_c^2}{2\bar{Y}}\right]^{\frac{2m+3}{2}}} - \frac{3\sqrt{P_0} N T_c \Gamma\left(\frac{2m+1}{2}\right) \left(\frac{m}{\Omega}\right)^m}{4\sqrt{2\pi} \bar{Y}^{\frac{5}{2}} \Gamma(m) \left[\frac{m}{\Omega} + \frac{P_0 N^2 T_c^2}{2\bar{Y}}\right]^{\frac{2m+1}{2}}}. \quad (D.12)$$

The third derivative  $f^{(3)}(\bar{Y})$  is

$$\begin{aligned} f^{(3)}(\bar{Y}) = & \frac{P_0^{\frac{5}{2}} R_0^5 N^5 T_c^5}{8\sqrt{2\pi} \bar{Y}^{\frac{11}{2}}} e^{\frac{-P_0 R_0^2 N^2 T_c^2}{2\bar{Y}}} - \frac{5P_0^{\frac{3}{2}} R_0^3 N^3 T_c^3}{4\sqrt{2\pi} \bar{Y}^{\frac{9}{2}}} e^{\frac{-P_0 R_0^2 N^2 T_c^2}{2\bar{Y}}} + \\ & \frac{15P_0^{\frac{1}{2}} R_0 N T_c}{8\sqrt{2\pi} \bar{Y}^{\frac{7}{2}}} e^{\frac{-P_0 R_0^2 N^2 T_c^2}{2\bar{Y}}}. \end{aligned} \quad (D.13)$$

Then  $A_3$  is obtained as

$$\begin{aligned} A_3 = & \frac{P_0^{\frac{5}{2}} N^5 T_c^5 \Gamma\left(\frac{2m+5}{2}\right) \left(\frac{m}{\Omega}\right)^m}{8\sqrt{2\pi} \bar{Y}^{\frac{11}{2}} \Gamma(m) \left[\frac{m}{\Omega} + \frac{P_0 N^2 T_c^2}{2\bar{Y}}\right]^{\frac{2m+5}{2}}} - \frac{5P_0^{\frac{3}{2}} N^3 T_c^3 \Gamma\left(\frac{2m+3}{2}\right) \left(\frac{m}{\Omega}\right)^m}{4\sqrt{2\pi} \bar{Y}^{\frac{9}{2}} \Gamma(m) \left[\frac{m}{\Omega} + \frac{P_0 N^2 T_c^2}{2\bar{Y}}\right]^{\frac{2m+3}{2}}} + \\ & \frac{15P_0^{\frac{1}{2}} N T_c \Gamma\left(\frac{2m+1}{2}\right) \left(\frac{m}{\Omega}\right)^m}{8\sqrt{2\pi} \bar{Y}^{\frac{7}{2}} \Gamma(m) \left[\frac{m}{\Omega} + \frac{P_0 N^2 T_c^2}{2\bar{Y}}\right]^{\frac{2m+1}{2}}}. \end{aligned} \quad (D.14)$$

The fourth derivative of  $f(\bar{Y})$  is

$$\begin{aligned} f^{(4)}(\bar{Y}) = & \frac{P_0^{\frac{7}{2}} R_0^7 N^7 T_c^7}{16\sqrt{2\pi} \bar{Y}^{\frac{15}{2}}} e^{\frac{-P_0 R_0^2 N^2 T_c^2}{2\bar{Y}}} - \frac{21P_0^{\frac{5}{2}} R_0^5 N^5 T_c^5}{16\sqrt{2\pi} \bar{Y}^{\frac{13}{2}}} e^{\frac{-P_0 R_0^2 N^2 T_c^2}{2\bar{Y}}} + \\ & \frac{105P_0^{\frac{3}{2}} R_0^3 N^3 T_c^3}{16\sqrt{2\pi} \bar{Y}^{\frac{11}{2}}} e^{\frac{-P_0 R_0^2 N^2 T_c^2}{2\bar{Y}}} - \frac{105P_0^{\frac{1}{2}} R_0 N T_c}{16\sqrt{2\pi} \bar{Y}^{\frac{9}{2}}} e^{\frac{-P_0 R_0^2 N^2 T_c^2}{2\bar{Y}}}. \end{aligned} \quad (D.15)$$

Then  $A_4$  is given by

$$\begin{aligned} A_4 = & \frac{P_0^{\frac{7}{2}} N^7 T_c^7 \Gamma\left(\frac{2m+7}{2}\right) \left(\frac{m}{\Omega}\right)^m}{16\sqrt{2\pi} \bar{Y}^{\frac{15}{2}} \Gamma(m) \left[\frac{m}{\Omega} + \frac{P_0 N^2 T_c^2}{2\bar{Y}}\right]^{\frac{2m+7}{2}}} - \frac{21P_0^{\frac{5}{2}} N^5 T_c^5 \Gamma\left(\frac{2m+5}{2}\right) \left(\frac{m}{\Omega}\right)^m}{16\sqrt{2\pi} \bar{Y}^{\frac{13}{2}} \Gamma(m) \left[\frac{m}{\Omega} + \frac{P_0 N^2 T_c^2}{2\bar{Y}}\right]^{\frac{2m+5}{2}}} + \\ & \frac{105P_0^{\frac{3}{2}} N^3 T_c^3 \Gamma\left(\frac{2m+3}{2}\right) \left(\frac{m}{\Omega}\right)^m}{16\sqrt{2\pi} \bar{Y}^{\frac{11}{2}} \Gamma(m) \left[\frac{m}{\Omega} + \frac{P_0 N^2 T_c^2}{2\bar{Y}}\right]^{\frac{2m+3}{2}}} - \frac{105P_0^{\frac{1}{2}} N T_c \Gamma\left(\frac{2m+1}{2}\right) \left(\frac{m}{\Omega}\right)^m}{16\sqrt{2\pi} \bar{Y}^{\frac{9}{2}} \Gamma(m) \left[\frac{m}{\Omega} + \frac{P_0 N^2 T_c^2}{2\bar{Y}}\right]^{\frac{2m+1}{2}}}. \end{aligned} \quad (D.16)$$